IMPROVED AIR QUALITY FROM SUSTAINABLE CITY DEVELOPMENT IN THE UNITED STATES, INDIA, AND CHINA

A Dissertation
Presented to
The Academic Faculty

by

Raj M. Lal

In Partial Fulfillment
of the Requirements for the Degree
Doctor of Philosophy in the
School of Civil and Environmental Engineering

Georgia Institute of Technology
May 2020

IMPROVED AIR QUALITY FROM SUSTAINABLE CITY DEVELOPMENT IN THE UNTIED STATES, INDIA, AND CHINA

Approved by:

Dr. Armistead Russell, Advisor
School of Civil and Environmental Engineering
Georgia Institute of Technology

Dr. Anu Ramaswami
Civil and Environmental Engineering, Institute for International and Regional Studies, and Princeton Environmental Institute
Princeton University

Dr. James Mulholland
School of Civil and Environmental Engineering
Georgia Institute of Technology

Dr. Jennifer Kaiser
School of Civil and Environmental Engineering and School of Earth and Atmospheric Sciences
Georgia Institute of Technology

Dr. Rodney Weber
School of Earth and Atmospheric Sciences
Georgia Institute of Technology

Date Approved: [March 2, 2020]

ACKNOWLEDGEMENTS

I sincerely acknowledge all those who helped me, either with schoolwork or in other matters, over the last six years. Particularly my primary thesis advisor, Dr. Armistead Russell, for always providing guidance, knowledge, and not only allowing us to pursue our own research interests, but encouraging us to do so. I also thank Dr. Anu Ramaswami for always giving me her time (no matter where in the world she was), whether it was going line by line on paper reviews with me over video calls or working with me late into the night on slides for upcoming presentations. I would also like to thank my other committee members for their inputs and comments on my thesis work, Dr. Rodney Weber, Dr. Jennifer Kaiser, and Dr. James Mulholland. I have definitely learned to become more independent and confident as a researcher thanks to them.

Also many thanks to each of my groupmates, students in the air department, and other friends in the area. I particularly would like to thank senior graduate students and post-docs Sunni Ivey, James Hite, Ajay Nagpure, and Petrul Vasilakos for their continuous support, mentorship, and friendships.

TABLE OF CONTENTS

LIST OF TABLES

LIST OF FIGURES

SUMMARY

It is estimated that ~70% of people will live in cities by 2050 compared to ~55% present-day, an increase of 2.5 billion globally. Because of such growth, there are pressing needs to study sustainable city management, develop and utilize new methods to obtain fine-scale data, and identify infrastructure to support future development to improve public health. Exposure to ambient air pollution is associated with adverse health outcomes and is one of the leading causes of premature mortality globally, estimated to contribute to 6.5 million deaths each year, many of which occur in the United States (~70,000), India (1.4 million), and China (~650,000). In addition, these three countries are the top-three CO_2-emitting countries globally, accounting for ~50% of global emissions. The work presented in this thesis explores strategies to improve ambient air quality, reduce carbon emissions, assess $PM_{2.5}$ spatial patterns in US cities, and study fine-scale linkages between various environmental indicators.

The Taj Mahal is an iconic Indian monument and one of the Seven Wonders of the World but its marble surface has been discolored with time. Previous emission-reduction interventions have been proposed and implemented in Agra, but the soiling of the iconic monument has persisted. A recent source apportionment study estimated that ~40% of the Organic Matter (OM) deposited to its surface was from biomass burning emissions, and as a result, the City of Agra banned dung cake burning, a common fuel source for cooking and heating, in the area. However, the impacts from municipal solid waste (i.e., trash) burning may be more significant for the discoloration and public health in Agra. We used spatially detailed emission estimates using on-site developed inventories and air quality modeling to estimate biomass (e.g., municipal solid waste (MSW) and dung cake) burning contributions to the discoloration. We found that MSW burning contributed to 4.3 $\mu g\ m^{-3}$ of PM2.5 to the Taj Mahal while primary emission from dung cake burning led to about 0.34 $\mu g\ m^{-3}$. We found that open MSW burning leads to about 150 ($\pm$ 130) mg $m^{-2}\ yr^{-1}$ of $PM_{2.5}$ being deposited to the surface of the Taj Mahal compared to about 12 ($\pm$ 3.2) mg $m^{-2}\ yr^{-1}$ from dung cake burning. Those two sources, combined, also lead to an estimated 713 (377-1050) premature mortalities in Agra each year, dominated by waste burning in socioeconomically lower status neighborhoods. Interventions to improve waste

management in Agra can not only prevent the discoloration of that Taj Mahal but also have large public health benefits.

National Chinese $PM_{2.5}$ and CO_2 emission reductions from novel, urban-industrial symbiosis strategies were assessed, including waste heat re-use from electric generating and industrial sources for district commercial and residential heating and cooling. Such cross-sectoral strategies—enabled by compact urban design and circular economy policies—contribute an additional 15%–36% to national CO_2 mitigation, compared to conventional single-sector strategies. As a co-benefit, ~25,500 to ~57,500 deaths annually are avoided from air pollution reduction.

The relationship between air quality with neighborhood infrastructure and affective subjective well-being, i.e., emotional well-being, was characterized to provide supportive data for more equitable outcomes for future city development. In this work, $PM_{2.5}$ was measured using low-cost sensing technologies in six neighborhoods of varying characteristics (e.g., household income (medium-SES vs. low-SES), access to light rail, urban vs. suburban) in Minneapolis, MN. Concurrently, residents of the neighborhoods took real-time well-being assessments using a novel, phone application Daynamica. R-Line was used to simulate on-road mobile-source NO_x concentration impacts throughout Minneapolis. We found lower income neighborhoods tended to have higher $PM_{2.5}$ concentrations than mid-income neighborhoods, and urban-designated neighborhoods had higher average on-road mobile-source NO_x impacts than their suburban counterparts. Home-based exposure assessments found that $PM_{2.5}$ was negatively correlated with positive emotions such as happiness and to net affect (the sum of positive and negative emotion scores), and positively correlated (i.e., a higher $PM_{2.5}$ concentration led to higher scores) for negative emotions such as tiredness, stress, sadness, and pain. Simulated mobile-source NO_x, assessed from both home-based exposures and in-situ exposures, had a near-zero relationship with all EWB indicators, which was attributed to the generally low and relatively similar concentrations in the study neighborhoods and throughout Minneapolis. None of the air quality and EWB relationships were found to be statistically significant (α=0.05), which may in part be attributed to the relatively small sample size from this study.

The near-road environment has historically been one of the highest pollution areas in U.S. cities. The US EPA recently implemented the Near-road (Monitoring) Network to measure NO_2 concentrations at high-traffic roads in cities and many sites also measure $PM_{2.5}$ and CO, as well. We compared two-year average concentrations (2017 and 2018) at these near-road monitors with nearby non-near-road monitors within the same cities. After controlling for primary emissions from the target highways, we found similar and suggestively no difference ($\alpha = 0.05$) in $PM_{2.5}$ concentrations between the near-road and non-near-road urban sites (δ = 0.42 (-0.08-0.90) μg m^{-3}, n=35 comparisons). NO_2 and CO levels, on average were significantly higher at the near-road sites compared to the non-near-road urban sites by 5.0 (3.4-6.5) ppb (n=44 comparisons) and $9.2x10^{-2}$ (0.04-0.14) ppm (n=42 comparisons), respectively. The similar levels of $PM_{2.5}$ in the near-road and non-near-road environments can be explained by cleaner vehicle fleets, formation of secondary PM from on-road emissions occurring downwind (i.e., away from the road), decreased SOA formation rates in the near-road environment, the prevalence of other low-volume vehicular and local, non-vehicular sources of emissions at the non-near-road sites (e.g., railyards, truck yards, ports, biomass-fueled heating, backyard barbecuing, and commercial cooking, etc.) and local meteorology (e.g. wind speed and wind direction) impacting near-road observations. The same observational data was used to assess mobile source emission estimates from the EPA National Emission Inventory, and analysis of the observations are in rough agreement with the current ratio of NO_x to CO from on-road mobile sources.

Finally, power plant and industrial waste heat to electricity and coal fly-ash material exchanges were assessed in India to estimate air pollution and carbon mitigation of such strategies there. Currently, residential biomass burning used for cooking and heating is the leading contributor to ambient $PM_{2.5}$ in India, while the leading CO_2-emitting sector is Thermal Power Systems (TPSs). Previously published emission estimates projected to 2050 find coal-fired TPSs will be the leading source of ambient $PM_{2.5}$, due in part to reductions in residential biomass burning emissions and widespread projected expansion in coal generating capacity nationwide. Here, we quantify the total amount of electricity that can be generated from low- and medium-grade waste heat at coal-fired TPSs and other large sources (e.g., cement plants, iron and steel plants, open agricultural burning) using

Organic Rankine Cycles (ORCs). This same amount of electricity is offset by coal consumption reductions at TPSs to offer a first-order assessment of the CO_2 emission and air quality impacts of such strategies in 2015 and under three scenarios projected to 2050 using various levels of policy adoption (2050-REF: business as usual; 2050-S2: effective achievement of currently-proposed targets under the Perform, Achieve, and Trade (PAT) scheme; 2050-S3: ambitious regulatory achievement). In addition, we assess material exchange pathways that re-utilize coal fly-ash for material substitution in brick and cement reduction, offering local CO_2 and air pollution emission reductions. We find such waste-heat re-use strategies to generate an additional 17 (9% of total coal-fired TPS generating capacity), 27 (6%), 19 (8%), and 5 (4%) GW of electricity in the 2015, 2050-REF, 2050-S2, and 2050-S3 scenarios, respectively, and preliminary modeling results find population-weighted $PM_{2.5}$ improvements ranging from 1.2-6.6% for the three 2050 scenario projections.

CHAPTER 1. INTRODUCTION

Exposure to elevated levels of ambient air pollution is associated with adverse health outcomes that result in premature mortality and reduced life expectancy (5-8), with the vast majority (~95%) of air pollution-related mortality linked to fine particulate matter ($PM_{2.5}$, particulate matter whose aerodynamic diameter is less than 2.5 microns) (6, 9). About 6.5 million deaths worldwide annually are attributed to air pollution exposure, of which 1.4 million are in India, 650,000 in China, and another 70,000 in the United States. In addition, many sources of air pollutants are also sources of climate-forcing greenhouse gases (GHGs), so benefits of air pollution emission reductions could be multi-dimensional. Despite some of the differences between the countries and their respective states of development, China, the United States, and India are the 1st, 2nd, and 3rd leading GHG-emitting countries globally, contributing 26%, 15%, and 6.5% of global emissions, respectively.

By 2050, it is estimated that ~70% of people will live in cities, an increase of 2.5 billion globally (10). As a result of such growth, there are pressing needs to study cities and identify infrastructure (defined as systems that provide water, energy, food, shelter, transportation/communication, waste management, and public spaces (11)) to support the expected development. These seven infrastructure sectors are associated with ~87% of global anthropogenic GHG emissions and contribute to ~19.5 million deaths annually, many of which will occur within cities themselves (12). Developing sustainable cities in the United States, India, and China can lead to outcomes associated with healthier populations, global environmentally friendly practices, and improved well-being (12).

Studying cities in countries like the United States, India, and China offers unique insights for sustainable city development as these countries are at very different stages of their developments. The United States is a developed nation with a human development index (HDI) of 0.92, China's HDI is 0.75, and India's HDI is 0.64. The UN HDI (scale 0:1, with one the highest achievable score) is a comprehensive statistic that considers life expectancy, education, and income per capita indicators and is used as a measure of a country's level of human development. This thesis will outline infrastructure interventions, synergies between infrastructure indicators, and characterizations of pollution and emission levels in the United States, India, and China to achieve goals associated with sustainable city development for improved air quality.

Chapter 2 addresses how biomass burning, including emissions from municipal solid waste (MSW) and dung cake burning, is discoloring the surface of the Taj Mahal, an iconic Indian monument and one of the Seven Wonders of the World. Previous interventions such as restricting vehicles near the complex, requiring nearby iron foundries to install scrubbers and filters on their smokestacks, and prohibiting new polluting enterprises from being built within a defined buffer zone surrounding the mausoleum have been administered to reduce pollution near the monument, but the haze and darkening has persisted. PM responsible for the soiling has been attributed to a variety of sources, but a recent source apportionment study concluded that biomass burning (MSW, dung cake, wood, crop, etc.) contributed ~40% of the deposited organic matter (OM, a component of PM) (13). Dung cake burning, used extensively for cooking in the region, was the suggested culprit and banned within the city limits. In this work, I helped develop spatially detailed emission estimates of MSW and dung cake burning from on-site fieldwork (14). I

used an air quality model to simulate $PM_{2.5}$ impacts in Agra and found that MSW burning contributed 12 times more $PM_{2.5}$ than dung cake burning emissions at the Taj Mahal. I estimated the combined amount of pollutant deposition to be 162 mg m^{-2} yr^{-1}. In addition, in conjunction with detailed population and demographic data, 713 premature mortalities each year are attributed to exposures of $PM_{2.5}$ from MSW and dung cake burning emissions (14).

Chapter 3 assesses the potential of a novel urban-industrial symbiosis strategy for carbon mitigation with local health co-benefits in 637 Chinese cities (15). Cities offer unique strategies to reduce fossil fuel use through the exchange of energy and materials across homes, businesses, infrastructure, and industries co-located in urban areas. Here, novel cross-sectoral strategies, which includes the use of waste heat re-use for commercial and district energy and heating, were assessed throughout China, and we found these interventions could contribute an additional 15-36% to national CO_2 emission reductions when compared to conventional single-sector strategies. As a co-benefit, ~25,500 to ~57,500 deaths annually are avoided from air pollution reduction. My contribution to this work was performing the air pollution modeling of the base case emissions and the emissions under the urban-industrial symbiosis strategies. The benefits are highly variable across cities, ranging from <1%–37% for CO_2emission reduction and <1%–47% for avoided premature deaths. These results that use multi-scale, multi-sector physical systems modelling identify cities with high carbon and health co-benefit potential and show that urban–industrial symbiosis is a significant carbon mitigation strategy, achievable with a combination of existing and advanced technologies in diverse city types.

Chapter 4 explores the links between air quality and emotional well-being (EWB) and air quality and neighborhood infrastructure in Minneapolis, MN. Cities in the United States have announced initiatives to make them more sustainable, healthier, resilient, livable, and environmentally friendly. However, indicators of measuring outcomes related to these targets and the synergies between them have not been well defined and studied. I collected ambient $PM_{2.5}$ measurements using low-cost air quality sensors (16) and modeled mobile-source NO_x using the Research-LINE (R-LINE) source dispersion model for near-surface releases. Residents of the six study neighborhoods (each with varying infrastructure parameters including middle-income vs. low-income, urban vs. rural, and access to light rail) concurrently took real-time EWB assessments using a smart phone application, Daynamica, to gauge their emotional state, including happiness, tiredness, stress, sadness, and pain. No statistically significant (α=0.05) $PM_{2.5}$ differences were found between urban poor and urban middle-income neighborhoods, but average mobile-source NO_x was statistically significantly (α=0.05) higher in the four urban neighborhoods than in the two suburban neighborhoods. Close proximity to light rail had no observable impact on average observed $PM_{2.5}$ or simulated mobile-source NO_x. Home-based exposure assessments found that $PM_{2.5}$ was negatively correlated with positive emotions such as happiness and to net affect (the sum of positive and negative emotion scores), and positively correlated (i.e., a higher $PM_{2.5}$ concentration led to higher scores) for negative emotions such as tiredness, stress, sadness, and pain. Simulated mobile-source NO_x, assessed from both home-based exposures and in-situ exposures, had a near-zero relationship with all EWB indicators. This was attributed to low

NO_x levels throughout the study neighborhoods and at locations were the EWB-assessed activities took place, both owing to low on-road mobile-source NO_x emissions.

Chapter 5 compares $PM_{2.5}$, NO_2, and CO at near-road sites with other non-near-road, regulatory monitors within U.S. cities. Emissions from mobile sources have historically been an important anthropogenic contributor to ambient air pollution leading to high levels of air pollution near major roadways (17). The US EPA recently implemented the Near-Road (monitoring) Network to measure NO_2 concentrations by heavily trafficked roadways in urban centers throughout the US, as these locations were believed to characterize worst-case human exposures to traffic-related pollutants. Some near-road sites also include CO and $PM_{2.5}$ measurements, which along with the NO_2 observations, were compared against companion non-near-road monitors located within the city boundary or a 10-mile (~city scale) radius. After controlling for primary emissions from the target highways, we found no statistical difference ($\alpha = 0.05$) in $PM_{2.5}$ concentrations between the near-road and non-near-road urban sites ($\delta = 0.42$ (-0.08-0.90) $\mu g\ m^{-3}$, n=35 comparisons). NO_2 and CO levels, on average were significantly higher at the near-road sites compared to the non-near-road urban sites by 5.0 (3.4-6.5) ppb (n=44 comparisons) and $9.2x10^{-2}$ (0.04-0.14) ppm (n=42 comparisons), respectively. The average $PM_{2.5}$ difference found here is 5%, and at 14 of the 35 (~40%) urban monitor comparisons and 28 of the 72 (~39%) overall comparisons, $PM_{2.5}$ is actually higher at the non-near-road site relative to its near-road pair. The same observational data was used to assess mobile source emission estimates from the EPA National Emission Inventory, and analysis of the observations are in rough agreement with the current ratio of NO_x to CO from on-road mobile sources.

Chapter 6 investigates the air quality and CO_2 emission impacts of waste heat to electricity and material exchange pathways at coal-fired Thermal Power Stations (TPSs) and other large emission sources in India. Currently, residential biomass burning used for cooking and heating is the leading contributor to ambient $PM_{2.5}$ in India, while the leading CO_2-emitting sector is Thermal Power Systems (TPSs). Previously published emission estimates projected to 2050 find coal-fired TPSs will be the leading source of ambient $PM_{2.5}$, due in part to reductions in residential biomass burning emissions and widespread projected expansion in coal generating capacity nationwide. Previous assessments have found that clean-energy generation using renewable technologies (e.g., PV solar, wind, etc.) will have large carbon and air quality benefits, but the installation costs have been a barrier for implementation thus far throughout India. Coal combustion, particularly with Indian coal, is highly inefficient and produces large amounts of waste heat. Here, we quantify the total amount of electricity that can be generated from low- and medium-grade waste heat at coal-fired TPSs and other large sources (e.g., cement plants, iron and steel plants, open agricultural burning) using Organic Rankine Cycles (ORCs). This same amount of electricity is offset by coal consumption reductions at TPSs to offer a first-order assessment of the CO_2 emission and air quality impacts of such strategies in 2015 and under three scenarios projected to 2050 using various levels of policy adoption (2050-REF: business as usual; 2050-S2: effective achievement of currently-proposed targets under the Perform, Achieve, and Trade (PAT) scheme; 2050-S3: ambitious regulatory achievement). In addition, we assess material exchange pathways that re-utilize coal fly-ash for material substitution in brick and cement reduction, offering local CO_2 and air pollution emission reductions. We find such waste-heat re-use strategies to generate an additional 17 (9% of

total coal-fired TPS generating capacity), 27 (6%), 19 (8%), and 5 (4%) GW of electricity in the 2015, 2050-REF, 2050-S2, and 2050-S3 scenarios, respectively. These inventories were used as input to the GEOS-Chem model to simulate ambient $PM_{2.5}$ and two-week simulation results presented here find improvements in population-weighted average concentrations, ranging from 1.2% to 6.6% reductions.

CHAPTER 2. MUNICIPAL SOLID WASTE BURNING AND DUNG CAKE BURNING: DISCOLORING THE TAJ MAHAL AND HUMAN HEALTH IMPACTS IN AGRA

As published in *Environmental Research Letters*

Abstract

The Taj Mahal – an iconic World Heritage monument built of white marble – has become discolored with time, due, in part, to high levels of particulate matter (PM) soiling its surface (13). Such discoloration has required extensive and costly treatment (18) and despite previous interventions to reduce pollution in its vicinity, the haze and darkening persists (13, 18). PM responsible for the soiling has been attributed to a variety of sources including industrial emissions, vehicular exhaust and biomass burning, but the contribution of the emissions from the burning of open municipal solid waste (MSW) may also play an important role. A recent source apportionment study of fine particulate matter ($PM_{2.5}$) at the Taj Mahal showed biomass burning emissions, which would include MSW emissions, accounted for nearly 40% of organic matter (OM) – a component of PM – deposition to its surface (13); dung cake burning, used extensively for cooking in the region, was the suggested culprit and banned within the city limits (18), although the burning of MSW, a ubiquitous practice in the area (2), may play a more important role in local air quality. Using spatially detailed emission estimates and air quality modeling, we find that open MSW burning leads to about 150 ($\pm$ 130) mg m^{-2} yr^{-1} of $PM_{2.5}$ being deposited to the surface of the Taj Mahal compared to about 12 ($\pm$ 3.2) mg m^{-2} yr^{-1} from dung cake burning. Those two sources, combined, also lead to an estimated 713 (377-1050) premature mortalities in Agra each year, dominated by waste burning in

socioeconomically lower status neighborhoods. An effective MSW management strategy would reduce soiling of the Taj Mahal, improve human health, and have additional aesthetic benefits.

2.1 Introduction

The Taj Mahal in Agra, India is a UNESCO World Heritage Site that attracts millions of tourists each year. However, its surface has been soiled over time, discoloring its white marble façade. Studies have recognized that poor air quality is responsible for the soiling and discoloration (13, 19-22) and measures have been taken to curb the impact of local air pollution around the Taj Mahal including restricting vehicles near the complex, closing over 200 enterprises in Agra, requiring iron foundries to install scrubbers and filters on their smokestacks, prohibiting new polluting enterprises from being built within a defined buffer zone around the mausoleum, and most recently, banning cow dung cake burning as cooking fuel (18). A recent source apportionment study of fine particulate matter ($PM_{2.5,}$ whose particles are less than 2.5 μm in aerodynamic diameter) at the Taj Mahal found that biomass burning accounts for nearly 40% of all organic matter (OM) deposition to its surface (13). Two sources of biomass burning $PM_{2.5}$ in Agra, which would be included in the measurement of deposited OM, are the open combustion of municipal solid waste (MSW) and dung cake burning (2). The high particulate matter (PM) loadings in Agra also reduce visibility, further impairing the aesthetic beauty of the Taj Mahal.

While the discoloration of the Taj Mahal and the deterioration of visibility may be the most immediately noticeable outcome of MSW and dung cake burning in the area, human health is of concern as well. The Global Burden of Disease (GBD) found that of 67 environmental factors associated with premature mortality, exposure to ambient PM pollution is the 6th leading cause of premature mortality in India after dietary risks, high blood pressure, indoor air pollution (which is also affected by dung cake burning), smoking

and diabetes-related diseases (23). Additionally, residential and commercial energy use, including biomass burning used for heating and cooking, is responsible for the largest impact on mortality linked to outdoor air pollution throughout India (9).

Rapid growth in Agra, coupled with a limited MSW management infrastructure, has resulted in less effective waste management that leaves large volumes of trash accumulating in the streets (2, 24). Further, generated waste is openly and frequently burned on roadsides and in residential and commercial areas in Agra (2) and throughout India (24), leading to byproducts of poor combustion and increased pollutant emissions (25-27). The Central Pollution Control Board of India estimated MSW-burning to contribute between 5 to 11% of primary PM emissions from sources within cities (28). MSW emissions include combustion byproducts of plastics and other waste in addition to biomass, which can contain chlorinated organics, dioxins, polyaromatic hydrocarbons (PAHs), numerous volatile organic compounds (VOCs) and heavy metals including lead, cadmium and mercury (29, 30). Health impacts specific to these toxic compounds are not specifically addressed in the GBD approach.

Dung cake burning used as cooking fuel has been more studied in Indian cities (31-33); 11% of rural Indian households depend on cow dung as their primary cooking fuel (33). Open MSW burning and dung cake burning tends to be more concentrated in areas of poorer populations (2, 34-38), exacerbating exposures to more vulnerable populations. MSW and dung cake emissions can also influence radiative balance and lead to regional and global change (25, 39, 40).

In this paper, the contributions of MSW and dung cake burning to ambient OM and BC (pollutants known to discolor surfaces (41)) concentrations in Agra, the deposition to and soiling of the Taj Mahal, and health impacts are assessed by quantifying location specific MSW and dung cake burning emissions, performing air quality and deposition modeling,

and conducting a health impact assessment. Such information can be used to evaluate the potential benefits of policy interventions, including improved MSW collection management practices and the associated infrastructure in and around Agra.

2.2 Methods

2.2.1 Open Municipal Solid Waste and Dung Cake Burning Inventories

Waste burn rate inventories were generated in Agra using a recently developed field transect approach to quantify the spatial and temporal trends of open MSW burning (2). In this method, researchers move along the transect (route/line) and record burning incidents, approximate weight, and composition of MSW in a predetermined distance from the line of the transect (route/line) (typically visible range is used as the distance). MSW burning incident density is then estimated by the total MSW burning incidents count and surveyed area. Two separate transect routes in Agra that covered 35 and 45 km^2, respectively (Figure A-1 & Figure A-2), were used in this study over three days for each route between May 30 and Jun 2, 2015 to quantify the waste burn density, composition, and the mass of waste burn. These surveys assessed MSW burning by socioeconomic status (SES) based on census data (32) at the neighborhood level and represented 14 neighborhoods of different SES (Figure A-1). Satellite-driven studies at the global scale cannot capture the very high levels of waste burning found in neighborhoods or near roads (9), thus the on-ground field approach is an important part of developing an improved PM emission inventory from MSW burning.

The open waste burn rate, TWB_i (g-MSW day^{-1}), within an electoral ward, *i*, from the SES-based waste burning rates is quantified by:

$$TWB_i = WBR_{lowSES} * POP_{i,lowSES} + WBR_{highSES} * (1 - POP_{i,lowSES}) \quad (1)$$

where WBR_{lowSES} = daily per capita waste burn rate of the low SES, $POP_{i,lowSES}$ = illiterate population within the ward as reported in the 2011 census (32), and $WBR_{highSES}$ = daily per capita waste burn of the high SES. Literacy was the primary indicator of SES used in this study; the total reported literacy rate in Agra is 64% (32). Waste burn inventories were generated on an electoral ward basis and each ward was modeled as its own emission grid, as were five additional zones (Figure A-3).

Data on the use of cow-dung cakes as fuel for food preparation data was assessed from the census (32). The census gave the percentage of households at the ward/precinct level using different types of fuel for cooking. Annual per household consumption of cow dung was then multiplied with the number of households using cow dung as a fuel for cooking (Figure A-4) within each ward/precinct to determine electoral-ward based burning inventories, computed on an annual basis and then converted to daily average emission rates. Applying the same method, air quality impacts from two additional sources, firewood and crop residue, were also modeled for comparison.

2.2.2 *Human Health Risk Assessment from Open MSW and Dung Cake Burning Emissions*

Premature mortality attributable to $PM_{2.5}$ (BC + OM) emissions from MSW and cow dung cake burning were determined using concentration response function (CRFs) based equations. Five major diseases – acute respiratory lung infection (ALRI), chronic obstructive pulmonary disease (COPD), ischemic heart disease (IHD), cerebrovascular disease (stroke) and lung cancer (LC) – associated with $PM_{2.5}$ mortality risks were assessed in this study. COPD, IHD, stroke, and LC related mortality were determined for adults (age ≥ 25 years), while mortalities related to ALRI were estimated for children under five years of age. Disease-specific relative risk equations use a CRF, incidence rate for premature mortality, change (increment) in ambient pollution concentration, and exposed population to estimate the mortality. The CRFs data and equation (2) used integrated-exposure response functions (IERs) to estimate specific health impacts (42).

$$\begin{cases} RR = 1 + a\{1 - \exp[-b(\Delta C)^{p}]\}, \text{for } \mathrm{C} > \mathrm{C_o} \\ RR = 1, \text{for } \mathrm{C} \le \mathrm{C_o} \end{cases} \tag{2}$$

$$PAF = \frac{\sum_{i=1}^{n} P_i(RR_i - 1)}{\sum_{i=1}^{n} P_i(RR_i - 1) + 1} \tag{3}$$

$$P_h = B_i * PAF * P_i \quad (4)$$

where RR is the relative risk or CRFs, ΔC is the increase of ambient $PM_{2.5}$ concentrations due to dung cake and MSW burning emissions, C_o is the baseline $PM_{2.5}$ concentration (considered 0 for this source impact application), and a, b, and p are parameters that determine the relationship of concentration to response and are discussed further in Burnett et al., 2014 (42). PAF is the population attributable fraction, i.e., the proportion of the disease incidence on the exposed population that can be attributed to the exposure, P_i is the fraction of the population in exposure category, i, and n is the number of exposure categories, where exposure categories were defined by five-year age increments with available CRFs. P_h is the premature mortality associated with $PM_{2.5}$ exposure and B_i is the baseline population incidence of given health effects (i.e. death per 100,000). The exposed population within each modeling grid was retrieved from the 2015 Worldpop Database. A growth factor for the total population within the study domain for the Worldpop Database reported population compared to the 2014 projected population from the census (32) was used, as the modeling results presented are for 2014.

Also determined were disability adjusted life years (DALY), which estimate the current discounted value of future years of health life lost due to morbidity and future year of human years of life lost (YLL) due to premature mortality. Since air pollutants are not a primary cause of mortality, but rather contributory, DALY can be a better indicator of health risks than premature mortality (43). The DALYs are calculated as the total of the

YLL due to premature mortality and years lost due to disability (YLD) because of morbidity. In this study, we only estimated the premature deaths due to $PM_{2.5}$ emissions associated with biomass and MSW burning and thus considered YLL as the measure of DALYs. YLL were calculated using the following equation:

$$YLL = B_i * PAF * POP_i * LE \quad (5)$$

where POP_i is the exposed population (i.e., the population within each modeled grid) and LE is the standard life expectancy at age of death (in years).

2.2.3 Municipal Solid Waste and Dung Cake Burn Inventories to AERMOD Dispersion Modeling

Open MSW and dung cake burn rates were applied in AERMOD, a Gaussian plume dispersion model (44), to spatially characterize the ambient, annually-averaged $PM_{2.5}$ concentrations from MSW and dung cake burning. AERMOD is a recommended regulatory air pollution dispersion model, but has limitations as it doesn't include atmospheric chemical processes or secondary pollution formation (44). The findings presented here are specific source impacts from emissions within the study domain, i.e., background transport is not considered. Integrated hourly surface data from the National Climatic Data Center (NCDC) at the Agra Station from the National Oceanic and Atmospheric Administration (NOAA) and upper air data from the US National Weather Service (NWS) at the Delhi Station were used in AERMET, a meteorological input to AERMOD. Digital Elevation Models from the Global 30 Arc-Second Elevation (GTOPO30) were used in AERMAP, a terrain processing input to AERMOD.

OM and BC source emission rates from both MSW and dung cake burning were determined using emission factors from the literature (45, 46) (Table A-2). $PM_{2.5}$ component-specific emission factors for MSW burning used here are from measurements of trash burning in peri-urban communities near Mexico City at varying combustion stages (45). Christian et al. (45) found emission factors of OC = 5.3 (± 4.9) and BC = 0.65 (± 0.27) g kg^{-1} burned. These emission factors are within the reported range of 0.04 – 9.97 g BC kg^{-1} burned from recent measurements of trash burning in Nepal where some samples were enriched for specific compositions of plastic and foil (47), but lower than the reported range of 8.4-73.9 g OC kg^{-1} burned. MSW emissions can vary significantly and have high uncertainties due to the composition of the waste and stage of combustion (27, 48). Emission factors applied for dung cake burning were measured in households throughout the Indo-Gangetic Plain (46). An OM/OC factor of 2.1 (49) was applied to the OC emission factors; OM is related to OC as the former accounts for specific elements other than carbon associated with the organic compounds.

2.2.4 Dry Deposition to and Pollutant Covering of the Taj Mahal

Pollutant deposition to the surface of the Taj Mahal contributes to its browning (13), so the impacts of wet and dry deposition from MSW and dung cake emissions were quantified. Dry deposition rates were calculated using modeled concentrations, measured size distributions and size-dependent deposition velocities. Deposition velocity is a variable that incorporates the aerodynamic transport through the atmospheric surface layer, the transport across the quasi-laminar sublayer, and the uptake at the surface into a single parameter (50, 51). Imaging from a scanning electron microscopy (SEM) (LEO 1530, Carl Zeiss Microscopy) and energy dispersive X-ray (EDX) spectroscopy (Oxford Instruments

X_{max} detectors) were used to measure the average particle size of carbonaceous PM species at the surface of the Taj Mahal (13). The average particle size was found to be ~ 1 μm.

The $PM_{2.5}$ component specific mass fluxes (g m^{-2} s^{-1}), F_i, of OM and BC to the surface of the Taj Mahal by dry deposition were found as:

$$F_i(t) = -V_{D,i}(d_{p,ave}) * [C_i(t)] \quad (6)$$

where V_D is the size-specific surface deposition velocity (m s^{-1}) and $d_{p,ave}$ is the average particle diameter. The pollutant concentration, $[C_i(t)]$, used here is the annual average, ambient pollutant concentration from open waste and dung cake burning at the Taj Mahal as determined in AERMOD. Wet deposition was considered in this analysis to account for rain, and the wet deposition loadings were small compared to dry deposition (see A.3 for a detailed assessment).

The fraction of the Taj Mahal's surface covered by pollutant deposition from MSW and dung cake burning emissions was also quantified from the modeled number of particles deposited per area of the surface and the total surface area of the aerosol deposited per area of the surface. The number of particles per unit area (particles m^{-2}), N, from each source and pollutant, i, was determined by:

$$N_i = \frac{\sigma_i}{\rho_i d_{p,ave}{}^3 / 6} \quad (7)$$

where σ_i (mg m^{-2} yr^{-1}) is the specific pollutant loading for each source, ρ_i is the pollutant (OM or BC) density (52, 53), and $d_{p,ave}$ is the average particle diameter from on-site measurements (~ 1 μm).

Combined with the average surface area per particle, the fractional cover of $PM_{2.5}$ emissions from MSW and dung cake burning in one year, Ω_i, was then calculated as:

$$\Omega_i = \frac{6\sigma_i}{\rho_i d_{p,ave}} \quad (8)$$

2.3 Results and Discussion

2.3.1 Open Municipal Solid Waste and Dung Cake Burning Emissions to Modelled Concentrations throughout Agra and Model Evaluation

Employing the field transect method developed by Nagpure et al. (2), the total average waste burn rate in Agra was estimated at 130 g MSW capita^{-1} day^{-1} with higher per capita burn rates observed in low SES areas (Table 2-1). Burn rates were higher in the morning than the evening within the city, but showed less diurnal difference in the rural areas (areas outside of the city boundaries). If Agra's per capita average waste burn rate is applied to the entire population of India, the annual nationwide burn rate would be 68,000 Gg yr^{-1}, consistent with model findings of Wiedinmyer et al. of 35,000 – 75,000 Gg yr^{-1} for India (54). The total cow dung cake burning emissions on a ward-by-ward basis within Agra were calculated from household fuel use data (31, 32) (Figure A-4) and ranged between 0 – 9,100 kg day^{-1} ward^{-1} within the study domain, compared to 490 – 25,000 kg day^{-1} ward^{-1} from open waste burning (Table A-1). A report on sustainable solid waste management in India reported the average waste generation rate in Agra as 580 g MSW

capita^{-1} day^{-1} (55). Applying this MSW generation rate, the average burn rate of MSW in Agra is 23%, higher than the 5-10% estimates from previous waste burning studies in Indian cities (24, 56, 57).

Applying emission factors from the literature (45, 46) in conjunction with observed burn rates resulted in annual combined emissions in Agra from open waste and dung burning to be 2500 ($\pm$ 2200) kg yr^{-1}and 150 ($\pm$ 58) kg yr^{-1}for the OM and BC components of $PM_{2.5}$, respectively. Annual average $PM_{2.5}$ component concentrations due to open waste and dung cake burning throughout Agra, simulated by AERMOD, found concentrations at the Taj Mahal to be 4.1 ($\pm$ 3.8) and 0.24 ($\pm$ 0.10) μg m^{-3} for OM and BC from MSW burning and 0.32 ($\pm$ 9.1 x 10^{-2}) and 0.019 ($\pm$ 9.7 x 10 $^{-4}$) μg m^{-3} for OM and BC from dung cake burning (Figure 2-1 & Figure A-5). Uncertainty was assessed just for the emission factors, as that is where much of the uncertainty lies due to variations in waste composition and stage of combustion. The calculation does not consider secondary formation of $PM_{2.5}$ due to gaseous emissions from those sources. These results were evaluated using measurements from a recent $PM_{2.5}$ source apportionment study at the Taj Mahal that found that the contribution of biomass burning emissions to OM (which can be from a variety of combustion activities including wood, crop, dung and MSW burning) at the Taj Mahal to be 12 μg m^{-3} (13). While the sum of the four sources assessed here (MSW, dung cake, firewood, and crop residue) is 5.9 ($\pm$ 4.7) μg m^{-3}, suggesting regional transport of additional OM, MSW is the highest contributor of modeled biomass burning sources (Figure A-6).

Table 2-1: Diurnal per capita open waste burn rates (g capita^{-1} day^{-1}) in Agra categorized by socioeconomic status (SES) using a recently developed field transect approach. Higher per capita open waste burn rates were observed in regions of lower SES

	Morning Transect	Evening Transect	Full Day
High SES	73.0	20.9	93.9
Low SES	157	39.3	196
Rural Areas	73.5	106	180

Maximum combined annual-averaged impacts on $PM_{2.5}$ in Agra were 33 ($\pm$ 30) μg m^{-3} from MSW burning and 3.3 ($\pm$ 0.90) μg m^{-3} from dung cake burning (Figure 2-1 & Figure A-7). High levels were found in neighborhoods with lower SES where MSW and dung-cake burning are most prevalent. The contribution from open MSW burning is greater than for dung cake burning throughout Agra, except in the rural areas where dung cake burning is a primary fuel source for cooking (31, 32). The combined annually-averaged ambient $PM_{2.5}$ concentration averaged throughout Agra from open waste and dung cake burning was 4.3 ($\pm$ 3.8) μg m^{-3} for OM and 0.25 ($\pm$ 0.10) μg m^{-3} for BC. Recent ambient OC and elemental carbon (EC) concentration measurements throughout Agra have been reported between 10.2 ($\pm$ 7.2) – 30 ($\pm$ 13) μg m^{-3} and 1.3 ($\pm$ 0.8) – 4.0 ($\pm$ 1.5) μg m^{-3} (48, 58), which suggest the source impact modeling results averaged over the study domain are in line with ambient measurements.

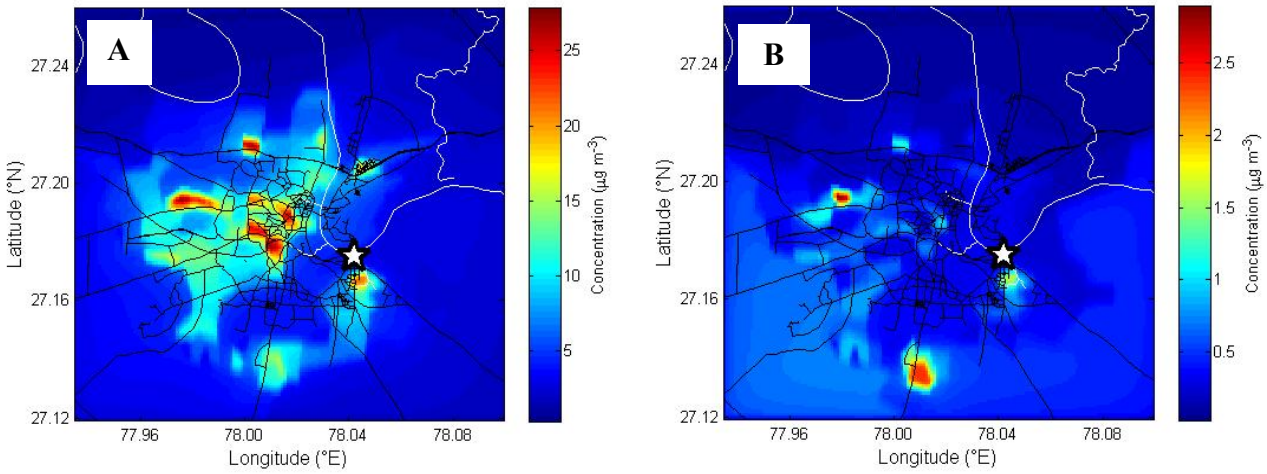

Figure 2-1: Annual average fine particulate matter ($PM_{2.5}$) concentrations in Agra from: a, open MSW burning b, dung cake burning. Modeled [$PM_{2.5}$] at the Taj Mahal (depicted by the white star) was 4.3 ($\pm$ 3.9) µg m^{-3} from MSW emissions and 0.34 ($\pm$ 9.1 x 10^{-2}) µg m^{-3} from dung cake burning emissions.

2.3.2 Adverse Health and Premature Mortality Assessments

Estimation of premature mortality associated with $PM_{2.5}$ ($BC + OM$) emissions from dung cake and MSW burning suggest that these two sources are responsible for 713 (377-1050) cases of premature mortalities from outdoor exposure in Agra annually, 380 (247-540) attributed to IHD, 231 (98-362) attributed to stroke, 94 (31-170) attributed to COPD, and 7 (1-12) attributed to LC for adults (age $\geq$ 25 years). Premature mortality due to ALRI from MSW and cow dung cake burning contributes an additional 1 (0-2) case (age $\leq$ 5 years) annually in Agra. For all-cause mortality (i.e., ALRI, COPD, IHD, stroke and LC) attributable to $PM_{2.5}$ emissions from MSW and cow dung cake burning, the total human YLL is estimated at 10,087 years (5480-14,520) from one year's exposure, where IHD (56%) is the highest contributor followed by stroke (32%), COPD (11%), and LC (1%).

2.3.3 Deposition and Soiling of the Taj Mahal

The deposition of MSW and dung cake burning emissions to the Taj Mahal via dry and wet deposition was quantified using the simulated concentrations, along with observed size distributions and rainfall data. Detailed size distributions measured on-site showed the average surface area median diameter of the carbonaceous particles deposited to outdoor surfaces at the Taj Mahal to be ~ 1 μm (13), which was used in conjunction with deposition velocity relationships to derive a deposition velocity of 0.11 cm sec^{-1} (59). Similar deposition velocities have been measured for particles of similar size and composition in previous studies in urban areas (60-63).

Estimated total annual combined $PM_{2.5}$ dry deposition to the Taj Mahal is 150 ($\pm$ 130) mg m^{-2} from open waste burning and 12 ($\pm$ 3.2) mg m^{-2} from dung cake burning (Table 2-2). The wet deposition loadings were small compared to dry deposition and detailed findings are available in A.3. While the mass loading of organic species, which contains light-absorbing brown carbon (BrC), is nearly eight times more than BC loading, BC is a strong light absorber (13, 64). Emission factor measurements do not consider secondary formation, so this analysis is likely underestimating the total OM deposition from the two sources as both also have gaseous emissions (25, 48).

Additionally, the pollutant coverage of the Taj Mahal's surface was quantified to better gauge discoloration – if the fractional surface area coverage exceeds 1, its perceived color will likely be impacted. MSW burning emissions showed a fractional cover of 0.73 ($\pm$ 0.67) while dung cake burning emissions contributed an additional 5.7 x 10^{-2} ($\pm$ 1.6 x 10^{-2}) annually. Treatment cleanings have occurred four times since 1994. Given the time

between cleanings, the influence of MSW and dung cake burning emissions is likely to exceed a fractional coverage of 1, suggesting their combined deposition will lead to surface discoloration.

Table 2-2: Comparison of the dry total organic matter (OM) and black carbon (BC) deposition (mg m^{-2}) to the surface of the Taj Mahal from open waste and dung cake burning in 2014.

	OM	BC	Total Combined Deposition
MSW	140 ($\pm$ 130)	8.3 ($\pm$ 3.4)	150 ($\pm$ 130)
DC	11.0 ($\pm$ 3.1)	0.66 ($\pm$ 3.4 x 10^{-2})	12 ($\pm$ 3.2)

2.4 Conclusion and Implications

Our model finds that open MSW-burning and dung cake burning led to estimated $PM_{2.5}$ impacts of 4.3 and 0.34 μg m^{-3} (annually averaged) at the Taj Mahal, respectively, and up to 33 and 3.3 μg m^{-3} in Agra, with the highest levels in low SES neighborhoods. The increased OM and BC $PM_{2.5}$ from those sources at the Taj Mahal lead to an increase of 160 mg m^{-2} yr^{-1} of $PM_{2.5}$ deposition to its surface, 150 mg m^{-2} yr^{-1} from open waste burning and 12 mg m^{-2} yr^{-1} from dung cake burning. The amount of $PM_{2.5}$ deposited, along with the optical characteristics of the particles (13, 25, 27) lead to substantial soiling and discoloration of the Taj Mahal, and also reduced visibility, further degrading the aesthetic beauty of the site. A population, concentration-weighted exposure and health assessment finds that chronic exposure to MSW and dung burning related ambient $PM_{2.5}$ was found to increase premature deaths by approximately 713 per year. While more difficult to quantify, acute exposures to the high $PM_{2.5}$ levels can have additional health impacts, e.g., to visitors.

Potential interventions can address the soiling of the Taj Mahal, degraded visibility, and human health in the area. In addition to improving ambient air quality, the recently promulgated ban on dung cake burning can improve indoor air quality, magnifying the estimated health benefits beyond those found based on improving ambient air quality alone. However, the benefits from its proposed implementation will be dependent upon more than 50,000 homes using cleaner sources for cooking (65, 66). Better MSW management and prevention of garbage-burning in Agra were explored previously (67) but were not considered as high impact options to protect the Taj Mahal and public health. This paper indicates that preventing MSW burning can have a higher impact compared to the recently enacted dung cake burning ban on reducing $PM_{2.5}$ concentrations affecting health and $PM_{2.5}$ deposition that soils the Taj Mahal. Policies and action to reduce MSW burning should therefore be considered in the portfolio of actions to preserve the Taj and improve urban public health in Agra, particularly in low SES areas where people are disproportionately exposed to MSW and dung cake burning emissions.

Interventions leading to better waste management have not been a high priority in previous efforts to address air pollution in Indian cities. Agra Municipality has shown the initiative to implement policies designed to reduce soiling of the Taj Mahal, including limiting mobile source emissions near the landmark, banning polluting enterprises nearby, and prohibiting dung cake burning. Our results suggest that implementing a better waste management infrastructure (67) can be a high impact action that can improve ambient air quality in Agra, decrease soiling of the Taj Mahal and reduce adverse health outcomes.

2.5 Acknowledgements

This work was supported by NSF PIRE Grant No. 1243535, NSF SRN Grant No. 1444745, USAID PEER, and instruments were available from grants from the Ministry of Human Recourse Department (3-21/2014-TS.1), Government of India and IIT-K grant for PG Teaching and Research. In addition, Cesunica Ivey at Georgia Institute of Technology contributed to the model development. Fernando Garcia Menendez at Massachusetts Institute of Technology provided ArcGIS files for emission grids. Heidi Vreeland at Duke University assisted with creating figures for publication. Vipul Lalchandani and Shamjad PM assisted with field work and data collection in Kanpur. Gratitude is expressed toward Prakash Bhave of ICIMOD, Robert Yokelson at the University of Montana and Elizabeth Stone at the University of Iowa for providing detailed data for past and in progress studies.

CHAPTER 3. AIR POLLUTION MODELING OF "URBAN CROSS-SECTOR ACTIONS FOR CARBON MITIGATION WITH LOCAL HEALTH CO-BENEFITS IN CHINA"

As published in Nature Climate Change

Abstract

Cities offer unique strategies to reduce fossil fuel use through the exchange of energy and materials across homes, businesses, infrastructure and industries co-located in urban areas. However, the large-scale impact of such strategies has not been quantified. Using new models and data sets representing 637 Chinese cities, we find that such cross-sectoral strategies—enabled by compact urban design and circular economy policies—contribute an additional 15%–36% to national CO_2 mitigation, compared to conventional single-sector strategies. As a co-benefit, ~25,500 to ~57,500 deaths annually are avoided from air pollution reduction. The benefits are highly variable across cities, ranging from <1%–37% for CO_2 emission reduction and <1%–47% for avoided premature deaths. These results, using multi-scale, multi-sector physical systems modelling, identify cities with high carbon and health co-benefit potential and show that urban–industrial symbiosis is a significant carbon mitigation strategy, achievable with a combination of existing and advanced technologies in diverse city types. My direct contribution to this work was the air quality modeling for each Chinese province under the base-case and urban, industrial symbiosis strategy.

3.1 Introduction

Energy supply to support urban homes, businesses, industries, transportation, construction, water and waste infrastructure sectors is associated with >70% of global carbon (CO_2) emissions (12). Further, fossil-fuel-related outdoor/ambient air pollution by fine particulate matter (<2.5 μm: $PM_{2.5}$) contributes to more than 4.7 million premature deaths worldwide (6), a majority occurring in populous urban areas. Therefore, city strategies that reduce fossil fuel use have great potential to achieve both global carbon mitigation and local health protection goals. However, quantifying carbon and health co-benefits potential has been challenging for cities, summarized below.

First, to quantify contributions toward global CO_2 emissions, individual cities are now including both territorial (direct) fuel use as well as transboundary CO_2 emissions embodied in supply chains that support their residential, commercial, and industrial activities through different footprinting perspectives (68). Although CO_2 emissions footprints of several individual cities and a few city-typologies worldwide have been reported (69, 70), quantifying total urban contributions toward national or global CO_2 emissions has been challenging, because we do not yet have energy-use and energy-supply data for all city activity sectors, for all cities in a nation, with attention to local specificity.

Second, the unique opportunities that cities provide for CO_2 mitigation through co-location of residential–commercial and industrial activities have not been fully assessed. Most CO_2 mitigation strategies modeled in global scenario models (71) and in individual cities (72, 73) focus on energy efficiency within single sectors (for example, industry,

power plants, transportation or building energy use). Uniquely urban cross-sectoral actions that advance system-wide energy efficiency by reutilizing 'waste' energy or materials across co-located homes, commercial buildings, industries and the various infrastructure sectors in cities, have not been quantified to date in energy futures models. Examples include advanced fourth-generation district heating/cooling systems (74) that enable use of presently unutilized low-grade industrial waste heat up to 30 km to heat and cool buildings in cities, energy exchanges across co-located industries (75), and strategic material exchanges such as substituting fly ash and steel slag for energy-intensive production of Portland cement used in construction (76). Compact urban design and spatial urban infrastructure planning that supports district energy, along with circular economy policies, are essential for implementing such cross-sectoral symbiosis in cities, highlighting the unique urban nature of these strategies.

Third, CO_2 and $PM_{2.5}$ co-benefits experienced by individual cities due to fuel-use reductions both within and outside the boundary, arising from city actions, are of interest. However, few models are available to address CO_2 and $PM_{2.5}$ co-benefits at the city scale. The emerging co-benefits literature largely focuses on national-scale aggregate co-benefit estimation (77), with a few models evaluating fuel use, CO_2 and air pollution interactions at regional scales (78). Of interest to cities is the distribution of CO_2 and health co-benefits across different cities in a nation.

Specifically in this work, I used AERMOD (79) to simulate $PM_{2.5}$ concentrations in a base-case scenario and under the interventions outlined by the urban-industrial symbiosis pathway (15).

3.2 Methods

To quantify the collective contribution of urban-scale actions toward national CO_2 mitigation, we develop a new and comprehensive Chinese City Industry-Infrastructure (CCII) database that represents energy use in co-located homes, businesses and industries—for all 637 cities in mainland China in the Year 2010. Energy-cascading and material-exchange algorithms are developed in conjunction with the CCII data set to quantify the potential for urban–industrial symbiosis in individual cities utilizing co-location data. This yields a conservative first-order estimate of cross-sectoral urban–industrial symbiosis potential in Chinese cities, beyond reuse levels already occurring in 2010.

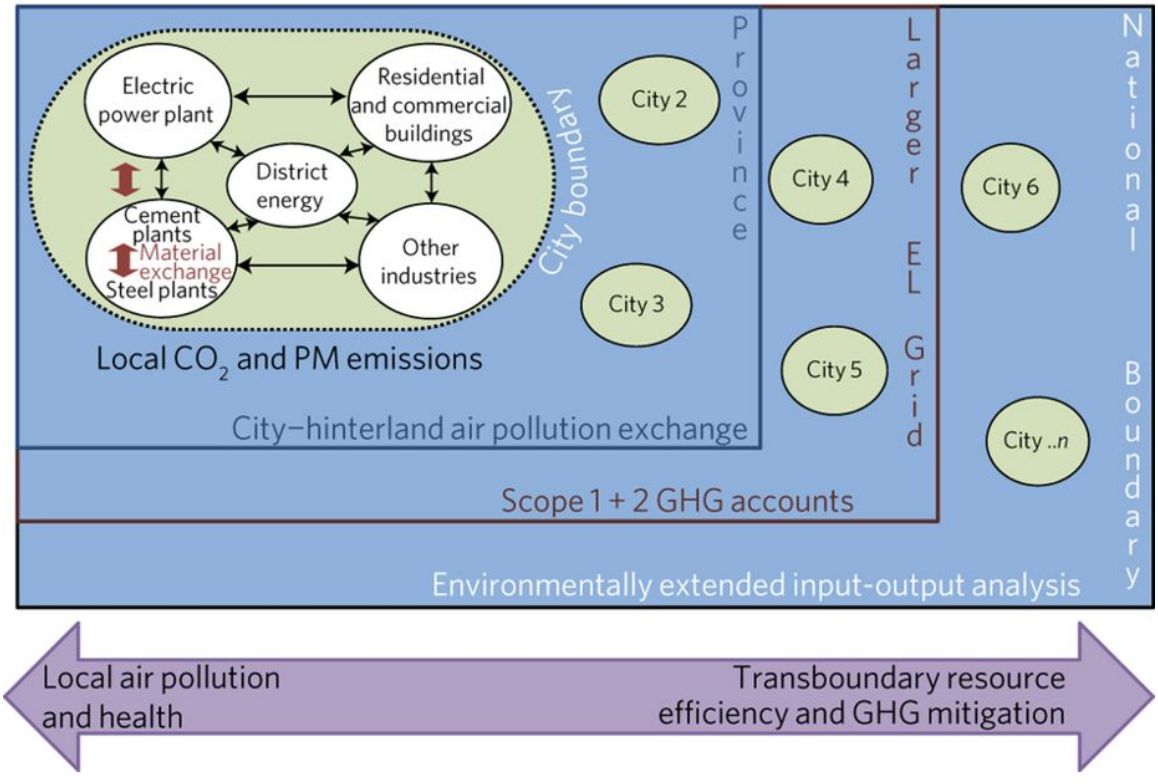

Figure 3-1: Multi-scale modeling of linkages across intra-city, hinterland, provincial, grid region and national scales to assess local health and national CO_2 benefits of urban-industrial symbiosis.

Because cross-sectoral symbiosis potential decreases when individual sectors become more efficient, urban cross-sectoral symbiosis scenario strategies are modelled after applying conventional single-sector efficiency actions nationwide in buildings, power plants, cement, steel, and other sectors, assuming near-term efficiency targets specified in China's Five-Year Plan (FYP 2010–2015) are achieved. This is referred to as the FYP-Efficiency-plus-Symbiosis scenario (Table 3-1).

Table 3-1: Strategies and technological pathways and assumptions identified in the Five Year Plan- Efficiency-plus-Symbiosis scenario

Strategies	Technology pathways and assumptions
High-grade waste heat (>400 °C) to electricity (generates 14.6 TWh)	Commercially available Organic Rankine Cycle (ORC) to convert high-grade waste heat to electricity at 15% efficiency to displace grid electricity production
Medium-grade waste heat (100–400 °C) to other industries and district energy system	**Cascade 1*:** Heat is first applied to food/beverage and other low temperature industries **Cascade 2:** Remaining heat is reused in current district heating system to displace heating fuel use **Cascade 3*:** Heat displaces electricity via ORC
Low-grade waste heat (<100 °C) to new district energy systems	Heat is applied in new 4th generation district heating systems circulating low temperature hot water (30–70 °C) to energy efficient buildings only in the urban core of cities
Material exchange—fly ash from power sector to cement	Fly ash reuse beyond current provincial reutilization rates (50–90%) to achieve 35% saturation of fly ash by mass in cement
Material exchange—steel slag to cement	Steel slag from dry slag granulation reutilized to displace cement up to 25% by mass plus waste heat to electricity
Unutilized low-grade waste heat	Can displace heating fuels in future 4th generation district heating systems. Range indicates fuel displaced: coal (high

	CO_2 savings) or natural gas (lower CO_2 savings)

Transboundary air pollution modelling tracks air pollution dynamics between cities and their surrounding hinterland areas; both of which are impacted (although not equally) by system-wide fossil fuel reductions from single- and cross-sector urban actions. Transboundary pollution modelling is important because even if cities reduce fuel combustion and corresponding $PM_{2.5}$ emissions within their boundaries, their local airborne $PM_{2.5}$ concentration can be affected by wind-blown transport of $PM_{2.5}$ from surrounding polluted areas into cities, and vice versa. Here, $PM_{2.5}$ was modeled using AERMOD (79). Each Chinese province was modeled independently of one another and emission grids were defined from local Shiqu and Xianji Shi boundaries (Figure B-1). Health benefits, that is, premature deaths avoided due to reduction in $PM_{2.5}$ concentration in each individual city, are computed by applying concentration-response functions (80) to the age-distributed population of that city.

3.3 Results and Discussion

The bottom-up CCII data set effectively represents co-location of energy use in multiple sectors along with energy generation systems in 637 diverse Chinese cities, consistent with China's national energy balance statistics (81). Direct territorial CO_2 emissions (Scope 1) from the 637 cities add up to 62% of China's total CO_2.

CO_2 Mitigation potential in the What-If FYP-Efficiency-plus-Symbiosis scenario is shown in Figure 3-2. China's 2010 five-year plan (FYP) single-sector efficiency targets, applied across all industries and aggregated nationally, assuming they are fully met, yield ~9.0% (754 million tonnes (Mt)) CO_2 mitigated compared to the 2010

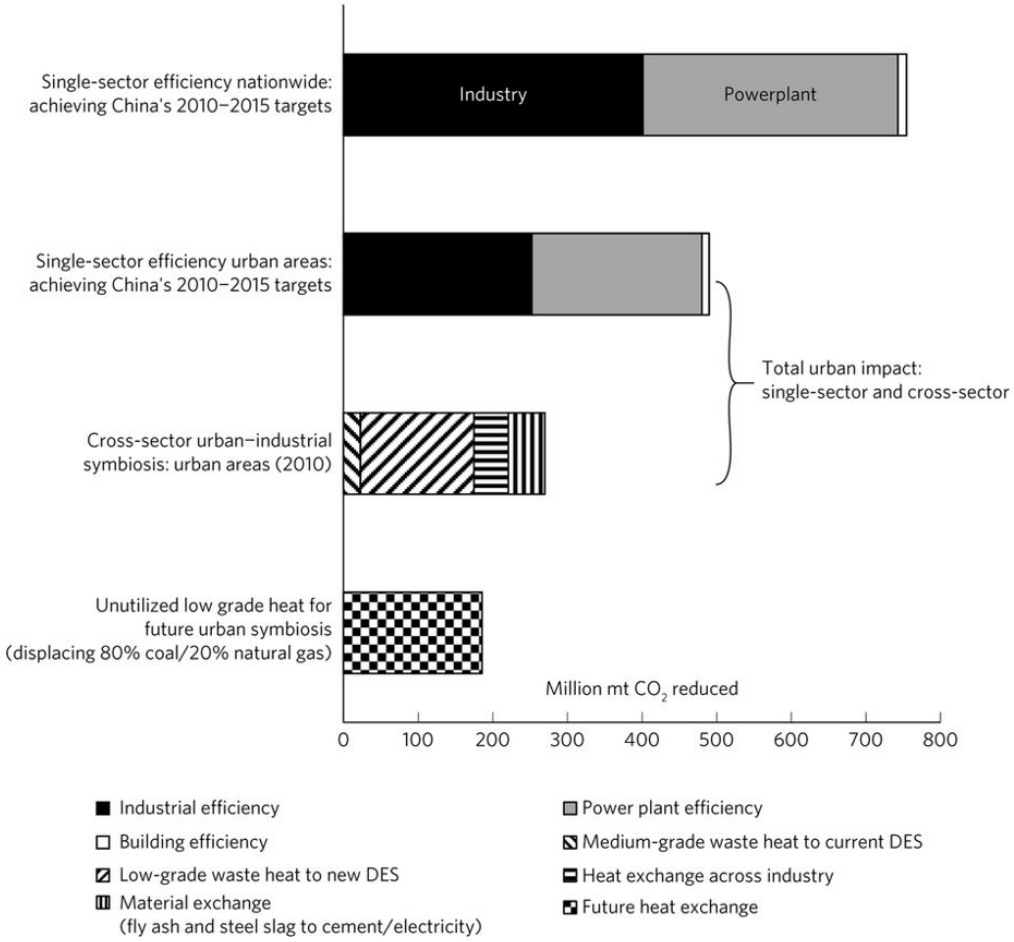

Figure 3-2: National territorial CO_2 mitigation in China under Year 2010 What-If FYP-Efficiency-plus-Symbiosis scenario compared to base-case 2010 emissions (8,800 million metric tons)

baseline, of which 65% (490 Mt) occurs geographically within cities. Urban cross-sectoral symbiosis interventions evaluated in this paper (Table 3-1) contributed an additional 3.1% (270 Mt) reduction of national CO_2 emissions (Figure 3-2: National

territorial CO2 mitigation in China under Year 2010 What-If FYP-Efficiency-plus-Symbiosis scenario compared to base-case 2010 emissions (8,800 million metric tons)Figure 3-2).

Total base-case annual average $PM_{2.5}$ emissions from all sectors (excluding agriculture) normalized per unit geographic area ranged from <1 to 30.6 g m^{-2} yr^{-1} across cities and are in the range reported by others (1) (Figure B-2). The modelled airborne $PM_{2.5}$ concentrations (μg m^{-3}) in the Year 2010 Base-Case were within the range of those measured in Chinese cities (82), illustrating the model results are reasonable. Application of the What-If FYP-Efficiency-plus-Symbiosis scenario showed $PM_{2.5}$ reductions between <1 to 49% aggregated across cities (Figure 3-3). Aggregated across urban China, the health benefits—that is, the overall reduction in premature deaths per year in the What-If FYP-

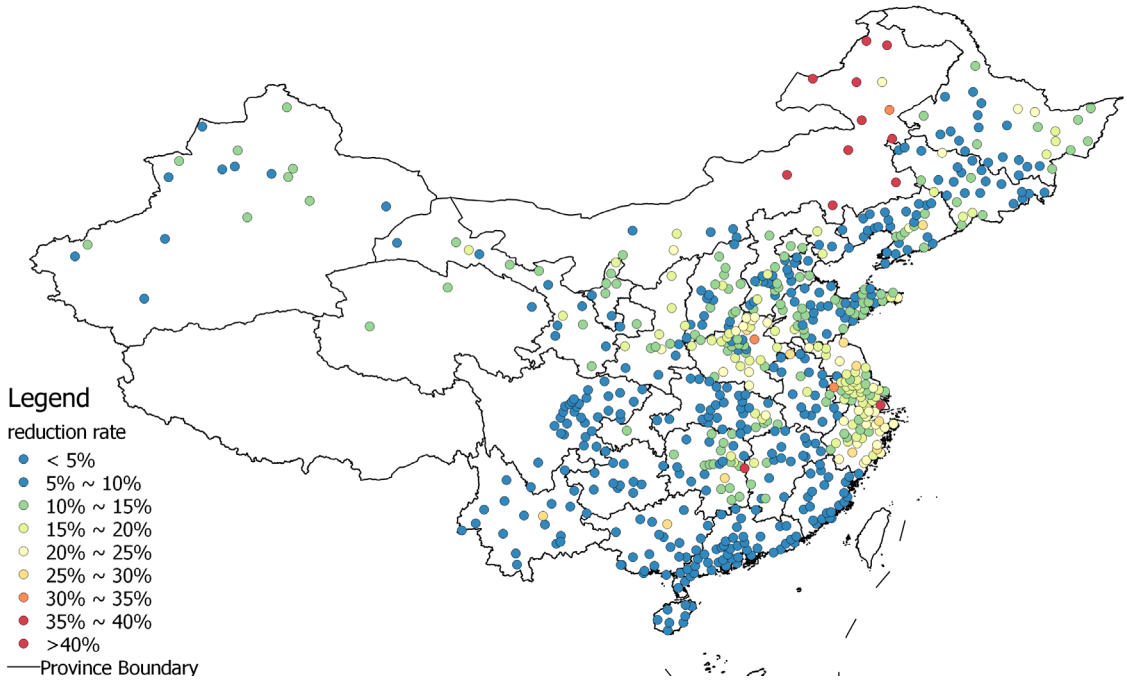

Figure 3-3: Percentage reduction in city $PM_{2.5}$ concentrations under the five-year-plan-efficiency-plus-symbiosis scenario

Efficiency-plus-Symbiosis scenario compared to the Base-Case—are 47,230 (+10,240/−21,874) deaths per year. This estimate is probably conservative as we do not consider secondary $PM_{2.5}$ formation from gaseous SO_2 and NO_x emissions from industries that would be similarly reduced by the efficiency and cross-sector (material and energy) symbiosis strategies assessed in the scenario versus Base-Case. Reductions in $PM_{2.5}$ concentrations in air (and hence avoided premature mortality) are less correlated with reductions in $PM_{2.5}$ emission intensities ($R^2 = 0.65$), because of transboundary air pollution dynamics with the rest of province.

3.4 Conclusion

With China contributing ~27% of global anthropogenic CO_2 emissions, Chinese cities can be significant players in national (and hence global) CO_2 mitigation efforts. Further, Chinese cities are experiencing high levels of air pollution, with annual average ambient airborne $PM_{2.5}$ concentrations (82) exceeding international guidelines, contributing to more than 4,000 pollution-related daily deaths in China. China's commitments to the Paris Accord, along with clean air commitments, provide impetus for identifying urban strategies that simultaneously yield large carbon reductions and provide local health co-benefits.

Urban–industrial symbiosis potential is likely to be substantial in industrial nations such as China, where 70% of national total fossil fuel use occurs in industry and power sectors that generate waste heat, compared to only 20% in the commercial–residential sectors that could reuse such waste heat, maximizing exchange potential. For example, low-grade heat that dominates industrial waste heat output has few

applications within industry, but can effectively be used for space heating in advanced district energy systems recently implemented in the EU (74). Thus, technology innovation and widespread implementation of urban–industrial symbiosis in China can contribute significantly to national decarbonization, while reducing fuel-related $PM_{2.5}$ emissions.

Uniquely urban cross-sectoral strategies that cities offer today for decarbonization, as well as local health co-benefits, have not been integrated in international assessments because their analysis requires co-location information, urban–industrial symbiosis algorithms, and multi-scale carbon, air pollution, and health risk models. In this assessment we were able to address these concerns while specifically targeting $PM_{2.5}$ impacts from novel, urban-industrial symbiosis strategies. Simulations showed reductions in $PM_{2.5}$ concentrations ranging between <1-49% in cities from the urban-industrial efficiency scenario, highlighting the potential air quality benefits of this novel mitigation strategy.

CHAPTER 4. CONNECTING AIR QUALITY WITH EMOTIONAL WELL-BEING AND INFRASTRUCTURE IN A U.S. CITY

As submitted to *Environmental Health Insights*

Abstract

Cities in the United States have announced initiatives to become more sustainable, healthy, resilient, livable, and environmentally friendly. However, indicators for measuring all outcomes related to these targets and the synergies between them have not been well defined or studied. One such relationship is the linkage between air quality with emotional well-being (EWB) and neighborhood infrastructure. Here, regulatory monitoring, low-cost sensors (LCSs), and air quality modeling were combined to assess exposures to $PM_{2.5}$ and traffic-related NO_x in six Minneapolis neighborhoods of varying infrastructure parameters (median household income, urban vs. suburban, and access to light rail). Residents of the study neighborhoods concurrently took real-time EWB assessments using a smart phone application, Daynamica, to gauge happiness, tiredness, stress, sadness, and pain. Both LCS $PM_{2.5}$ observations and mobile-source simulated NO_x were calibrated using regulatory observations in Minneapolis. No statistically significant (α=0.05) $PM_{2.5}$ differences were found between urban poor and urban middle-income neighborhoods, but average mobile-source NO_x was statistically significantly (α=0.05) higher in the four urban neighborhoods than in the two suburban neighborhoods. Close proximity to light rail had no observable impact on average observed $PM_{2.5}$ or simulated mobile-source NO_x. Home-based exposure assessments found that $PM_{2.5}$ was negatively correlated with positive emotions such as happiness and to net affect (the sum of positive and negative emotion scores), and

positively correlated (i.e., a higher $PM_{2.5}$ concentration led to higher scores) for negative emotions such as tiredness, stress, sadness, and pain. Simulated mobile-source NO_x, assessed from both home-based exposures and in-situ exposures, had a near-zero relationship with all EWB indicators. This was attributed to low NO_x levels throughout the study neighborhoods and at locations were the EWB-assessed activities took place, both owing to low on-road mobile-source NO_x emissions. Although none of the air quality and EWB responses were determined to be statistically significant (α=0.05), due in part to the relatively small sample size, the results are suggestive of linkages between air quality and a variety of EWB outcomes.

4.1 Introduction

Cities in the United States have announced initiatives to become more sustainable, healthy, resilient, livable, and environmentally friendly (12, 83). However, assessing these outcomes has been challenging, as metrics to define the outcomes and their interrelationships are limited (84-86). This is due, in part, to the fine scale data needed to study these factors and interactions. Studying these fine scales is challenging because of personnel limitations, data and instrumentation barriers, and high costs (86). Nonetheless, cities are evolving, and it is helpful to understand these relationships to achieve desired goals.

A potentially important set of relationships involves local air quality, neighborhood-scale infrastructure, and subjective well-being (SWB). Air quality, typically characterized by air pollutant concentrations, has both chronic and acute health responses (5, 6, 87, 88). Neighborhood infrastructure is related to the services, accessibilities, and social capital provided at the neighborhood level (89), and can impact both air quality and well-being (90, 91). SWB is defined as an individual's cognitive and affective evaluation of his/her life (92, 93). Cognitive well-being relates to what an individual *thinks* about his/her life and is often associated with long-term well-being while affective SWB, or emotional well-being (EWB), refers to what an individual *feels* about his/her life. Emotional well-being is more sensitive to short-term environment changes (94); hence, this study considered EWB. Typical studies of EWB track a range of positive and negative emotions such as happiness, anger, aggression, pleasure, fatigue, stress, sadness, etc. (95, 96).

EWB has often been associated with health as the two influence each other; better health often leads to higher EWB and vice versa (97). High EWB involves frequent pleasant emotions, infrequent unpleasant emotion, the net of which is one measure of EWB called net affect; high well-being also includes cognitive aspects, i.e., high levels of life satisfaction/evaluation. Poor health, separation (encompassing widowhood, divorce, or separation), unemployment, and lack of social contact are factors of strong, negative associations to EWB (98). Intra-personal personality traits can also influence subjective self-assessments of well-being. In addition, neighborhood level infrastructure has also been shown to impact health and EWB (99-101). Access to convenient and affordable transportation enables participation in activities that can improve life, including gainful employment, improved education, and social interactions (102, 103). Exposure to poor air quality, particularly $PM_{2.5}$, has been found to be one of the largest factors leading to disease burden globally, as it has both chronic and acute adverse health outcomes (5, 6, 87, 88). In addition, $PM_{2.5}$ affects visibility, which is an additional socioeconomic burden that influences EWB (104).

Traditionally, air pollution has been measured using expensive, bulky, and sparsely located monitors (105). New techniques to generate fine scale measurements have been developed and studied in recent years, including the use of low-cost sensing technologies (106). Low-cost sensors (LCSs) have advantages as they are cheaper and smaller, providing widespread spatial coverage that has not been viable in the past, and are easier to transport and operate than regulatory or research-grade instruments. However, evaluation of their performance is inconsistent (16, 106-109). City-scale modeling of air pollutants is often done using dispersion models, but the modeled concentrations do not

always agree with observations, due in part to emission uncertainties, omission of complex atmospheric chemistry, and no default depositional loss mechanisms in the model. Much of the local gradients of pollution concentrations, particularly NO_x (a combustion byproduct), is driven by mobile sources in cities (110), so fine-scale dispersion simulations from on-road mobile sources can provide additional understanding of neighborhood air pollution levels and their impacts on EWB.

Historically, EWB was measured using retrospective self-reports, in which participants would reflect on certain past events and attempt to recall their feelings. The results from these studies were accordingly limited due to recall bias. Following self-reporting, the next advancement in measuring EWB was with experience sampling methods (ESMs). ESMs involve repeated sampling of subjects' behaviors in real time in natural environments (111). ESMs assess specific events in subjects' lives or assess subjects at periodic intervals by random time sampling (112). While ESMs allow for advancements of studying EWB, they do not offer continuous measurements of it.

The day reconstruction method (DRM) asks the respondent to reconstruct the entire sequence of daily activities and emotional experiences during each activity, which offers a more comprehensive measurement of EWB than ESMs and captures more completely the time-variant nature of EWB (113). Recent mobile technology advancements, including smartphone applications, allow for opportunities to collect EWB data near real-time (survey subjects often fill the responses throughout the day and not necessarily following each event, so their real-time EWB emotions may not be fully captured) using the DRM approach (114, 115). Smartphone-enabled DRM approaches allow for comprehensive data acquisition throughout the day as opposed to single snapshots. Using smart phones for the

surveys provides additional benefits including: (1) accurate location identification using the Global Positioning System (GPS) (116), (2) additional characterization of activity attributes using smartphone built-in sensors for user inputs (e.g., transportation mode, companionship/event partnerships, etc.), and (3) for information on the temporal sequence of activities and experiences (117-120).

Recent studies have addressed environmental justice and air pollution exposure based on socioeconomic status (SES) and have generally found that poor and racial minority communities are disproportionately affected with lower air quality (121-124). However, no studies to our knowledge have explicitly addressed the relationship between air quality with EWB and neighborhood-level infrastructure. This first-of-its-kind study explored the relationship between air quality (measured using LCS sensors and simulated with a mobile-source dispersion model) with EWB (assessed using a novel phone application) and neighborhood infrastructure (assessed from census-level data) in Minneapolis, MN using a combination of low-cost sensors, air quality modeling, and dynamic well-being sampling using a phone-based application.

4.2 Methods

This study examined the relationship between ambient air quality with neighborhood infrastructure and individual's emotional well-being (EWB) using concurrent air quality measurements, mobile source modeling of a traffic-related air pollutant (TRAP), and individual's EWB assessments in six neighborhoods of varying infrastructure parameters in Minneapolis, MN.

4.1.1 Neighborhood Selection

The study's six Minneapolis neighborhoods included Phillips, Near North, Brooklyn Center, St. Anthony Park, Blaine, and Prospect Park (Table 4-1 and Figure C-1). Infrastructure quality was assumed to be correlated with median household income (with income class breaks designated from literature on income and health-based disparities (125)), access to light rail (access defined as the neighborhood either containing a light rail station or one block away from at least two light rail stations), and urban or suburban (inside the city boundaries of Minneapolis and St. Paul considered urban and outside considered suburban) (Table 4-1 and Figure C-1). Because the intensity of the data collected limits the size of the panel to be studied, only six neighborhoods were used in this study; however, these six neighborhoods still allowed for studying combinations of the infrastructure criteria. The study period was from October 2016 to April 2017.

4.1.2 Air pollution measurements and modelling

This study focuses on $PM_{2.5}$ and NO_2 air quality as these pollutants show more heterogeneity than a secondary pollutant like ozone and both are found to contribute significantly to the overall health burden (6, 9, 126). There are nine regulatory $PM_{2.5}$ monitors in the study domain and four are defined to capture pollutant concentrations representative of neighborhoods (127) (Table C-1). However, the neighborhoods housed by three of these four monitors did not meet our other neighborhood criteria, so to measure suitable neighborhood $PM_{2.5}$ levels we use low-cost air quality sensors that were deployed and evaluated during a number of previous studies (4, 128-130). In this study, the monitors were deployed in the backyards of residents' homes. The selection criteria for the homes

included no close-proximity (within 10s of meters) sources, (e.g., fire pit, back alleyways for cars/parking, lawn mowing; the study was conducted from October to April, limiting

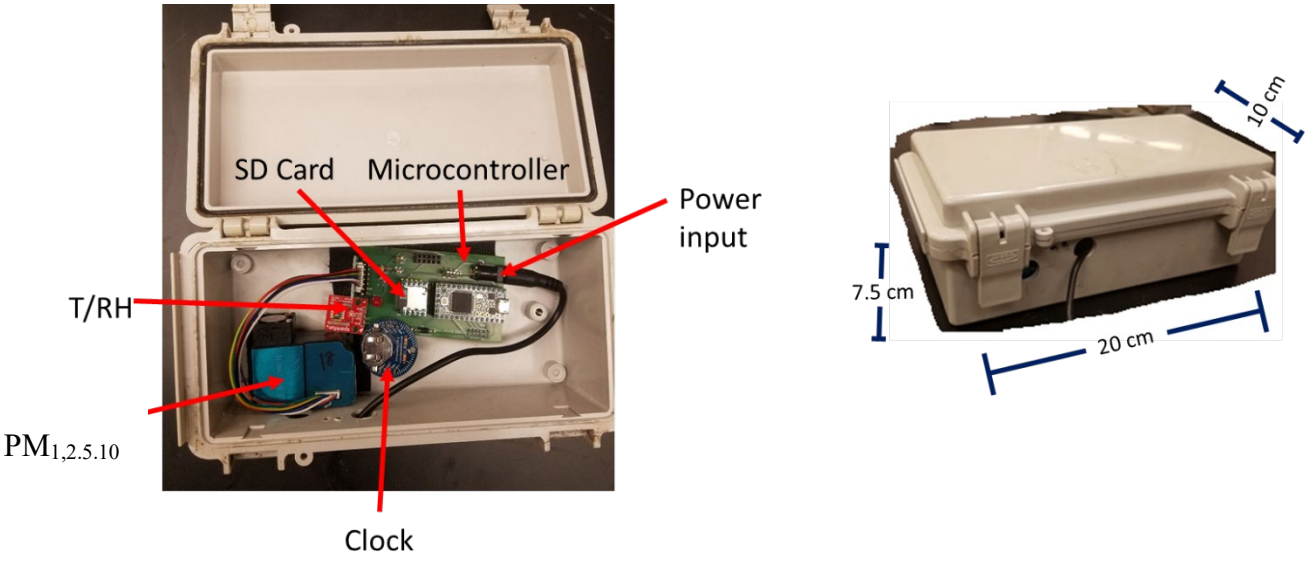

Figure 4-1: Air quality and meteorological sensing system.

lawn mowing and similar activities), no nearby construction (also limited by the choice of study period), and being at least one house away from a street intersection. The monitors were zip-tied to fences or posts approximately at the inhalation height, ~1.5m off the ground (Figure C-3). The LCS measured $PM_1/PM_{2.5}/PM_{10}$ using a Plantower PMS3003 with no upstream drier (Figure C-3 for schematic) and relative humidity and temperature with a Sensiron SHT 15.

The sensors were calibrated using a co-location approach with an EPA Near-Road (monitoring) Network (NRN) site in Minneapolis (Minneapolis – Near Road I-35/I-94). The LCS were co-located with a dry $PM_{2.5}$ measurement (Beta Attenuation Monitor, BAM) at the NRN site. Initial $PM_{2.5}$ calibration (using the manufacturer reported $PM_{2.5}$ output)

results showed a piecewise continuous response that split at ~10 μg m^{-3}, which has been observed in other studies (3). An RH correction to the sensor $PM_{2.5}$ data (level 2A correction (131)) was employed (4), which provided an estimate of dry $PM_{2.5}$. Calibrations lasted two days and were conducted every two weeks during the study period to account for any drifts that occur. A linear fit was then used to calibrate the LCS with the reference site measurements. The sensor calibration data were then applied to the neighborhood sampling data by time-weighted averaging. The sampling frequency used in these samples was minute data; however, to be consistent with the NRN monitor data, levels were averaged hourly. A recent evaluation of the Plantower PMS3003 with a BAM in a US city showed the BAM to have a high noise-to-signal ratio at low concentrations (4), similar to levels that would be observed in Minneapolis; future work with the Plantower sensors may consider longer averaging times during the calibrations to smooth out the noise. Uncertainty was assessed from the slope and intercept uncertainty from the co-location calibration. Uncertainties were propagated through the sampling period for each hour's pollutant measurement.

While LCS can provide additional monitoring, they still do not provide comprehensive spatial coverage, so R-Line (132) was used to simulate mobile source NO_x impacts for the same hours that the EWB assessments were conducted. Modeling of mobile-source impacts on $PM_{2.5}$ was not used because $PM_{2.5}$ impacts from mobile sources are understood to be low (133, 134), leading to issues with relying on R-Line results. Mobile sources contribute to 18% of primary $PM_{2.5}$ emissions in Minneapolis (https://www.pca.state.mn.us/air/statewide-and-county-air-emissions). While NO_x was the

only traffic-related air pollutant (TRAP) modeled here, those levels would be indicative of exposure to other TRAP emissions, as well.

R-Line uses a similar approach to AERMOD, the EPA recommended regulatory dispersion model. R-Line is formulated specifically to address line (vs. point or area) sources. In addition, R-Line has updated plume spread (σ_y and σ_z) parametrizations, specific for near-surface dispersion (132, 135). National land cover data from the multi-resolution land characteristic consortium (MRLC) were used in AERSURFACE to generate monthly surface properties in Minneapolis to estimate the Bowen ratio, surface roughness length, and albedo. This, in combination with surface data from the Minneapolis airport and upper air data from nearby Chanhassen, MN (WMO# 72649) was then processed in AERMET to generate meteorological fields, including hourly boundary layer heights.

Mobile source emission estimates were generated using annual average daily traffic (AADT) counts from the Minnesota Department of Transportation (MNDOT; http://www.dot.state.mn.us/traffic/data/data-products.html) in combination with representative emission factors used in the EPA National Emission Inventory (NEI). The AADT counts for each road link were from 2017 counts or from the most recent estimates on each road if 2017 data did not exist. Fleet composition data were available for 1,040 links in Minneapolis. A weighted average by vehicle type and vehicle count was then used to estimate the fleet composition for the remaining road links used in the simulations (N~34,459). Diurnal and day-of-the-week trends measured in Minneapolis, MN. (136) were used alongside the AADT data to develop hourly vehicle counts for each link. Emission factors used to convert activity data to emissions were from the NEI and were a

function of vehicle type, season (gasoline formulation), temperature, and relative humidity. A 380 m (E-W) x 500 m (N-S) resolution receptor network spanning 46 km (E-W) x 60 km (N-S) was used in R-Line.

The R-Line simulations gave hourly mobile source impact estimates for NO_x, and concentrations were determined for each of the study neighborhoods. R-Line modeling has been found to lead to unrealistically high simulated pollutant values, which may be attributed to the model itself, i.e., due to no default loss mechanisms or an over estimation of modeled emissions (137, 138), both of which led to approaches to calibrate simulated values (139). Here, 24 correction factors were generated, one for each hour of the day. The correction was developed from linear fits between the R-Line simulation results for each hour of the day and an estimate of the true mobile source impact from observations, (i.e., the difference between the I-35/I-94 NRN monitoring site [AQS Site ID# 27-053-0962] and a background, regulatory EPA site observation [AQS Site IDs# 27-003-1002]). The correction approach resulted in the reduction of the model's initial, high-simulated concentrations (see Appendix C.1 for more details on the correction methodology).

4.1.3 Emotional well-being (EWB) assessments

EWB assessments were recorded using Daynamica™ (114), a smart phone application available on Android phones (Figure C-4). Neighborhood residents took entry and egress surveys for demographic and personal characteristics. Survey respondents were not informed of the ongoing air pollution study. Residents of the six homes in which the LCSs were housed did not participate in the EWB assessments. Daynamica™ scaled EWB on a scale from 1 (not at all) to 7 (strongly), and five emotions were assessed: happiness,

sadness, stress, pain, and tiredness (114). The net affect, defined as the positive category (happiness) less the average of the four negative ones (sadness, stress, pain, and tiredness), was also assessed. This was the same approach that has been used in other studies to determine the U-index, an oft-applied misery index (i.e., a measure of time that people spend in an unpleasant state) (140).

The application tracked the users' movements for a period of seven consecutive days. Next, users would subsequently identify the activity completed and when it occurred and then respond to a series of EWB questions. There were 371 users, and 26,313 responses were gained from all users (see Appendix C.2 for more details on the respondent selection criteria and respondent demographic and SES background). More detailed assessment of the EWB results can be found in Fan et al. (141). Oftentimes, the event to which the EWB recording was associated lasted over multiple hours. The midpoint of the start time and end time was used as the hour of the EWB recording for analysis. Because multiple responses existed in a given hour from a single person or from a person in the same neighborhood, the EWB assessment results in the same hour were averaged.

4.1.4 Linking air quality, infrastructure, and emotional well-being (EWB)

We analyzed the relationships between the EWB assessments with the neighborhood $PM_{2.5}$ measurements (home-based LCS exposure), the R-Line NO_x model results evaluated at the same location where the $PM_{2.5}$ measurements existed (home-based R-Line exposure), and the R-Line NO_x model results at the location of the EWB respondent's activity (in-situ R-Line exposure). Only the hours that included both a EWB neighborhood response and LCS $PM_{2.5}$ measurement or R-Line NO_x result were used in

the analysis. There were 2,806, 4,732, and 5,126 hourly EWB responses used in the comparison with the $PM_{2.5}$ observations, home-based mobile-source NO_x simulations, and in-situ mobile-source NO_x simulations, respectively (see Table C-2 for neighborhood breakdown). Neighborhood averages for hours when the $PM_{2.5}$ observation / NO_x simulation and EWB response all existed were determined. The uncertainty for the R-Line simulations was not estimated (which was consistent with other R-Line studies (133, 139)). The average EWB was reported with one standard deviation of all measurements. Tests for statistical significance (Appendix C.3) on the regressions comparing LCS $PM_{2.5}$, R-Line home-based NO_x exposures, and R-Line in-situ NO_x exposures with EWB were performed.

The extent to which high-pollution events, including a two-day lag period, affected EWB was also explored. We include the two-day lag period as it is a lag time that is used in epidemiology studies involving air pollution exposure impacts with health outcomes (142). Here, high-pollution events were considered as the top 10% of $PM_{2.5}$ observations or NO_x simulations for each of the neighborhoods, independently, or the top 10% of overall in-situ NO_x concentrations where a EWB response existed. We also wanted to explore the EWB outcomes of National Ambient Air Quality Standard (NAAQS) exceedance events, but there were no exceedances of the 24-hour average $PM_{2.5}$ standard during the study period. There were four simulated hours that exceeded the 100 ppb NAAQS hourly NO_2 standard, but considering the inherent uncertainty of the simulations, the findings are not included in the main text (see Appendix C.4).

4.2 Results

4.2.1 Low-cost sensor (LCS) $PM_{2.5}$ performance and findings

The RH-corrected LCS $PM_{2.5}$ observations resulted in a linear relationship between the LCS data and regulatory instrument (BAM) at the NRN site, and Pearson correlation coefficients were consistently between 0.8 and 0.9 (see Figure C-5 for a sample co-location calibration result and Table C-3 for calibration fits for the entire study period). Elevated $PM_{2.5}$ levels were observed at the beginning of the study period in October/November and toward the end of the study period in April. Minnesota Pollution Control Agency (MPCA) sites within the study domain showed similarly elevated levels during the same hours (Figure C-5). High concentrations are typically driven by meteorology (e.g., low inversion heights, low wind speeds) though they also reflect increased emission events (e.g., rush-hour traffic and residential wood burning, a common approach to home heating throughout Minneapolis (143)). The calibrated LCS observations were compared against the reference measurements for the entire study domain, and agreement was found between the neighborhood levels and the reference sites (R^2 ~ 0.30-0.61; Figure C-6 and Figure C-7 and Table C-4).

The LCS measurements showed similar average $PM_{2.5}$ concentrations in five of the six neighborhoods, with Blaine (the middle-income, suburban neighborhood) being statistically significantly (α=0.05) cleaner than each of the other five neighborhoods. Here, concentrations were compared only when observational data existed for all six neighborhoods. The highest observed average $PM_{2.5}$ concentration was in Prospect Park (the middle-income, urban with access to light rail neighborhood), but there was no statistical difference between the mean $PM_{2.5}$ in Prospect Park and each of the other neighborhoods except Blaine (Table 4-1). Although Brooklyn Center is a suburban neighborhood, it showed similar measured levels as the urban neighborhoods. Brooklyn

Center is just outside the Minneapolis city boundary (Figure C-1) and would thus be subject to similar urban emissions. The neighborhood $PM_{2.5}$ observations followed similar time series (Figure C-6), which further supports that much of the particulate pollution in the area was from regional sources and/or driven by meteorological factors. The results suggest that there were no noticeable rail access impacts on $PM_{2.5}$ levels. It is understood that current-day $PM_{2.5}$ emissions from mobile-sources are generally low; the displacement of vehicles from riders choosing light-rail over personal vehicles will not affect local $PM_{2.5}$ levels. In addition, public transportation only accounts for 13% of Minneapolis' commute modeshare (144), of which 68% is by bus commute and 29% by the light rail (145). The light-rail system does not displace a large fraction of personal use vehicles.

Table 4-1: Neighborhoods used in this study, including neighborhood infrastructure characteristics, study-average observed $PM_{2.5}$ concentrations (95% confidence interval) from low-cost sensors (LCS) and R-Line simulated mobile-source NO_x concentrations (95% confidence interval). The $PM_{2.5}$ concentrations were only considered for hours where observations existed in all six neighborhoods. See Figure C-1 for a detailed spatial map of the study neighborhoods and Table C-5 for entire sampling average concentrations.

Neighborhood	Urban status	Low-income status	Rail access	Distance to central city (mi.)	Population density (people/acre)	Median household income ($/HH)	Low-cost sensor $PM_{2.5}$ ($\mu g\ m^{-3}$)	R-Line NO_x (ppb)
Prospect Park	X		X	3.5	6.0	75,800	7.8 (7.5-8.2)	8.2 (7.8-8.6)
St. Anthony Park	X			4.4	5.2	79,800	7.5 (7.2-7.7)	8.0 (7.7-8.4)
Phillips	X	X	x	1.8	20.8	32,200	7.5 (7.2-7.9)	8.2 (7.8-8.6)
Brooklyn Center		X		7.4	6.1	56,300	7.6 (7.2-7.9)	6.4 (6.1-6.7)
Near North	X	X		2.5	12.5	36,200	7.5 (7.1-7.8)	7.4 (7.1-7.7)
Blaine				15.3	5.1	90,400	6.4 (6.2-6.7)	3.8 (3.6-4.0)

4.2.2 R-Line mobile source NO_x modeling calibration and performance

The re-scaling of mobile source NO_x contributions resulted in improved agreement between the simulated mobile-source impact and the true mobile-source impact evaluated at the NRN site (Appendix C.1). As expected, the modeled on-road mobile source impacts closely followed the major roadways in Minneapolis (Figure 4-2). A large NO_x concentration difference was not found between urban neighborhoods with access to light rail (Phillips and Prospect Park) and neighborhoods without such access (Near North and St. Anthony Park). Access to light rail was expected to reduce mobile-source NO_x impacts considering the proximity of alternative-fuel transportation modes, i.e., electric light rail. However, this can be offset by increased traffic arriving at the light-rail stations or because these four study neighborhoods were centrally located and thus, subject to high vehicle counts along common routes. Phillips, Prospect Park, St. Anthony Park, and Near North

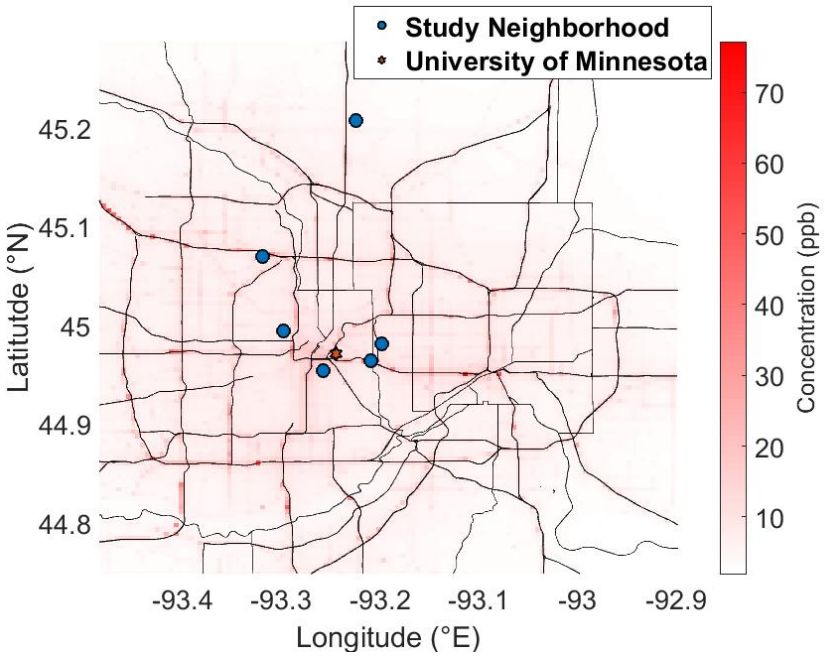

Figure 4-2: Average mobile-source NO_x impacts simulated using R-Line for Minneapolis, MN. from October 2016 to April 2017. The blue dots indicate locations of neighborhoods where concurrent air quality measurements and emotional well-being (EWB) assessments were performed. The red star is the location of the University of Minnesota.

(the urban neighborhoods) had the highest average simulated NO_x impacts with higher simulated NO_x concentrations than the two suburban neighborhoods (Brooklyn Center and Blaine). This is due to the higher vehicle counts in the urban areas.

4.2.3 Linking low-cost sensor (LCS) $PM_{2.5}$ and emotional well-being (EWB)

The findings in Minneapolis for the low-cost sensor (LCS) $PM_{2.5}$ was negatively correlated (i.e., a higher $PM_{2.5}$ concentration led to a lower EWB score) with happiness and positively correlated (i.e., a higher $PM_{2.5}$ concentration led to a lower EWB score) with all of the negative emotions, including tiredness, stress, sadness, and pain (Figure 4-3). A negative correlation was also found for the net affect (sum of the five EWB indicators) assessment. None of the relationships were found to be statistically significant (α=0.05), which may in part be explained because amongst most of the neighborhoods, the difference between $PM_{2.5}$ concentrations was not significantly (α=0.05) different (Table 4-1). In addition, this assessment was conducted using home-based $PM_{2.5}$ exposures, which had limitations, as the respondents' $PM_{2.5}$ exposure pathways are not fully captured throughout the day.

4.2.4 Linking R-Line NO_x (home-based and in-situ exposures) and emotional well-being (EWB)

Stress, sadness, and pain were positively correlated with simulated neighborhood mobile-source NO_x levels, while tiredness and happiness were negatively associated with home-based NO_x concentrations (Figure 4-3). Net affect was also negatively associated with mobile-source NO_x concentrations (home-based exposure). For the in-situ exposures, we found tiredness, sadness, and net affect to be positively associated with simulated NO_x concentrations, and happiness, stressed, and pain to be negatively associated. Happiness

and net affect were expected to be EWB indicators negatively correlated with mobile-source NO_x concentrations.

All of the regression relationships between NO_x and EWB, for both home-based and in-situ exposures were near-zero, suggesting that the influence of mobile source pollution had little impact on immediate EWB (Figure 4-3). Although the majority of anthropogenic NO_x emissions (~59% (110)) come from mobile sources in the United States, mobile-source NO_x emissions have reduced ~80% since the Clean Air Act was passed in 1970 (134), resulting in relatively low average concentrations in the six study neighborhoods and at the locations where the associated activity for the EWB response took place (Table 4-1 and Figure 4-3). The range of average NO_x concentrations was 3.8-8.2 ppb in the six study neighborhoods, far below the annual NO_2 NAAQS standard of 53 ppb. Thus, the average NO_x levels might not have been high enough for its effects on EWB to be observed, and further, NO_2 has little impact on visibility at such low levels (146).

Other factors that can influence the findings presented have not been controlled for in the analysis. The respondent took the survey at various times during the day (they could take the questionnaire right after completing an activity or hours after the activity) which could bias results. Confounding variables that could have major impacts on EWB assessments against a single indicator using this dataset are discussed further in Fan et al. (141). Furthermore, the EWB outcomes were not mutually exclusive of one another, i.e., if someone is feeling pain, it is possible they feel stressed, too. This inter-relationship among the indicators was difficult to quantify and can influence results. Also, we have not included any correction or re-scaling of the data due to personality or other demographic (e.g., age, gender, ethnicity, etc.) effects.

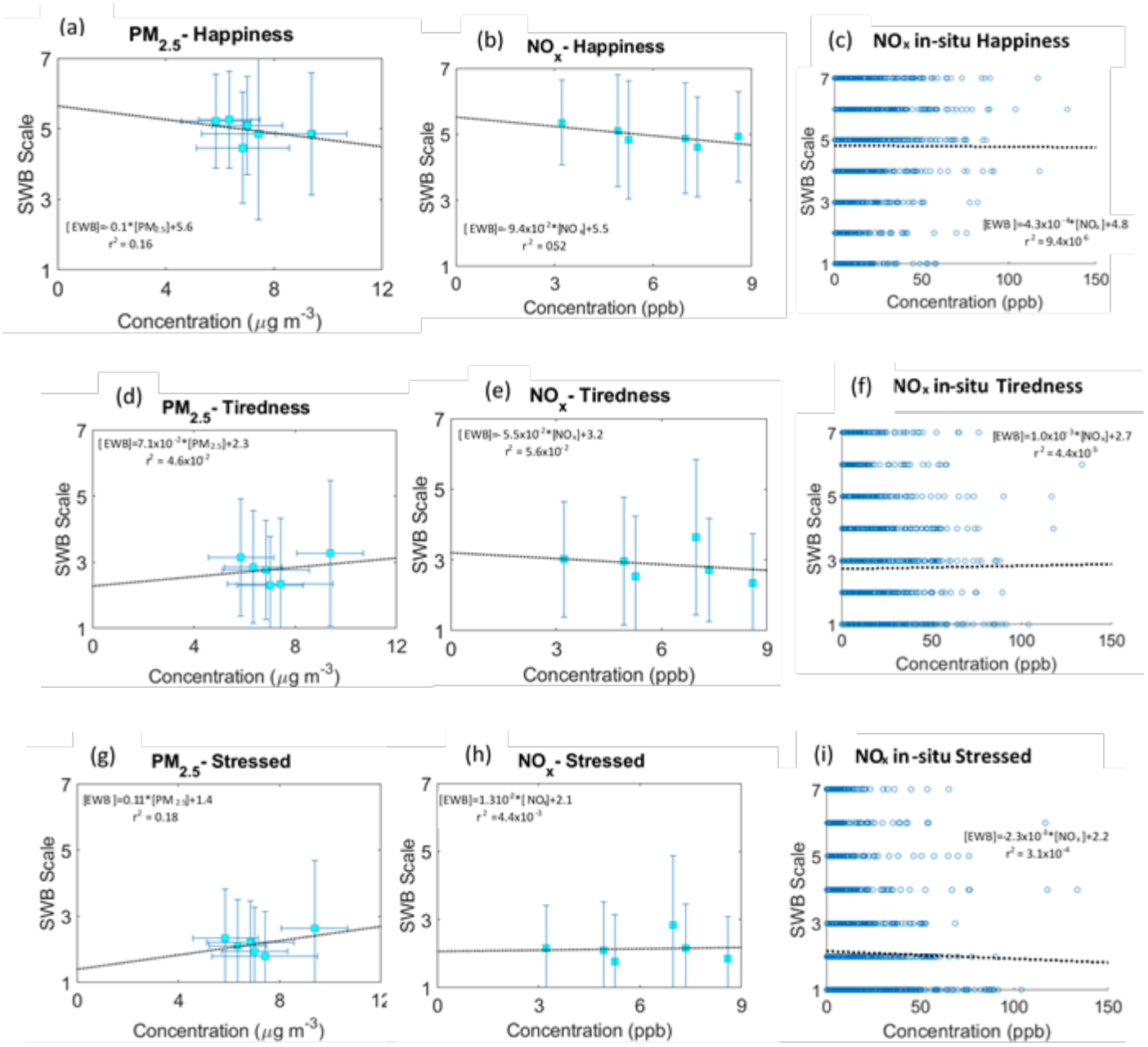
(a) PM2.5 - Happiness
SWB Scale
Concentration (μg m-3)
(b) NOx - Happiness
Concentration (ppb)
(c) NOx in-situ Happiness
(d) PM2.5 - Tiredness
(e) NOx - Tiredness
(f) NOx in-situ Tiredness
(g) PM2.5 - Stressed
(h) NOx - Stressed
(i) NOx in-situ Stressed

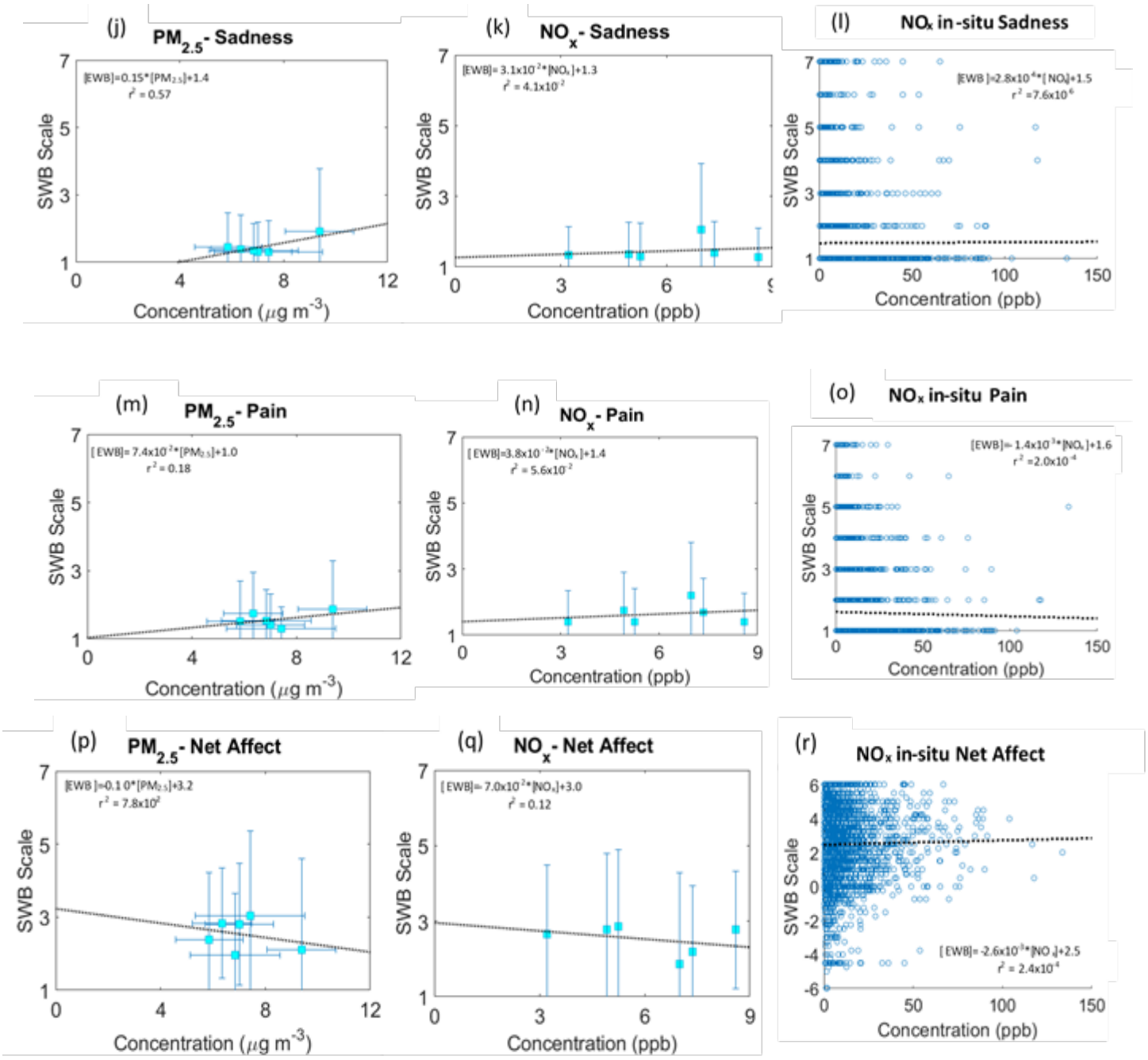

Figure 4-3: (left column) Average neighborhood low-cost sensor (LCS) $PM_{2.5}$, (middle column) R-Line mobile-source NO_x home-based exposure, and (right column) R-Line mobile-source NO_x in-situ exposure against concurrent emotional well-being (EWB) measurement (n = 5,126) for (a-c) happiness, (d-f) tiredness, (g-i) stress, (j-l) sadness, (m-o) pain, and (p-r) net affect. A higher EWB score means "more" emotion (e.g., a higher EWB happiness score means happier). None of the relationships were statistically significant (α=0.05).

4.2.5 High pollution events and emotional well-being (EWB) impacts

No noticeable trends were found when exploring the top 10% of neighborhood $PM_{2.5}$ concentrations, home-based mobile-source NO_x levels, or in-situ mobile-source NO_x levels, including a two-day lag, on any of the EWB outcomes (Table 4-2, Table 4-3, Table 4-4, and Figure C-7). The $PM_{2.5}$ finding was likely due to the little difference between $PM_{2.5}$ concentrations in the top 10% of hours with the remaining concentrations (Table C-6), while the NO_x finding could be explained from the low mobile-source NO_x to EWB relationship. There were no noticeable trends of EWB impacts from high NO_x or $PM_{2.5}$ events in the six neighborhoods with respect to access to light rail, income levels, or urban versus suburban.

Table 4-2: Average difference between emotional well-being (EWB) indicators for the top 10% of $PM_{2.5}$ hourly concentrations (including a two-day lag) and the 90% cleanest hours in each neighborhood. See Table C-6 for the cutoff concentrations. Positive values indicate the top 10% EWB average value was higher than the bottom 90% value (i.e., a positive score means the EWB outcome was higher in the high $PM_{2.5}$ days). The asterisk (*) indicates the difference is statistically significant (α=0.05).

EWB indicator	Phillips	Near North	Prospect Park	St. Anthony Park	Blaine	Brooklyn Center
Happiness	-0.95*	-4.2×10^{-2}	-0.18	-0.51*	1.2×10^{-2}	0.15
Tiredness	0.21	0.49*	1.0*	-0.23*	-0.16	-6.6×10^{-2}
Stress	0.18	0.26	0.65*	-2.3×10^{-2}	-0.16*	1.3×10^{-2}
Sadness	0.11	0.12	0.41*	-7.3×10^{-2}	-3.6×10^{-2}	-1.9×10^{-2}*
Pain	0.33*	-3.8×10^{-2}	0.34*	-0.13	0.35*	-7.3×10^{-3}
Net affect	*-1.23**	*-0.13*	*-0.69**	*-0.34**	*-0.19*	*0.13*

Table 4-3: Average difference between emotional well-being (EWB) indicators for the top 10% of mobile-source NO_x hourly concentrations (including a two-day lag) and the 90% cleanest hours in each neighborhood. See Table C-6 for the cutoff concentrations. Positive values indicate the top 10% EWB average value was higher than the bottom 90%

value (i.e., a positive score means the EWB outcome was higher in the high NO_x days). The asterisk (*) indicates the difference is statistically significant (α=0.05).

EWB indicator	Phillips	Near North	Prospect Park	St. Anthony Park	Blaine	Brooklyn Center
Happiness	0.16	-0.28*	-0.25*	-0.36*	-0.14	0.37*
Tiredness	-0.18	0.35*	0.20*	$-1.6x10^{-2}$	-0.16	-0.20
Stress	-0.37*	0.30*	$7.3x10^{-2}$	$-1.6x10^{-2}$	$-6.0x10^{-2}$	$7.9x10^{-2}$
Sadness	-0.12	0.59*	$8.9x10^{-2}$	$-7.6x10^{-2}$	$-9.8x10^{-2}$	0.13*
Pain	-0.32*	0.23*	-0.16*	-0.42*	$1.8x10^{-2}$	-0.10
Net affect	*0.64**	*-0.41**	*-0.21**	*-0.23**	*-0.23*	*0.26*

Table 4-4: Average difference between emotional well-being (EWB) indicators for the top 10% of in-situ mobile-source NO_x hourly concentrations (concentrations > 19.6 ppb; including a two-day lag) and the 90% cleanest hours in each neighborhood. Positive values indicate the top 10% EWB average value was higher than the bottom 90% value (i.e., a positive score means the EWB outcome was higher in the high NO_x days). The asterisk (*) indicates the difference is statistically significant (α=0.05).

EWB indicator	Happiness	Tiredness	Stress	Sadness	Pain	Net affect
	-0.24*	-0.13*	-0.19*	$-6.7x10^{-2}$	$1.5x10^{-2}$	-0.11

4.3 Conclusions

This exploratory research used a novel approach to characterize the relationships between air quality with emotional well-being (EWB) and neighborhood infrastructure. This study integrates low-cost sensing for $PM_{2.5}$ and R-Line modeling for mobile-source NO_x with a novel phone application for near real-time EWB assessments. From the observational data in six neighborhoods of varying socioeconomic-status (SES) and light-rail access, poorer neighborhoods tended to have higher $PM_{2.5}$ concentrations than their mid-SES counterparts in Minneapolis, MN. Simulated NO_x levels from mobile sources were significantly (α=0.05) higher in the urban neighborhoods than the suburban ones, which was expected, considering higher average traffic counts in the urban neighborhoods. There was little influence of light rail access on neighborhood air quality (for both

measured $PM_{2.5}$ and modeled mobile-source NO_x). When compared to concurrent EWB assessments from neighborhood respondents, neighborhood $PM_{2.5}$ had a negative response (i.e., a higher $PM_{2.5}$ concentration resulted in a lower EWB outcome) for happiness and net affect, but a positive response (i.e., a higher $PM_{2.5}$ concentration resulted in a higher EWB outcome) for tiredness, stress, sadness, and pain. None of the air pollution relationships were found to be statistically significant (α=0.05) with EWB, and though from a relatively small sample size associated with this exploratory research, these results are suggestive of more measureable affects given larger sample sizes or greater pollutant variability. Future work linking air quality to EWB should consider multivariate regressions including personality, age, gender, ethnicity, etc. Both mobile-source and in-situ NO_x had a minimal and near-zero regression relationship with all EWB indicators, which may have been a result of reductions in mobile source emissions as well as increased exposure measurement error versus having observed levels.

4.4 Acknowledgements

This work was supported by NSF SRN Grant No. 1444745. In addition, Colin Schladweiler at the University of Minnesota assisted with data collection in Minneapolis. Rick Strassman, Margaret McCourtney, and Daniel Dix from the MPCA provided valuable insight on local air quality measurements and modeling results. Lara Clark at the University of Washington assisted with the study set up. Dong Gao and James Hite at Georgia Tech helped with sensor testing. Jennifer Moutinho and XinXin Zhai at Georgia Tech, and Cesunica Ivey at University of California- Riverside helped with R-Line modeling.

Christina Norris at Duke University helped with the low-cost sensor Arduino setup. Gertrude Pavur at Georgia Tech edited the manuscript.

CHAPTER 5. ASSESSMENT OF THE NEAR-ROAD (MONITORING) NETWORK INCLUDING COMPARISON WITH NEARBY MONITORS WITHIN U.S. CITIES: NEW FINDINGS FROM NATIONWIDE OBSERVATIONS WITH IMPLICATIONS FOR URBAN ENVIRONMENTAL HEALTH OUTCOMES

As in revision at *Environmental Research Letters*

Abstract

Emissions from mobile sources have historically been an important anthropogenic contributor to ambient air pollution leading to high levels of air pollution near major roadways. The US EPA recently implemented the Near-Road (monitoring) Network to measure NO_2 concentrations by high-traffic roadways in urban centers throughout the US, as these locations were believed to characterize worst-case human exposures to traffic-related pollutants. Many near-road sites also include $PM_{2.5}$ and CO measurements, which along with the NO_2 observations, were compared in a pairwise manner against non-near-road monitors located within the city-scale boundary. After controlling for primary emissions from the target highways, we found no statistical difference ($\alpha = 0.05$) in $PM_{2.5}$ concentrations between the near-road and non-near-road urban sites ($\delta = 0.42$ (-0.08-0.90) $\mu g\ m^{-3}$, n=35 comparisons). NO_2 and CO levels, on average were significantly higher at the near-road sites compared to the non-near-road urban sites by 5.0 (3.4-6.5) ppb (n=44 comparisons) and $9.2x10^{-2}$ (0.04-0.14) ppm (n=42 comparisons), respectively. The average $PM_{2.5}$ difference found here is 5%, and at 14 of the 35 (~40%) urban monitor comparisons and 28 of the 72 (~39%) overall comparisons, $PM_{2.5}$ is actually higher at the non-near-road site relative to its near-road pair. Cleaner vehicle fleets, formation of secondary PM from

on-road emissions occurring downwind (i.e., away from the road), decreased SOA formation rates in the near-road environment, the prevalence of other low-volume vehicular and local, non-vehicular sources of emissions at the non-near-road sites (e.g., railyards, truck yards, ports, biomass-fueled heating, backyard barbecuing, and commercial cooking, etc.) and local meteorology (e.g. wind speed and wind direction) explain this finding. The same observational data was used to assess mobile source emission estimates from the EPA National Emission Inventory, and analysis of the observations are in rough agreement with the current ratio of NO_x to CO from on-road mobile sources.

5.1 Introduction

High levels of air pollution in US cities have often been observed near major roadways, largely due to the proximity of on-road mobile sources (herewith referred as mobile sources) (17). Despite large reductions in mobile source emissions in the US, they are expected to continue to be a large fraction of the total anthropogenic emissions as other sources, e.g. power plants, industrial emissions, etc., have also become increasingly well controlled over time (147). Since 1970 emissions from mobile sources in the US have dropped 82% for CO, 81% for VOCs, 58% for NO_X, and 58% for fine particulate matter ($PM_{2.5}$, particulate matter, PM, whose aerodynamic diameter is less than 2.5 microns) (110, 134), but mobile sources still contribute 59% of all anthropogenic NO_x, 54% of all anthropogenic CO, and 18% of all anthropogenic primary $PM_{2.5}$ (110).

Exposure to air pollution is associated with adverse health outcomes that result in premature mortality and reduced life expectancy (5-8), with the vast majority (~95%) of air pollution-related mortality linked to $PM_{2.5}$ (6, 9). Past exposure assessments have estimated that roadway-associated exposures account for elevated $PM_{2.5}$ and NO_2 exposures (148, 149), raising environmental justice concerns for residents near roadways. Mobile source impacts have been found to disproportionately affect poorer, racial minority, and vulnerable populations whose residents live near major highways (150, 151). As a result, there have been more recent efforts to characterize pollution exposures targeting the near-road environment (152-155), with a trend to finding lower near-road increments (156-159) .

The United States EPA initiated the Near-Road (monitoring) Network as part of the 2010 NO_2 National Ambient Air Quality Standards (NAAQS) review because these sites, which are located at high-traffic locations in cities where peak ambient NO_2 concentrations are expected to occur as a result of on-road mobile source emissions, would represent the worst-case population exposures (160). All near-road sites are required to measure NO_2; $PM_{2.5}$ and CO are required in every core-based statistical area (CBSA) with 1 million or more persons (161). Some sites include NO, NO_x, VOCs, and black carbon (BC) monitoring instruments as well.

Previous assessments of city-scale (e.g., Detroit, MI. (150), Houston, TX. (162) and Boise, ID., Des Moines, IA., St. Louis, MO., Detroit, MI., New York City, NY, and Los Angeles, CA. (163)) and regional-scale (e.g. DeWinter and colleagues (164) and Seagram and colleagues (165)) comparisons of near-road observations to very nearby non-near-road monitors have been infrequent and limited. The NO_2 city-scale studies (150, 163) found

that the near-road environment had higher NO_2 concentrations for each hour of the day than a background, non-near-road site measurement, while the $PM_{2.5}$ city-scale study (162) showed 24-hr $PM_{2.5}$ in Houston was 23% higher than background observations. DeWinter and colleagues (164) and Seagram and colleagues (165) compared near-road $PM_{2.5}$ concentrations with all EPA Air Quality System (AQS) sites within 25 km, 50 km, and 100 km using datasets from 2015 and 2016, respectively, that included Phase 1 (of 2) near-road sites and found higher annual-average $PM_{2.5}$ at the near-road sites by 15%. However, there was no focus on the comparison with other surrounding non-near-road urban sites <25km, where the majority of the population would be subject to similar urban emissions. This scale is particularly important to address issues of urban-scale environmental disparities.

More novel approaches to measuring on-road pollution, including via bicycles (166) and Google Street View Cars (156) regularly find elevated levels of $PM_{2.5}$ and BC on high-traffic roads or roads near highly localized mobile-source emissions (intersections along a major truck route, vehicle repair facilities, etc.). However, these approaches mostly capture on-road (or trail) observations and cannot compare concentrations with non-road/trail areas. In addition, such on/very near-roadway observations can miss the importance of how near-road environmental conditions (e.g., wind speed and wind direction) can impact $PM_{2.5}$ levels, the formation of secondary $PM_{2.5}$ from on-road emissions, and other factors impacting local $PM_{2.5}$ concentrations in cities. Further, such studies have found that some PM hot spots may be driven by non-mobile sources within cities (156).

Here, we: (1) present a nationwide, pairwise comparison of near-road observations against non-near-road observations within the city/urban-area scale (2) compare the

seasonal trends of the $PM_{2.5}$, NO_2, and CO concentration differences, (3) evaluate observed levels at each site with the corresponding NAAQS level, (4) compare near-road $PM_{2.5}$, NO_2, and CO concentrations with annual average daily traffic (AADT) and fleet-equivalent AADT (FE-AADT), (5) assess local wind speed and wind direction impacts on observed $PM_{2.5}$, NO_2, and CO concentrations at the near-road sites, (6) utilize the NO_x and CO concentration difference data to evaluate mobile-source emission estimates in the National Emission Inventory (NEI), and (7) discuss the potential human health-related outcomes of the findings from this work.

5.2 Methods and Materials

The Near-Road (monitoring) Network is a regulatory network that began monitoring in 2014 to characterize NO_2 in the near-road environment. The network contained 70 active, operational sites (referred to herewith as near-road sites) located in 62 continental U.S. cities and one site situated in San Juan, PR as of May 2017 (Figure D-1). Near-road sites are intended to measure at locations that would result in peak NO_2 concentrations related to mobile source emissions, presumably associated with high-trafficked spots in cities. Near-road sites (which can also be influenced from other non-mobile source emissions) used in this analysis sample within 50 meters of the intended high-traffic roadway. The location of near-road sites are not necessarily representative of other locations on the same road and caution has been recommended from a previous study on using near-road sites for exposure studies (167). NO_2, $PM_{2.5}$, and CO are monitored at 69 (no data at the Des Moines, IA. site), 43, and 56 of the near-road sites, respectively. The $PM_{2.5}$ instruments used at the near-road sites are either a Met One Beta Attenuation Monitor (BAM) 1020, a TEI 5014i BAM, a Grimm 180, or a TEI 1405-DF Tapered

Element Oscillating Microbalance (TEOM). Previous assessments of co-located Federal-Equivalent Method (FEM) monitors have shown variability (168, 169), including differences approaching 10% on 24-hour averaged $PM_{2.5}$ levels (170). The biases between the measurement approaches are attributed to local ambient conditions (e.g., temperature, relative humidity, and aerosol composition) (171). In this work, we do not perform any additional quality assurance or quality control to the reported concentrations.

Observations used in this study were from the continental US near-road monitors along with regulatory monitors within the same city or within 10 miles of a near-road site (referred to herewith as non-near-road sites; see Table D-1 for a complete list of sites in the study). The 10-mile condition is applied as some non-near-road monitors are across city lines (e.g., state borders) but still likely subject to the same urban emission profile. The average size of the top 50 most populous U.S. cities is ~300 sq. miles (172), and considering that near-road sites are often centrally located, the 10-mile radius is appropriate to capture observations that may be affected by the same urban emission profile. The non-near-road sites used in this study are regulatory monitors that can represent a general population or capture areas that may be sited in response to a specific nearby-source, and may be a part of other monitoring networks.

We compared the hourly concentrations for $PM_{2.5}$, NO_2, and CO for hours where data existed at both the near-road site and non-near-road pair site; the non-near-road sites were not necessarily sited for the purpose of pairing with a near-road site, but we use those data to do the comparisons. For many near-road sites, there were multiple non-near-road sites within the city boundary/10-mile radius (e.g., Figure D-2). Each non-near-road site was compared against the near-road site within the city boundary/10-mile radius. The non-

near-road sites were characterized as urban, suburban, or rural as given in the Air Quality System (AQS) dataset (173). The focus of this assessment is on urban sites; there are no urban-designated sites identified in the same city as the near-road site that are also outside the 10-mile radius. However, there are suburban- and rural-designated sites that could be impacted by the same urban emissions profile but are not within the city boundary or 10 miles of the near-road site.

Non-near-road sites may be affected by on-road emissions (e.g., from the roads next to which near-road monitors are located), but past studies have found that mobile-source emitted pollutants decay within a few 100 meters of the road for all pollutants (156, 160). To control for such target highway emissions, we use previous findings that estimate BC (surrogate to $PM_{2.5}$) and NO_2 decay to background at 350m and 970m (156). There are no recent studies that estimate CO decay to background from mobile source emissions, so we treat the CO decay to background distance to be the same as the NO_2 decay to background distance. We exclude any comparison pairs where the non-near-road site is within these distances of the target near-road roadway from the analysis (these sites are indicated in Table D-1; we exclude 11 $PM_{2.5}$ comparisons, 37 NO_2 comparisons, and 35 CO comparisons).

There were 72 comparisons at 30 near-road sites for $PM_{2.5}$, 91 comparisons at 55 near-road sites for NO_2 (NO_2 measurements are at each near-road site, but for some near-road sites the non-near-road site pair was within the NO_2 decay distance, while other near-road sites do not have a corresponding comparison site within the city boundary/10-mile radius), and 70 comparisons at 36 near-road sites that measure CO (Table D-2). Because of measurement limitations (i.e., no monitor or recorded data at the near-road site, no non-

near-road site within the city boundary/10-mile radius, and/or no non-near-road site outside the pollutant decay distance to background zone), some of the most populous cities in the US were not included in this study. This includes Chicago, IL and Salt Lake City, UT for NO_2, CO and $PM_{2.5}$, Atlanta, GA for NO_2 and $PM_{2.5}$, San Antonio, TX for $PM_{2.5}$ and CO, and San Diego, CA, Dallas, TX, and Houston, TX for $PM_{2.5}$ comparisons.

The assessment period covers two years (Jan. 2017 – Dec. 2018). The start date of this analysis was 2017 as this was the latest start year of the most recent list of active, near-road monitors. Hourly $PM_{2.5}$, NO_2, and CO concentrations were retrieved from the AQS database pre-generated data files for 2017 and 2018 and were downloaded following the May 1st, 2019 EPA data certification deadline. In addition, hourly NO_x concentrations were retrieved from the same sites that also had an NO_2 measurement, where available.

Here, we examined the hypothesis that two-year average $PM_{2.5}$, NO_2, and CO concentrations are elevated at the near-road sites when compared to nearby (~city scale) non-near-road sites. A one-tailed t-test (H_0: $\mu_{diff} = 0$; H_a: $\mu_{diff} > 0$ ($\mu_{non\text{-}near\text{-}road} > \mu_{near\text{-}road}$); $\alpha = 0.05$) was performed to assess the statistical significance of the concentration differences at a 95% confidence level for each pollutant. A one-tailed t-test was selected so that the alternative hypothesis, H_a, could be defined as the unexpected situation that the non-near-road concentration is greater than the near-road concentration. Seasonal and monthly trends of the concentration differences were assessed. The measurements were evaluated against the US NAAQS levels and near-road concentrations were compared against annual average daily traffic (AADT) and fleet-equivalent annual average daily traffic (FE-AADT) to gauge mobile source impacts. The same analysis was performed for BC, which would be a more direct combustion emission surrogate, but there were only four

cities where the appropriate data existed for comparison (see Appendix D.1 for BC findings). In addition, coefficients of divergence (COD), a measure of spatial heterogeneity (174), were computed to gauge the spatial variability among the near-road and non-near-road monitors for each pollutant (Appendix D.2). Inverse-distance weighting of the pollutant concentration differences between the near-road and non-near-road sites was assessed (Appendix D.3). Further, NO_2 to NO_X ratios were assessed at the near-road and non-near-road sites (Appendix D.4), which is useful to estimate the fraction of ambient NO_x that has undergone oxidation from the primarily-emitted NO (175).

The local meteorology (e.g., wind speed (WS) and wind direction (WD)) and local configuration (vehicle-induced turbulence, physical barriers, monitor distance to highway, depressed roadways, etc.) of near-road sites influence how traffic emissions from the target roadways can effect observed concentrations (164, 165, 176). In this work, we relate the observed near-road $PM_{2.5}$, NO_2, and CO concentrations with near-road site monitored wind direction and wind speed (n=41). We do not assess configuration affects in this analysis. Downwind was when the angle between the target highway and near-road site was in-line with the observed wind direction (+/- a 90° buffer; we choose a wide angle window under the rationale that at non-perpendicular angles an air parcel travels over more roadway length and thus receives more emissions (177)). The remaining conditions were treated as upwind conditions. Wind speed conditions were split as either less than or equal to 1 m s^{-1} or greater than 1 m s^{-1}, consistent with wind speeds used in DeWinter et al. (164). Here, we compare the following four combinations of hourly wind conditions on hourly near-road $PM_{2.5}$, NO_2, and CO observations: (1) WS < 1 m s^{-1} and near-road site upwind, (2) WS < 1 m s^{-1} and near-road site downwind (expected to give the highest average

concentration at each site), (3) WS > 1 m s^{-1} and near-road site upwind (expected to give the lowest average concentration at each site), and (4) WS > 1 m s^{-1} and near-road site downwind. The results presented are two-year averages for each of the four combinations.

Recent studies have questioned the accuracy of on-road mobile emission estimates from the EPA National Emissions Inventory (NEI) (178, 179); we use two approaches from the available data to evaluate the NO_x to CO ratio given in the inventory (110). The NEI estimates mobile-source NO_x and not NO_2. We cannot explicitly evaluate emission estimates from the dataset used here, but we can estimate ratios of the emissions from the concentration differences. The first approach was to estimate a NO_x to CO ratio from the slope of the orthogonal regression curve fitting two-year average CO concentration differences to two-year average NO_x concentration differences for each near-road and non-near-road site combination. The second approach took the ratio of the average enhancement (i.e., the average concentration difference) of NO_x between all near-road and non-near-road observations to the average enhancement of CO between all near-road and non-near-road observations (Appendix D.5). These approaches both assume the enhancement of NO_x and CO at the near-road sites is driven by the difference in mobile source emissions affecting the near-road site minus the mobile source emissions affecting a paired non-near-road site, only. We consider both cases where negative concentration differences, i.e., the near-road annual average observation is less than the non-near-road annual average, are and are not included (Appendix D.5).

5.3 Results and Discussions

5.3.1 Comparisons of near-road and non-near-road $PM_{2.5}$, NO_2, and CO

Average levels of $PM_{2.5}$, NO_2, and CO as well as the differences between the Near-Road (monitoring) Network (near-road sites) and non-near-road sites, were calculated using observational data from 2017 and 2018, further considering if the non-near-road sites were designated as urban, suburban, or rural (Table 5-1). The $PM_{2.5}$, NO_2, and CO concentration differences between near-road and non-near-road sites were 0.50 μg m^{-3} (95% CI: 0.17-0.84 μg m^{-3}), 6.2 ppb (95% CI: 5.2-7.1 ppb), and $9.2x10^{-2}$ (95% CI: $5.8x10^{-2}$-0.13 ppm), respectively. The $PM_{2.5}$ concentration difference between the urban non-near-road sites and the near-road sites (δ = 0.42 μg m^{-3}) was not statistically significant (H_0: $\mu_{diff} = 0$; H_a: $\mu_{diff} > 0$ ($\mu_{non\text{-}near\text{-}road} > \mu_{near\text{-}road}$); p = 0.051, α = 0.05, 95% CI: -0.08-0.90 μg m^{-3}) (Table 5-1 and Appendix D.6 and Table D-3). No statistically significant difference was found between near-road $PM_{2.5}$ and the rural designated pairs either; however, there was a limited number of sample comparisons for these comparisons, and we do not include all rural monitors that could be affected by the urban emission profile as they fell outside the city/10-mile criteria radius.

Thirty-nine percent (28 out of 72) of the non-near-road sites have a higher two-year average $PM_{2.5}$ value than the corresponding near-road site, with the highest difference being 3.2 μg m^{-3} between Oakland West (AQS Site ID# 06-001-0011) and the Berkeley near-road site (AQS Site ID# 06-001-0013) (Figure 5-1, Figure D-3 and Figure D-4, and Table D-4). The Oakland West monitoring site began operation in 2009 to capture downwind emissions from the nearby Port of Oakland, a major source of diesel PM (180). We reviewed city and state air monitoring plan handbooks and found 10 of the 72 non-near-road sites from the paired comparisons were sited as source-oriented or highest

concentration sites, and four of them actually had lower concentrations than the corresponding near-road site (Table D-5).

The average difference between near-road NO_2 measurements and corresponding non-near-road sites is 6.2 ppb (95% CI: 5.2-7.1 ppb, $p = 1.9 \times 10^{-22}$). Five (out of 45) cities (St. Louis, MO., Buffalo, NY., Queens, NY., Philadelphia, PA., and Detroit, MI.) had one or more non-near-road monitors with higher average NO_2 than the companion near-road site (Figure 5-1, Figure D-4, and Table D-4). The seven (out of 92) non-near-road sites that exceed the corresponding near-road NO_2 level are all either in industrial areas or closely located to major waterways, which could be subject to local boating and shipping emissions, a source whose emissions are growing (181, 182) and are not well controlled (182). As expected, average levels decreased (in order) from the near-road, to urban, suburban, and rural environments, and the average urban, suburban, and rural differences were all statistically significant (Table 5-1 and Figure 5-1).

CO was 9.7×10^{-2} ppm higher (95% CI: 6.0×10^{-2}-0.13 ppm, $p = 6.1 \times 10^{-7}$) on average at the near-road sites than the non-near-road sites (Table 5-1). The spatial pattern of the non-near-road vs. near-road difference for CO was similar to NO_2 (Figure 5-1 and Figure D-3 and Figure D-4), which was expected considering that mobile sources account for the majority of anthropogenic CO and NO_2 emissions. There are 15 (out of 70) comparisons where the average CO concentration is higher in the non-near-road environment than at the near-road monitor (Table D-4). The highest difference is 0.40 ppm between the Indianapolis – Illinois St. monitor (AQS Site ID# 18-097-0072) and the Indianapolis – I-70E near-road monitor (AQS Site ID# 18-097-0087). The Illinois St. monitor, located downtown in a commercial area, may observe higher CO concentrations due to the building

canyon effect, trapping CO near the surface. This site does not measure NO_2 or $PM_{2.5}$, so it is difficult to assess what else may be causing the relatively elevated CO levels. Like NO_2, average CO levels decreased from the near-road, to urban, suburban, and rural environments (Table 5-1 and Figure 5-1).

Table 5-1: (Left) $PM_{2.5}$, NO_2, and CO two-year average (± 1σ) concentrations at the near-road sites and non-near-road sites. (Right) $PM_{2.5}$, NO_2, and CO two-year average (95% Confidence Interval) concentration differences between the near-road and non-near-road sites. A positive value indicates the near-road sites have higher two-year average concentration than the non-near-road sites. Only paired comparisons where the non-near-road monitor fell outside a "decay to background" distance of 350m for $PM_{2.5}$ or 970m for NO_2 and CO from the target highway were included in the analysis. The asterisk (*) indicates the concentration difference is *not* statistically significant (H_0: $\mu_{diff} = 0$; H_a: $\mu_{diff} > 0$ ($\mu_{non\text{-}near\text{-}road} > \mu_{near\text{-}road}$); $\alpha = 0.05$).

	Two-year average (± 1σ) concentrations				**Two-year average (95% CI) concentration differences**		
	$PM_{2.5}$ (μg m^{-3})	NO_2 (ppb)	CO (ppm)		$PM_{2.5}$ (μg m^{-3})	NO_2 (ppb)	CO (ppm)
All Sites	9.5 (±1.7)	12.8 (±5.9)	0.37 (±0.13)		0.50 (0.17-0.84)	6.2 (5.2-7.1)	0.09 (0.06-0.13)
Near-road sites	9.8 (±1.4)	15.9 (±5.8)	0.42 (±0.13)		N/A	N/A	N/A
Non-near-road sites	9.2 (±2.0)	9.7 (±4.1)	0.32 (±0.10)		N/A	N/A	N/A
Urban non-near-road sites	9.4 (±1.4)	11.4 (±3.6)	0.33 (±0.11)		0.42* (-0.08-0.90)	5.0 (3.4-6.5)	0.09 (0.04-0.13)
Suburban non-near-road sites	9.0 (±1.9)	8.4 (±3.8)	0.30 (±0.10)		0.52 (-0.02-1.1)	6.4 (5.3-7.4)	0.10 (0.04-0.17)
Rural non-near-road sites	8.1 (±1.2)	5.3 (±1.7)	0.19 (±0.04)		0.92* (-0.63-2.5)	10.9 (6.2-15.6)	0.10* (-0.26-0.45)
All sites range	N/A	N/A	N/A		-3.2 to 3.8	-2.7 to 21.5	-0.40 to 0.56

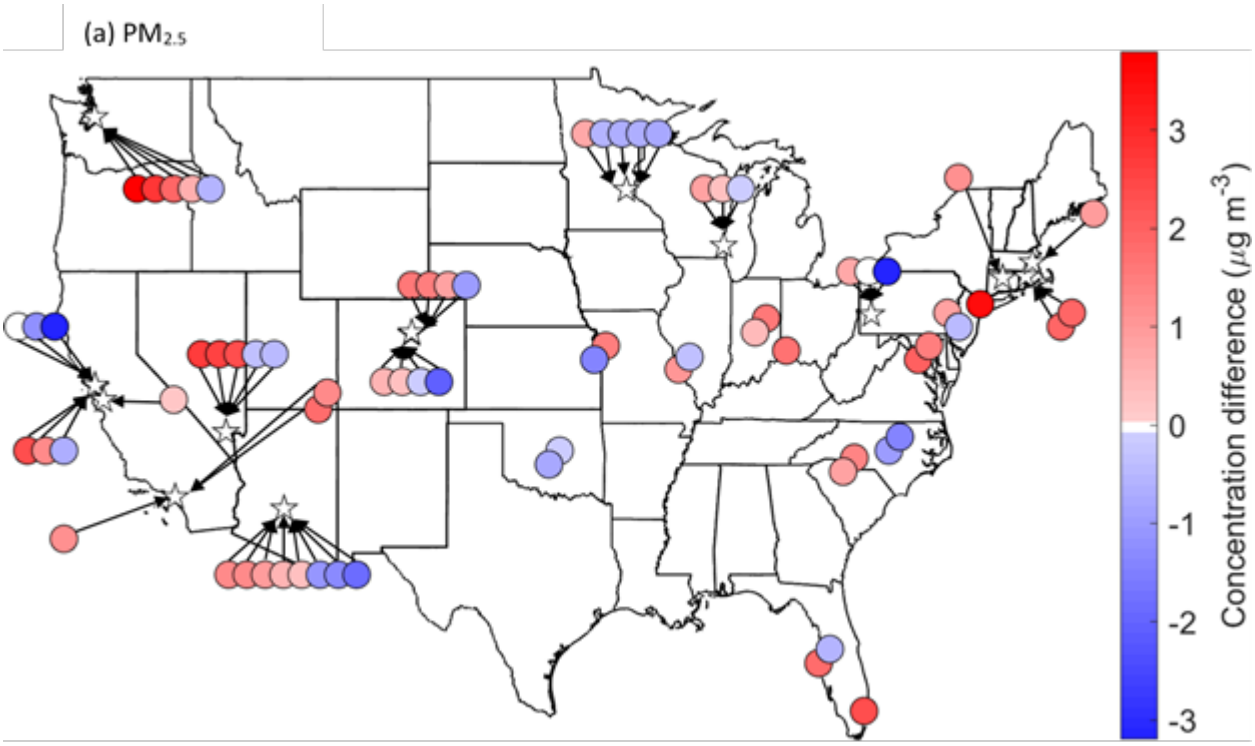
(a) PM2.5
3
2
1
0
-1
-2
-3
Concentration difference (μg m-3)

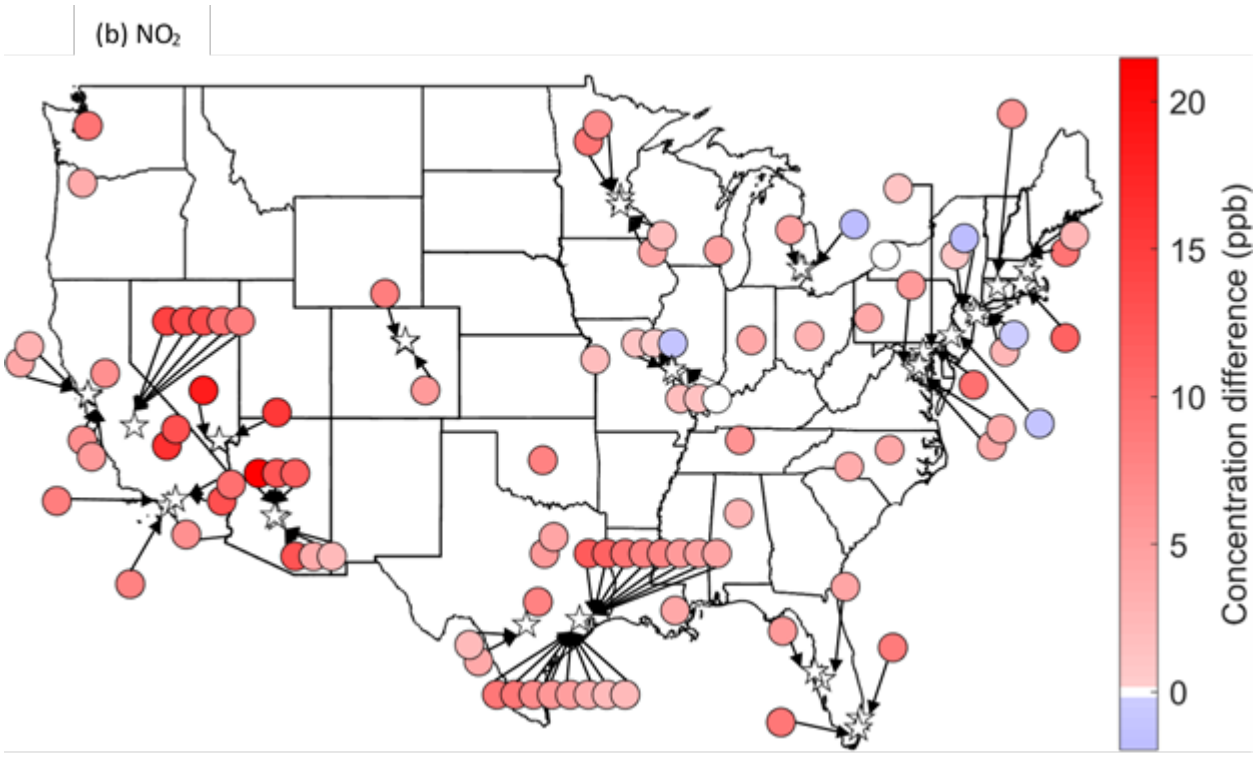
(b) NO2
20
15
10
5
0
Concentration difference (ppb)

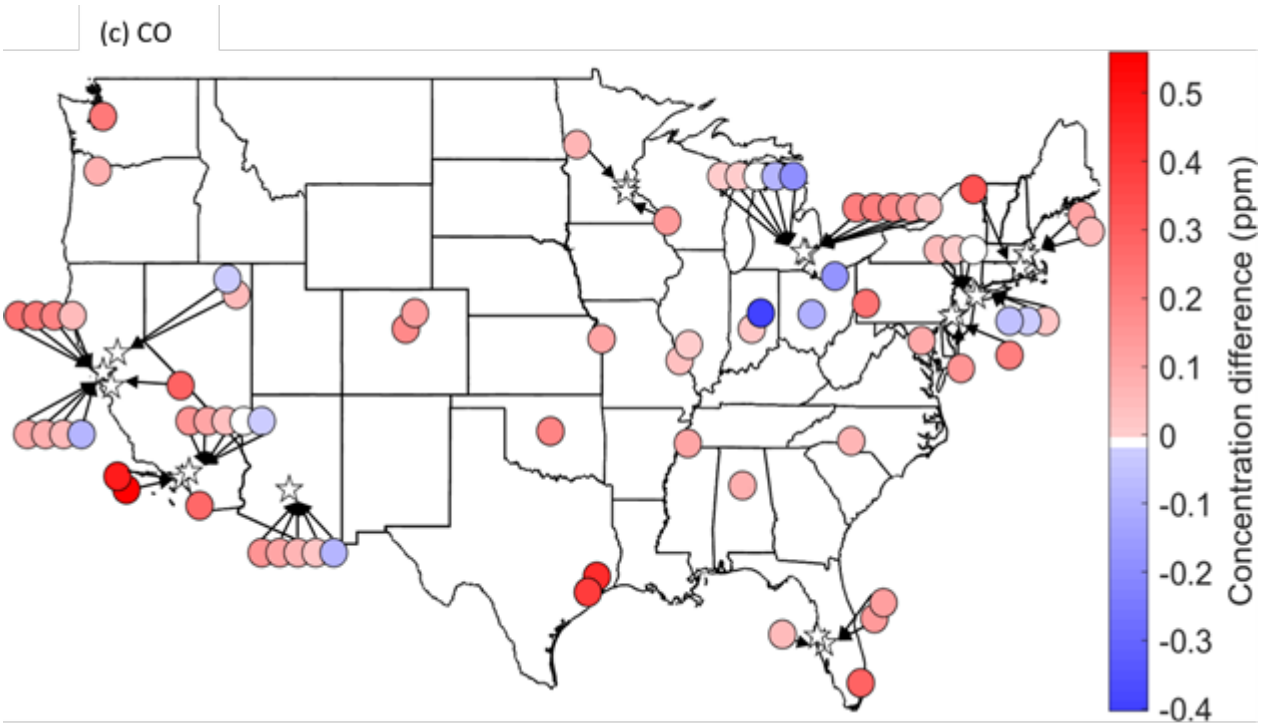

Figure 5-1: Two-year average concentration differences between near-road sites and companion non-near-road sites for (a) $PM_{2.5}$ (µg m^{-3}) (n= 72) (b) NO_2 (ppb) (n=91), and (c) CO (ppm) (n=70). Positive values indicate near-road sites have higher two-year average concentrations than a companion non-near-road site. Only paired comparisons where the non-near-road monitor fell outside a "decay to background" distance of 350m for $PM_{2.5}$ or 970m for NO_2 and CO from the target highway were included in the analysis. Some near-road sites have multiple non-near-road pair comparisons. The stars indicate a near-road site location, and arrows from the circles (two-year average concentration differences) indicate the comparison is made at that near-road site. See Figure D-4 for city-averaged comparisons.

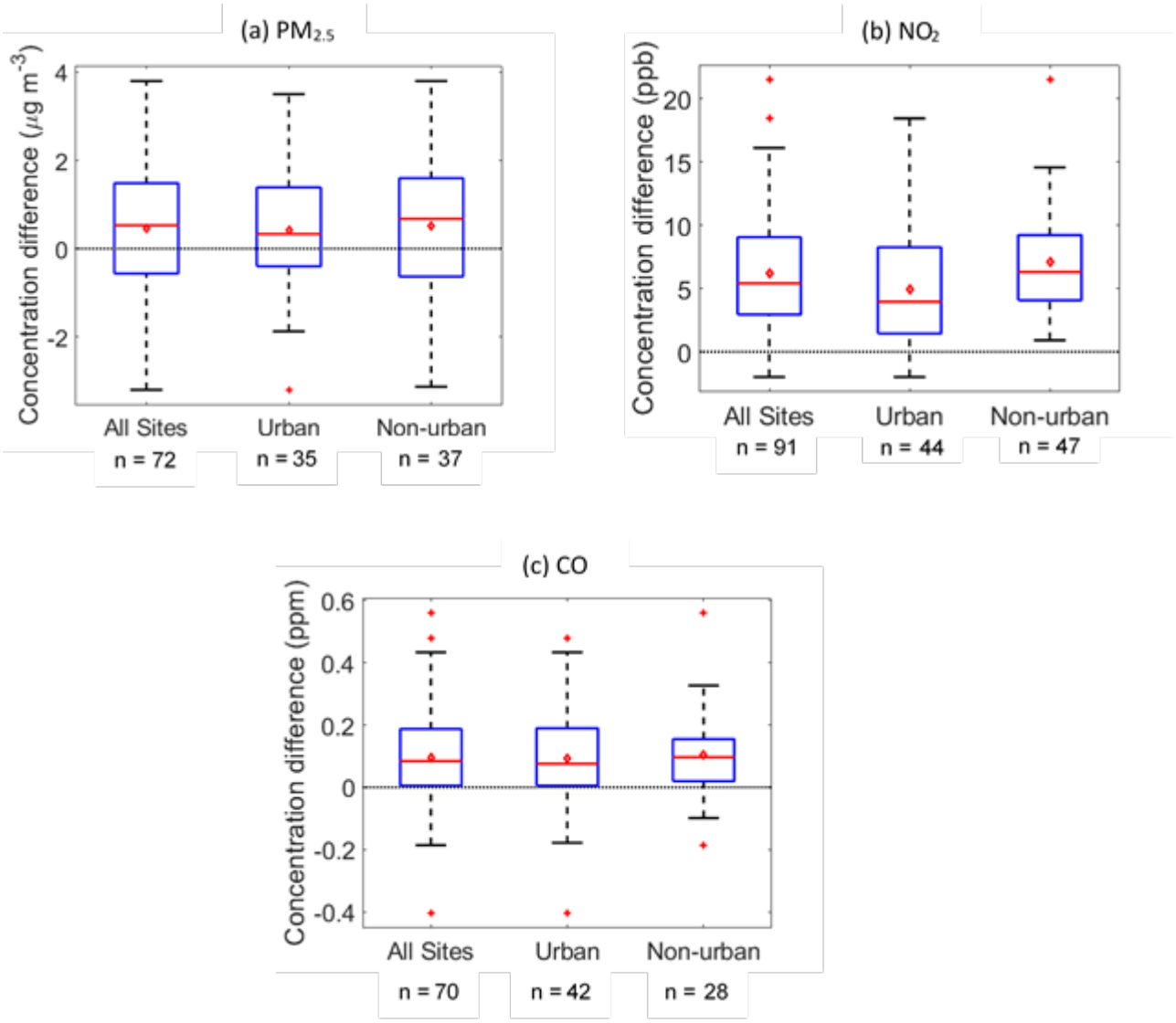

Figure 5-2: Box-plot two-year average concentration differences between (a) $PM_{2.5}$ (b) NO_2 and (c) CO near-road sites and all non-near-road sites, urban non-near-road sites, and non-urban (suburban and rural) non-near-road sites. Positive values indicate near-road sites have higher two-year average concentrations than the non-near-road sites. The boxes, red line, and red diamond represent the interquartile range (25%-75%), the median, and the average concentration difference, respectively.

5.3.2 Seasonal variation of the $PM_{2.5}$, NO_2, and CO concentration differences

$PM_{2.5}$ experienced the greatest seasonal variation in the near-road and non-near road site differences (Table 5-2 and Figure D-5). The wintertime (Dec.-Feb.) urban $PM_{2.5}$ difference is higher than the other season average differences which may be explained by higher wintertime $PM_{2.5}$ tailpipe emissions (183) and lower temperatures, the latter reducing volatilization of semi- and intermediate volatility organic aerosols (184, 185). Further, secondary organic and inorganic aerosol formation is depressed in the wintertime due to decreased photochemical activity, decreasing the impact of on-road emissions of PM precursors on secondary PM levels on urban scales. There is little observed seasonal difference of CO concentration differences, on average, between the near-road and non-near-road sites (Table 5-2 and Figure D-5). Wintertime (Dec.-Feb.) NO_2 concentration differences are slightly lower, on average, compared to the other seasons, which is likely due to lower average mobile-source NO_x emissions in the winter and a longer NO_2 lifetime, providing for further downwind NO_2 transport and city-wide buildup (186). Surprisingly, both CO and NO_2 have an opposite trend to $PM_{2.5}$ in the winter (i.e., it is the season where the smallest differences between the near-road and non-near-road sites are observed), so decreased wintertime mixing would not appear to be a major factor for the increased wintertime $PM_{2.5}$ differences.

Table 5-2: Seasonal differences of two-year average (95% Confidence Interval) $PM_{2.5}$, NO_2, and CO concentrations between the near-road sites and non-near-road sites. A positive value indicates the near-road sites have higher two-year average concentrations than the non-near-road sites. See Table D-6 and Figure D-6 for monthly comparisons.

	$PM_{2.5}$ ($\mu g\ m^{-3}$)		NO_2 (ppb)		CO (ppm)	
	All sites	*Urban sites*	*All sites*	*Urban sites*	*All sites*	*Urban sites*
Winter	0.65 (0.15-1.15)	0.83 (0.16-1.49)	5.5 (4.5-6.5)	4.0 (2.6-5.5)	0.07 (0.03-0.10)	0.07 (0.03-0.12)
Spring	0.39 (0.08-0.70)	0.32 (-0.08-0.74)	6.4 (5.4-7.4)	4.9 (3.4-6.5)	0.09 (0.05-0.12)	0.08 (0.04-0.13)
Summer	0.34 ($8.1x10^{-3}$-0.67)	0.20 (-0.26-0.66)	6.4 (5.4-7.3)	5.5 (3.9-7.0)	0.10 (0.07-0.14)	0.10 (0.05-0.15)
Fall	0.39 (0.11-0.84)	0.28 (-0.19-0.75)	6.2 (5.2-7.2)	5.2 (3.6-6.8)	0.10 (0.06-0.13)	0.08 (0.04-0.13)

5.3.3 National Ambient Air Quality Standards (NAAQS) Exceedances

The observed data at the near-road and non-near-road sites were compared against the NAAQS levels for each pollutant. Three (of the 29) near-road sites (*San Francisco - Laney College, Los Angeles -Long Beach, and Los Angeles – Ontario*) and five (of the 65) non-near-road sites (*Oakland West, Pittsburgh – Liberty, Los Angeles - Long Beach-South, Los Angeles - Upland, and Los Angeles Mira Loma Van Buren*) used in this study exceeded the annual mean $PM_{2.5}$ primary standard of 12 μg m^{-3} (NAAQS standard is annual mean averaged over three years; here, we average over two years; Table D-7). The Pittsburgh monitor that exceeds the standard is sited as a highest-concentration site, is downwind of a steel plant, and is located on top of a school building adjacent to the bus loop – subject to local emissions from both sources. Each of the other non-near-road and near-road sites are where annual standard exceedance occur are in areas that have been prone to wildfires in recent years (187). There were seven (of the 29) near-road sites and 11 (of the 65) non-near-road sites that exceeded the 35 μg m^{-3} 24-hour standard at least once (98^{th} percentile, NAAQS standard is averaged over three years, here we average over two years; Table D-7), each of which are also locations prone to wildfire plumes.

All near-road and non-near-road sites in the United States are below the hourly and annual NO_2 and hourly and annual CO NAAQS. There were no NO_2 or CO exceedances of the standard in 2017 or 2018, an improvement compared to the first two years of the network's inception when exceedances occurred (164), and the maximum levels observed at the near-road sites over these two years were lower than those from 2016 at the near-road sites (165). The highest observed NO_2 annual mean amongst the sites used in this study was 32 ppb at the Ontario, CA. Route 60 near-road site (AQS Site ID# 06-071-0027)

in 2017, below the 53 ppb NAAQS standard. The highest 98th percentile of 1-hour daily maximum concentrations averaged over the two year study period was 89 ppb at the Long Beach, CA. near-road site (AQS Site ID# 06-37-4008), below the 100 ppb NAAQS standard (which is averaged over three years). The highest CO 8-hour average is 4.5 ppm at the Minneapolis Near-Road I-35/I-94 site (AQS Site ID# 27-053-0962), below the NAAQS of 9 ppm that is not to be exceeded more than once per year. The highest 1-hour reporting from observations used in this study is 9.0 ppm at the Pittsburgh Parkway East Near-Road site (AQS Site ID# 42-003-1376), well below the 35 ppm hourly NAAQS that is not to be exceeded more than once per year.

5.3.4 Annual Average Daily Traffic (AADT) and Fleet-Equivalent AADT (FE-AADT) against near-road $PM_{2.5}$, NO_2, and CO

Comparison of average pollution levels at the near-road sites with AADT found positive, statistically significant (α=0.05) correlations for NO_2 and CO, and a weaker, insignificant relationship for $PM_{2.5}$. On the other hand, the comparison of NO_2, CO and $PM_{2.5}$ with FE-AADT at the near-road sites found positive, statistically significant (α=0.05) correlations for all three pollutants (Figure 5-3). FE-AADT gives heavy-duty vehicles 10 times the vehicle count of a standard vehicle as defined by:

$$FE - AADT = (AADT - HD_c) + (10 * HD_c)$$

where HD_c is the total number of heavy-duty vehicles. In the most recently reported Vehicle Inventory and Use Surveys (VIUS), approximately 87% of heavy-duty vehicles (>26,001 pounds) have diesel engines. Current literature now finds that diesel vehicles equipped with a diesel particulate filter (DPF) actually have lower $PM_{2.5}$ exhaust emissions per amount of fuel burned than gas direct inject (GDI) engines (188, 189); though older

non-DPF-equipped diesels still dominate primary carbonaceous emissions from on-road mobile sources (188, 190). In addition, the majority of particle emissions from engine exhaust occur in the PM_1 (D_p < 1 μm) range (191, 192) and emissions from diesel particulate filter (DPF) equipped heavy-duty diesel vehicles (HDDV) are almost exclusively in the ultrafine (D_p < 0.1 μm) range (193). Thus, the mass concentration implications may be small relative to the particle number concentration relationships. We find a lower CO correlation coefficient in the FE-AADT comparison compared to the correlation coefficient for either NO_2 or $PM_{2.5}$. First, FE-AADT is adjusted for the presence of trucks that are primarily diesel-powered, and diesels are not large contributors to CO emissions. Second, photochemical CO production from isoprene and other volatile organic compounds (VOCs) vary regionally and temporally. Global estimates show that isoprene oxidation contributes to about 13% (9-16%) of the CO budget (194), and CO production from isoprene is more efficient in high NO_x environments (e.g., near roadways) (195). Although the NO_x and CO relationships with both AADT and FE-AADT are significantly significant, the low correlations suggest near-road monitors are influenced by local characteristics (e.g., wind speed, wind direction, vehicle-induced turbulence, physical barriers, monitor distance to highway, depressed roadways, etc.) and emissions other than those from mobile sources.

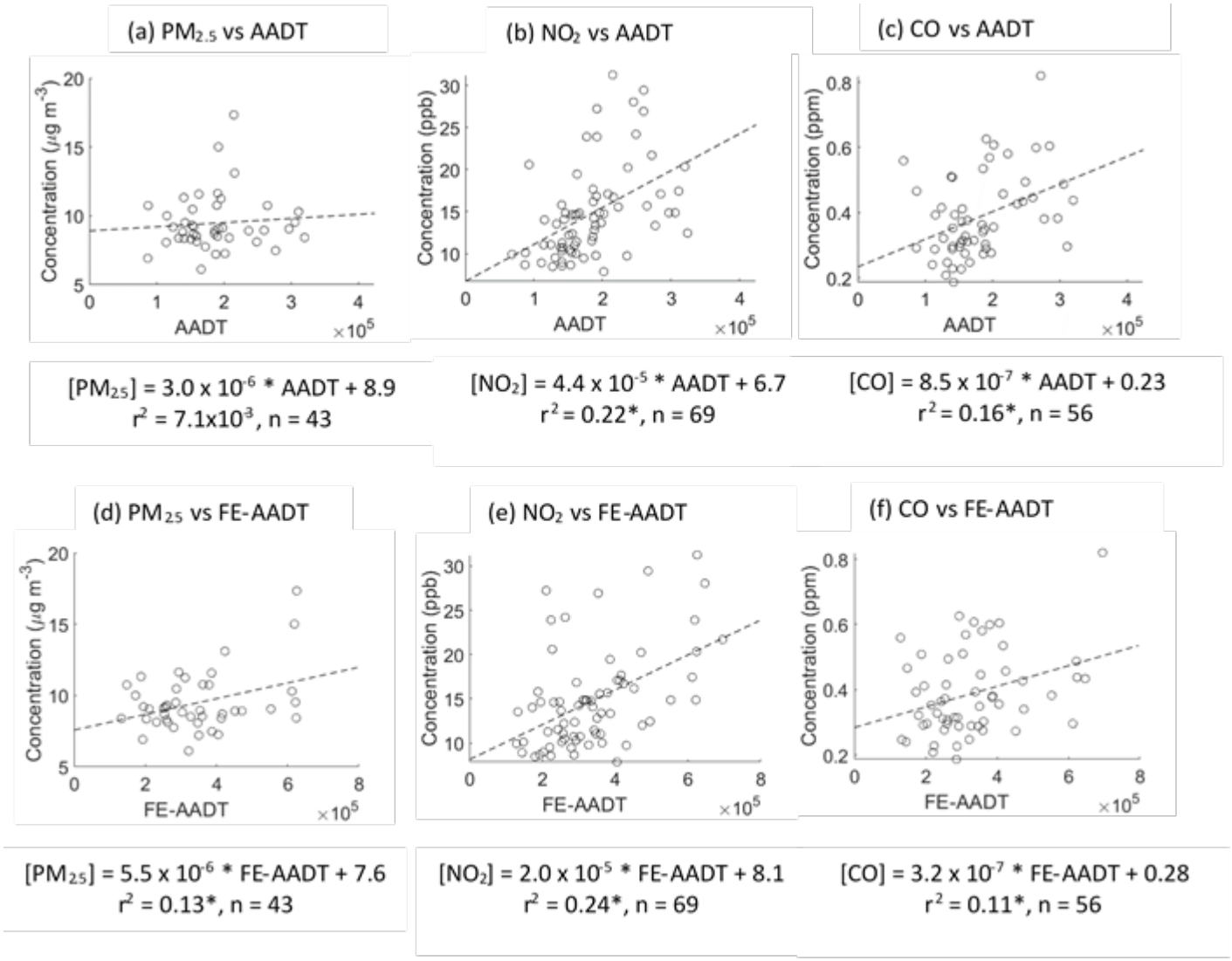

Figure 5-3: Near-road site two-year average concentrations versus (top) Annual Average Daily Traffic (AADT) and (bottom) Fleet-Equivalent AADT (FE-AADT) for (a & d) $PM_{2.5}$ (μg m^{-3}) (b & e) NO_2 (ppb) and (c & f) CO (ppm). The asterisk (*) indicates regressions that were found to be statistically significant (α=0.05)

5.3.5 Wind speed and wind direction on near-road $PM_{2.5}$, NO_2, and CO observations

The near-road site downwind and wind speed (WS) < 1 m s^{-1} criteria often results in the highest average observed $PM_{2.5}$, NO_2, and CO concentrations as expected (Figure 5-4). However, for four (of the 21) near-road $PM_{2.5}$ observations, 22 (of the 41) near-road

NO_2 observations, and 19 (of the 30) near-road CO observations, the downwind and WS < 1 m s^{-1} does not result in the highest average concentration. At three of the four PM sites where this occurs (Riverside AQS Site ID# 06-071-0027, Las Vegas AQS Site ID# 32-003-1501, San Antonio AQS Site ID# 48-029-1069), the downwind and WS < 1 m s^{-1} condition does not give the highest average concentration for NO_2 or CO, either. However, at the Indianapolis near-road site (AQS Site ID# 18-097-0087), the downwind and WS < 1 m s^{-1} condition does result in the highest average NO_2 and CO concentrations. Brown and colleagues (177) conducted a detailed assessment of meteorological factors influencing the Indianapolis near-road site and found a weak correlation between NO_x and $PM_{2.5}$ during high $PM_{2.5}$ hours, suggesting mobile sources are not a dominant contributor to high $PM_{2.5}$ hours. They attributed the high $PM_{2.5}$ hours that often occur at night to residential wood burning and low inversion heights. Further investigation finds upwind (wind moving in the direction of the road from the near-road site) conditions during these times of the day in Indianapolis. 52% of the total wind direction observations used in this analysis were during hours when the near-road site was upwind of the target highways, which suggests that the near-roadway site may not be the most equipped method to identify the effects of vehicular emissions on near-road air quality.

The low wind speed (WS < 1 m s^{-1}) and downwind condition does not result in the highest average concentration at the majority of the near-road sites for NO_2 and CO. For 15 (of the 22) NO_2 sites, 13 (of the 19) CO, and zero (of the four) $PM_{2.5}$ sites where this occurs (Table D-8), there is another major highway or interstate nearby (not the target highway) that is within the decay to background distance buffer ($L_{PM2.5}$ = 350m and L_{NO2}= L_{CO} = 970m) whose emissions will influence the monitor at a different wind direction

range. The hours of calm wind speeds and the monitor downwind of the target highway may not be during peak emission hours. In addition, the actual highway configuration (e.g., vehicle-induced turbulence, physical barriers, depressed roadways, etc.) will also impact near-road observations. Assessing these conditions on near-road monitors would require detailed meteorology, temporally-resolved emission inventories, and near-road dispersion modeling that considers the local roadway configuration.

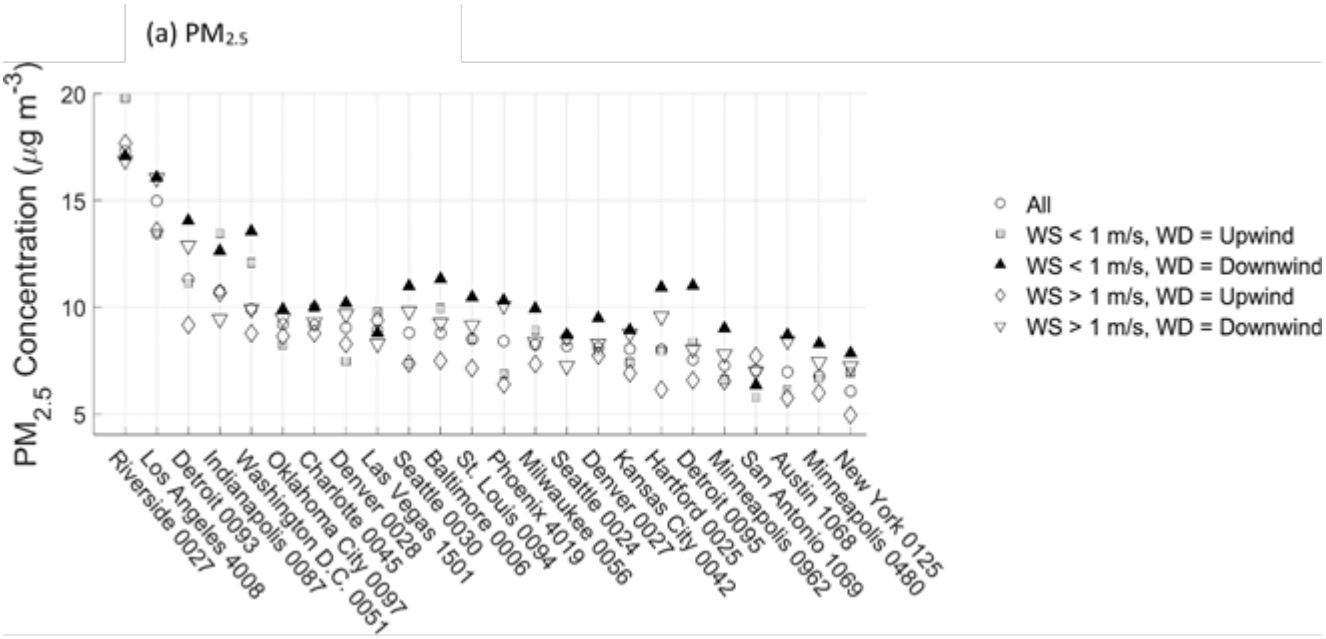

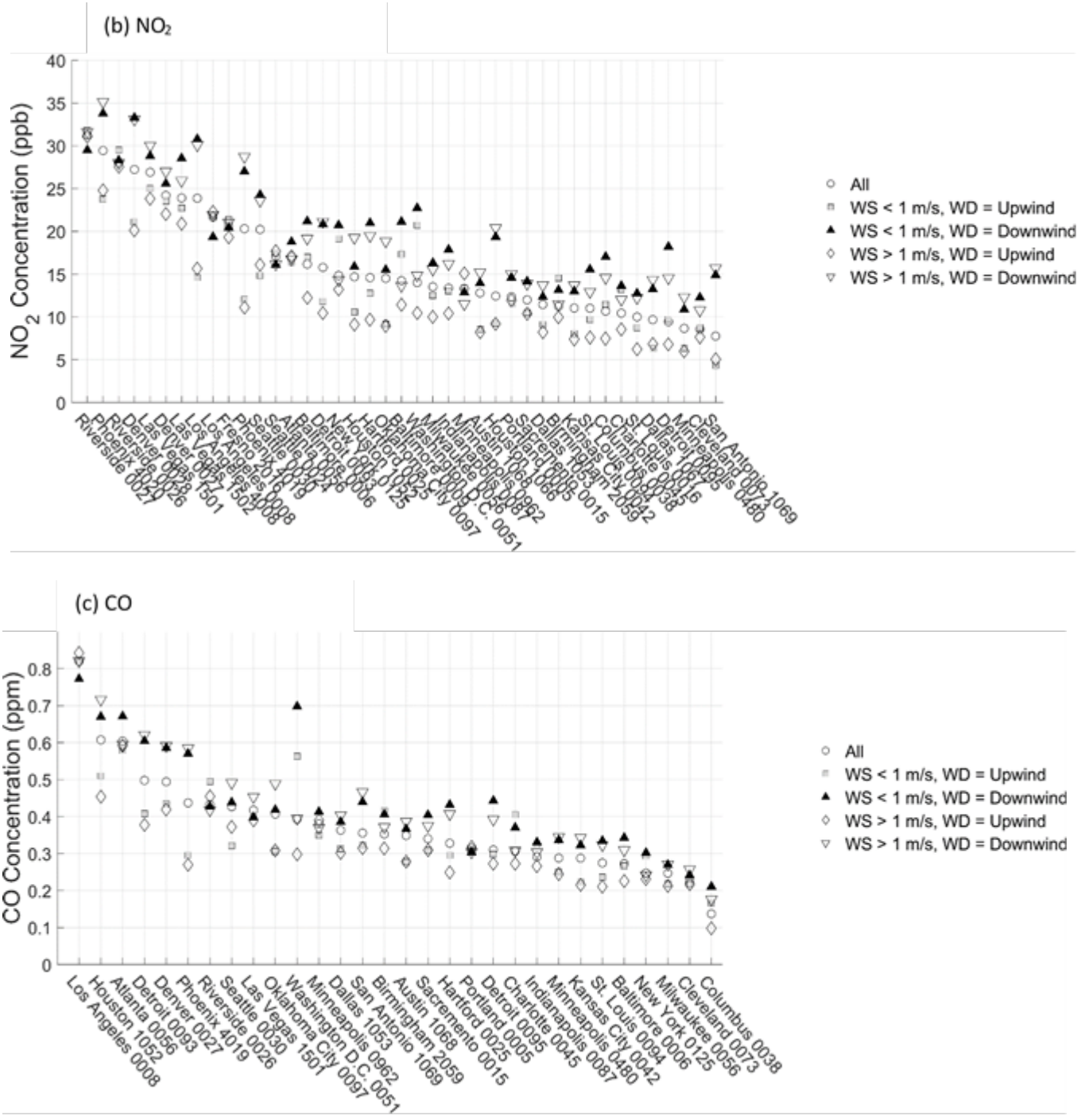

Figure 5-4: Wind speed and wind direction impacts on near-road site (a) $PM_{2.5}$ (µg m^{-3}) (b) NO_2 (ppb) and (c) CO (ppm) observations. The data presented here, including the average values, is only for hours when both wind data and pollutant concentrations exist in 2017-2018. The city names and the last four digits of the AQS Site ID are given for each near-road site.

5.3.6 *Using NO_x and CO concentration differences to assess the National Emission Inventory (NEI) mobile-source emission estimates*

NO_x and CO concentration differences between near-road and companion non-near-road site pairs that monitor both pollutants are positively correlated with each other (Figure 5-5), which is expected considering mobile sources contribute the majority of NO_x and CO emissions in the US (110). On-road mobile NO_x emission estimates according to the NEI are 5.8 x 10^9 kg yr^{-1} while CO on-road mobile emission estimates are 2.9 x 10^{10} kg yr^{-1} (110), a NO_x to CO ratio of 0.20. The slope of the orthogonal best-fit regression between CO and NO_x concentration differences is 172 (95% CI: 90 - 310) ppb NO_x (ppm $CO)^{-1}$ (~0.27 (0.14 - 0.49) μg m^{-3} NO_x (μg m^{-3} $CO)^{-1}$), slightly higher the ratio in the NEI of 0.20 (Figure 5-5, Appendix D.6 for significance tests, and Appendix D.5 for unit conversion explanation). The NO_x to CO ratio using the average enhancement of NO_x (16 ppb) and CO (0.14 ppm) where both sets of measurements exist between the near-road and non-near-road measurements (n = 31) is 0.17 μg m^{-3} NO_x (μg m^{-3} $CO)^{-1}$, in line with the NEI NO_x to CO estimate (see Appendix D.5 for the case where negative concentration differences were removed). Recent studies have questioned the accuracy of the NEI's on-road mobile emission estimates (178, 179), but the findings presented here suggest good agreement between observations and the NEI NO_x to CO estimate (other pollutant emissions and ratios might still have high uncertainties). There was little correlation between $PM_{2.5}$ differences to NO_x or CO differences, as expected, further emphasizing that there is relatively less $PM_{2.5}$ enhancement from mobile sources on near-road observations (Figure D-7). The average NO_2 to NO_x at the near-road sites was 0.63 and was 0.81 for the non-near-road sites (Appendix D.4).

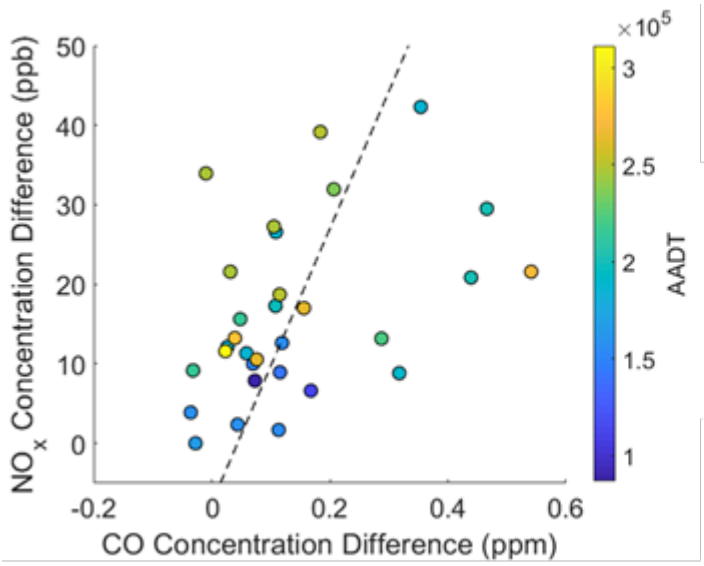

$$\partial[NO_x] = 172 \frac{ppb\ NO_x}{ppm\ CO} * \partial[CO] - 7.5\ ppb\ NO_x$$

$$r = 0.42$$

$$n = 31\ (n_{urban} = 18; n_{suburban} = 12; n_{rural} = 1)$$

Figure 5-5: The difference in two-year average NO_x and CO concentrations between a near-road site and non-near-road site. The positive values indicate the near-road annual average concentration is higher than the non-near-road concentration. Three cases exist where the CO concentration difference falls below zero. The regression was found to be statistically significant (α=0.05).

5.3.7 Explanations for having no statistically significant (α=0.05) $PM_{2.5}$ difference between near-road and non-near-road urban observations in U.S. cities

Historically $PM_{2.5}$, NO_2, and CO have been higher near major roads when compared to other, non-near-road locations in US cities (17, 164, 165). Recent assessments using various approaches, including fine-scale reduced-complexity models (159), emission inventory trends (134), distance decay transect studies (156, 157), and land-use regression predictions (158), have found that mobile sources generally contribute to low amounts of ambient $PM_{2.5}$ but still lead to enhancements near major highways. Here, using nationwide observations from the Near-Road (Monitoring) Network and nearby non-near-road monitors, we also find a slight near-road enhancement for $PM_{2.5}$ (~5% difference). The average difference between near-road and non-near-road monitors was not statistically significant (H_0: $\mu_{diff} = 0$; H_a: $\mu_{diff} > 0$ ($\mu_{non\text{-}near\text{-}road} > \mu_{near\text{-}road}$); $\alpha = 0.05$, $p = 0.051$). A

number of factors have led to lower near-road PM levels. First, modern automobiles and trucks have low primary $PM_{2.5}$ exhaust emissions, and the majority of this PM occurs in the PM_1 ($D_p < 1$ μm) range, with mass-median diameter generally between 100 and 200 nm (191, 192). Near-road sites are also alongside high-traffic interstates and likely not subject to cold start emissions, which are estimated to contribute the majority of tailpipe PM emissions (196) and select VOC emissions from mobile sources (197). Further, higher NO_x levels, like those observed in a near-road environment, are associated with lower secondary organic aerosol (SOA) yields (198-200) and reduce the rate of VOC oxidation to SOA precursor species. These reasons would only explain why the levels are not as elevated now as in the past, not why there is very little difference between near-road and nearby non-near-road observations.

Recent lab experiments estimate that SOA formation exceeds primary organic aerosol (POA) emissions after a few hours of atmospheric oxidation for most vehicles (201, 202), which would contribute to downwind $PM_{2.5}$ observations from mobile sources. Despite high fleet turnover rates, and less total SOA formation, newer vehicles tend to have higher SOA yields (SOA produced per unit mass of reacted precursor) (201, 203). Gordon et al. concluded that some vehicles generate as much as six times the amount of SOA as primary PM under typical oxidant levels (201). Further, Zhao et al. showed that changing tailpipe emissions (i.e., the ratio of non-methane organic gases (NMOG) to NO_x) and atmospheric chemistry (SOA yields) may result in the same SOA production from cleaner vehicle fleets compared to previous fleets, despite large reductions in direct tailpipe precursor emissions (204). These emissions would affect downwind, background observations more than the near-road PM observations.

The finding that $PM_{2.5}$ is similar near-road and at other urban monitoring areas in U.S. cities suggests that other non-major-road sources in US cities play an increasingly important role in air quality considering the large mobile source reductions. High-emitting local sources (e.g., commercial cooking, barbecuing, biomass-fueled residential heating emissions that escape outdoors, rail yards, truck yards, ports, school busses, etc.) and lower-volume vehicular sources can also play a role at non-near-road monitoring sites. Aligned with nationwide observations that organic carbon is becoming a major fraction of $PM_{2.5}$ loadings (205), the low $PM_{2.5}$ difference between near-road and non-near-road observations and low levels, in general, supports findings of the potential importance of biogenic emissions and volatile consumer products (206, 207).

5.3.8 Human health implications

The near-road environment having similar levels of $PM_{2.5}$ to adjacent areas has implications for health outcome assessments. $PM_{2.5}$ has been implicated as having the highest disease burden of air pollutants by the Global Burden of Disease (~95%) (6, 9), and recent health effect studies in the near-road environment have found excess risk for near-road populations (208-210). However, the finding of a low near-road $PM_{2.5}$ increment, which is consistent with recent near-road studies that used other approaches (e.g., fine-scale reduced-complexity models (159), distance decay transect studies (156, 157), and land-use regression predictions (158)), suggests that $PM_{2.5}$ mass may not be the best indicator of potential health impacts of traffic-related air pollutants.

Health studies that aim to understand the biological mechanism triggering health outcomes from air pollution exposure have implicated that small amounts of metals,

including iron (Fe) and copper (Cu) ions, both of which are generated from tailpipe and non-tailpipe (mechanical abrasion and road dust) vehicle emissions, can trigger oxidative stress in biological systems (211, 212). Increased oxidative stress is linked to the pathogenesis of cardiovascular and pulmonary diseases (213, 214). In addition, some of the organic species that are byproducts of incomplete fossil fuel combustion (i.e., particle-bound PAHs) enhance ROS generation (215) and potentially could be elevated in the near-road environment (216, 217), though atmospheric processing may increase PM oxidative potential away from roadways (218). Recent on-road measurements have found that near-road areas experience elevated levels to such primary pollutants (i.e., trace metals, PAHs, BC, etc.). In an on-road measurement campaign in Pittsburgh, PA., Gu and colleagues found a 1-2 $\mu g\ m^{-3}$ increase in PM_1 in traffic locations compared to urban background areas, with most of the difference attributable to primary carbonaceous aerosols (BC and hydrocarbon like organic aerosol (HOA)) (157).

Because of their potential significance to environmental health, the results found in this paper should continue to be evaluated through further air quality comparisons in the near road and non-near road environment as there are significant uncertainties when interpreting the results from near-road monitors. Future work should include consideration of additional pollutants (e.g., $PM_{2.5}$ species and oxidative potential) as $PM_{2.5}$ measured at near-road monitors may not be a robust indicator of traffic related air pollutant emissions on health outcomes.

5.4 Acknowledgements

Funding for this work was from National Science Foundation Sustainability Research Network Grant No. 1444745 and National Science Foundation Partnerships for International Research and Education Grant No. 1243535. We thank Cesunica Ivey at UC-Riverside, Jennifer Moutinho at ExxonMobil, James Hite, Rodney Weber, Masayuki Takeuchi, Sally Ng, Yongtao Hu, and Huizhong Shen at Georgia Tech, Steven Brown at Sonoma Tech Inc., and Sina Hasheminassab at SCAQMD for insightful discussion and guidance for preparing figures. In addition, Nealson Watkins, Halil Cakir, and Nick Mangus at the US EPA provided valuable insights on Near-Road (Monitoring) Network monitors and data.

CHAPTER 6. AIR QUALITY AND CO_2 EMISSION IMPACTS OF WASTE-HEAT TO ELECTRICITY AND MATERIAL EXCHANGE PATHWAYS AT COAL-FIRED POWER PLANTS AND OTHER LARGE SOURCES IN INDIA

Abstract

India is home to 1.3 billion people who are exposed to some of the highest levels of ambient air pollution of any country in the world, and exposure to fine particulate matter ($PM_{2.5}$) is estimated to contribute to 600,000 premature mortalities each year nationwide. In addition, India is the fastest-growing carbon emitter of the global super-emitters. Currently, residential biomass burning used for cooking and heating is the leading contributor to ambient $PM_{2.5}$ in India, while the leading CO_2-emitting sector is Thermal Power Systems (TPSs). Previously published emission estimates projected to 2050 find coal-fired TPSs will be the leading source of ambient $PM_{2.5}$, due in part to reductions in residential biomass burning emissions and widespread projected expansion in coal generating capacity nationwide. Previous assessments have found that clean-energy generation using renewable technologies (e.g., PV solar, wind, etc.) will have large carbon and air quality benefits, but the installation costs have been a barrier throughout India. Coal combustion, particularly with Indian coal, is highly inefficient and produces large amounts of waste heat. Here, we quantify the total amount of electricity that can be generated from low- and medium-grade waste heat at coal-fired TPSs and other large sources (e.g., cement plants, iron and steel plants, open agricultural burning) using Organic Rankine Cycles (ORCs). This same amount of electricity is offset by coal consumption reductions at TPSs to offer a first-order assessment of the CO_2 emission and air quality impacts of such

strategies in 2015 and under three scenarios projected to 2050 using various levels of policy adoption (2050-REF: business as usual; 2050-S2: effective achievement of currently-proposed targets under the Perform, Achieve, and Trade (PAT) scheme; 2050-S3: ambitious regulatory achievement). In addition, we assess material exchange pathways that re-utilize coal fly-ash for material substitution in brick and cement reduction, offering local CO_2 and air pollution emission reductions. We find such waste-heat re-use strategies to generate an additional 17 (9% of total coal-fired TPS generating capacity), 27 (6%), 19 (8%), and 5 (4%) GW of electricity in the 2015, 2050-REF, 2050-S2, and 2050-S3 scenarios, respectively. These inventories were used as input to the GEOS-Chem model to simulate ambient $PM_{2.5}$ and two-week simulation results presented here find improvements in population-weighted average concentrations, ranging from 1.2% to 6.6% percent reductions. Previously assessed strategies, including cleaner fuel sources and implementation of emission-control technologies, offer much larger air quality and carbon mitigation benefits in India and are the ideal path toward improved air quality and carbon mitigation efforts in India.

6.1 Introduction

Exposure to elevated levels of ambient air pollution, namely fine particulate matter ($PM_{2.5}$), is associated with adverse health outcomes and is estimated to contribute to 600,000 premature mortalities each year in India (219). India experiences some of the highest levels of ambient pollution in the world and the most recent World Health Organization (WHO) dataset found nine of the 10 most polluted cities in the world are in India. In addition, India is the third-highest carbon (CO_2 and CH_4) emitter in the world, emitting 3,100 Mt of CO_2-equivalent in 2017, which is approximately 7% of the global total. Carbon emissions from India are growing at approximately 6% yr^{-1} while emission rates in China and the U.S., the only two countries that emit more carbon than India, have remained steady and decreased, respectively, over the last few years (220). Recent studies have characterized carbon emissions and poor air quality throughout India and have identified various strategies for emission mitigation (14, 221); despite these efforts, carbon emissions have continued to increase (220) and there has been no noticeable improvement in ambient air quality in the last decade and a half (222). Furthermore, forecasts of both carbon and $PM_{2.5}$ emission rates expect large emission increases throughout India over the coming decades (223, 224).

Currently, residential biomass burning (including wood, crop, and dung cake) used as fuel for cooking and heating is the largest contributor to ambient $PM_{2.5}$ pollution in India, despite being an indoor activity (9, 223). Total emissions from residential biomass burning are expected to decrease in magnitude as cleaner fuel sources in households will continue to be introduced throughout India (225). Greenhouse gas (GHG) emissions in India, on the

other hand, are dominated by emissions from the power sector; the power sector in India contributes to half of the present-day GHG emissions of the total organized sectors (226).

At present, India has ~210 GW of electricity generation capacity, with the majority of it (57-76%) coming from coal-fired power plants (227-229). The generation capacity from coal will continue to grow in the coming years as new plants will be coal-fired. The current and next five-year plans call for 76 GW and 93 GW coal expansion, respectively, and Prayas and colleagues (230) have reported that 700 GW of power generation from coal is forthcoming, including from new Ultra Mega Power Projects (UMPP). UMPPs are coal-fired power plants each with generating capacity of 4 GW or more. These have begun to be commissioned throughout India with the aim of generating 100 GW of additional capacity by 2022. It is expected that each UMPPs will emit 28-29 Mt of CO_2 each year (231), which means that each plant will emit more than 1% of the total current national CO_2 emissions. The total coal consumption is projected to increase by a factor of three over the next decade and a half (660 millions tons $year^{-1}$ in 2014 to 1800 millions tons $year^{-1}$ in 2030) (232-234), and the current coal growth rate is expected to generate more than 1 billion tons of additional carbon emissions yearly within two decades (220). The anticipated growth in coal-fired power plants and industry activity will result in future (in 2050) $PM_{2.5}$ source contributions in India dominated by power plant and industrial coal combustion emissions (33%) (followed by dust (20%) and residential biomass burning (13%)), so strategies aimed to reduce carbon emissions from power plants can also greatly improve ambient air quality (223).

With the expected growth of coal-fired power plants, there is a pressing need to reduce carbon and air pollution emissions from these sources. All Indian coal-fired TPSs

have electrostatic precipitators (ESPs) currently on-site to control for PM emissions (227) and the Central Pollution Control Board (CPCB) finds the ESP efficiencies to be 99.5 to 99.9% (235); the fraction for $PM_{2.5}$ from ESPs is slightly lower at ~98% (236). The Indian Ministry of Environment and Forest (MoEF) issued a draft notification in 2015 to control for SO_2 (precursor to aerosol sulfate), NO_x (precursor to aerosol nitrate), PM, and Hg, and that power plants were to comply by Dec. 2017. However, by this date, almost no plants had installed controls and the deadline was extended to 2022 (237). Compliance of such standards will have large benefits for ambient air quality (227). Previous studies have assessed the potential of renewable energy production in India and have found such approaches will result in large carbon and air pollutant emission reductions (223, 238). The high primary installation costs of renewables has been a barrier of widespread implementation, but recent studies have found that when considering government subsidies, the cost of investing in renewable energy in India is similar to the operating cost of fossil-fuel based power plants (237, 239).

Coal-fired power plants (and other large sources like cement facilities, iron and steel plants, and agricultural burning) emit large amounts of waste-heat and re-utilizing such waste-heat offers additional opportunities to generate electricity. The Organic Rankine Cycle (ORC) utilizes low- and medium-grade waste heat to be recovered from industrial processes and operates similarly to a traditional steam Rankine cycle except that it uses an organic working fluid as opposed to steam. The organic working fluid (e.g., R-134a, R-236ea, R-245fa, etc.) has a lower boiling point and a higher vapor pressure than water, thus allowing the ORC to re-utilize lower temperature exhaust. ORC technology has been implemented in a cement (4 MW recovery) and iron and steel plant (125 KW

recovery) in India, and a recent report from an Indo-German Energy Forum specifically indicated that waste-heat recovery can be undertaken in the cement industry, iron and steel industry, and with large-scale open biomass burning in India (240).

The anticipated growth in coal consumption can also lead to opportunities for increased fly-ash re-utilization at cement and brick production plants. Indian coal is ~35% (28-42) fly-ash content (241-243) and presently the re-utilization rate in cement and bricks industries is considerably lower than industry standards.

Using an all-India emission inventory in 2015 (base year) projected to 2050 under various policy adoption strategies, we will estimate the additional carbon emission offsets and $PM_{2.5}$-air quality impacts that can be achieved from power plant and industrial waste-heat to electricity using Organic Rankine Cycles (ORCs) and material exchange pathways (e.g., coal fly-ash as substitute for brick and cement production).

6.2 Methods and Materials

The emission inventory used in this work is the most comprehensive and complete emission inventory over India to date and is explained in more detail in: Venkataraman and colleagues (223), Pandey and Venkataraman (244), Pandey and colleagues (245), and Sadavarte and Venkataraman (226). Briefly, the inventory includes spatially-resolved (25km x 25km) $PM_{2.5}$, black carbon (BC), organic carbon (OC), SO_2, NO_x, and non-methane volatile organic compounds (NMVOCs) from major Indian sources including power plants (coal-fired and natural gas-fired), industries (e.g., cement, brick kilns, steel, etc.), residential biomass (e.g., cooking, heating, and lighting), transportation, distributed diesel, open burning, and anthropogenic dust. The inventory includes a base year emission

in 2015 and three scenarios projected to 2050. The 2015 inventory is based on an engineering technology-linked energy emission modeling approach that includes technology parameters for process and emissions control technologies, including technology type, efficiency, or specific fuel consumption and technology-linked emission factors (g pollutant kg^{-1} fuel) to estimate emissions (223). The 2050 projected emissions are defined in three pathways: (1) 2050 Reference Scenario (2050-REF); (2) 2050 Aspirational Scenario (2050-S2); and (3) 2050 Ambitious Scenario (2050-S3). The 2050 scenario inventories were developed with expected future evolution of sectoral demand from the 2015 inventory and capture varying levels of emission control adoption (e.g., changing fuel sources and adopting control technologies). 2050-REF corresponds to slow uptake of new, cleaner technology, 2050-S2 corresponds to effective achievement of currently-proposed targets under the Perform, Achieve, and Trade (PAT) scheme, and 2050-S3 corresponds to ambitious regulatory achievement. Specifically from the power supply sector, the 2050-REF projection has a low influx of renewable energy, the 2050-S2 scenario assumes 40% achievement of renewable energy share by 2030 (one of the targets identified in India's agreement into the Paris Climate Accord), and the 2050-S3 scenario achieves 75-80% of non-fossil power generation and 80-95% of flue-gas desulphurization controls (Table 6-1).

The cascading scenarios assessed here first estimate the amount of electricity that can be generated from waste-heat-powered ORCs at coal-fired Thermal Power Stations (TPSs) and large point sources (e.g., cement industry, iron and steel industry, and agricultural burning). This amount of generated electricity will equivalently be offset at coal-fired TPSs by reduced coal consumption. Following the coal consumption offsets

attributed to the additional electricity generated from waste-heat capture with ORCs, material exchange pathways of coal fly-ash to brick and cement production are assessed.

6.2.1 Electricity generated from Organic Rankine Cycles (ORCs) at Thermal Power Stations (TPSs) and large point sources added to the National Grid to offset coal-consumption at TPSs

Coal combustion at thermal power stations (TPSs) in India is generally inefficient, and it can be estimated that each unit of coal combusted gives ~33% electricity generation, 56% waste heat, and the remaining 11% is lost (15, 227). Waste heat is split into different grades (high-grade >400°C, medium-grade 100~400°C, low-grade <100°C) and the efficiency of Organic Rankine Cycle (ORC) recovery is a function of temperature (246). We assume no high-grade waste heat is lost from TPSs, as high-grade heat should be previously converted to electricity. We assume the waste-heat is distributed evenly between medium-grade waste heat and low-grade waste heat, consistent with previous literature on waste-heat recovery from power plants (15). Low- and medium-grade waste heat conversion to electricity efficiencies at coal-fired TPSs will be disrupted by SO_2 fouling, and we use literature estimates of the fouling efficiencies by waste-heat grade in this analysis (15). We assume the ORC efficiency is 20% for the medium-grade waste heat and 10% for low-grade waste heat, a conservative efficiency estimate based on modeling results or ORC efficiencies (246) (Figure E-1). Emission pathways in the 2050 inventories used here anticipate higher natural gas generating capacity in India in 2050 (although the fraction of coal will still be 48% in 2050-REF, 25% in 2050-S2, and 13% in 2050-S3) (223). Current natural gas plants in India are all combined cycles (247), so we anticipate any new natural gas plant will also be a combined cycle. Although previous studies have explored ORC implementation as the bottoming cycle of a combined cycle plant (248), we

could not find any literature or evidence on further ORC utilization of post-combined-cycle waste heat. As a result, we do not estimate any additional amount of electricity that potentially can be generated from waste-heat at combined-cycle natural gas facilities. Coal consumption at TPSs equivalent to the amount of electricity that was produced from ORC waste-heat reclamation at coal-fired TPSs is offset in the scenario tests. The findings here should be interpreted as a first-order approximation; the coal needs to be combusted for the available waste-heat to generate electricity from the ORC, but will subsequently be offset by the initial coal consumption.

Next, we estimate the amount of electricity that can be generated from ORC waste-heat recovery at cement plants throughout India. A cement plant in Andhra Pradesh currently utilizes an Organic Rankine Cycle (ORC) for on-site electricity generation, and the electricity generation rate measured there was 1.6 MW 2,500 $tons^{-1}$ day (at an average exhaust temperature of 320°C) (240, 249). Without more detailed information in India on specific, individual cement-plant technologies or waste-heat characteristics (e.g., temperature exhaust distributions from the various processes), this same production to electricity (which is at a conservative 10% ORC efficiency) is used for each cement plant. Cement plants in India are mostly coal-fired and captive power plants; they generate power on-site to avoid higher grid costs and to avoid power shortages and power failures (250), so ORC-generated electricity could potentially be utilized on-site, which could lead to local coal consumption reductions. A previous case-study in India estimates that ORC on-site waste-heat exhaust recovery can be equivalent to 30% of the electricity used in a cement plant (251). However, without site-specific data of electricity demand from the grid at each plant and co-generated electricity on-site from traditional recovery processes, we are

unable to assess how much of the waste-heat ORC-generated electricity could be re-utilized locally, so we will apply the generated electricity to the national grid. Currently, only five (out of an estimated 150) cement plants have adopted waste-heat to electricity systems (250). To account for the current efficiency, the generation efficiency at the Andhra Pradesh plant (1.6 MW from ORC 2,500 $tons^{-1}$ day) is scaled by 0.953 (5/150). In this analysis, we will apply the estimated cement plant ORC-generated electricity to the national grid and subsequently offset the associated emissions to generate that same amount of electricity from coal-fired TPSs.

Open waste burning is a growing phenomenon throughout India, particularly during the agricultural burning seasons and has become a growing concern to air quality in India, especially in the Delhi-National Capital Region (Delhi-NCR) (252). Crop residue burning to electricity generation has been commissioned in a few Indian states (253), and there is a large amount of surplus residue throughout India that gets burned that could be re-utilized for energy generation (254). The electric generating potential of agricultural burning is estimated as:

$$Q_i = (ARB_i * LHV_i) * \eta$$

Where $Q_i$is the energy potential (GJ $year^{-1}$) from agricultural product, i, ARB is the agricultural residue burned (tons $year^{-1}$), LHV is the lower heating value (GJ ton^{-1}) found in Singh et al. (255), and η is the ORC efficiency, here conservatively estimated as 0.2. This analysis does not consider the emissions associated with collecting or transporting large amounts of crop residue to centralized ORC facilities or emissions associated with the ORC installation. The equivalent amount of electricity generated from the ORCs by

agricultural residue burning will be offset by reduction in coal consumption (and associated air pollution and CO_2 emissions) at coal-fired TPSs.

India is the fourth largest producer of crude steel and the largest producer of sponge iron (also referred to as direct reduced iron (DRI)) globally (256, 257). Waste heat is generated at multiple processes during steel production including at rolling units, forging units, strip processing units, heat treatment units, blast furnaces, sinter, and electric arc furnaces (EAFs). However, exhaust gas from each of these activities are highly contaminated and "present a challenge for economic waste-heat recovery" (240). Literature assessments have found ORC waste-heat systems are suitable for energy recovery at the exhaust stream of rolling units and at EAFs. Data from ORCs that were deployed at representative rolling mill (n=362) and EAF (n=190) sites throughout Europe (no literature was found in India) found the average electricity generating rate at rolling mills (with exhaust at 400°C) to be 1.23 kW ton-steel^{-1} and 4.3 kW ton-steel^{-1} at EAFs (258). In this analysis, we will apply the potential ORC-generated electricity from steel plants (rolling mills and EAFs only) to the national grid and subsequently offset the equivalent coal consumption (and associated air pollution and CO_2 emissions) at coal-fired TPSs.

6.2.2 Coal fly ash from Thermal Power Stations (TPSs) material exchange pathway for re-utilization in cement and brick plants

Coal ash is a nutrient rich by-product of coal combustion and is used in India and the rest of the world as material addition for various industrial processes, including cement production and brick production (259). Indian coal is ~35% (28-42) fly-ash content (241-243), and considering the projected increases in coal consumption, fly-ash will continue to be available as material substitution in both the cement and brick industries. According to

the Central Electricity Authority (CEA) ~170 MT of fly ash was generated from 155 TPSs from which data was received (capacity = 157.4 GW; coal consumed = 510 MT) (242). In the emission inventory used here, the estimated total capacity of the coal-fired TPSs is 196, 490, 250, and 125 GW in the 2015, 2050-REF, 2050-S2, and 2050-S3 scenarios, respectively. Using the same ratio of fly-ash generated to electricity produced as reported by the CEA, we estimate 193, 500, 248, and 130 MT of total fly-ash from TPSs is available for re-utilization in cement and brick production in the four scenarios. Without more detailed data available, we assume all of the ash generated is fly-ash that is collected from electrostatic precipitators (ESPs), which are installed at all coal-fired TPSs in India.

In 2015, 60.8% of generated fly-ash has been utilized already in various applications, including: cement production, brick and tile production, roads, reclamation of low lying areas, etc. (259). Present CEA estimates find that 40 MT of fly ash is going to cement production out of an estimated 330 MT cement produced each year (12% of total cement mass) (242, 260), but the Bureau of Indian Standards (BIS) suggests that cement can be 35% by mass fly-ash. A recent study of Indian cement found that the performance (e.g., compressive strength) of cement does not significantly change when the fly-ash content is increased to 50% by mass (261). For this analysis, though, we will re-utilize fly-ash up to the BIS prescribed standard of 35% by mass. If additional fly-ash is available following reclamation pathways in cement production, fly-ash to brick production will then be administered. We choose to apply coal fly-ash to cement production first because more spatially-resolved emission estimates are available for the cement industry and there are fewer cement plants (n ~=210) than traditional brick kilns (n ~=100,000) throughout India, which can allow for more feasible fly-ash transport. Further, the brick production industry

is highly unorganized in India (262) and the nationwide emission estimates used here are built using proxies for brick kiln locations. Currently 3% of brick is fly-ash, but bricks achieve the same standards and mechanical properties of standard clay bricks with fly-ash content up to 20% by weight (263). Here, we only consider these material pathways for coal fly-ash reclamation, as we do not have spatially resolved emission estimates for other industries that may utilize fly ash. The available coal fly ash first goes toward cement production, and if any coal-fly ash remains, then it goes toward brick production. In this analysis, the generated fly-ash at coal-fired TPSs is only allowed to transfer up to 300 km away from the TPS, consistent with current maximum distances transported for fly-ash reutilization (242). The impacts on the 2050 projected emission scenarios will use the same methods outlined in the 2015 scenarios for NON-PAT cement and traditional brick kiln sectors, but in the 2050-S2-WHME scenarios we assume the default fly-ash re-utilization rate to increase to 20% for cement production and 10% for brick production.

Opportunities for on-site material exchanges may currently be happening with bottom-ash (larger and of different chemical composition than fly ash) that deposit to the base of the exhaust chimney. However, without any documented control technologies to capture fly ash at either cement or brick production facilities, it is unlikely that any generated fly ash is being used for material substitution at non-PAT cement and traditional brick kilns in India. Thus, we do not assess on-site generated fly-ash material pathways for local emission reductions. The CO_2 and air pollution emissions at the local cement and brick production facilities are perturbed with the rationale that the fly ash does not need to be fired during production, i.e., for every unit percent fly-ash mass re-utilization at cement and brick plants, local on-site coal-combustion is reduced by one unit percent. The

maximum achievable emission reductions from non-PAT cement plants is 23% in 2015-WHME, 2050-REF-WHME, and 2050-S2-WHME (35% BIS standard minus 12% current fly-ash by mass) and 15% in 2050-S3 (35% BIS standard minus 20% fly-ash by mass). The maximum emission reductions from traditionally-fired brick production plants is 17% in 2015-WHME, 2050-REF-WHME, and 2050-S2-WHME (20% fly-ash standard minus 3% current fly-ash by mass) and 10% in 2050-S3-WHME (20% fly-ash standard minus 10% current fly-ash by mass).

6.2.3 Air pollution modeling in GEOS-Chem, evaluation with U.S. Embassy monitor observations in five Indian cities, and CO_2 emission inventory accounting

The four initial inventories (2015, 2050-REF, 2050-S2, and 2050-S3) and the four waste-heat and material exchange (WHME) inventories applied "on top" of the four initial inventories (2015-WHME, 2050-REF-WHME, 2050-S2-WHME, and 2050-S3-WHME) are used as input to the GEOS-Chem Model to simulate surface-level $PM_{2.5}$ in India. GEOS-Chem is a global 3-D model of atmospheric chemistry that uses meteorological input from the Goddard Earth Observing System (GEOS) (264). Meteorology used in these simulations were from the 2015 GEOS-Forward Processing (GEOS-FP) product. Here, we use GEOS-Chem v12.6.3 (DOI: 10.5281/zenodo.3552959) to simulate $PM_{2.5}$ concentrations at a 0.25° x 0.3125° resolution nested-grid over India following a three-month global spin-up that was done at a 2° x 2.5° resolution. In the global spin-up and the nested simulations, the emission inventories (2015, 2050-REF, 2050-S2, 2050-S3, 2015-WHME, 2050-REF-WHME, 2050-S2-WHME, and 2050-S3-WHME) masked emissions over India from other regional and global inventories. Ammonia emissions from industry, power supply, residential, transport, and agriculture are included from the Asia-MIX inventory (265), and we use the same inventory for the 2015 and each of the 2050 runs,

consistent with previous model methodologies outlined in Venkataraman et al. (223). For this analysis we use the same meteorology (i.e., 2015 GEOS-FP) for 2015 and all 2050 simulations (Table 6-1). The meteorology and atmospheric conditions over India will change between 2015 and 2050, due in part to both climate- and aerosol-forcing effects, and projecting future meteorology in-line with emissions or under climate-change scenarios is out of the scope of this analysis. The simulated results for 2015 are evaluated against five surface-level observations from the US Embassy/consulate stations in Chennai, Kolkata, Hyderabad, Mumbai, and Delhi. We do not compare the results here against simulation findings presented in Venkataraman and colleagues (223) as those results were generated using an older version of Geos-Chem (v.10.01) and the meteorological fields were from 2012 not 2015 as there was a change in the GEOS assimilation system during that time which did not allow them to assess 2015 meteorology. We report population-weighted concentrations and assume the population distribution is the same in each of the 2050 scenarios as in the 2015 scenario.

Table 6-1: Overview of 2015 and 2050 scenarios before and after waste-heat and material exchange (WHME) pathways. The waste-heat to electricity pathway is through Organic Rankine Cycles (ORCs) at coal-fired Thermal Power Stations (TPSs) and at other large sources (cement, iron and steel, and agricultural burning). The generated electricity from ORCs at these sources offsets coal consumption at an equivalent amount of electricity produced at TPSs. Material exchanges assessed here are for coal fly-ash reclamation for cement and brick production, which offsets local production emissions.

	Base Inventories from Venkataraman et al.	**Waste-Heat and Material Exchange Extensions**
Air pollution modeling configuration **MODEL**: GEOS-Chem v12.6.3	**2015**: Base-case 2015 emissions	**2015-WHME**: Base inventory with waste-heat to electricity and material exchange pathways
	2050-REF: All emission sectors are projected under current regulation for energy efficiency and emission controls	**2050-REF-WHME**: 2050 REF inventory with waste-heat to electricity and material exchange pathways

METEOROLOGY: GEOS_FP **INDIA NEST RESOLUTION**: 0.25° x 0.3125°	**2050-S2**: All emission sectors are projected broadly under promulgated future policies	**2050-S2-WHME**: 2050-S2 scenario with waste-heat to electricity and material exchange pathways
	2050-S3: All emission sectors are projected with ambitious adoption of cleaner technologies, beyond what has been proposed in S2	**2050-S3-WHME**: 2050-S3 scenario with waste-heat to electricity and material exchange pathways

6.3 Results

6.3.1 Electricity generated from waste-heat reclamation at coal-fired Thermal Power Stations (TPSs) and other large sources (cement plants, iron and steel plants, open agricultural burning) and associated coal consumption offsets at coal-fired TPSs

Organic Rankine Cycle (ORC) waste-heat to electricity recovery at Thermal Power Stations (TPSs) and other large sources in India including cement plants, iron and steel plants, and open agricultural burning leads to an estimated 16.9, 27.3, 19.4, and 4.5 GW of electricity recovery in the 2015-WHME, 2050-REF-WHME, 2050-S2-WHME, and 2050-S3-WHME scenarios, respectively. This account for 8.6% (6.3%), 5.6% (2.7%), 7.8% (1.9%), and 3.6% (0.4%) of the coal-fired (and total) electricity generated in the four scenarios. The amount of electricity generated in each of the scenarios corresponds to 26%, 17%, 24%, and 11% of total coal consumption offsets and emission reductions at coal-fired TPSs, respectively (Table 6-2). The total amount of electricity recovered is highest in the 2050-REF-WHME scenario, but the percent of coal offset due to the recovery is lower than in 2015-WHME or 2050-S2-WHME scenarios, which is explained by the larger amount of coal consumed in the 2050-REF-WHME scenario (490 GW electricity production from coal-fired power plants). In each of the four scenarios, the waste-heat to electricity potential is highest at coal-fired TPSs and for open burning than at either cement plants or iron and steel plants, the two industries where ORCs have been administered already in India. The

ORC potential for agricultural burning stays relatively constant between 2015-WHME and the 2050-REF-WHME and 2050-S2-WHME scenarios because the amount of generated crop residue is projected to remain constant (223).

At TPSs specifically, ORC-generated electricity from waste-heat reclamation at TPSs offers 7.1, 17.8, 9.1, and 4.5 GW of additional electricity in the 2015-WHME, 2050-REF-WHME, 2050-S2-WHME, and 2050-S3-WHME scenarios, respectively (Table 6-2). The amount of total electricity produced per unit input coal increases to 36.64% from 33% using ORC-recovery systems (Figure E-1), and as a first-order approximation, this will reduce the combusted coal at each coal-fired TPS by 11.0% to produce the equivalent amount of electricity. This is a first-order approximation; the electricity generated from waste heat here requires the coal to be combusted at the power plant. However, if the coal is not combusted, the waste heat is not available to generate additional electricity.

6.3.2 Local cement and brick production emission reductions from coal fly-ash material exchanges from coal-fired Thermal Power Stations (TPSs)

Following the coal consumption reductions at TPSs due to the additional electricity supplied by ORCs, the potential for material exchanges with the coal fly ash to brick and cement production were assessed. The generated fly ash from the four scenarios (2015-WHME, 2015-REF-WHME, 2050-S2-WHME, and 2050-S3-WHME) following ORC-related coal reductions at TPSs is estimated to be 193, 500, 248, and 130 MT of coal fly-ash, respectively. Following the assumption that coal is re-utilized already at 60.8% (259) for the 2015 and 2050-REF scenarios and is re-utilized at 80% in the 2050-S2 scenario, the available coal fly-ash for material exchanges to the cement and brick sector is found to be 76, 196, and 50 MT of cement in the three respective scenarios (Table 6-2). In 2050-S3,

the cement and brick production facilities are projected to be zero emissions, so despite coal fly-ash availability, we assume none will go towards offsetting any local cement or brick production emissions.

Table 6-2: Estimated electricity generation potential from ORC technologies at Thermal Power Stations (TPSs) and other large source activities (cement production, iron and steel production, and open burning) in 2015 and 2050 projected under three policy-adoption scenarios

	2015		2050-REF		2050-S2		2050-S3	
Traditional Energy Generation								
All power plants (MW)	270e3		1020e3		1020e3		1020e3	
Coal-fired power plants (MW)	196e3		490e3		250e3		125e3	
Sectors for waste-heat to electricity generation	Amount of electricity generated (MW)	Percent of TPS Coal reduced*	Amount of electricity generated (MW)	Percent of TPS Coal reduced*	Amount of electricity generated (MW)	Percent of TPS Coal reduced*	Amount of electricity generated (MW)	Percent of TPS Coal reduced*
Thermal Power Stations	7.1e3	11%	17.8e3	11%	9.1e3	11%	4.5e3	11%
Cement plants	485	0.74%	888	0.55%	792	0.96%	0	0
Iron and Steel plants	148	0.12%	210	0.13%	196	0.23%	0	0
Open burning	9.2e3	14.10%	9.3e3	5.70%	9.3e3	11.3%	0	0
Material Exchange	Mass of fly-ash re-utilized (MT)	Percent of maximum re-utilization	Mass of fly-ash re-utilized (MT)	Percent of maximum re-utilization	Mass of fly-ash re-utilized (MT)	Percent of maximum re-utilization	Mass of fly-ash re-utilized (MT)	Percent of maximum re-utilization
Additional fly-ash re-utilization for cement production	75.3	100%	196.4	59%	49.7	15%	0	0%
Additional fly-ash re-utilization for brick production (MT fly-ash)	0.5	<0.1%	8	<0.1%	4	<0.1%	0	0%

The maximum fly-ash potential in cement under the BIS standard of 35% is 75 MT in 2015 and 335 MT in the 2050-REF and 2050-S2 scenarios (this is a fraction of the amount of cement produced). For the cement exchange pathway, we find that there is enough available fly ash in 2015 to completely meet the BIS threshold for fly-ash re-utilization, but not enough in either the 2050-REF-WHME or 2050-S2-WHME scenarios even though more fly-ash is generated in these scenarios. This occurred because the growth rate in the cement sector (e.g., construction demand) exceeds the fly-ash production growth rate. The material exchange is associated with 23% emission reductions from cement plants in 2015 and 13% reductions in 2050-REF-WHME and 2.3% reductions in 2050-S2-WHME.

6.3.3 *Simulated $PM_{2.5}$ in GEOS-Chem and evaluation with U.S. Embassy monitors in five Indian cities*

The coal consumption offsets at TPSs and local reductions at cement and brick production facilities had a slight effect on nationwide population-weighted $PM_{2.5}$ levels as simulated in GEOS-Chem (Figure 6-1).

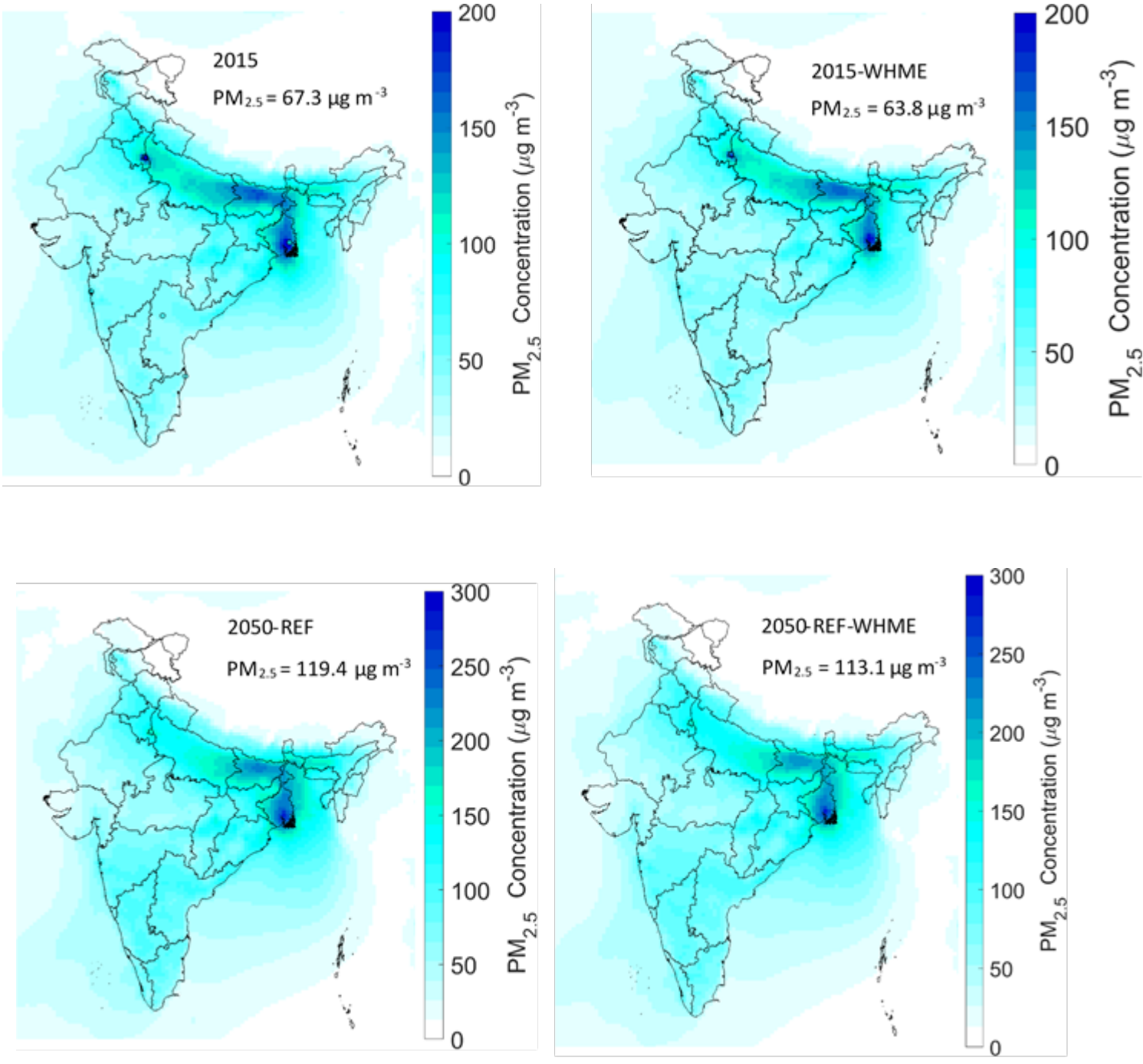

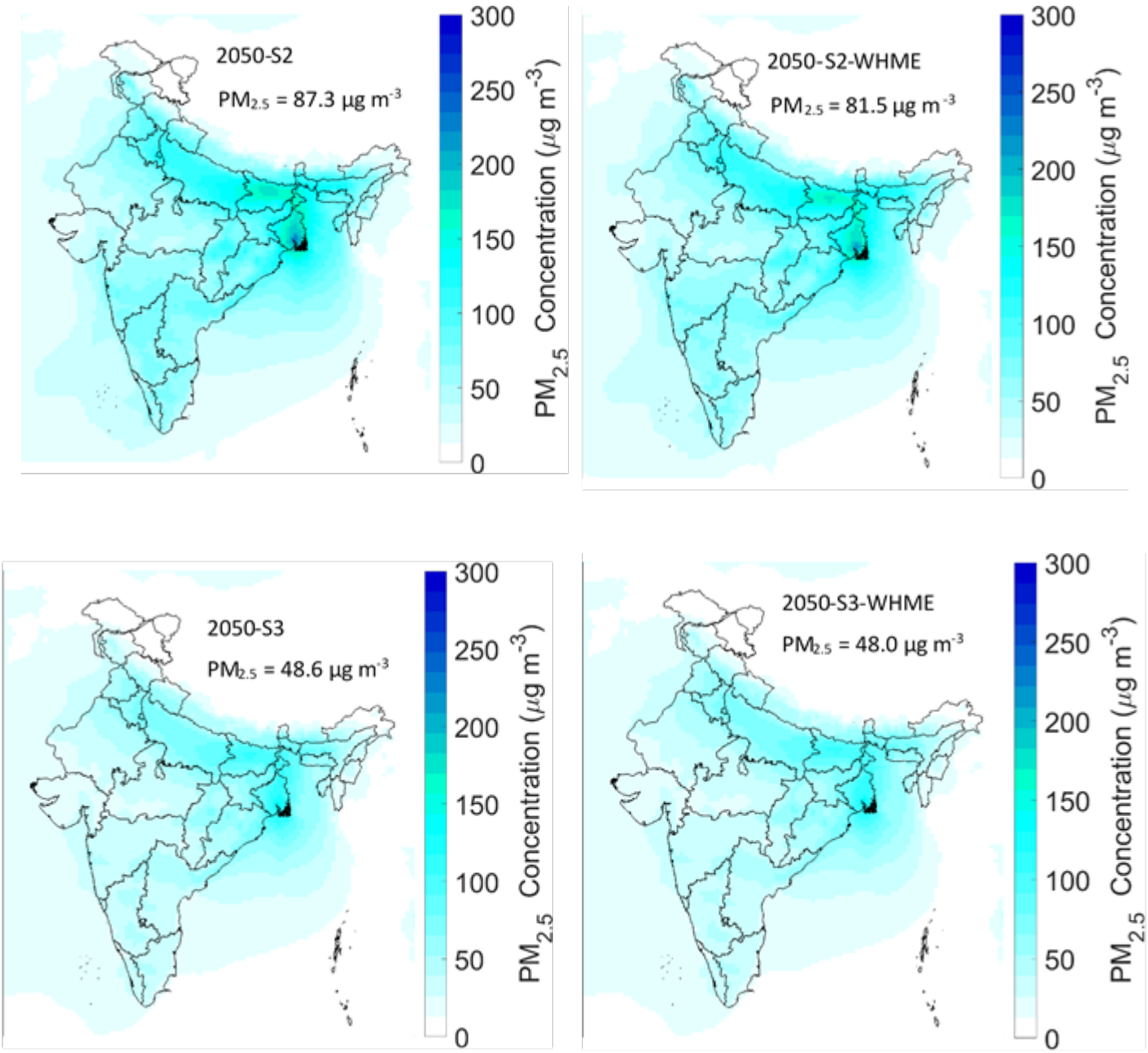

Figure 6-1: Two-week (Jan. 1, 2015 - Jan. 14, 2015) simulated $PM_{2.5}$ concentrations over India from the base inventories (2015, 2050-REF, 2050-S2, and 2050-S3) and the base inventories with waste-heat and material exchange (WHME) pathways (2015-WHME, 2050-REF-WHME, 2050-S2-WHME, and 2050-S3-WHME). The concentrations reported on each spatial map are population-weighted average concentrations. The colored circles in the 2015 concentration profile indicate average $PM_{2.5}$ measured at U.S. Embassy sites in Chennai, Kolkata, Hyderabad, Mumbai, and New Delhi. The 2015 profiles are also on a different color-scale axis.

The 2015 simulations were evaluated against averaged U.S. Embassy observations and showed varying levels of agreement (Figure 6-1 and Table 6-3). We saw very close agreement in New Delhi for the two-week simulation evaluation, but each of the other cities had at least a 10% difference between the GEOS-Chem simulations and the observed levels. The resolution of the GEOS-Chem model is 0.25° x 0.3125° and large concentration gradients will exist within each grid, which may not capture the local conditions at the Embassy monitoring locations. In addition, the Embassy monitors are typically representative of urban, background levels and are in relatively clean parts of the cities, which the emission inventories used here, at a 25 km x 25 km resolution cannot capture. In addition, the two-week simulation findings presented here will be largely influenced by the initial conditions and boundary conditions, and the results from the three-month spin-up for all eight scenarios were not used for the simulation results presented here.

Table 6-3: Evaluation of GEOS-Chem simulated $PM_{2.5}$ with observations from the U.S. Embassy sites throughout India in 2015

City	GEOS-Chem Simulated $PM_{2.5}$ ($\mu g\ m^{-3}$)	Observed $PM_{2.5}$ ($\mu g\ m^{-3}$)	Percent Difference
Chennai	32.0	58.8	-45%
Kolkata	170.0	139.1	22%
Hyderabad	55.9	64.1	-13%
Mumbai	70.7	85.4	-17%
Delhi	195.1	202.7	-4%

6.4 Conclusions

India is home to 1.3 billion people who are exposed to some of the highest levels of ambient air pollution in any country of the world. Exposure to $PM_{2.5}$ is estimated to contribute to 600,000 premature mortalities each year nationwide. In addition, India is the third-highest leading CO_2-eq emitting country in the world, and unlike China and the U.S., CO_2 emissions in India are increasing. Recent research studies (14, 223, 266) and research commentaries (267) have identified the urgent need to implement strategies to reduce both air pollutant and climate-forcing gas emissions and have indicated the strong environmental and human health benefits of such actions. The findings presented here assess the air quality and CO_2 emission impacts of re-utilizing waste-heat from coal-fired Thermal Power Stations (TPSs) and other large sources (cement production, iron and steel production, and open agricultural burning) to generate additional electricity and material exchange pathways using coal fly-ash in cement and brick production. We found these approaches offer modest improvements in $PM_{2.5}$-air quality and modest reductions in CO_2 emissions, and although still potentially helpful, ambitious regulatory achievement of cleaner fuel sources and cleaner technologies has been show to offer much larger air quality and human health benefits (223).

CHAPTER 7. CONCLUSIONS AND FUTURE WORK

The focus of the chapters presented in this thesis were to assess the air pollution and human health outcomes of various policy interventions in the United States, India, and China, explore relationships of air pollution with other environmental or sustainability outcomes, and to characterize air pollution spatial gradients within cities. The findings presented in this work have the opportunity to assist policy makers in designing more sustainable cities for improved air quality and air pollutant and greenhouse gas emission reductions.

First, as part of an interdisciplinary and intercultural team, I worked on a project to quantify how $PM_{2.5}$ emissions from biomass burning, including from municipal solid waste (MSW) and dung cake burning, are discoloring the surface of the Taj Mahal. The focus of this work was to address the discoloration of an icon of Indian culture as means to improve air quality and public health. In this work, I helped develop spatially detailed activity and emission estimates of MSW and dung cake burning from on-site fieldwork and found that Agra burns ~23% of its generated waste. I used an air quality model to simulate $PM_{2.5}$ impacts in Agra and found that MSW burning contributed 12 times more $PM_{2.5}$ at the Taj Mahal than dung cake burning, which was previously banned within the city. In conjunction with detailed population and demographic data, 713 premature mortalities each year are attributed to exposures of air pollution from MSW and dung cake burning emissions. The findings from this work resulted in citizen-led protests in Agra for action (which lead to a police lathicharge against them). Also, the Archaeological Society of India (ASI) initiated their own study of the sources of ambient air pollution near the monument in response to our findings and concluded that MSW burning was also a leading contributor

to the pollution at the Taj Mahal. More recently, under the guidance of the UN Environment Programme and Clean Air Asia, a multi-stakeholder Agra Air Action Plan was developed and indicated garbage and municipal solid waste burning needs to be addressed in Agra. Solutions for air pollution mitigation should be equitable, i.e., solutions must consider societal factors involved and disproportionately affect those who cannot protect themselves. The India government banned the burning of cow dung cake as cooking fuel following the source apportionment component of the study; however, they did not introduce cleaner cooking fuels as substitute. Such bans disproportionately affect poorer communities who do not have access to cleaner fuel sources. We recommended a better waste management infrastructure (and not a ban), which has previously been assessed and planned in an official Agra government document, as an equitable solution to control waste burning emissions, the discoloration of the Taj Mahal, and public health.

In the work presented in Chapter 3, I again had the opportunity to work on an interdisciplinary and intercultural team that assessed the potential of a novel urban-industrial symbiosis strategy for carbon mitigation with local health co-benefits in 637 Chinese cities. Here, novel cross-sectoral strategies, which includes the use of waste heat re-use for commercial and district energy and heating, were assessed throughout China, and we found these interventions could contribute an additional 15-36% to national CO_2 emission reductions when compared to conventional single-sector strategies. As a co-benefit, ~25,500 to ~57,500 deaths annually are avoided from air pollution reduction. The benefits are highly variable across cities, ranging from <1%–37% for CO_2 emission reduction and <1%–47% for avoided premature deaths. These results that use multi-scale, multi-sector physical systems modelling identify cities with high carbon and health co-

benefit potential and show that urban–industrial symbiosis is a significant carbon mitigation strategy, achievable with a combination of existing and advanced technologies in diverse city types.

The work presented in Chapter 4 explored the links between air quality and emotional well-being (EWB) and air quality and neighborhood infrastructure in Minneapolis, MN. I collected ambient $PM_{2.5}$ measurements using low-cost air quality sensors and modeled on-road mobile-source NO_x using the Research-LINE (R-LINE) source dispersion model for near-surface releases and found no statistically significant (α=0.05) $PM_{2.5}$ differences between urban poor and urban middle-income neighborhoods but did find average mobile-source NO_x was significantly (α=0.05) higher in the four urban neighborhoods than in the two suburban neighborhoods. Close proximity to light rail had no observable impact on average observed $PM_{2.5}$ or simulated mobile-source NO_x. Home-based EWB exposure assessments found that $PM_{2.5}$ was negatively correlated with positive emotions such as happiness and to net affect (the sum of positive and negative emotion scores), and positively correlated (i.e., a higher $PM_{2.5}$ concentration led to higher scores) for negative emotions such as tiredness, stress, sadness, and pain. Simulated mobile-source NO_x, assessed from both home-based exposures and in-situ exposures, had a near-zero relationship with all EWB indicators. This was attributed to low NO_x levels throughout the study neighborhoods and at locations were the EWB-assessed activities took place, both owing to low on-road mobile-source NO_x emissions. The findings from this work, although specific to Minneapolis, MN., suggest linkages between air quality, neighborhood infrastructure, and EWB that cities may utilize in future development.

Next, I compared $PM_{2.5}$, NO_2, and CO at near-road sites with other non-near-road, regulatory monitors within U.S. cities. After controlling for primary emissions from the target highways, we found no statistical difference ($\alpha = 0.05$) in $PM_{2.5}$ concentrations between the near-road and non-near-road urban sites (δ = 0.42 (-0.08-0.90) μg m^{-3}, n=35 comparisons). NO_2 and CO levels, on average were significantly higher at the near-road sites compared to the non-near-road urban sites by 5.0 (3.4-6.5) ppb (n=44 comparisons) and $9.2x10^{-2}$ (0.04-0.14) ppm (n=42 comparisons), respectively. The average $PM_{2.5}$ difference found here is 5%, and at 14 of the 35 (~40%) urban monitor comparisons and 28 of the 72 (~39%) overall comparisons, $PM_{2.5}$ is actually higher at the non-near-road site relative to its near-road pair. The same observational data was used to assess mobile source emission estimates from the EPA National Emission Inventory, and analysis of the observations are in rough agreement with the current ratio of NO_x to CO from on-road mobile sources. Most all of the recent health literature finds near-road inhabitants face higher levels of adverse health outcomes than their non-near-road counterparts from air pollution exposure; however, considering the findings here, it suggests that $PM_{2.5}$ itself is not the only traffic-related air pollutant contributing to higher rates of adverse health outcomes in the near-road environment.

Lastly, I am part of an interdisciplinary and intercultural team that is investigating the air quality and CO_2 emission impacts of waste heat to electricity and material exchange pathways at coal-fired Thermal Power Stations (TPSs) and other large emission sources in India. In the preliminary analysis, I have found waste-heat re-use to electricity using Organic Rankine Cycles (ORCs) can generate an additional 17 (9% of total coal-fired TPS generating capacity), 27 (6%), 19 (8%), and 5 (4%) GW of electricity in the 2015 and 2050

scenarios (2050-REF: business as usual; 2050-S2: effective achievement of currently proposed targets under the Perform, Achieve, and Trade (PAT) scheme; 2050-S3: ambitious regulatory achievement), respectively. In addition, the preliminary results show coal fly-ash material exchange pathways can offer additional local emission reductions at cement production facilities and brick kilns. Using these strategies in addition to perturbed emissions from IIT-Bombay, we find improvements in population-weighted average $PM_{2.5}$ concentrations ranging from 1.2% to 6.6%. The work presented here offers another potential strategy for air pollution and carbon emission mitigation in India.

7.1 Future Work

There are many research avenues and opportunities for future work with regards to air quality improvements and climate emission reductions from sustainability-targeted interventions. I hope to continue to do research that involves assessments of policies for air pollution and carbon mitigation in India and the United States.

Specifically in Agra, continued efforts can be made to reduce air pollution near the Taj Mahal, which in addition to preserving the iconic monument, will have public health benefits. For example, the entire Agra (and many other areas in North India, including Delhi-NCR) region is susceptible to impacts from large agricultural burning and recent emission inventories have been developed to estimate the crop burning activity throughout India. These inventories may be used to assess specific agricultural management strategies and the air quality impacts of such approaches on regional scales. In addition, related to many environmental justice studies conducted in the United States that find poorer, racial minority communities are disproportionately affected with higher levels of air pollution

exposure, similar equity studies should be performed in India. Poorer communities are often faced with many environmental challenges in India and as it relates to air pollution specifically, include residential biomass burning for cooking and heating, unpaved roads, large volumes of uncontrolled rickshaw emissions (oftentimes, which are idling from the congestion), etc.

Current work in both the U.S. and India for smart, connected cities (and assessment of other indicators including well-being) is ongoing and offers opportunities for studying environmental-related outcomes impacts in addition to emission abatement strategies (e.g., well-being, water consumption, health improvements from physical activity, etc.). Specifically to the work presented in this thesis (Chapter 4), future work with well-being studies and air pollution exposure should also control for other demographic and companionship factors of activities. Additional future work for studying cities can include larger, embedded system studies and characterize outcomes in addition to air pollution and carbon emissions. One such study in the U.S. could be comparisons of well-being indicators, air/carbon emissions, and health improvements from physical activity between transit riders on free public transportation (as has recently been announced in Kansas City and has been proposed in other cities in the U.S.) versus traditional commuters.

India, and other developing economies, are in a unique position to learn from the mistakes of developed countries and can bypass roadblocks by moving toward the most environmentally-friendly practices (clean energy production, embedded public transportation grids, etc.). Such development potential offers a unique testbed for novel emission reduction strategies, including assessments of "clean buildings" and technologies

that can lead to clean, net-positive cities, i.e., cities that cleanly produce more than consumed.

Specifically building off work detailed in this thesis, future work will include estimations of on-road mobile-source impacts in large Indian cities for evaluations of regional emission inventories. There is large uncertainty in the understanding of air pollution source impacts in Indian cities, which is due in part to the large number of sources, including unorganized source sectors that have not been well characterized (e.g., brick kilns, on-road mobile, MSW burning, etc.), and the high levels of pollution, a fraction of which is formed from gaseous precursor emissions. Receptor-based source apportionment results in urban areas finds a large influence of air pollution from on-road mobile sources; however, all-sector regional scale emission inventories in India generally find the contribution of mobile sources to contribute to <10% of ambient PM in urban areas. Using the recently developed EPA R-Line model offers an additional level of input to understand mobile-source impacts in Indian cities (e.g., New Delhi-NCR and Hyderabad). Another method to assess Indian (and U.S.) emission inventories includes comparison of model-simulated concentrations with satellite data. Future work can compare $PM_{2.5}$ and NO_2 (for estimation of on-road mobile and power generation) concentrations between simulated values and the satellite data.

APPENDIX A. SUPPLEMENTAL MATERIAL FOR CHAPTER 2

A.1 Open Municipal Solid Waste (MSW) and Dung Cake burning inventory generation and uncertainty

A field transect method developed by Nagpure et al.(2) was used to estimate the MSW burning incidents, approximate mass and composition in Agra. The average weight and composition of MSW burned per incident is then used to compute the MSW weight and composition per unit area. Transect lines were designed to sample each neighborhood in rough proportion to their areas. Latitude and longitude data of each transect and frequencies of observations were recorded by a hand-held Garmin GPS 72. High and low SES was determined within Agra's city boundary while the rural designation for burn rates was from survey findings outside of the city boundaries (129; Figure A-1).

There are limited studies that detail the mass of cow dung burned in homes in Indian cities. Here, we assess two approaches to estimate the mass of cow dung burned in Agra. Approach 1: We apply the census data to determine the percent of households within a ward using different types of fuels. Only one study has reported the mass of cow dung cake used for cooking in South Asia, which found in Bangladesh the mass of dung cake consumed in homes to be 42 kg per household; this approach is used in the paper due to the direct reporting of the mass of dung cake being burned (268). Further, this report, from the IARC, only discloses single fuel use for households, not multiple fuel use. Approach 2: We assess expenditures on multiple cooking fuels reported in samples of homes surveyed in rural and urban areas of Agra district, obtained from the National Sample Survey (269). Expenditures on dung are converted to mass based on price of Rs. 3 per kg dry cake in 2010 (32) (Table A-5). There is uncertainty in the price of dung cake, and

uncertainty due to the lower number of respondents using dung cake in urban areas and reporting a snapshot of monthly fuel expenses. Further, both dung cake and firewood are used occasionally in religious functions but not routinely in cooking in many homes, further confounding the extrapolation from a single month's expenditure data from a small numbers of respondents.

Approach 2, which uses household expenditures on multiple fuels used in cooking yields higher potential dung cake mass used in homes, and less firewood use, compared to Approach 1. Cow dung consumption was 11 Gg per year in Agra based off Approach 1 and 25 Gg per year based off Approach 2 (Table A-6). For firewood, we find 53 Gg (approach 1) versus 39 Gg per year in approach 2. Approach 1 was applied in this study as it has less embedded uncertainty.

A.2 Emission Rates from MSW, Dung Cake, Firewood and Crop Residue Burning to AERMOD Dispersion Model

Emission rates for MSW, dung cake, firewood and crop residue burning were determined on an electoral-ward basis, i.e., an electoral ward is an emission grid. Emission grids for Agra's 90 electoral wards, cantonment area, and four rural zones were modeled from the Agra Census map (270). We selected vertices from the census map (green dots of Figure A-3b) and used these vertices to create polygons of each electoral ward/emission grid. The $PM_{2.5}$ emission rate (g OM or BC m^{-2} s^{-1}) for MSW burning within each emission grid was determined as

$$E_i = \frac{TWB_i}{A_i} * EF \quad (1)$$

where A_i is the ward area (m^2) and EF is an emission factor (g-pollutant kg-burned^{-1}) for MSW.

The $PM_{2.5}$ emission rate (g OM or BC m^{-2} s^{-1}) for dung cake, firewood, and crop residue burning from each emission grid was determined as

$$E_i = \frac{TDCB_i}{A_i} * EF \quad (2)$$

where $TDCB_i$ is the total annual dung cake, firewood, or crop residue burned within each grid (kg-dung/firewood/crop yr^{-1}). Emission factors were used to find the amount of pollutant emitted per mass of biomass burned (Table A-2). Representative $PM_{2.5}$ emission factors for firewood and crop residue weren't available in the literature. The emission factors used in the study are total PM measurements. However, particulate emissions from biomass burning are mainly found in the accumulation mode (271-273), suggesting these emission factors can be appropriately considered as $PM_{2.5}$ emission factors.

In AERMET, 58 days had missing meteorology or other factors that resulted in null concentrations throughout the study domain. Dry deposition findings are not altered as the concentration used for analysis was the annual average from the non-null values. Because the influence of wet deposition was small compared to dry deposition, the days that had missing concentrations were ignored for wet deposition calculations; these missing data points resulted in an underestimate of the wet deposition loadings.

The modeling results for concentration profiles and the subsequent health impact assessment and pollutant deposition estimates are given for 2014. Full year publically

available meteorological data was available for 2014. The most recent census data (2011) at the time the modeling was performed was used to assess SES for the waste burning transect results. We assumed the SES data was the same in 2014 for this analysis. Receptor networks in AERMOD can be polar or Cartesian grids. Here we used a Cartesian receptor network. To align population data for the fine-scale health impact assessment, we applied satellite derived population data at the same resolution. Satellite data was available for 2015. Using annual growth rates between 2001-2011 from the census population data, we applied a growth factor to obtain Cartesian-gridded 2014 population. The transect study was performed in 2015, but Nagpure et al., 2015 (2) showed there is little annual variation of MSW burn rates.

A.3 Dry and Wet Deposition to the Taj Mahal

A detailed discussion on marble sampling and instrumentations used to measure carbonaceous species particle size at the Taj Mahal's surface is available from Bergin et al., 2014 (13). Pre-cleaned marble cuboids were fastened to Taj Mahal structures with double-sided tape at a variety of locations, and exposed from April to June 2012. Scanning electron microscopy (SEM) (LEO 1530, Carl Zeiss Microscopy) and energy dispersive X-ray (EDX) spectroscopy (Oxford Instruments Xmax detector) were carried out on two horizontally facing marble targets. Images were taken at various magnifications to capture the particles ranging from 100 nm to 100 μm diameter. The particle sizes and shapes were accessed through SEM images using image processing in a MATLAB program. EDX analyses were carried out on the same marble targets on ~1000 particles. The information gained from the SEM/EDX analyses allowed for the estimation of the particle number and surface area concentration, and chemical composition as a function of area of the marble

target. The measured size distribution can be found in Bergin et al., 2014 (13), and the average surface area median diameter, $D_{p,ave}$, was determined by

$$D_{p,ave} = \frac{\sum \frac{dSA}{d\log D_p} * D_p}{\sum \frac{dSA}{d\log D_p}} \quad (3)$$

Deposition of MSW and dung cake-related PM to the Taj Mahal's surface in 2014, σ (mg m^{-2} yr^{-1}), was calculated for both wet and dry deposition from detailed particle size measurements, and the ambient OM and BC concentrations from both sources as generated in AERMOD using

$$\sigma_i(t) = -V_{D,i}(d_p) * [C_i(t)] * t \quad (4)$$

where V_D is the size-specific surface deposition velocity (m s^{-1}), $[C_i(t)]$ used here is the annual average ambient pollutant concentration (μg m^{-3}) from open waste and dung cake burning at the Taj Mahal as determined in AERMOD, and t is the time interval of interest (yr).

Rain (e.g., from the monsoons) leads to wet deposition of pollutants to the Taj Mahal. The pollutant mass loading to the Taj Mahal by wet deposition is

$$\sigma(t) = WR * [C_i(t)] * p_o(t) * t \quad (7)$$

where $p_o(t)$ is the precipitation intensity (mm hr^{-1}) and WR is the washout ratio. It has been shown that the magnitude of washout ratios to pollution flux measurements account for

major uncertainties in atmospheric fluxes (274-276). Empirical studies of washout ratios for BC have ranged from 140 – 597 (277-279). This analysis considered the average of these reported values. Washout ratios for particulate organic carbon (POC) have been less studied, but Guo et al. found a relationship between precipitation intensity and POC washout ratio (280). Their logarithmic relationship only spanned precipitation intensities from 0 to 4.3 mm hr^{-1}, but will still be considered for this study despite measured precipitation intensities above their studied range.

Possible pollutant washoff during precipitation events was not considered in this analysis. Surface reactions, also, were not explored when quantifying the pollutant deposition. Water-insoluble particles like BC (52, 281) and a fraction of OM are likely not easily removed once deposited (13), although biomass burning aerosols are known to contain water-soluble organics (282). The absorption of volatile organic compounds (VOCs) and semi-volatile organics (SVOC) at the surface or the potential formation of secondary organic aerosol (SOA) from the gaseous emissions were not included in this analysis.

Rain data (Table A-3) was available in three-hour intervals. During the three hour wet-deposition interval, the ambient pollutant concentration will decrease and was accounted for using a mass balance design principles of a particle scrubber (283). Thus for successive wet deposition events, the initial concentration was determined from the preceding interval.

A mass balance on particle uptake by uniform size raindrops showed the particle collection efficiency, $E(t)$, in time t (hr) to be:

$$E(t) = 1 - e^{\frac{-1.5 * E * p_o * t}{D_{RD}}} \quad (5)$$

where E is the particle uptake efficiency (a function of particle size distribution and rain droplet size D_{RD}) (284) and p_o is the precipitation intensity (mm hr^{-1}) (283). Rain data was available in three hour intervals; the precipitation intensity was calculated as the total rainfall in each interval divided by three hours. On-site rain drop size measurements were unavailable during the monsoon season. The average rain drop diameter during a monsoon was taken as 1 mm (285). Similar to the deposition velocity term for dry deposition, the particle collection efficiency is a function of collected particle size. However, there are no distinguishable differences over such a narrow particle size (284), so one particle uptake efficiency is used in the proceeding analysis – 0.004. A constant mixing height of 1,000 m was used in the analysis and the OM emission rates within electoral ward 72, home of the Taj Mahal, were 2.13×10^{-8} and 2.79×10^{-9} g m^{-2} sec^{-1} and for BC 1.25×10^{-9} and 1.69×10^{-10} g m^{-2} sec^{-1} for open waste and dung cake burning, respectively. These emission rates were selected because the emissions from both sources aren't particularly buoyant and likely stay near source once emitted. Simulated concentrations in AERMOD were tabulated for maximum daily values at each receptor location as hourly output options were unavailable. For successive rainfall events, it was expected that the ambient concentration would decrease by

$$c(t) = c_o e^{\frac{-1.5 * E * p_o * t}{D_{RD}}} + \frac{EM * t}{H} \quad (6)$$

where EM is the emission rate (g m^{-2} s^{-1}) from MSW or dung cake burning in the Taj Mahal's electoral ward, and H is the mixing height (m). However, for 185 of the successive rainfall events for open waste and 187 for dung cake burning, the ambient concentration increased after the first event. This can be explained by low precipitation intensities that have minimal influence on ambient concentrations and no other sinks (i.e. advection losses) considered, despite a constant emission source. Compared to a constant concentration between successive events and ambient concentrations unaltered, the difference in wet deposition for these events was negligible.

Washout ratios were used to quantify the pollutant loading to the Taj Mahal by wet deposition.

$$WR = \frac{[P_i]_P}{[P_i]_A} \quad (7)$$

where $[P_i]_P$ is the pollutant concentration in precipitation and $[P_i]_A$ is the pollutant concentration in air.

Wet deposition from open waste burning, 2.0 ($\pm$ 1.8) mg m^{-2}, exceeds that from dung cake burning, 0.15 ($\pm$ 4.1 x 10^{-2}) mg m^{-2} (Table 2-2). Dry deposition occurring during wet deposition events was calculated to be 18 ($\pm$ 16) mg m^{-2} from MSW burning and 1.4 ($\pm$ 0.37) mg m^{-2} from dung cake burning. This can be explained by 317 of the 345 rainfall events considered having precipitation intensity less than 1 mm hr^{-1}. However, during significant wet deposition events – where the removal efficiency was at least 10% – the combined MSW and dung cake burning emissions influence by wet deposition

exceeded that by dry deposition 0.46 ($\pm$ 0.40) mg m^{-2} to 0.16 ($\pm$ 0.15) via dry during those intervals. Over the course of a year, the influence of dry deposition was greater than via wet processes (Table A-2).

The fractional cover of the pollutants to the surface of the Taj Mahal was estimated by determining the total surface area of the aerosol deposited per area of the surface. The number of particles per unit area (m^{-2}), N, was determined by

$$N = \frac{\sigma}{\rho D_{p,ave}{}^{3}/6} \quad (8)$$

where ρ is the species-specific particle density. From the surface area size distribution measured on-site, the average surface area per particle was determined. Combined with (8), the fractional cover, Ω, was calculated as

$$\Omega = \frac{6\sigma}{\rho D_{p,ave}} \quad (9)$$

A.4 Figures and Tables from the Supplementary Information

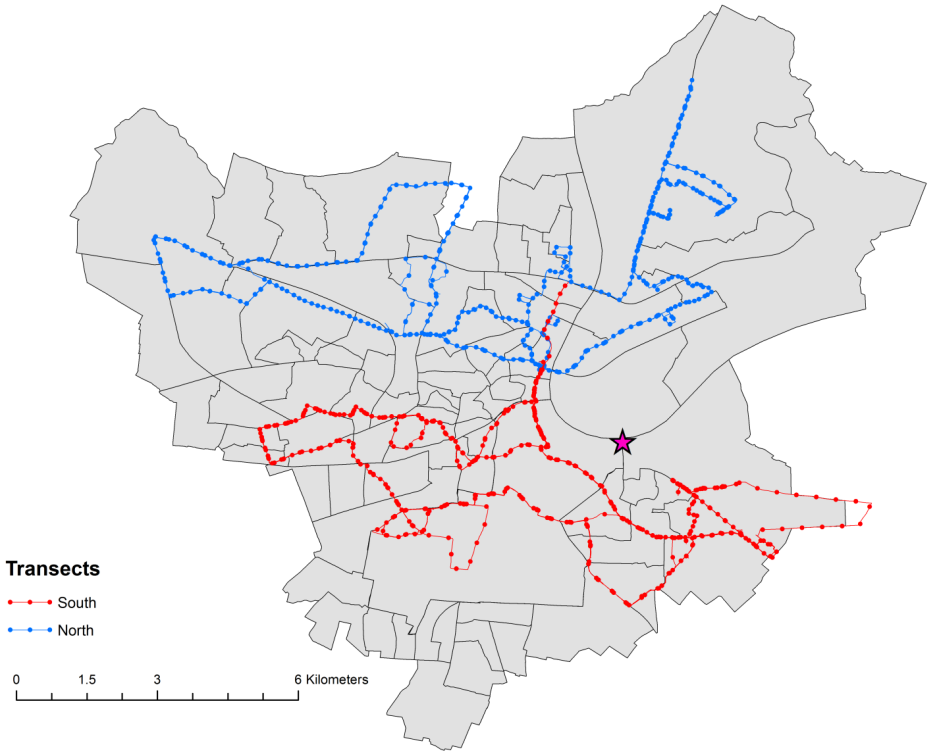

Figure A-1: The two transect routes in Agra, India, home of the Taj Mahal, used to characterize the spatial and temporal trends of open MSW burning. Using a method developed by Nagpure et al., 2015 (2), these routes helped quantify open MSW burn density, composition, and a coarse estimate of MSW burning mass.

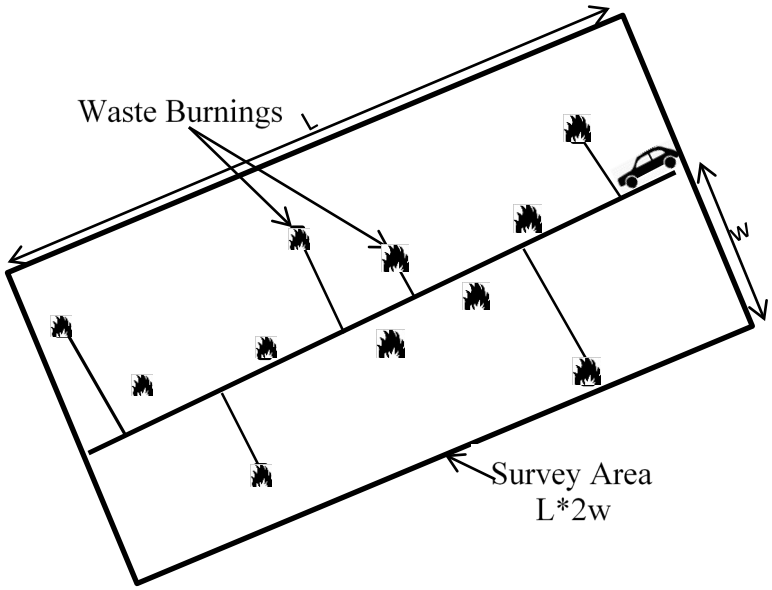

Figure A-2: Distance sampling (vehicle/line transect) methodology (2). Researchers move along the transect and record open waste burning incidents, approximate weight, and composition of MSW burning events.

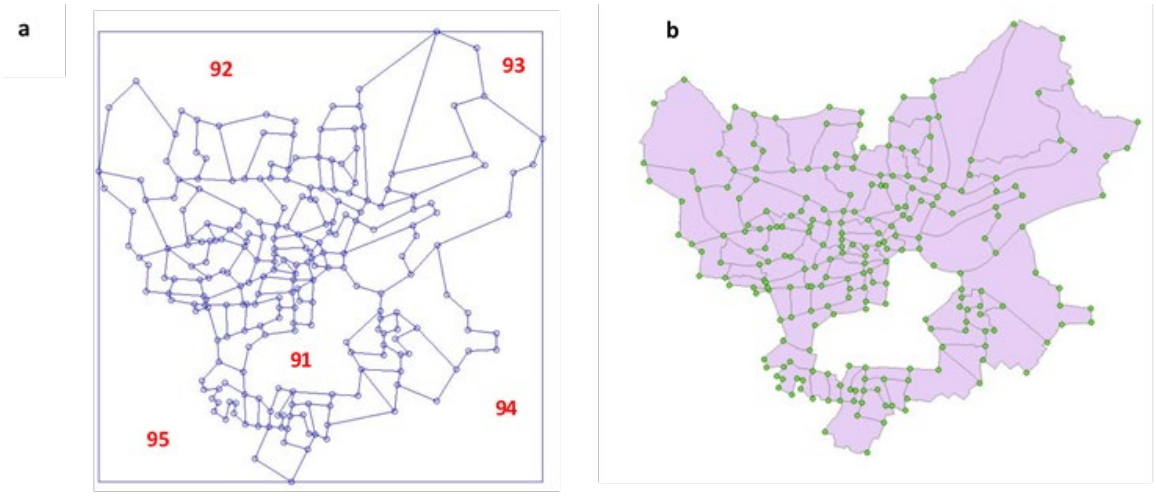

Figure A-3: a, Agra study domain with emission grids modeled as electoral wards from the b, 2011 Census map. Coordinates of the ward vertices (green dots) from the census map were used as vertices for each emission grid in AERMOD. These grids served as the study domain and were later applied in AERMOD to show the spatial variation of open waste and dung cake burning pollutant emission concentrations.

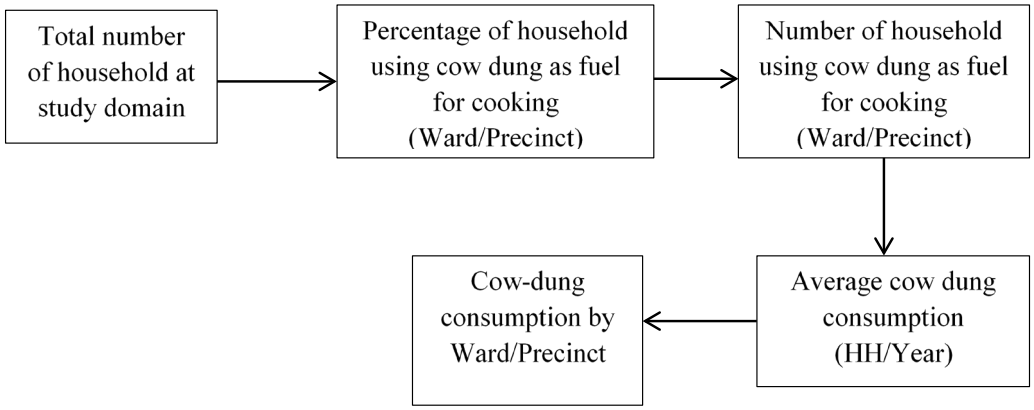

Figure A-4: Estimation methodology of cow dung consumption at ward/precinct level in Agra. Dung cake burning, which is usually associated with indoor exposure, was banned by Agra Municipality as a result of an earlier study at the Taj Mahal (13).

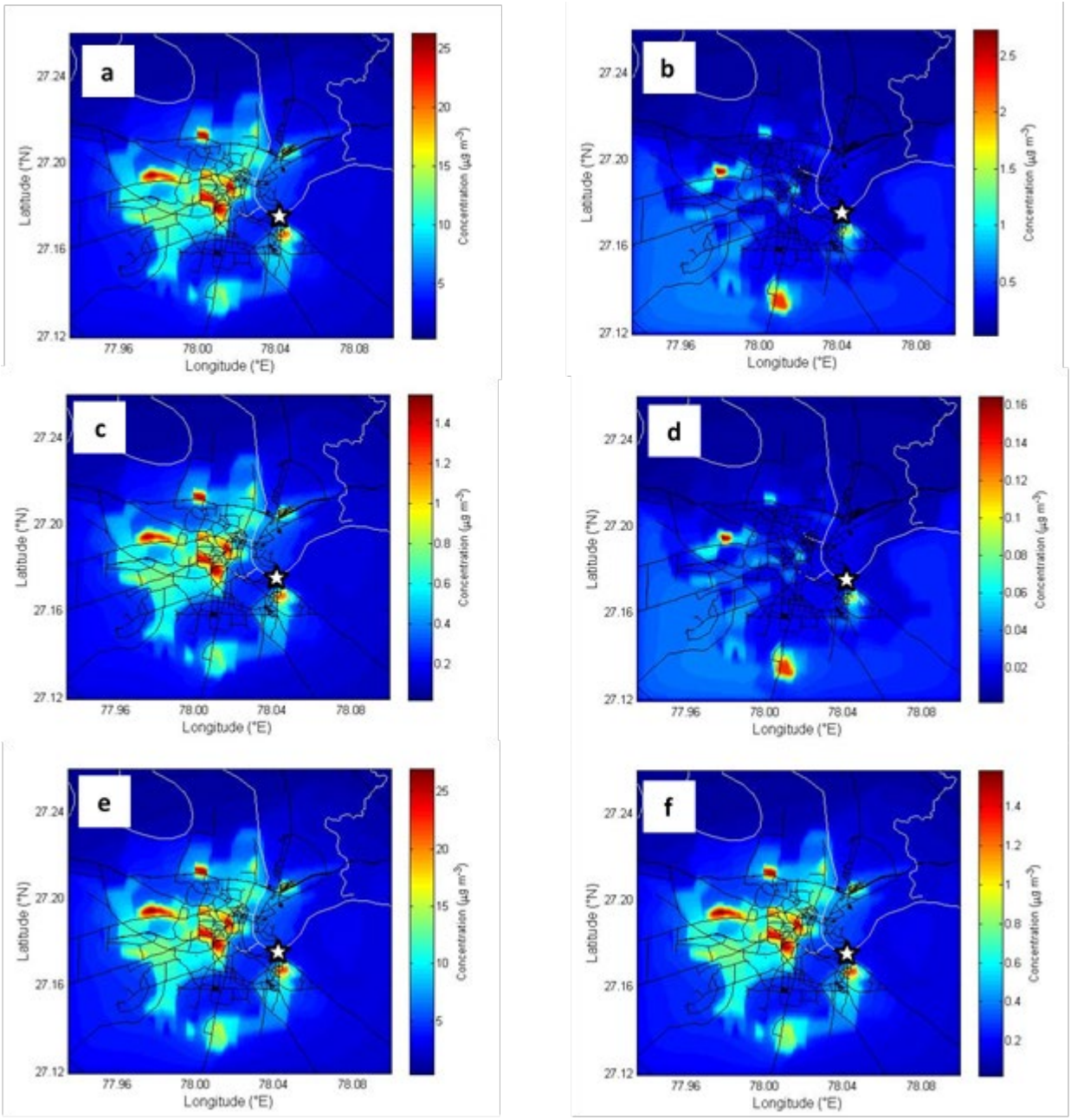

Figure A-5: AERMOD annual average $PM_{2.5}$-component concentration profiles from: a, Organic matter (OM) emissions from MSW burning b, OM emissions from dung cake burning c, black carbon (BC) emissions from open MSW burning d, BC emissions from dung cake burning e, combined organic matter (OM) emissions from open MSW and dung cake burning and f, combined BC emissions from open MSW and dung cake burning, The Taj Mahal (27.18°N, 78.04°E) is depicted by the white star.

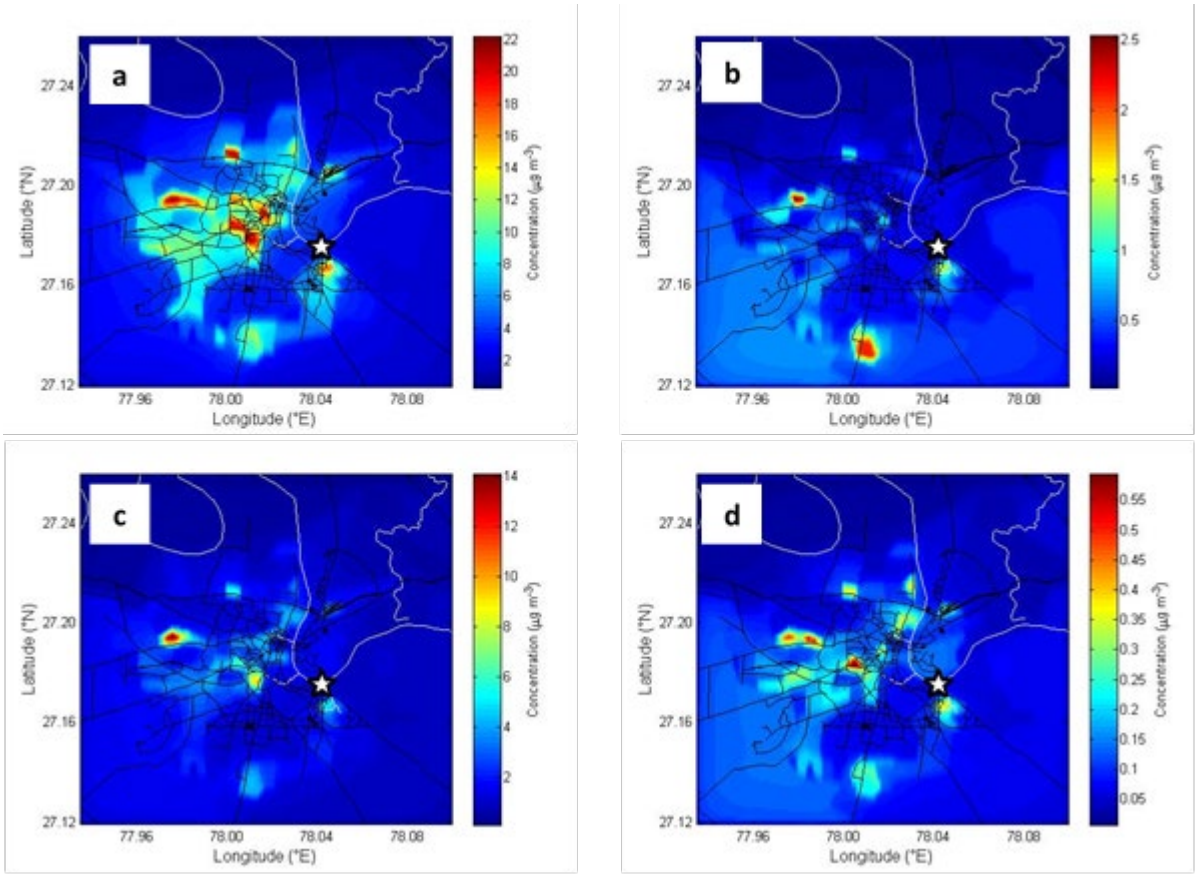

Figure A-6: Annual average organic matter (OM) concentrations in Agra from: a, open MSW burning b, dung cake burning c, firewood burning and d, crop residue burning. These models showed the combined OM concentrations at the Taj Mahal to be 5.9 ($\pm$ 4.7) µg m^{-3}, with component specific contributions of 4.1 ($\pm$ 3.8) µg m^{-3} from MSW, 0.32 ($\pm$ 0.091) µg m^{-3} from dung cake, 1.4 ($\pm$ 0.75) µg m^{-3} from firewood, and 0.080 ($\pm$ 0.070) µg m^{-3} from crop residue. The Taj Mahal (27.18°N, 78.04°E) is depicted by the white star.

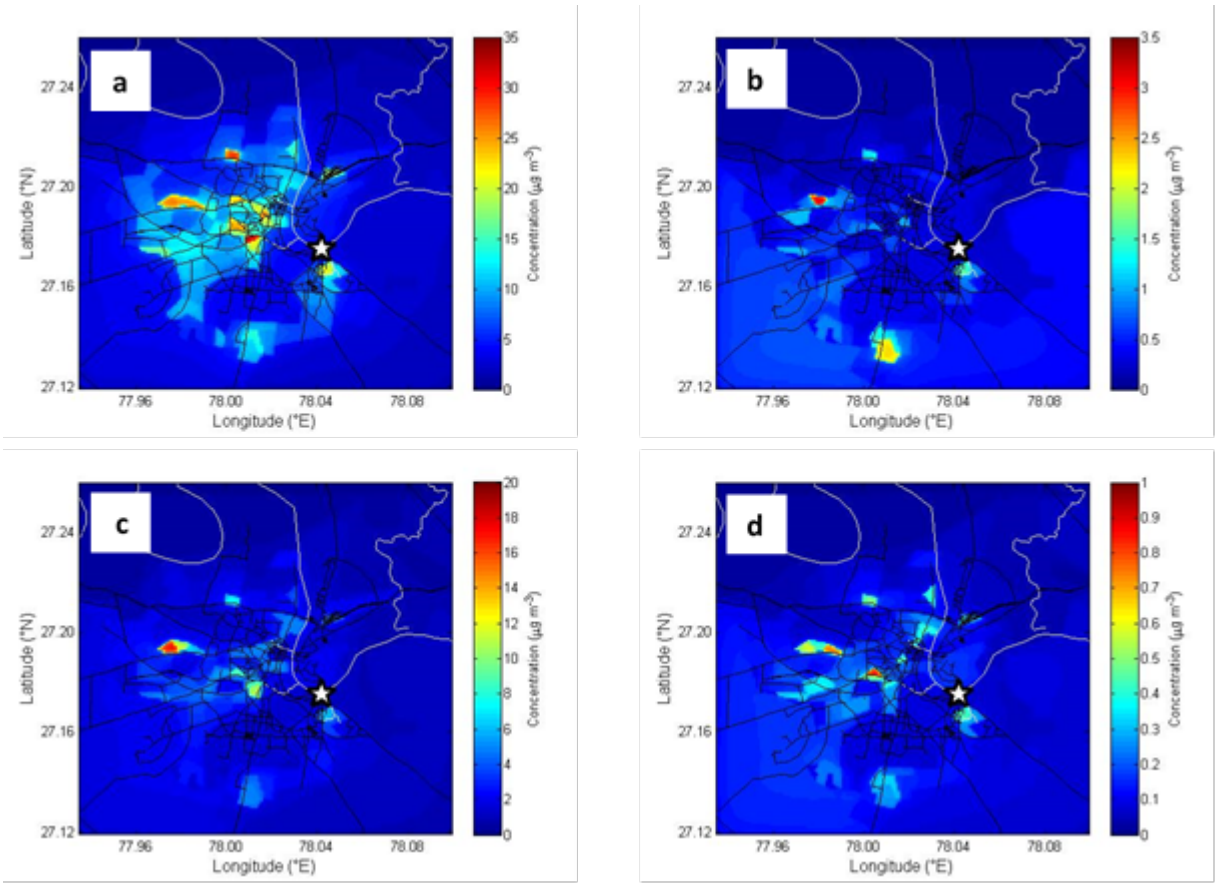

Figure A-7: Annual average organic matter (OM) concentrations in Agra before post-process smoothing from: a, open MSW burning b, dung cake burning c, firewood burning and d, crop residue burning. The Taj Mahal (27.18°N, 78.04°E) is depicted by the white star. These concentration profiles generated in AERMOD showed higher pollution from both forms of biomass burning concentrated in areas of lower SES.

Table A-1: A comparison of the total amount of open waste and dung cake burning (kg day^{-1}) in Agra for each of the 95 emission grids.

	MSW	DC
Average	2723	321
Range	494 – 24,709	0 – 9,114

Table A-2: Reported $PM_{2.5}$ organic matter (OM) and black carbon (BC/EC) emission factors (g-pollutant kg-$burned^{-1}$) for open MSW, dung cake, firewood and crop residue burning (45, 46, 286). An OM/OC ratio of 2.1 (49) was applied to OC emission factors provided in the literature. The emission factors used in the study for dung cake, firewood and crop residue burning are bulk PM measurements. However, particulate emissions from biomass burning are mainly found in the accumulation mode (271-273), suggesting these emission factors can be appropriately considered as $PM_{2.5}$ emission factors.

	OM	BC/EC
MSW (45)	11.1 (± 10.3)	0.65 (±0.27)
Dung Cake (46)	8.1 (±2.3)	0.49 (±0.025)
Firewood (286)	7.4 (±4.0)	1.1 (±0.50)
Crop Residue (286)	8.2 (±7.1)	1.3 (±1.1)

Table A-3: Measured precipitation in nearby New Delhi of at least 1 mm hr^{-1}. 344 rainfall events contributed to wet deposition and data was available in three-hour intervals throughout the year.

Date	Time	Rain (mm)	Precipitation Intensity (mm hr^{-1})
12-Sep-14	8:30 AM	62.5	20.83
12-Sep-14	11:30 AM	26.9	8.97
12-Sep-14	5:30 AM	20.7	6.90
4-Sep-14	8:30 AM	13	4.33
6-Aug-14	5:30 PM	12.1	4.03
9-Aug-14	5:30 PM	8.6	2.87
11-Sep-14	2:30 PM	7.7	2.57
3-Aug-14	5:30 PM	7.6	2.53
10-Aug-14	11:30 PM	7.6	2.53
2-Sep-14	11:30 PM	7.1	2.37
4-Aug-14	2:30 PM	6.1	2.03
6-Aug-14	8:30 PM	6.1	2.03
11-Sep-14	5:30 PM	5.6	1.87
28-Feb-14	8:30 PM	5.5	1.83
11-Aug-14	5:30 PM	5.5	1.83
4-Sep-14	8:30 PM	4.3	1.43
2-Aug-14	2:30 PM	4.1	1.37
18-Jul-14	11:30 AM	4	1.33
10-Aug-14	2:30 PM	4	1.33
22-Jan-14	2:30 PM	3.9	1.30
10-Aug-14	8:30 PM	3.9	1.30
18-Jul-14	2:30 PM	3.8	1.27
22-Jan-14	8:30 PM	3.7	1.23
13-May-14	8:30 PM	3.4	1.13
9-Aug-14	2:30 PM	3.3	1.10
13-Oct-14	8:30 PM	3.2	1.07
6-Aug-14	2:30 PM	3.1	1.03
5-Sep-14	5:30 PM	3	1.00

Table A-4: Comparison of the wet and dry total organic matter (OM) and black carbon (BC) deposition (mg m^{-2}) to the surface of the Taj Mahal from open waste and dung cake burning in 2014.

	OM – Dry	OM – Wet	BC – Dry	BC – Wet	Total Combined Deposition
MSW	141 (± 130)	1.95 (± 1.8)	8.29 (± 3.4)	3.65×10^{-2} (± 1.5 x 10^{-2})	151 (± 136)
DC	11.0 (± 3.1)	0.144 (± 4.1 x 10^{-2})	0.661 (± 3.4 x 10^{-2})	2.76×10^{-3} (± 1.4 x 10^{-4})	11.8 (± 3.22)

Table A-5: Household fuel use by primary fuel users in Agra (approach 2 for cow dung consumption estimation)

Primary fuel use		**Firewood HH/Mo (kg.)**	**Cowdung cake HH/Mo (kg.)**	**kerosene HH/Mo (Ltr.)**	**LPG_PNG HH/Mo (kg.)**	**Sample Size**
Firewood	Urban	40.7 ± 90.8	21.8 ± 50.2	1.07 ± 2.76	0	7
	Rural	54.0 ± 24.0	23.0 ± 12.8	2.35 ± 0.88	1.26 ± 2.01	20
Cow Dung	Urban	36.7 ± 23.0	27.4 ± 5.54	1.17 ± 1.77	0	3
	Rural	52.6 ± 29.8	60.7 ± 29.0	2.74 ± 0.79	1.84 ± 3.16	45

Table A-6: Monthly household cooking fuel consumption comparison: Approach 1 and 2 (Gg yr^{-1})

	Firewood	**Cowdung cake**
Approach 1: Single Cooking Fuel Method based on IARC	53	11
Approach 2: Multiple Fuel Method Based on HH Expenditure Survey	39	25
Higher limit of Approach 2	97	57

APPENDIX B. SUPPLEMENTAL MATERIAL FOR CHAPTER 3

B.1 Figures and Tables from the Supplementary Information

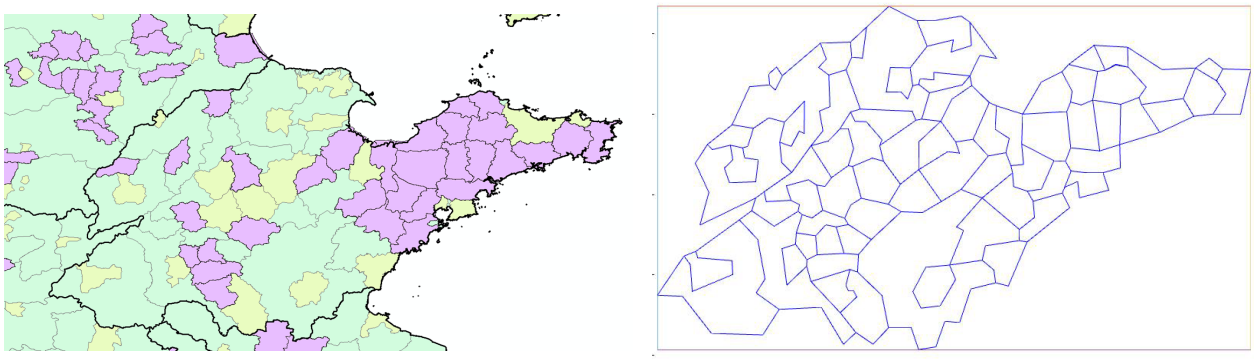

Figure B-1: Sample mapping of provincial urban administrative districts (shiqu, purple girds) and county-level cities (xianji shi, yellow-green grids) into emission grids (right) for application in AERMOD

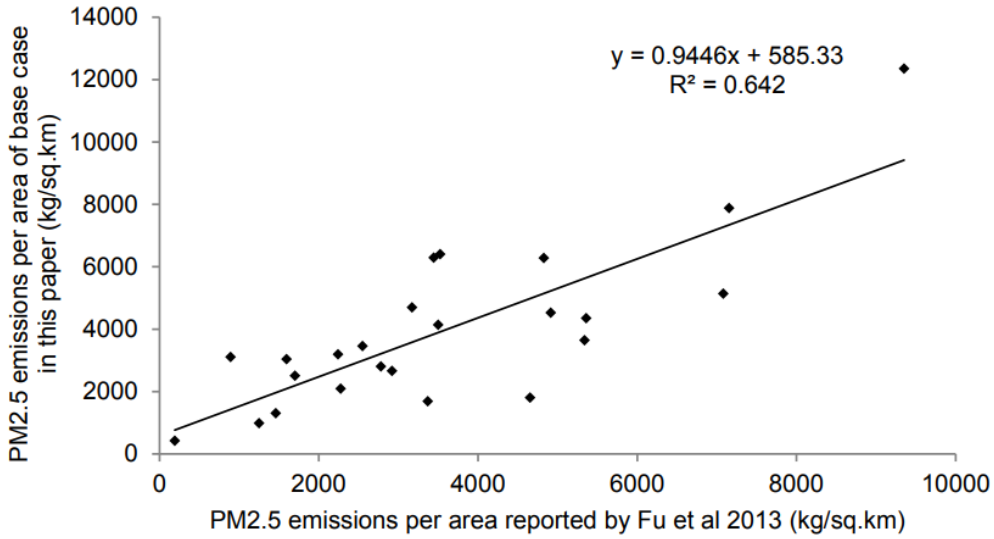

Figure B-2: Comparison of primary $PM_{2.5}$ emissions per area in our model compared with Yangtze River Delta cities reported by Fu et al, 2013 (1)

APPENDIX C. SUPPLEMENTAL MATERIAL FOR CHAPTER 4

C.1 Correcting R-Line Simulated NO_x impacts

R-Line simulation results for NO_x were not in agreement with the estimates of the true mobile source impact (Figure C-9). The true mobile source impact is estimated as the difference between the Near-Road (monitoring) Network (NRN) hourly NO_x concentration (AQS Site ID# 27-053-0962) and the average of the non-NRN NO_x concentrations within 10 miles of the NRN site (NO_x AQS Site IDs# 27-003-1002 & 27-037-0020 and $PM_{2.5}$ AQS Site IDs# 27-171-3201 & 27-139-0505 & 27-003-1002 & 27-053-0963 & 27-123-0871 & 27-123-0868). The difference between the NRN concentration and the average of the background concentrations for each hour was considered as the hourly mobile source impact at the NRN site. We could then estimate the hourly NOx spatial fields by evaluation of the initial model concentration at the NRN site with the true mobile source impacts. Each hour of the day was grouped against the corresponding mobile source impact for that hour (Figure C-10 for hourly comparisons), so that 24 unique comparisons could be made (Table C-7). From here, we used 24 linear corrections to correct the corresponding hourly R-Line simulations. This calibration approach reduced maximum simulated NO_x concentrations throughout the study period (Figure C-11), but other performance metrics, including average percent differences between the simulated mobile-source impacts and the "true" mobile-source impact determined from observations, did not show improvements, and oftentimes the performance metric was worse (Table C-8). This is likely attributed to the correction approach which would be driven by the high-concentration simulated values by the model.

The initial horizontal dispersion coefficient, σ_z, a measure of the plume spread, used in this is 2 meters, the default value suggested in R-Line. This value is on the high end of mobile source σ_z and slight increases in σ_z has little influence on the output concentrations.

C.2 Participant Selection Criteria

Residents of randomly selected blocks (921 of the 2443 census blocks in the study neighborhoods) in the study neighborhoods were recruited to participate in the study. All homes on the selected blocks were first post carded with a brief study description (which did not include any information of the concurrent air pollution sampling) and contact information for the research team. Once contacted, researchers explained the study in detail to the participants, individually, and those who chose to participate set an appointment with the survey team. The well-being assessments occurred in three stages, an entry survey, 7 days of episode level data collection, and an exit survey (Table C-9 for complete demographic breakdown of the study participants). The entry and exit surveys are used to collect information on cognitive SWB, socio-demographic parameters, neighborhood perceptions, and other variables that been known to influence SWB.

C.3 Statistical tests on regressions between air quality (observed $PM_{2.5}$ and mobile-source simulated NO_x) and emotional well-being (EWB) indicators

Significance on the correlation coefficients between air quality (observed $PM_{2.5}$ and mobile-source simulated NO_x) and the six EWB indicators was determined using

$$t = r * \sqrt{\frac{n-2}{1-r^2}}$$

Where t is the t-statistic, r is the square root of r^2, and n is the number of neighborhood assessments (6). None of the regressions were found to be statistically significant at $\alpha = 0.05$ (Table C-10).

C.4 NAAQs Exceedances on emotional well-being (EWB)

There were four simulated hours when the mobile source NO_x impact exceeded the hourly NO_2 NAAQs (100 ppb) in the neighborhoods when a concurrent EWB assessment existed (Table C-11). The NAAQs exceedance in Near North resulted in higher happiness and net affect, but lower tiredness, stress, sadness, and pain (Table C-12). This was the exact opposite of what was expected, and each of the responses was statistically significant (α=0.05). In Prospect Park, the statistically significant relationships between NO_x exceedances, and EWB were negative responses with happiness and net affect. Each of the companion EWB assessments during NO_x exceedance events were recorded as either at-home or leisure recreation activity types, which may both be indoor and subject to a variety of other confounding variables like the ongoing activity (watching TV, family time, reading, etc.). There were no $PM_{2.5}$ daily NAAQs exceedances when at least one EWB assessment existed for any of the neighborhoods.

C.5 Figures and Tables from the Supplementary Information

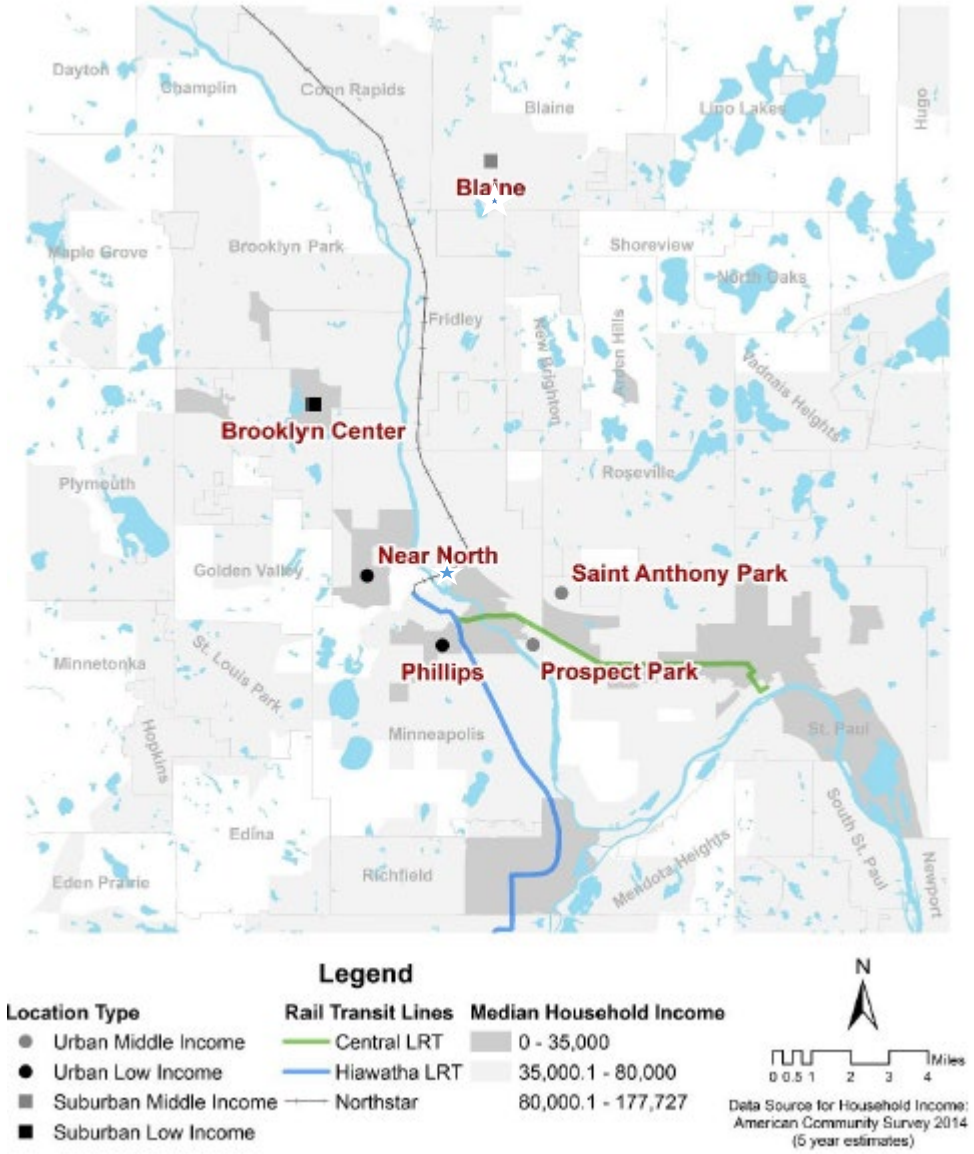

Figure C-1: Minneapolis-St. Paul city map with the study neighborhoods identified. The different shadings and lines represent household income and rail access, respectively. The blue stars are the locations of the Minnesota Pollution Control Agency (MPCA) air pollution monitoring sites that were used for low-cost sensor (LCS) evaluation and calibration.

Figure C-2: Sample of the low-cost sensor set up (within the red circle) in St. Anthony Park. In each neighborhood, monitors were ziptied to fences or other stationary spots outside the house that were isolated and away from emission sources. Monitors were elevated to approximately the inhalation height in each neighborhood.

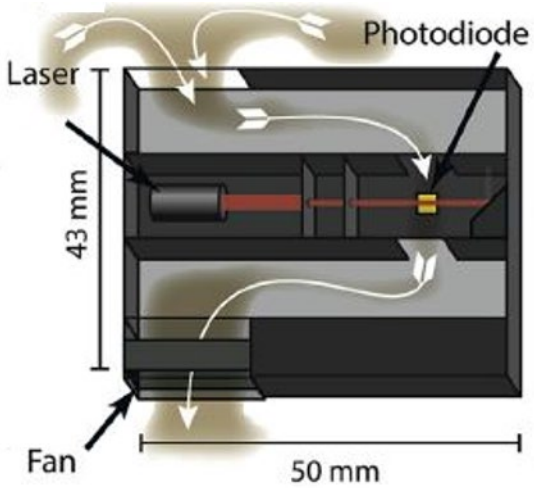

Figure C-3: Schematic of the Plantower PMS3003 (which measures PM_1, $PM_{2.5}$, and PM_{10}) as originally published in Kelly et al. (3). The figure is republished with permission from Kelly and colleagues. The output waveform produced by the photodiode estimates mass concentration from particle size (pulse amplitude) and number concentration (pulse frequency)

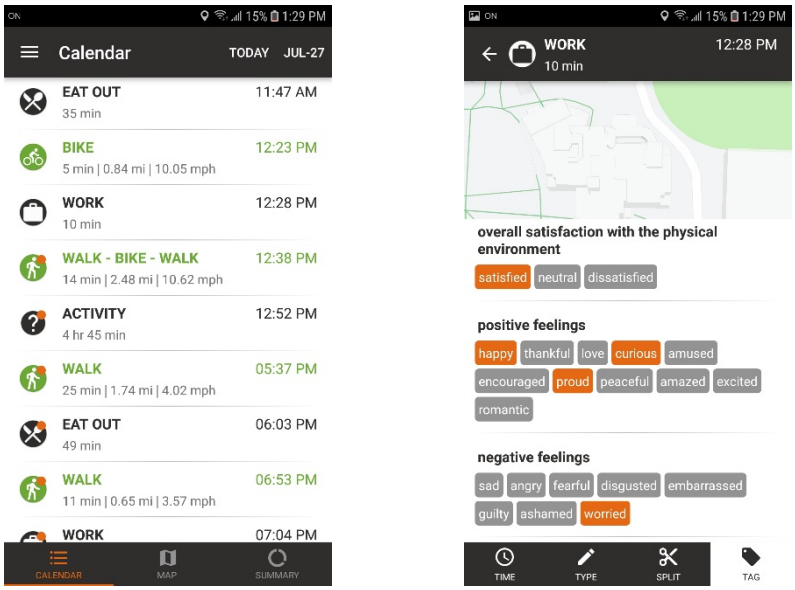

Figure C-4: Sample interface of Daynamica, the smartphone application used to assess well-being. Residents of the study neighborhoods responded to well-being surveys after completing activities throughout the day.

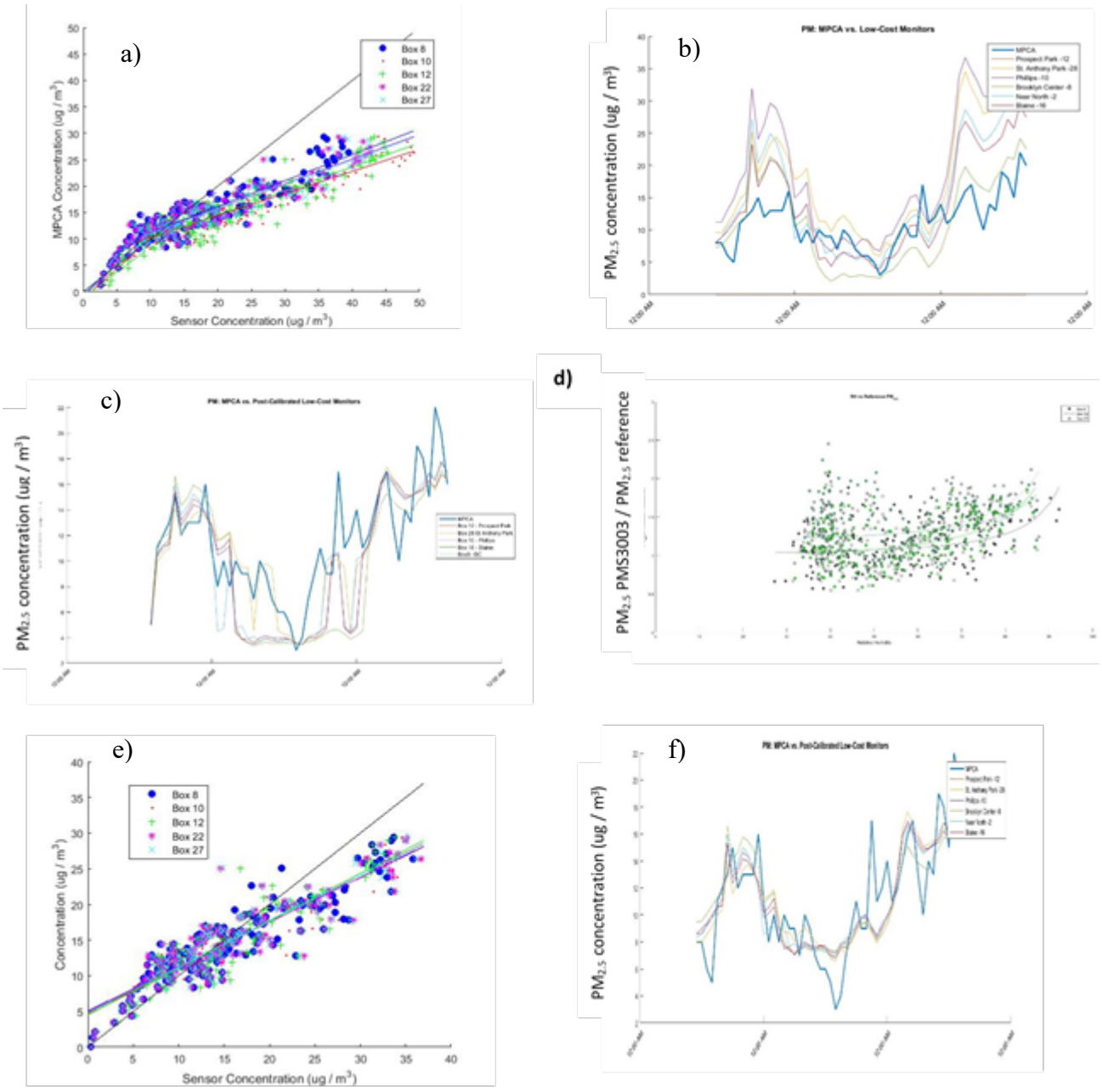

Figure C-5: Sample calibration results of the Plantower PMS 3003 sensor co-located with a Beta Attenuation Monitor (BAM) at a Minnesota Pollution Control Agency (MPCA) site (AQS Site ID# 27-053-0962). (a) *Pre-calibration scatter*: Comparison of 5 low-cost sensors (LCS) with BAM measurements. The best fit is a piecewise continuous fit. (b) *Pre-calibration time series*: $PM_{2.5}$ time series where the thick blue line is the BAM measurement and the thin lines are the LCS measurements. (c) *Piecewise correction without relative humidity correction*: The adjusted Plantower results following a piecewise adjustment (i.e., a fit was determined, and values below the split point were given one linear calibration, and sensor concentrations' above the split point were given a different calibration). (d) *Relative humidity correction method*: RH vs. $PM_{2.5}$ fit using Zheng, et al. (4). (e) *Post-RH Correction scatter*: Comparison of 5 LCS with BAM measurements following the RH correction. (f) *Post-RH Correction Calibration time series*.

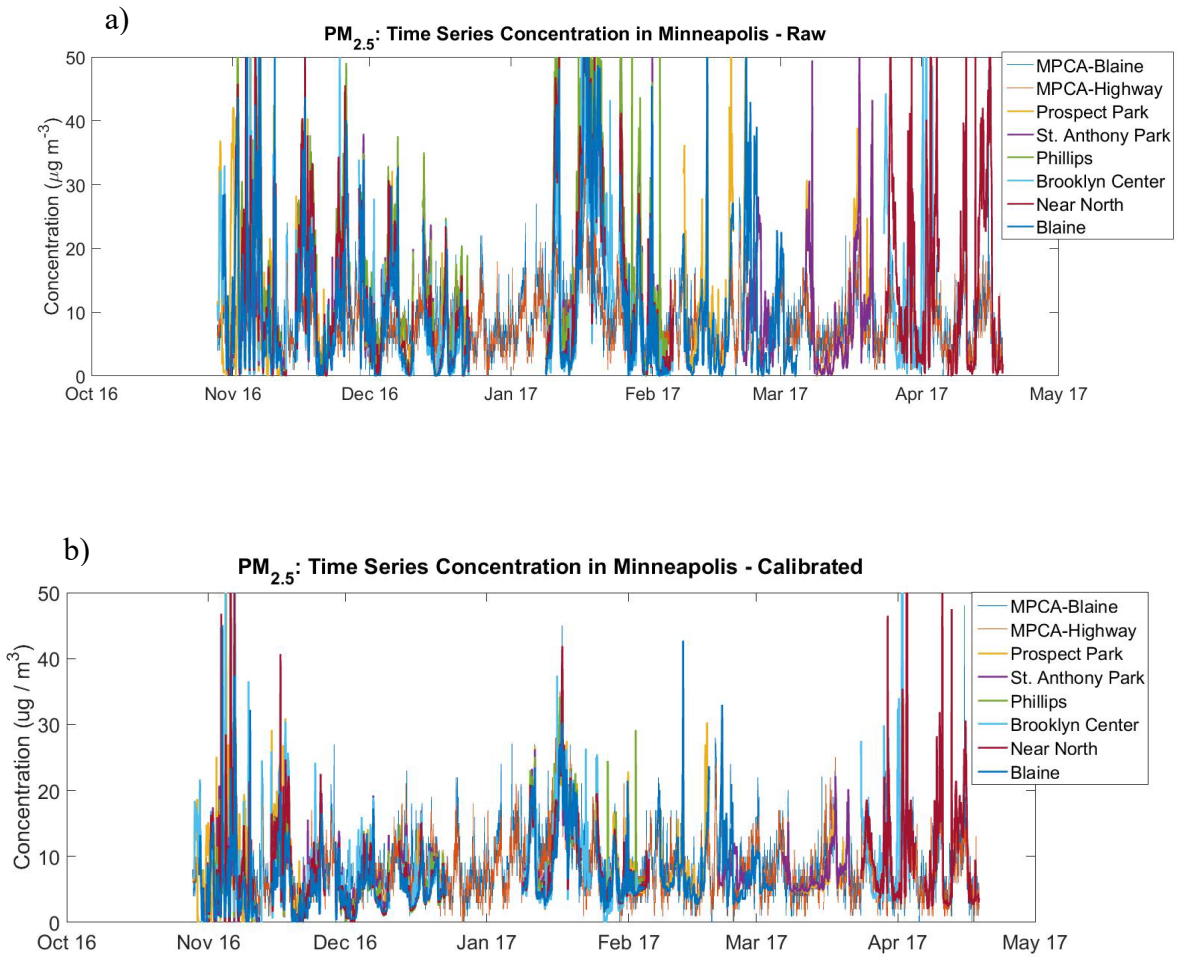

Figure C-6: Low-cost sensor raw and post-RH-corrected calibration time series in Minneapolis throughout the study period. The thicker lines represent low-cost sensor concentrations while the thin blue and orange lines are from two regulatory monitors (AQS Site IDs# 27-003-1002 & 27-053-0962) in the study domain: (a) Raw $PM_{2.5}$ and (b) Calibrated $PM_{2.5}$

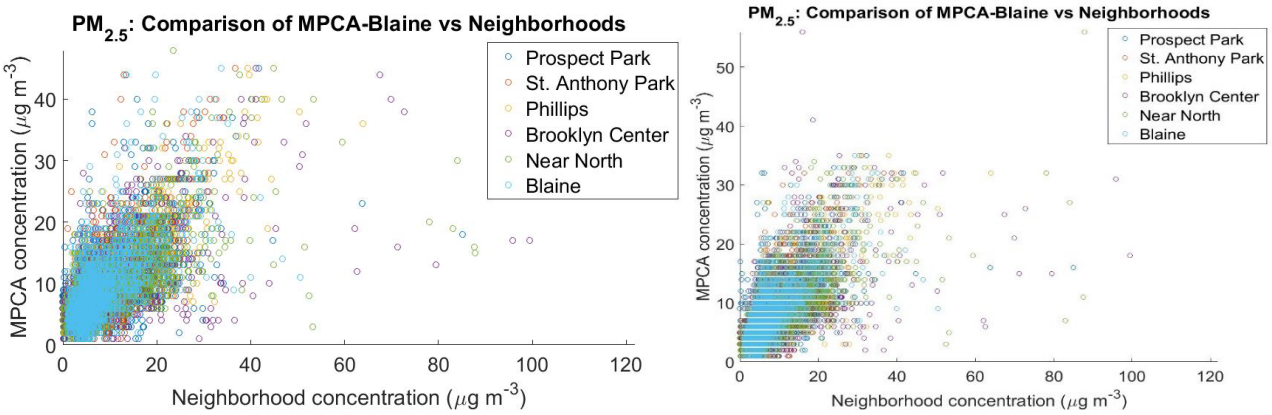

Figure C-7: Comparison of 1-hour neighborhood low-cost sensor $PM_{2.5}$ measurements against regulatory site (MPCA-Blaine and MPCA-NRN) measurements

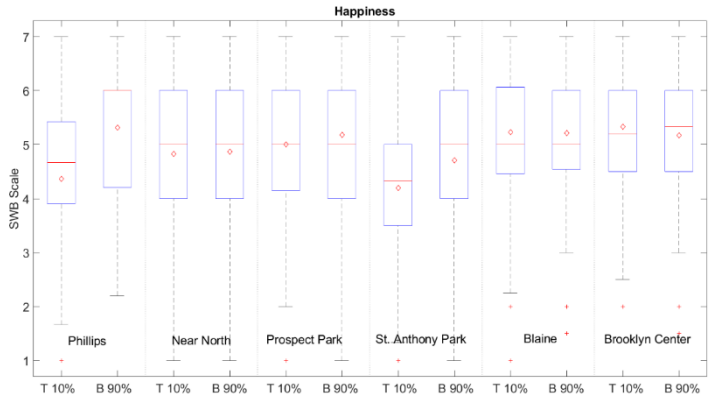
Happiness
SWB Scale
Phillips
Near North
Prospect Park
St. Anthony Park
Blaine
Brooklyn Center
T 10%
B 90%

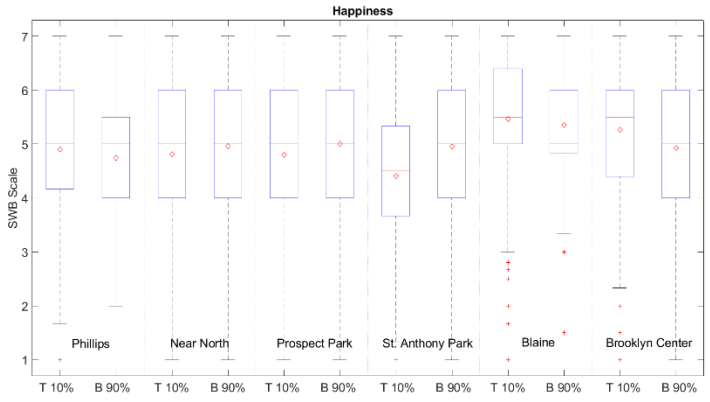
Happiness
SWB Scale
Phillips
Near North
Prospect Park
St. Anthony Park
Blaine
Brooklyn Center
T 10%
B 90%

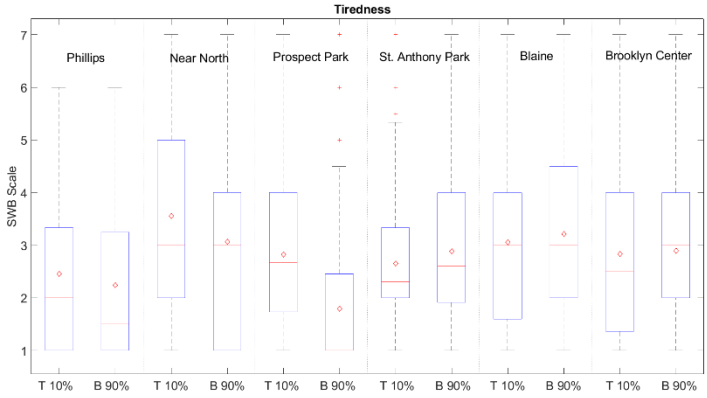
Tiredness
SWB Scale
Phillips
Near North
Prospect Park
St. Anthony Park
Blaine
Brooklyn Center
T 10%
B 90%

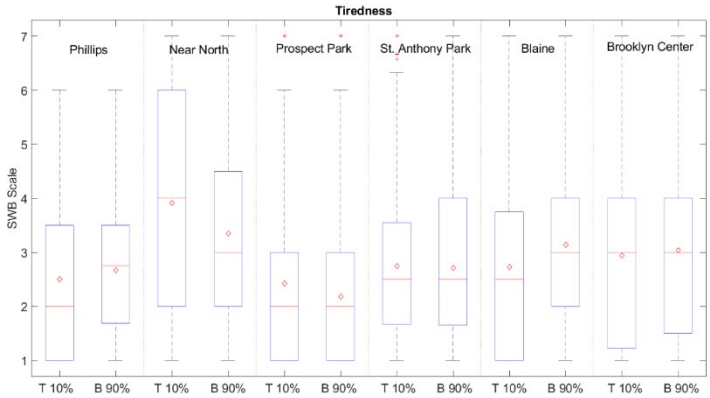
Tiredness
SWB Scale
Phillips
Near North
Prospect Park
St. Anthony Park
Blaine
Brooklyn Center
T 10%
B 90%

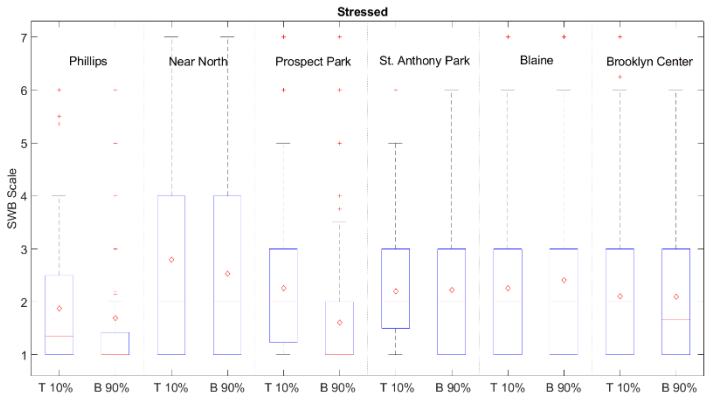
Stressed
SWB Scale
Phillips
Near North
Prospect Park
St. Anthony Park
Blaine
Brooklyn Center
T 10%
B 90%

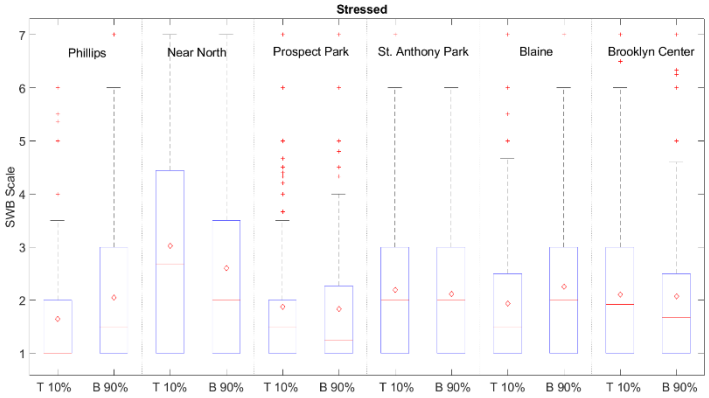
Stressed
SWB Scale
Phillips
Near North
Prospect Park
St. Anthony Park
Blaine
Brooklyn Center
T 10%
B 90%

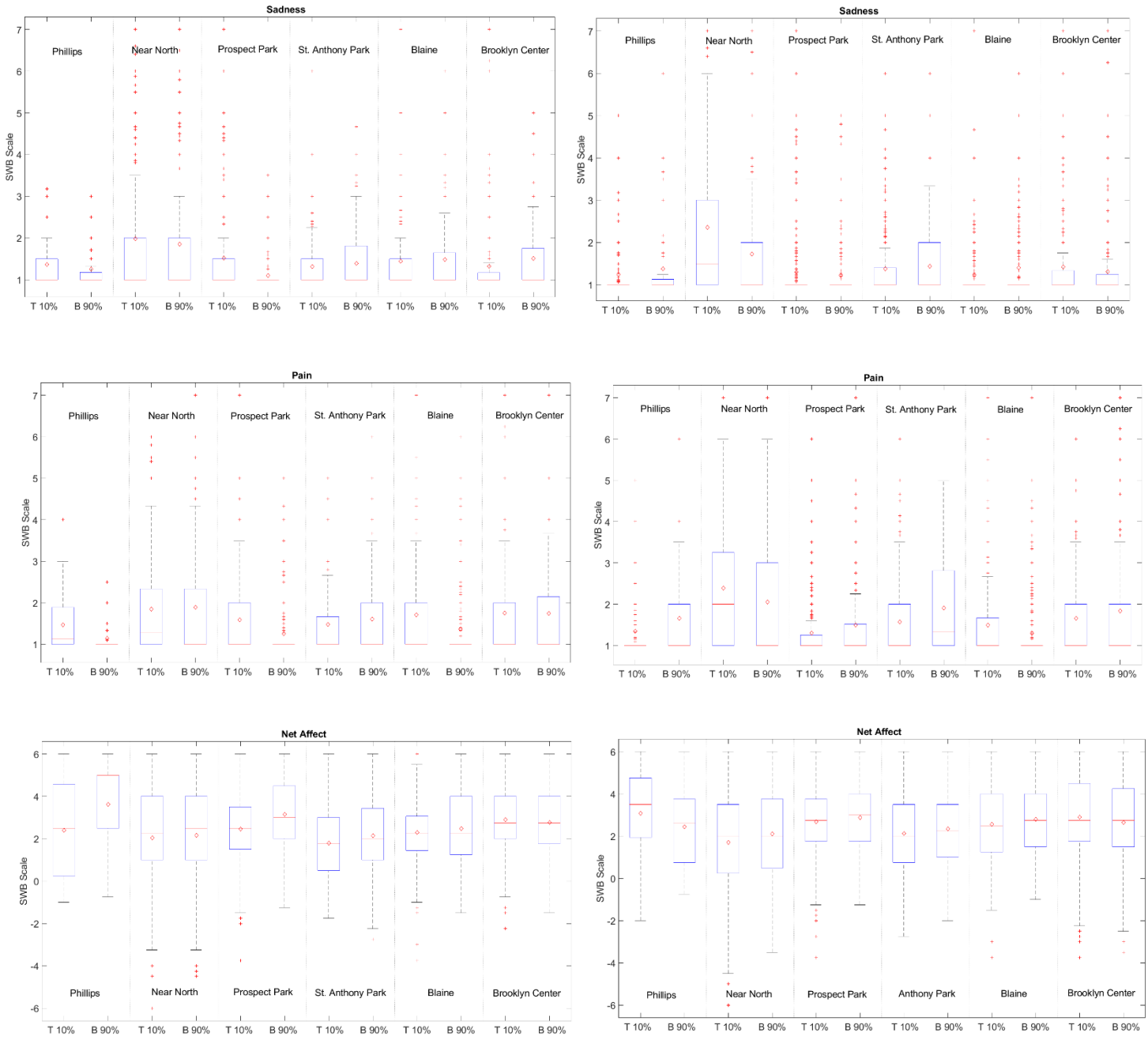

Figure C-8: Boxplots of the top 10% of pollution (low-cost sensor (LCS) $PM_{2.5}$ and R-Line simulated NO_x) on each of the six emotional well-being (EWB) indicators in the six study neighborhoods. The left column is for LCS $PM_{2.5}$ responses, and the right column is R-Line simulated NO_x home-based responses.

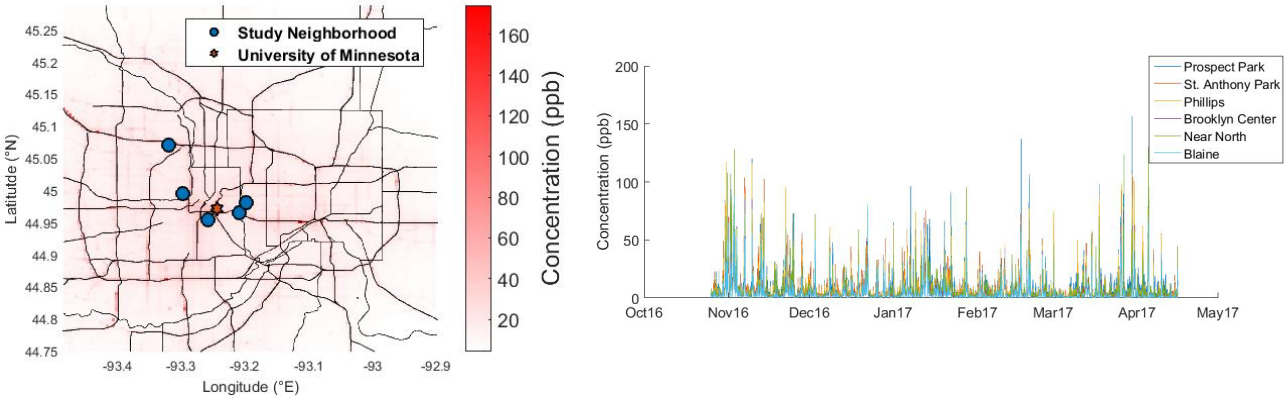

Figure C-9: Average R-Line simulated mobile source NO_x impacts before correction during the study period

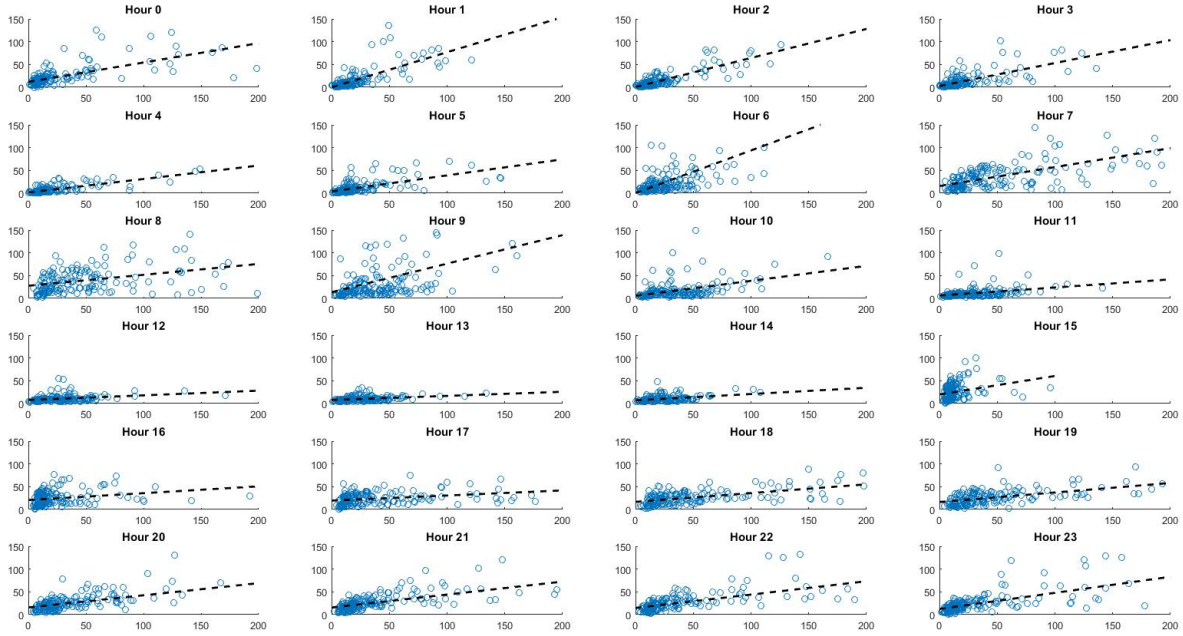

Figure C-10: Hourly R-Line simulated NO_x concentrations (x-axis) against the true mobile source impact (Near Road minus background measurement). The slope of the regression is used to adjust the R-Line NO_x outputs

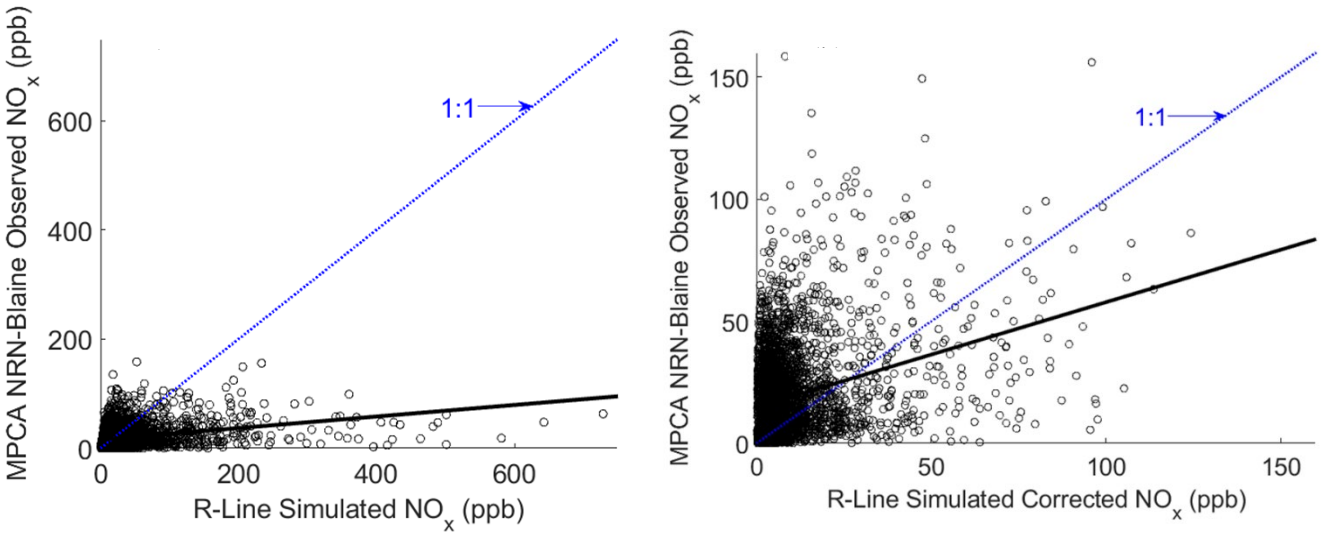

$NO_{x,observed} = 0.11 * NO_{x,R-Line\ simulated}$

$NO_{x,observed} = 0.43 * NO_{x,R-Line\ simulated}$

Figure C-11: Comparison of (a) R-Line initial simulated NO_x and (b) R-Line following calibration simulated NO_x against the estimated mobile-source impact at a Near-Road (Monitoring) Network (NRN) site (AQS Site ID# 27-053-0962) in Minneapolis. The mobile-source impact was estimated as the difference between the NRN site and a background NO_x observation (AQS Site ID# 27-003-1002).

Table C-1: Air Quality System (AQS) regulatory $PM_{2.5}$ and NO_2 monitors in the study domain. The asterisk (*) next to the site name indicates it is not a source-oriented site.

Site name	AQS Site ID#	Pollutants measured	Additional details
Blaine-Anoka Airport	27-003-1002	$PM_{2.5}$, NO_2	Housed at airport
Harding High School*	27-123-0871	$PM_{2.5}$	Urban neighborhood
Ramsey Health Center	27-123-0868	$PM_{2.5}$	Very near highway
Andersen School*	27-053-0963	$PM_{2.5}$	Urban neighborhood
St. Louis Park City Hall	27-053-2006	$PM_{2.5}$	Commercial, high-volume roads
Near-Road I-35/I-94	27-053-0962	$PM_{2.5}$, NO_2	Near-road site
Apple Valley*	27-037-0470	$PM_{2.5}$	Suburban neighborhood
B.F. Pearson School*	27-139-0505	$PM_{2.5}$	Suburban neighborhood
Near-Road I-35	27-037-0480	$PM_{2.5}$, NO_2	Near-Road I-35

Table C-2: The number of emotional well-being (EWB) responses that coordinated with an air quality (Low-cost sensor or R-Line) data point for the same hour for each of the six study neighborhoods

	Number of EWB assessments for measured $PM_{2.5}$ comparison	Number of EWB assessments for simulated mobile source NO_x home-based comparison	Number of EWB assessments for simulated mobile source NO_x in-situ based comparison
Phillips	102	271	406
Near North	612	858	897
Prospect Park	520	833	861
St. Anthony Park	677	1,172	1,297
Blaine	496	805	778
Brooklyn Center	399	793	887
Total	*2,806*	*4,732*	*5,126*

Table C-3: Summary of LCS regressions from the co-location approach to calibrate LCS $PM_{2.5}$ with a Beta Attenuation Monitor (BAM) at the NRN site (AQS Site ID# 27-053-0962). A linear fit was used to correct the raw $PM_{2.5}$ data following an RH-correction as outlined by Zheng et al. (4). The asterisk (*) indicates that the sensor in the neighborhood changed to a different, but not necessarily new sensor that week. The "*x*" in the regression equation is the RH-corrected LCS $PM_{2.5}$ observation.

Calibration No.	Dates	NRN Average (Range) $PM_{2.5}$	Prospect Park		St. Anthony Park		Phillips		Brooklyn Center		Near North
			r^2	regression	r^2	regression	r^2	regression	r^2	regression	r^2
1	11/11/16-11/13/16	8.1 (1-24)	0.83	1.3*x-0.99	0.79	1.6*x-2.5	0.80	1.6*x-2.4	0.83	1.5*x-1.8	0.83
2	11/25 – 11/27	10.9 (4-27)	0.76	1.1*x-0.05	0.59	0.99*x-0.90	0.74	1.2*x-0.90	N/A		0.76
4	12/21-12/23	9.0 (2-22)	0.81	0.64*x+3.18	0.83	0.56*x+3.59	0.82	0.68*x+2.8	0.80	0.52*x+4.0	0.80
5	1/20-1/23	10.0 (4-21)	0.48	0.87*x+1.85	0.61	1.0*x+0.56	0.58	1.1*x-0.20	0.72	1.2*x-1.8	0.54
6	2/3-2/6	10.1 (3-22)	0.81	0.67*x+4.4	0.58	0.50*x+5.0	0.60	0.49*x+5.1	0.60	0.42+6.5	0.69
7	2/17-2/19	9.7 (-1-28)	0.85	0.65*x+1.7	N/A	N/A	N/A		N/A		N/A
8	3/3-3/5	9.9 (3-17)	0.42	0.52*x+5.0	0.42	0.54*x+4.8	N/A		N/A		N/A
10	4/3-4/5	6.1 (-1-13)	N/A		N/A		N/A		0.63	0.75*x+2.1	0.65
11	4/17-4/19	5.8 (0-13)	N/A		N/A		N/A		0.56	0.48*x+2.9	0.58

	Blaine									
	regression	r^2	regression							
	1.5*x-1.81	N/A	1.1*x-0.06	1.1*x-0.77	0.72	0.61*x+3.4	0.81	0.56*x+3.7	0.98*x+0.84	0.58	0.97*x+0.78	0.53*x+5.2	0.67	0.54*x+5.2		0.82	0.62*x+1.9		0.44	0.51*x+5.0	0.79*x+2.0	N/A	N/A	0.49*x+2.8	N/A	N/A

Table C-4: Summary statistics of the comparison between the neighborhood low-cost sensor (LCS) $PM_{2.5}$ measurements against regulatory site measurements for the entire study period. The asterisk (*) denotes the location of the closest neighborhood to the regulatory site.

	Near Road Network: I-35/I-94			**Blaine**		
	R^2	Slope	Intercept	R^2	Slope	Intercept
Prospect Park	0.29	0.49	4.5	0.30	0.46	4.2
St. Anthony Park	0.34	0.69	2.9	0.44	0.68	2.4
Phillips	0.61*	0.62	3.7	0.58	0.57	3.5
Brooklyn Center	0.35	0.41	5.5	0.33	0.38	5.0
Near North	0.45	0.45	4.8	0.47	0.45	4.1
Blaine	0.29	0.62	4.2	0.49*	0.63	3.2

Table C-5: Study-average observed $PM_{2.5}$ concentrations (95% confidence intervals) from low-cost sensors and simulated mobile-source NO_x concentrations (95% Confidence Interval) modeled in R-Line.

	Low-cost sensor $PM_{2.5}$ ($\mu g\ m^{-3}$)	**R-Line NO_x (ppb)**
Prospect Park	7.8 (7.5-8.0)	8.2 (7.8-8.6)
St. Anthony Park	7.4 (7.2-7.6)	8.0 (7.7-8.4)
Phillips	7.5 (7.2-7.8)	8.2 (7.8-8.6)
Brooklyn Center	8.0 (7.7-8.4)	6.4 (6.1-6.7)
Near North	8.2 (7.9 -8.5)	7.4 (7.1-7.7)
Blaine	6.7 (6.4-6.9)	3.8 (3.6-4.0)

Table C-6: The concentration cutoff between the top 10% of $PM_{2.5}$/mobile-source NO_x hours and the 90% cleanest hours in each neighborhood.

	Phillips	Near North	Prospect Park	St. Anthony Park	Blaine	Brooklyn Center
NO_x cutoff (ppb)	10.5	17.4	20.1	17.5	7.2	11.5
$PM_{2.5}$ cutoff ($\mu g\ m^{-3}$)	18.4	18.5	14.1	13.7	11.4	12.6

Table C-7: Hourly regression results for the R-Line NO_x corrections. R-Line results were biased high, so the initial outputted model results were corrected based on hour.

Hour	regression	r^2
0	$[NOx]_{corrected} = 0.42 \times [NOx]_{R\text{-}Line} + 12$	0.42
1	$[NOx]_{corrected} = 0.72 \times [NOx]_{R\text{-}Line} + 9.3$	0.45
2	$[NOx]_{corrected} = 1.1 \times [NOx]_{R\text{-}Line} + 5.1$	0.33
3	$[NOx]_{corrected} = 0.95 \times [NOx]_{R\text{-}Line} + 7.8$	0
4	$[NOx]_{corrected} = 2.0 \times [NOx]_{R\text{-}Line} + 4.7$	0
5	$[NOx]_{corrected} = 1.1 \times [NOx]_{R\text{-}Line} + 9.1$	0
6	$[NOx]_{corrected} = 0.41 \times [NOx]_{R\text{-}Line} + 18$	0.44
7	$[NOx]_{corrected} = 0.23 \times [NOx]_{R\text{-}Line} + 24$	0.19
8	$[NOx]_{corrected} = 0.16 \times [NOx]_{R\text{-}Line} + 32$	7.3×10^{-2}
9	$[NOx]_{corrected} = 0.25 \times [NOx]_{R\text{-}Line} + 33$	0
10	$[NOx]_{corrected} = 0.11 \times [NOx]_{R\text{-}Line} + 38$	0
11	$[NOx]_{corrected} = 0.54 \times [NOx]_{R\text{-}Line} + 28$	0
12	$[NOx]_{corrected} = 0.86 \times [NOx]_{R\text{-}Line} + 21$	0
13	$[NOx]_{corrected} = 1.1 \times [NOx]_{R\text{-}Line} + 16$	0
14	$[NOx]_{corrected} = 0.92 \times [NOx]_{R\text{-}Line} + 17$	0
15	$[NOx]_{corrected} = 0.36 \times [NOx]_{R\text{-}Line} + 23$	0
16	$[NOx]_{corrected} = 0.05 \times [NOx]_{R\text{-}Line} + 22$	2.1×10^{-2}
17	$[NOx]_{corrected} = 0.07 \times [NOx]_{R\text{-}Line} + 21$	0
18	$[NOx]_{corrected} = 0.09 \times [NOx]_{R\text{-}Line} + 21$	0
19	$[NOx]_{corrected} = 0.17 \times [NOx]_{R\text{-}Line} + 18$	9.0×10^{-2}
20	$[NOx]_{corrected} = 0.24 \times [NOx]_{R\text{-}Line} + 38$	0
21	$[NOx]_{corrected} = 0.31 \times [NOx]_{R\text{-}Line} + 28$	0
22	$[NOx]_{corrected} = 0.24 \times [NOx]_{R\text{-}Line} + 28$	0
23	$[NOx]_{corrected} = 0.35 \times [NOx]_{R\text{-}Line} + 13$	0.35

Table C-8: Hourly percent differences comparing R-Line initial and post-calibrated mobile-source NO_x simulations extracted at the Near-road (Monitoring) Network (NRN) site (AQS Site ID# 27-053-0962) against the true mobile source impact assessed at the NRN site. The mobile-source impact was estimated as the difference between the NRN site and a background NO_x observation (AQS Site ID# 27-003-1002). The negative values indicates the model result is biased low relative to the NRN observation.

Hour	Initial simulation percent difference (%)	Post-calibration percent difference (%)
0	-33	65
1	-36	-13
2	-63	4.8
3	-48	14
4	-2.4	-29
5	66	-3.2
6	51	-60.4
7	-4.3	-10
8	-44	-60
9	-63	-30
10	-48	-56
11	-2.4	-10
12	-44	-2.2
13	-48	-14
14	22	-2.4
15	94	-18
16	123	-67
17	105	-23
18	58	-35
19	53	-19
20	55	-8.2
21	43	-2.7
22	13	-3.8
23	-23	18

Table C-9: Summary of demographic and economic status of the participants for the emotional well-being (EWB) assessments in Minneapolis neighborhoods

Variable	Total	Phillips	Near North	Prospect Park	St. Anthony Park	Blaine	Brooklyn Center
Female	268	48	46	43	55	37	39
Living with Spouse/partner	238	34	27	48	56	40	33
Age (median)	52	44	55	57	58	43	54
Employed Full Time	163	17	18	30	33	30	35
Disabled	79	20	20	8	10	8	13
Children Under 18 Present	122	30	25	11	20	21	15
White	309	42	32	65	74	48	48
Asian	15	4	1	2	3	4	1
Black	43	11	27	0	0	1	4
American Indian	9	9	0	0	0	0	0
Multiple	21	9	2	3	1	2	4
Low income (< 25K)	83	31	24	9	9	3	7
Med income (25-75K)	138	25	28	20	19	17	29
High income (75K +)	176	18	10	41	51	35	21
Total Sample Number	*398*	*75*	*62*	*70*	*79*	*55*	*57*

Table C-10: t-statistics on the relationship between low-cost sensor (LCS) $PM_{2.5}$ and R-Line mobile source simulated NO_x against emotional well-being (EWB) assessments in the study neighborhoods. None of the regressions are statistically significant at $\alpha = 0.05$.

	LCS $PM_{2.5}$	R-Line NO_x
Happiness	0.87	2.1
Tiredness	0.44	0.48
Stressed	0.95	0.13
Sadness	2.3	0.41
Pain	1.0	0.49
Net affect	0.58	0.75

Table C-11: NO_x NAAQS exceedances (NO_2 hourly standard) in the neighborhoods for hours when concurrent emotional well-being (EWB) assessments existed.

Neighborhood	Date and time	R-Line simulated NO_x (ppb)
Near North	Nov. 3, 2016 (8:00 pm)	115.1
Prospect Park	Nov. 11. 2016 (7:00 pm)	108.1
Prospect Park	Feb. 19, 2017 (2:00 am)	136.6
Prospect Park	Feb. 21, 2017 (1:00 am)	106.4

Table C-12: Average difference between emotional well-being (EWB) indicators for hours (including a two-day lag) when the R-Line simulated mobile-source NO_x concentration exceeded the hourly NO_2 NAAQS (100 ppm). Positive values indicate the EWB where NAAQS exceedance occurrences were higher than the non-NAAQs exceedances (i.e., a positive value means the EWB outcome was higher in the NAAQs exceedance days). The asterisk (*) indicates the difference is statistically significant (α=0.05).

EWB indicator	Near North	Prospect Park
Happiness	1.2*	-0.83*
Tiredness	-1.1*	0.30
Stress	-1.4*	$5.4x10^{-2}$
Sadness	-0.98*	$-7.6x10^{-2}$
Pain	-0.97*	$-2.4x10^{-2}$
Net affect	*2.5**	*-0.67**

APPENDIX D. SUPPLEMENTAL MATERIAL FOR CHAPTER 5

D.1 Black Carbon Near-road (monitoring) Network against non-near-road findings

Black carbon (BC) comparisons were only available for 4 cities (Boston, MA., Indianapolis, IN., Providence, RI., and Sacramento, CA.) resulting in 5 comparisons in 2017. The average difference between the near-road and non-near-road sites was 0.81 µg m^{-3}, with the highest difference of 1.2 µg m^{-3} observed in Providence, RI. between the Providence Building Rooftop (AQS Site ID# 44-007-1010) and Providence near-road site (AQS Site ID# 44-007-0030) (Figure D-8 and Figure D-9). BC, on average was 0.81 (0.21-1.23, n=5) µg m^{-3} higher at the near-road sites than at the non-near-road sites. Much of the anthropogenic BC in cities is emitted directly from combustion activities, so we expect the near-road to usually be higher in BC than a non-near-road site unless a nearby source is by the non-near-road monitor.

Similar to $PM_{2.5}$, NO_2, and CO, we examined the relationship between Fleet-Equivalent Annual Average Daily Traffic (FE-AADT) and AADT with the near-road site BC concentrations (n=10). In line with expectations we found a statistically significant (α=0.05), positive correlation for both traffic count measures (Figure D-10). BC, a component of $PM_{2.5}$, is emitted as a byproduct of incomplete combustion and on-road emissions contribute ~70% of BC emissions in North America (52).

D.2 Coefficients of Divergence (COD) for $PM_{2.5}$, NO_2, and CO concentration differences between the near-road and non-near-road sites

The coefficients of divergence (COD), a measure of similarity between pollutant concentrations at two different monitoring sites (174), was determined between each near-road and non-near-road pair. The COD is calculated as:

$$COD = \sqrt{\frac{1}{n}\sum_{i=1}^{n}\left(\frac{x_{if} - x_{ih}}{x_{if} + x_{ih}}\right)^2}$$

where n is the number of observations (for many of our comparisons $n \cong 17{,}000$, the number of hours in 2 years), $x_{if}\ and\ x_{ih}$ are the concentrations of one species for the ith time period at sites $f\ and\ h$. The COD between the near-road sites and the urban sites for NO_2, $PM_{2.5}$, and CO were 0.37 (95% CI: 0.34-0.39), 0.28 (0.26-0.29), and 0.31 (0.28-0.33), respectively (Table D-9). Using previous assessments of COD, Krudysz et al. (287) estimates a boundary COD of 0.20, where COD values >0.20 are defined as heterogeneous spatial distributions and values <0.20 represent spatially homogenous air pollutants. This is a misleading metric for the $PM_{2.5}$ comparison because >40% of the $PM_{2.5}$ comparisons have higher non-near-road two-year average concentrations than at the near-road sites, but COD is more valuable for assessing NO_2 and CO differences.

D.3 Inverse-Distance Weighting

We explore the relationship between distance to the near-road site and concentration difference using inverse-distance weighting of the form:

$$CD = \frac{1}{a * x^b}$$

where CD is the pollutant concentration difference between the near-road and non-near road site, a and b are fit coefficients, and x is the distance (miles) between the near-road and non-near road companion site. We unexpectedly see no relationship between the distance and the concentration difference for NO_2 or CO, but some relationship for $PM_{2.5}$

(Figure D-11). We expected as the distance increased away from the near-road site that the concentration difference would also increase. This may be attributed to varying wind speeds and directions.

D.4 NO_2 to NO_x ratio at near-road and non-near-road sites

NO_2 to NO_x ratios were investigated at the near-road and non-near-road sites. We find higher NO_2 to NO_x consistently at the non-near-road sites (Figure D-12), which was expected considering much of the direct NO_x emissions from vehicles is NO. In Denver, all four of the non-near-road sites had considerably lower NO_2 to NO_x ratios. Three of the sites were within close proximity to a major roadway and the fourth is stationed next to a major railway, which may lead to elevated NO levels. The NO_2 to NO_x average diurnal trend traced one another closely, with the NEAR-ROAD ratio lower (Figure D-13). This trend was expected with a morning rush hour leading to elevated NO emissions followed by ozone production during the day to consume NO. A slight seasonal trend of lower NO_2 to NO_x was observed during the winter months (Figure D-14). This again is likely due to the higher O_3 levels in the summer that converts NO to NO_2.

D.5 Estimating the NO_x to CO emissions ratios from observations

D.5.1 Approach 1: Line of best fit of the CO concentration difference between the NRN and non-NRN sites and the NO_x concentration differences between the NRN and non-NRN site

A linear regression was fit to the data of CO and NO_x concentration differences (Figure 5-5). The slope of this line can be considered as a proxy of the NO_x to CO emissions ratio. To convert the slope, 172 (90-300) ppb NO_x ppm CO^{-1}, to a mass basis, we use the ideal gas law:

$$(SI\ 1)\quad \frac{NO_x}{CO} = \frac{\frac{P_{atm} * MW_{NO_x} * Conc_{NO_x}(ppb)}{R * T_{atm}}}{\frac{P_{atm} * MW_{CO} * Conc_{CO}(ppb)}{R * T_{atm}}} = slope_{NO_x:CO} * \frac{MW_{NO_x}}{MW_{CO}}$$

$$= 172x10^{-3} * \frac{44}{28} = 0.27$$

D.5.2 Approach 2: Ratio of NO_x enhancement to CO enhancement

The NO_x to CO ratio is assessed using the ratio of the near-road enhancements for NO_x and CO. The NO_x enhancement, on average, was 16 ppb while for CO the average was 0.14 ppm. Using SI 1:

$$\frac{NO_x}{CO} = \frac{\frac{P_{atm} * MW_{NO_x} * Conc_{NO_x}(ppb)}{R * T_{atm}}}{\frac{P_{atm} * MW_{CO} * Conc_{CO}(ppb)}{R * T_{atm}}} = \frac{Conc_{NO_x}(ppb) * MW_{NO_x}}{Conc_{CO}(ppb) * MW_{CO}} = \frac{16 * 44}{140 * 28}$$

$$= 0.20$$

D.5.3 Doing Approach 1 with no negative concentration differences, i.e., the NRN NO_x and CO concentration is always higher than the non-NRN

To convert the slope, 165 (90-310) ppb NO_x ppm CO^{-1}, to a mass basis, we use the ideal gas law:

$$\frac{NO_x}{CO} = \frac{\frac{P_{atm} * MW_{NO_x} * Conc_{NO_x}(ppb)}{R * T_{atm}}}{\frac{P_{atm} * MW_{CO} * Conc_{CO}(ppb)}{R * T_{atm}}} = slope_{NO_x:CO} * \frac{MW_{NO_x}}{MW_{CO}} = 165x10^{-3} * \frac{44}{28}$$

$$= 0.26$$

D.5.4 Doing Approach 2 with no negative concentration differences, i.e., the NRN NO_x and CO concentration is always higher than the non-NRN

$$\frac{NO_x}{CO} = \frac{\frac{P_{atm} * MW_{NO_x} * Conc_{NO_x}(ppb)}{R * T_{atm}}}{\frac{P_{atm} * MW_{CO} * Conc_{CO}(ppb)}{R * T_{atm}}} = \frac{Conc_{NO_x}(ppb) * MW_{NO_x}}{Conc_{CO}(ppb) * MW_{CO}} = \frac{17 * 44}{160 * 28}$$

$$= 0.17$$

D.6 Statistical Tests for $PM_{2.5}$, NO_2, and CO concentration differences between the near-road sites against non-near-road sites

To evaluate the statistical differences between $PM_{2.5}$, NO_2, and CO near-road against AQS observations elsewhere in cities, we use a one-tailed t-test with H_0: $\mu_{diff} = 0$; H_a: $\mu_{diff} > 0$ ($\mu_{non\text{-}near\text{-}road} > \mu_{NEAR\text{-}ROAD}$); $\alpha = 0.05$ and we calculate the Coefficients of Divergence (COD). For the 95% confidence interval (CI) ranges reported in the manuscript, we run a two-tail t-test (H_0: $\mu_{diff} = 0$; H_a: $\mu_{diff} \neq 0$ ($\mu_{non\text{-}near\text{-}road} > \mu_{NEAR\text{-}ROAD}$); $\alpha = 0.05$). P-values of the one-tailed t-test show that there is a statistically significant difference between CO and NO_2 at the near-road sties compared against urban non-near-road sites, but found there is no statistically significant difference between $PM_{2.5}$ at the near-road sites and urban non-near-road sites (Table D-3). Statistically, there is no significant difference between suburban and rural $PM_{2.5}$ compared with the near-road monitors, either, based off observations used in this study. This, however, is misleading considering this analysis does not include all of the rural and suburban monitors that may be influenced by city emissions and there is a limited number of comparisons of rural-designated monitors within the city boundary or 10 miles of the companion near-road monitor. When combined with the suburban monitors as a "non-urban" comparison, we find a statistically significant difference between $PM_{2.5}$ the near-road monitors and the non-urban monitors (Table D-3).

Significance on the correlation coefficients between Fleet-Equivalent Annual Average Daily Traffic (FE-AADT) and AADT with near-road two-year average concentrations (Figure 5-3 and Figure D-10) and significance between the NO_x and CO concentration differences (Figure 5-5) were determined using:

$$t = r * \sqrt{\frac{n-2}{1-r^2}}$$

Where t is the t-statistic, r is the square root of r^2, and n is the number of samples. We find the t-values for $PM_{2.5}$, NO_2, CO, and BC to be 2.5, 4.6, 2.6, and 1.4, respectively, when compared against FE-AADT. All but BC are significant at α=0.05. The t-value of near-road $PM_{2.5}$ with AADT is 0.54, insignificant at α=0.05. In the comparison between NO_x and CO concentration differences, the t-value is 2.5 which is significant at α=0.05.

D.7 $PM_{2.5}$ and CO observations – using different monitors

The $PM_{2.5}$ annual average concentrations at the near-road sites (and presumably non-near-road sites) were measured with different federal equivalent method (FEM) monitors. The FEM $PM_{2.5}$ sensors used at the near-road sites are either a Met One Beta Attenuation Monitor (BAM) 1020, a TEI 5014i BAM, a Grimm 180, or a TEI 1405-DF Tapered Element Oscillating Microbalance (TEOM). Previous assessments of co-located FEMs show variability between monitors (168). In addition, many of the CO measurements only report data to one decimal, which may also bias the results. This uncertainty was not quantified. The instruments used for CO measurement are not detailed within the near-road handbook from the EPA website. The near-road sites were implemented, at earliest, in 2014, so it is possible the CO monitors here are newer than at the non-near-road sites.

D.8 Figures and Tables from the Supplementary Material

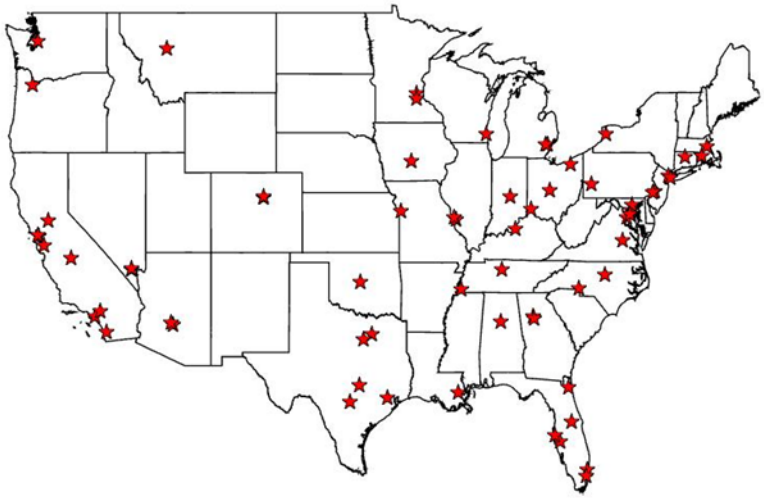

Figure D-1: The locations of the 69 active Near-road (monitoring) Network sites in the Continental US

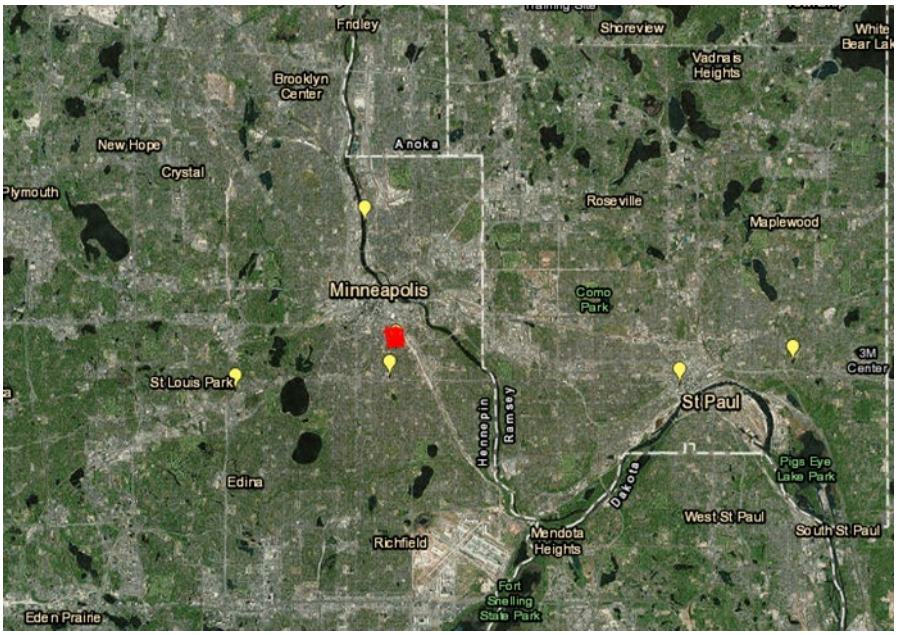

Figure D-2: $PM_{2.5}$ monitors in Minneapolis, MN. The yellow flags are $PM_{2.5}$ monitoring sites and the red block indicates the Near-road (monitoring) Network site. Each monitor within the Minneapolis-St. Paul city boundary or 10 miles of a near-road monitor (~city scale) was used for comparison in this study.

Figure D-3: City averaged comparison of two-year average concentrations of near-road sites against non-near-road sites for (a) NO_2 (ppb) (b) $PM_{2.5}$ (μg m^{-3}) and (c) CO (ppm). Positive values indicate near-road sites have higher two-year average concentrations than the non-near-road sites.

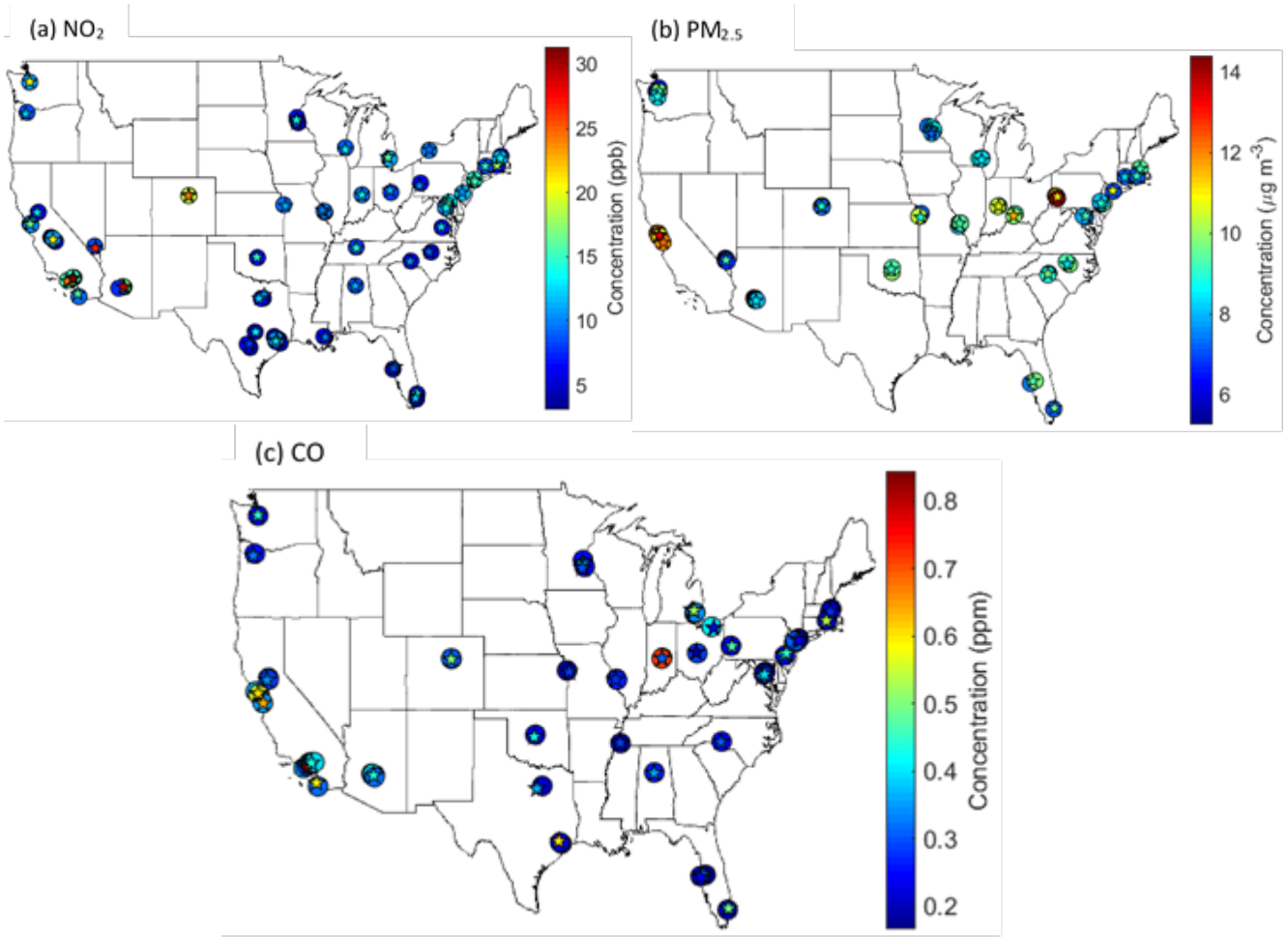

Figure D-4: The two- year average concentrations for (a) NO_2 (ppb) (b) $PM_{2.5}$ (µg m^{-3}) and (c) CO (ppm) at monitoring sites used in this study. Stars indicate near-road sites and the circles indicate non-near-road sites.

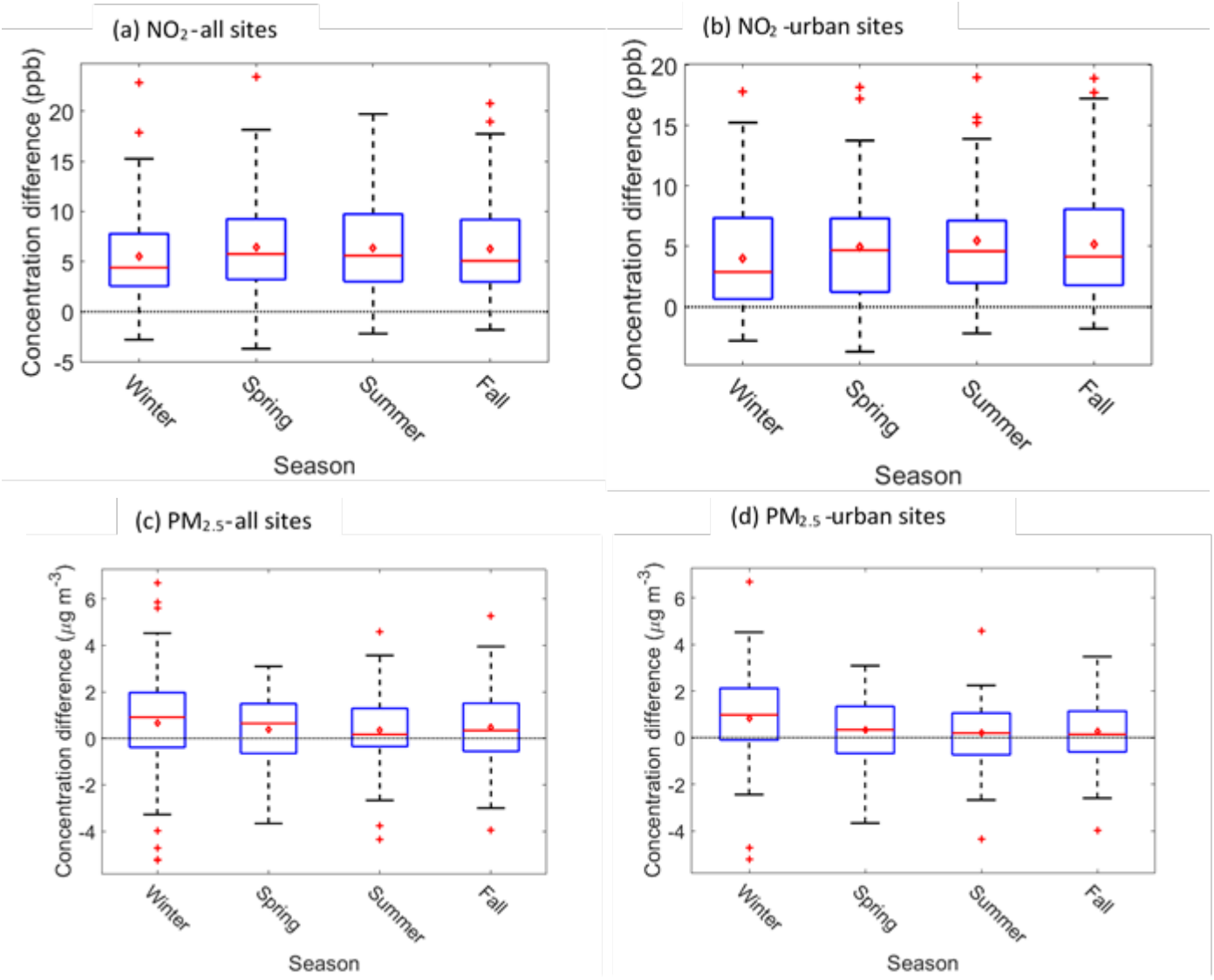
(a) NO2 -all sites
Concentration difference (ppb)
20
15
10
5
0
-5
Winter
Spring
Summer
Fall
Season
(b) NO2 -urban sites
Concentration difference (ppb)
20
15
10
5
0
Winter
Spring
Summer
Fall
Season
(c) PM2.5 -all sites
Concentration difference (μg m-3)
6
4
2
0
-2
-4
Winter
Spring
Summer
Fall
Season
(d) PM2.5 -urban sites
Concentration difference (μg m-3)
6
4
2
0
-2
-4
Winter
Spring
Summer
Fall
Season

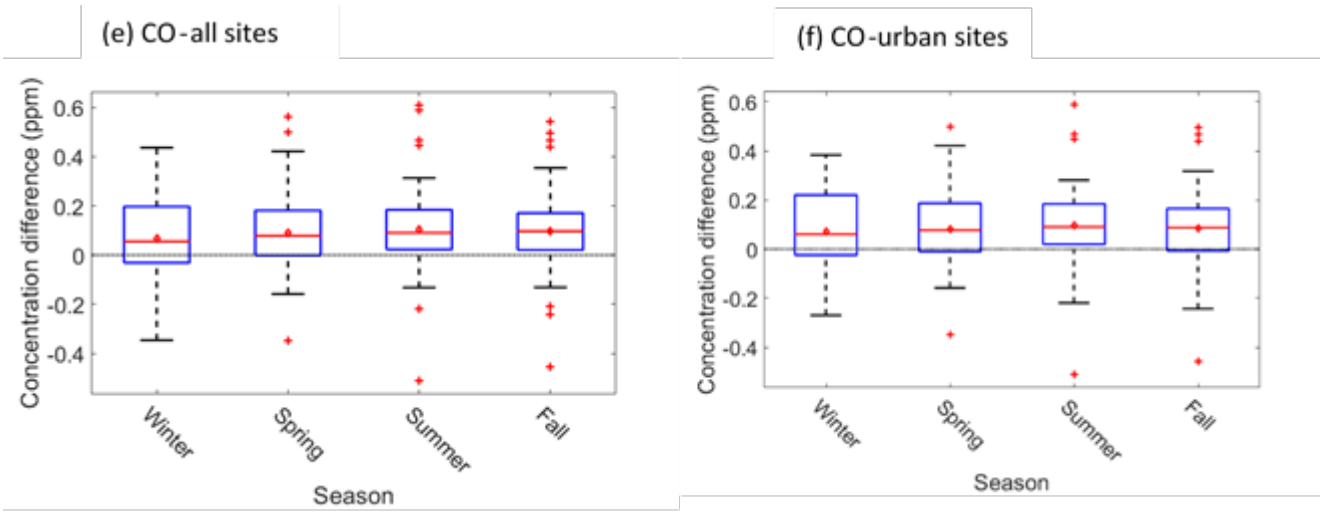

Figure D-5: Seasonal (a-b) NO_2, (c-d) $PM_{2.5}$, and (e-f) CO concentration differences between near-road sites and (left) all non-near-road sites and (right) urban non-near-road sites. Positive values indicate near-rad sites have higher two-year average concentrations than the non-near-road sites. The boxes represent the interquartile (25%-75%) range and the red line is the median. The red diamond represents the average concentration difference.

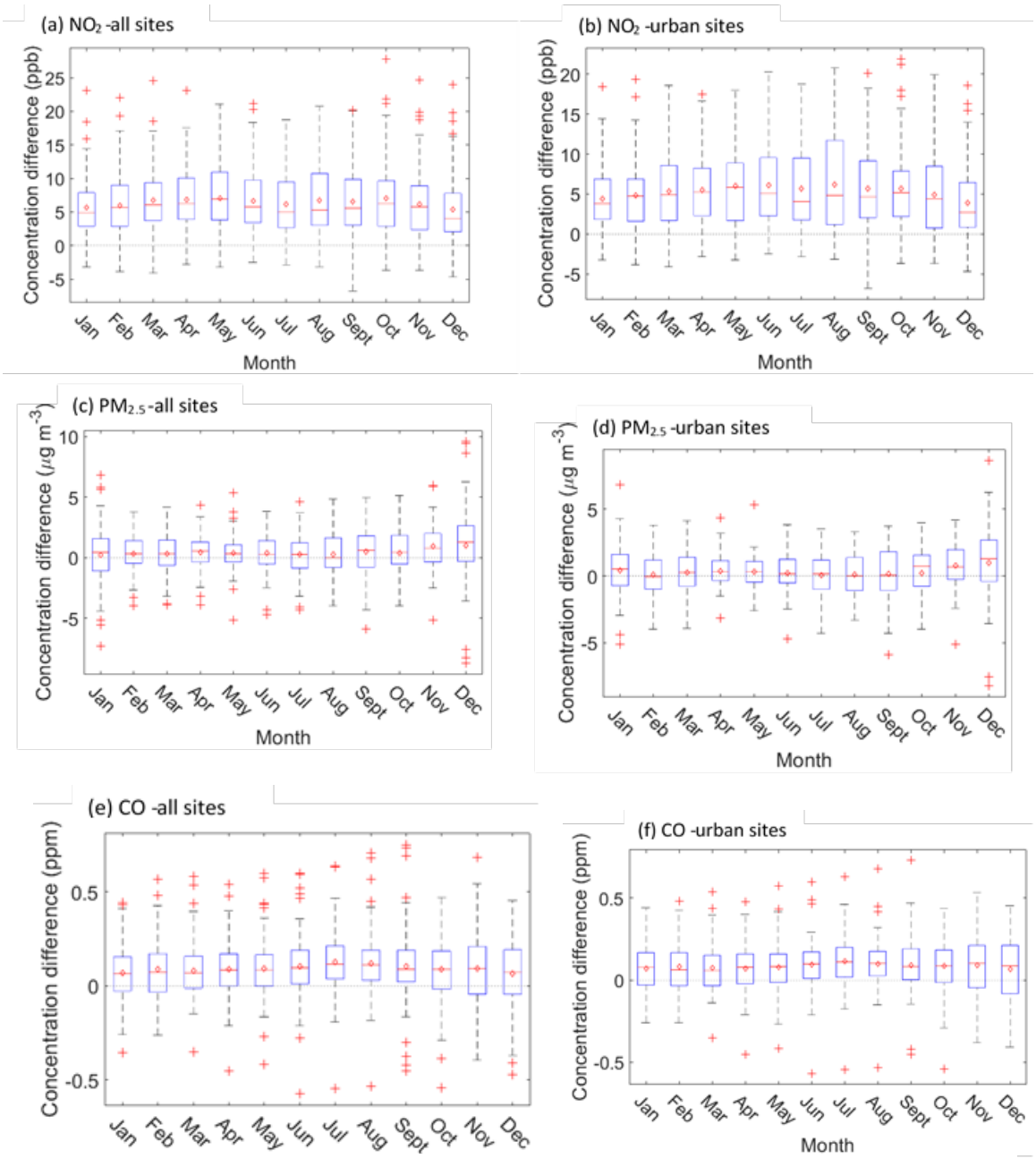

Figure D-6: Monthly (a-b) NO_2, (c-d) $PM_{2.5}$, and (e-f) CO concentration differences between Near-Road (monitoring) Network (NRN) sites and (left) all non-NRN sites and (right) urban non-NRN sites. Positive values indicate NRN sites have higher two-year average concentrations than the non-NRN sites. The boxes represent the interquartile range (25%-75%), the red line indicates the median, and the red diamond represents the two-year average concentration difference.

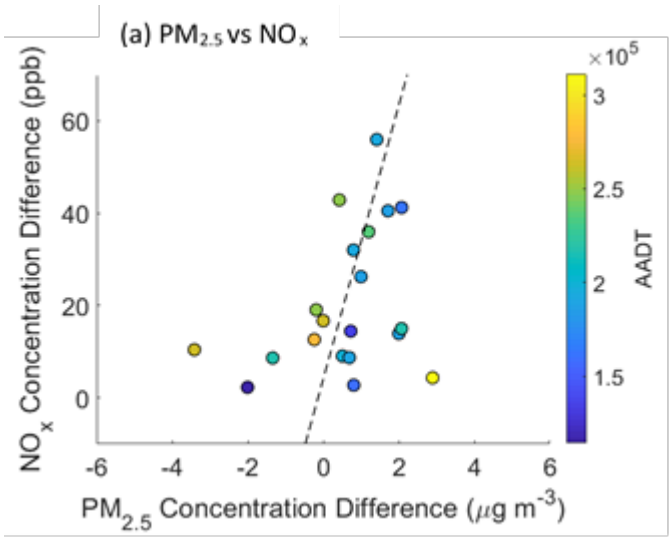

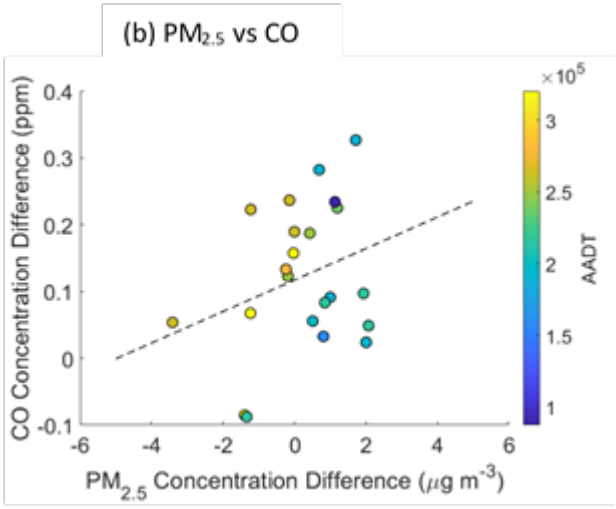

$$\partial[NO_x] = 30\frac{ppb\ NO_x}{\mu g\ m^{-3}\ PM_{2.5}} * \partial[PM_{2.5}] + 4\ ppb\ NO_x \qquad \partial[CO] = 24\frac{ppb\ CO}{\mu g\ m^{-3}\ PM_{2.5}} * \partial[PM_{2.5}] + 110\ ppb\ CO$$

Figure D-7: The difference in two-year average (a) $PM_{2.5}$ and NO_x and (b) $PM_{2.5}$ and CO concentrations between a Near-Road (monitoring) Network (NRN) site and non-NRN site. The positive values indicate the NRN concentration is higher than the non-NRN concentration. Few cases exist where either the CO or NO_x difference falls below zero.

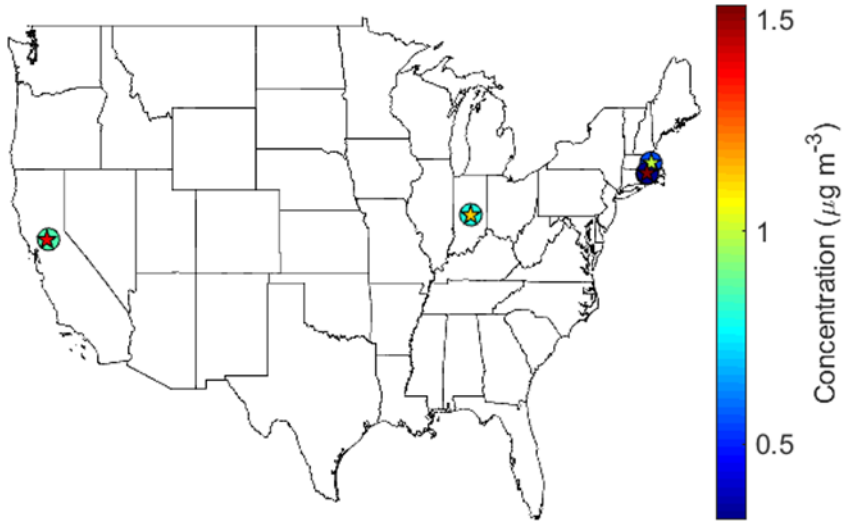

Figure D-8: The annual average concentration for BC (μg m^{-3}) at monitoring sites used in this study. Stars indicate near-road sites and the circles are regulatory sites within the city boundary / 10 miles of the near-road monitor.

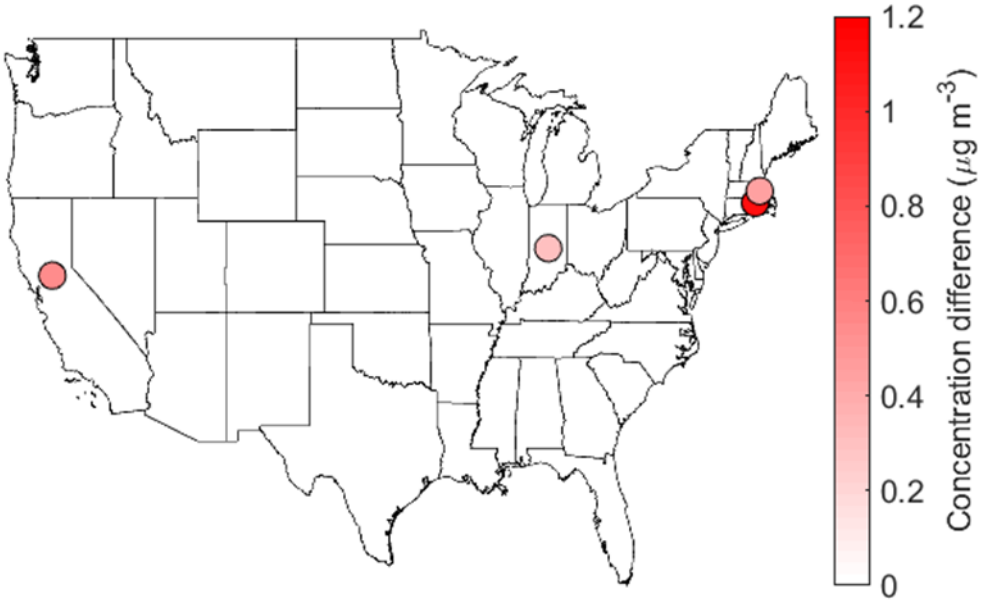

Figure D-9: Comparison of annual average concentrations of near-road sites against non-near-road sites for BC (µg m^{-3}). Positive values indicate locations where the average concentration at the near-road sites is higher than the non-near-road sites

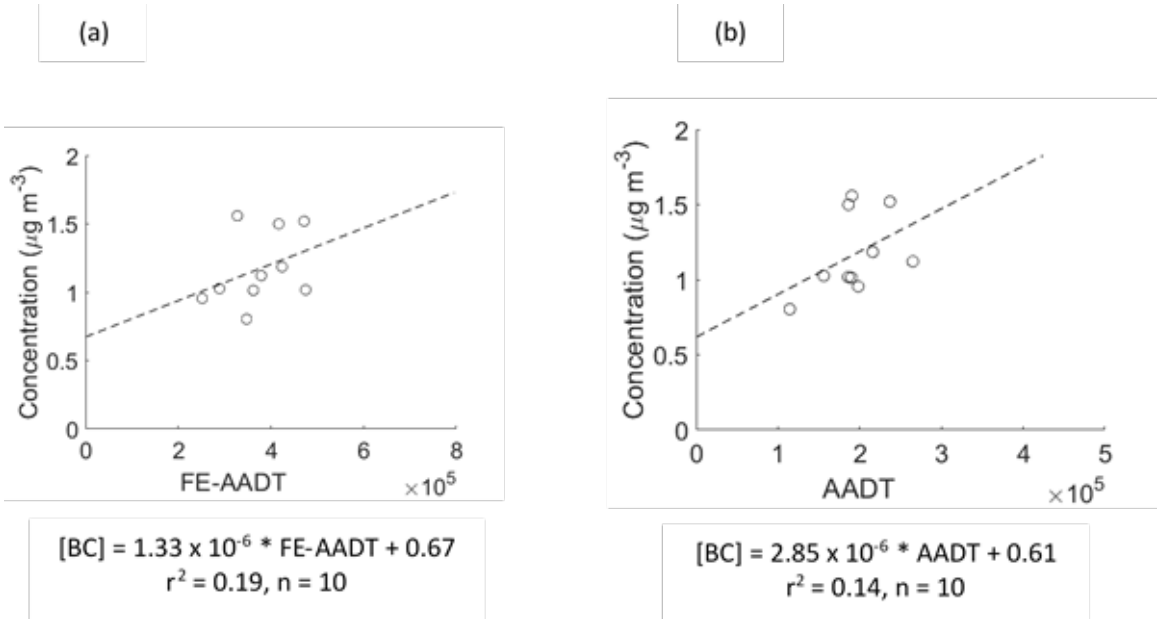

Figure D-10: (a) Fleet-Equivalent Annual Average Daily Traffic (FE-AADT) and (b) AADT versus near-road site annual average BC concentrations (µg m^{-3}).

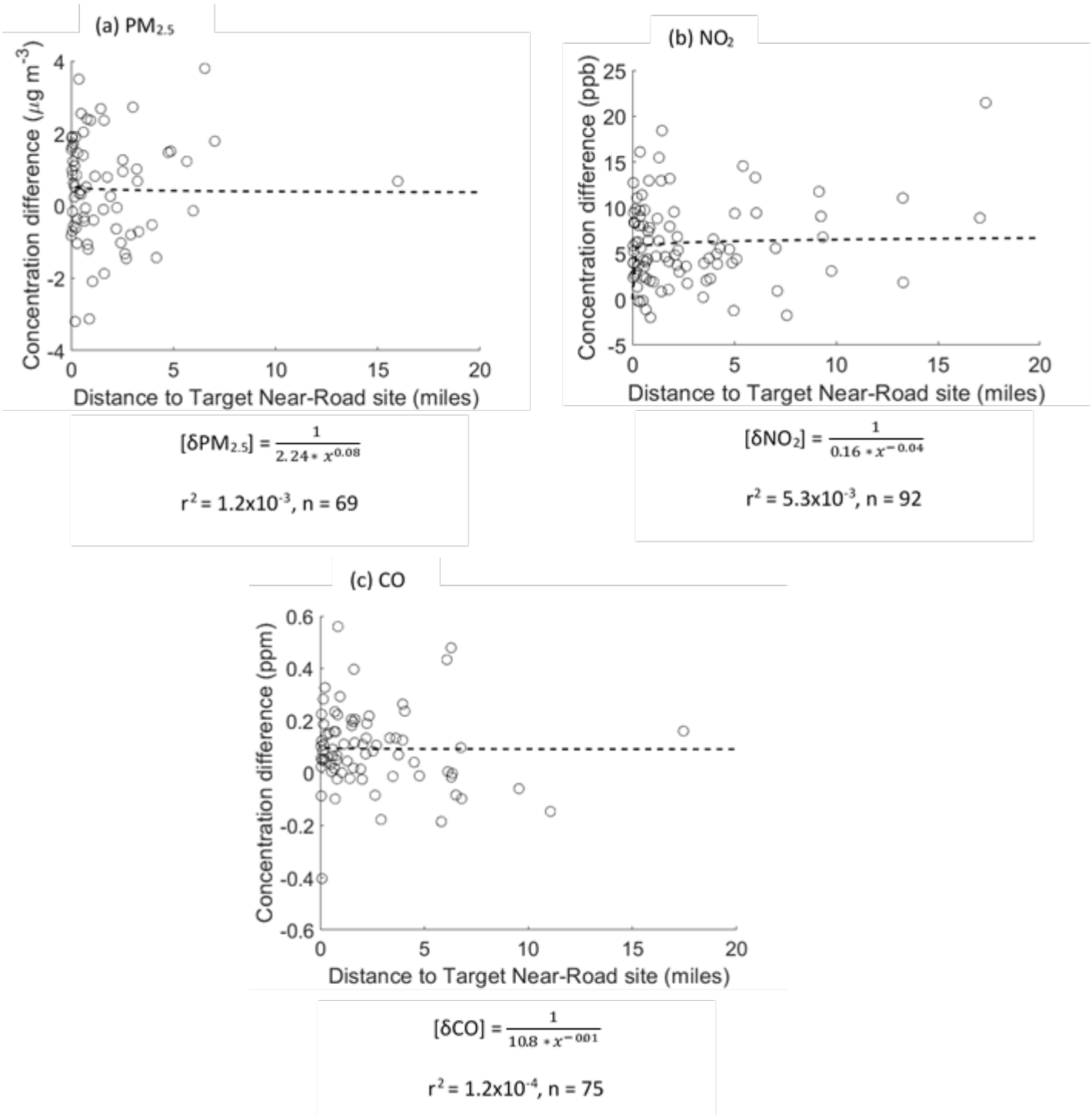

Figure D-11: Inverse distance weighting of the concentration differences between near-road and non-near-sites for (a) $PM_{2.5}$ (μg m^{-3}), (b) NO_2 (ppb), and (c) CO (ppm)

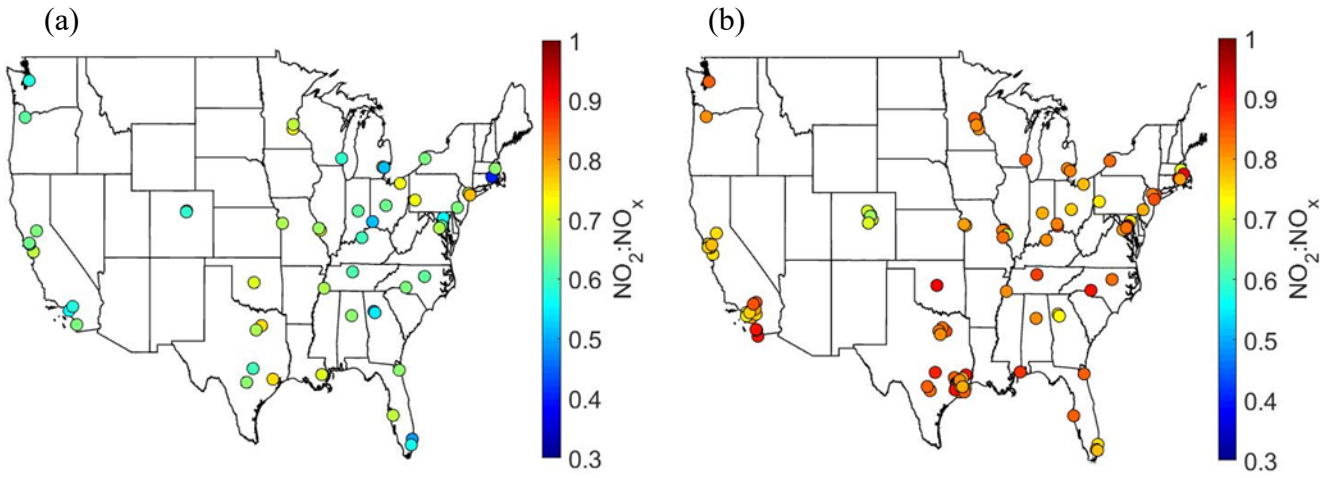

Figure D-12: NO_2:NO_x ratios at the (a) near-road sites and (b) the non-near-road sites

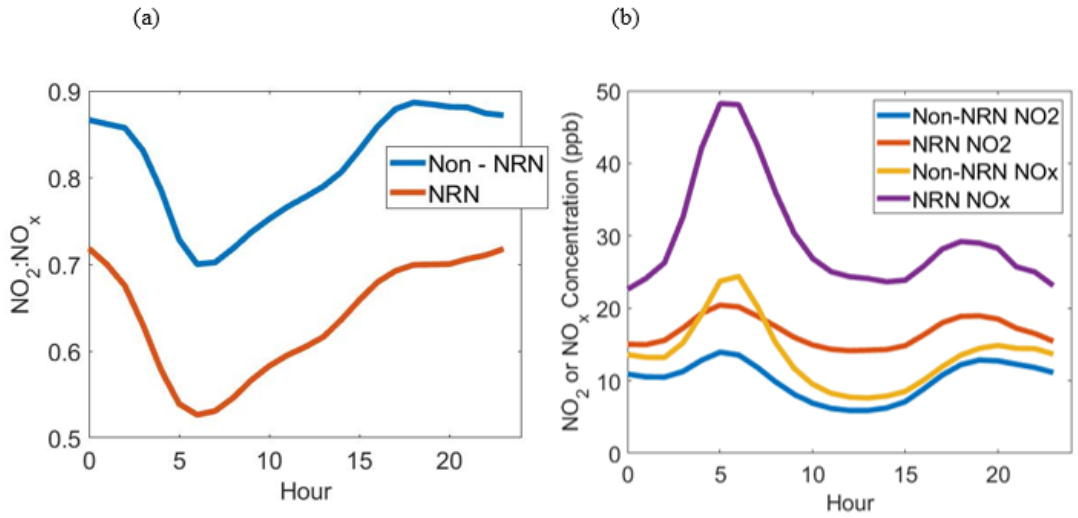

Figure D-13: Average diurnal pattern of the (a) NO_2:NO_x at the Near-Road (monitoring) Network (NRN) and non-NRN sites and (b) NO_2 and NO_x concentrations at the NRN and non-NRN sites

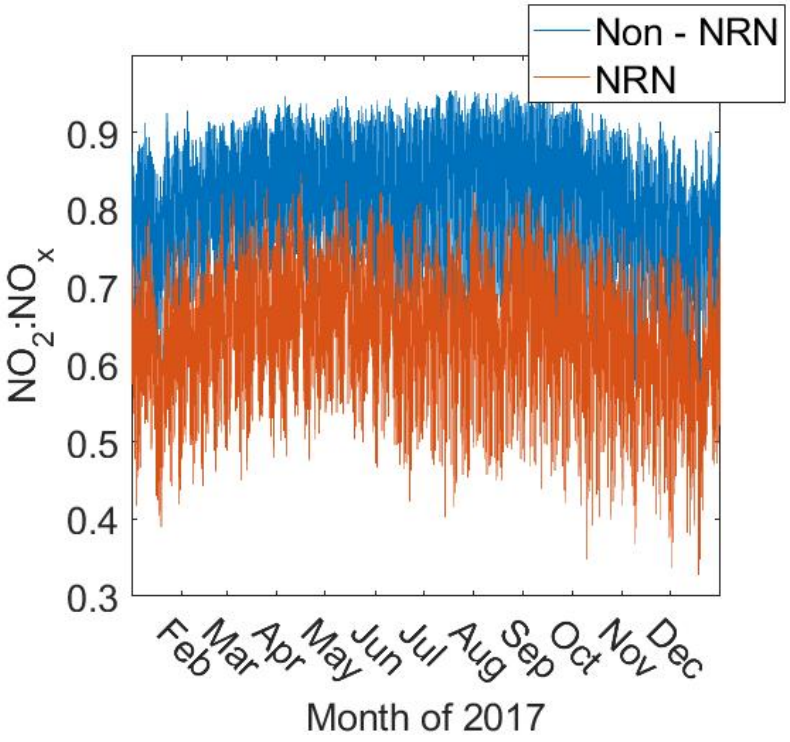

Figure D-14: Time series plot of the NO_2:NO_x at the Near-Road (monitoring) Network (NRN) and non-NRN in 2017

Table D-1: List of the near-road sites and the non-near-road sites that met the initial analysis criteria (i.e., either a near-road site or a non-near-road site within 10 miles of the near-road site) used in this analysis. Sites with the asterisk (*) indicates these non-near-road sites were removed from the pair comparison as they fell within a decay to background distance ($L_{PM2.5}$ = 350m and L_{NO2}= L_{CO} = 970m) of the target highway. In some instances, the non-near-road site is within the decay to background distance for NO_2 or CO, but not for $PM_{2.5}$. Such instances are indicated with the asterisk (*) on both the site name and the pollutants that were excluded from the paired comparisons. The buffer removed 11, 37, and 35 $PM_{2.5}$, NO_2, and CO comparisons, respectively.

Location	AQS Site ID No.	Site Name	NEAR-ROAD or non-near-road	Measured Pollutants
Anaheim, CA.	06-059-0008	NR - Anaheim Route 5	NEAR-ROAD	NO_2, NOx, CO
Anaheim, CA.	06-059-0007	Anaheim*	non-near-road	NO_2, NOx, CO
Anaheim, CA.	06-059-5001	La Habra	non-near-road	NO_2, NOx, CO
Atlanta, GA.	13-121-0056	NR – Georgia Tech	NEAR-ROAD	NO_2, CO
Atlanta, GA.	13-089-0003	NR-285	NEAR-ROAD	NO_2
Atlanta, GA.	13-089-0002	S. DeKalb*	non-near-road	NO_2, CO
Austin, TX.	48-453-1068	Near Road Austin North Interstate 35	NEAR-ROAD	NO_2, NOx
Austin, TX.	48-453-0014	Austin Northwest	non-near-road	NO_2, NOx
Baltimore, MD.	24-510-0040	Oldtown	non-near-road	NO_2, NOx
Baltimore, MD.	24-005-0009	NR Baltimore	NEAR-ROAD	NO_2, NOx
Baltimore, MD.	24-033-0030	HU-Beltsville	non-near-road	NO_2, NOx, CO, $PM_{2.5}$
Baltimore, MD.	24-027-0006	NR Baltimore Howard County	NEAR-ROAD	NO_2, NOx, CO, $PM_{2.5}$
Baltimore, MD.	24-031-3001	Rockville	non-near-road	$PM_{2.5}$
Birmingham, AL.	01-073-2059	NR Arkadelphia	NEAR-ROAD	NO_2, NOx, CO
Birmingham, AL.	01-073-0023	North Birmingham	non-near-road	NO_2, NOx, CO
Birmingham, AL.	01-073-1003	Fairfield*	non-near-road	CO
Boston, MA.	25-025-0044	Von Hillern St	NEAR-ROAD	NO_2, NOx, CO, $PM_{2.5}$, BC
Boston, MA.	25-025-0002	Boston Kenmore SQ*	non-near-road	NO_2, NOx,
Boston, MA.	25-025-0042	Dudley Square Roxbury	non-near-road	NO_2, NOx, CO, $PM_{2.5}$, BC
Boston, MA.	25-009-2006	Lynn Water Treatment Plant	non-near-road	NO_2, NOx, CO

Boston, MA.	25-025-0043	North End Site Central Artery*	non-near-road	$PM_{2.5}$
Buffalo, NY.	36-029-0023	Near Road Buffalo	NEAR-ROAD	NO_2, NOx, CO
Buffalo, NY.	36-029-0005	Buffalo	non-near-road	NO_2, NOx, CO
Charlotte, NC.	37-119-0045	NR-Remount	NEAR-ROAD	NO_2, NOx, CO, $PM_{2.5}$
Charlotte, NC.	37-119-0041	Garinger HS	non-near-road	NO_2, NOx, CO, $PM_{2.5}$
Charlotte, NC.	37-119-0042	Montclair Elem. School	non-near-road	$PM_{2.5}$
Cincinnati, OH.	39-061-0040	Taft	non-near-road	NO_2, NOx, CO, $PM_{2.5}$
Cincinnati, OH.	39-061-0048	Cincinnati Near Road	NEAR-ROAD	NO_2, NOx, CO, $PM_{2.5}$
Cincinnati, OH.	39-061-0006	Sycamore*	non-near-road	$PM_{2.5}$
Cleveland, OH.	39-035-0073	Cleveland NR	NEAR-ROAD	NO_2, NOx
Cleveland, OH.	39-035-0060	GT Craig	non-near-road	NO_2, NOx
Columbus, OH.	39-049-0034	Fairground	non-near-road	NO_2, NOx, CO
Columbus, OH.	39-049-0038	Smoky Row	NEAR-ROAD	NO_2, NOx, CO
Dallas, TX.	48-113-1067	Dallas LBJ Freeway	NEAR-ROAD	NO_2, NOx
Dallas, TX.	48-113-0075	Dallas North #2*	non-near-road	NO_2, NOx
Dallas, TX.	48-113-0069	Dallas Hinton*	non-near-road	NO_2, NOx
Dallas, TX.	48-113-0087	Dallas Redbird Airport Ex	non-near-road	NO_2, NOx
Denver, CO.	08-031-0002	Denver - Camp	non-near-road	NO_2, NOx, CO, $PM_{2.5}$
Denver, CO.	08-031-0027	I-25	NEAR-ROAD	NO_2, NOx, CO, $PM_{2.5}$
Denver, CO.	08-031-0028	Globeville	NEAR-ROAD	NO_2, NOx, $PM_{2.5}$
Denver, CO.	08-031-0026	La Casa*	non-near-road	*NO_2, *NOx, *CO, $PM_{2.5}$
Denver, CO.	08-001-3001	Welby*	non-near-road	NO_2, NOx, CO
Denver, CO.	08-031-0013	Denver – NJH-E	non-near-road	$PM_{2.5}$
Denver, CO.	08-001-0008	Tri County Health	non-near-road	$PM_{2.5}$
Detroit, MI.	26-163-0093	NR – Eliza Howell	NEAR-ROAD	NO_2, NOx, CO
Detroit, MI.	26-163-0095	NR - Livonia	NEAR-ROAD	NO_2, NOx, CO
Detroit, MI.	26-163-1011	Allen park	non-near-road	NO_2, NOx, CO
Detroit, MI.	26-163-1009	Mark Twain M.S.	non-near-road	CO
Detroit, MI.	26-163-1006	S. Fort St.	non-near-road	CO
Detroit, MI.	26-163-1005	NW Fort St.	non-near-road	CO
Detroit, MI.	26-163-1008	Fort St.	non-near-road	CO
Fresno, CA.	06-039-0004	Pump Yard	non-near-road	NO_2
Fresno, CA.	06-019-0242	Fresno-Sky Park	non-near-road	NO_2
Fresno, CA.	06-019-5001	Clovis-Villa*	non-near-road	NO_2

Fresno, CA.	06-019-0011	Garland	non-near-road	NO_2
Fresno, CA.	06-019-2016	Fresno-Foundry	NEAR-ROAD	NO_2
Fresno, CA.	06-019-0007	Drummond	non-near-road	NO_2
Fresno, CA.	06-019-4001	Parlier	non-near-road	NO_2
Ft. Lauderdale, FL.	12-011-8002	Dr. Von Mizell-Eula Johnson State Park	non-near-road	NO_2, NOx, CO
Ft. Lauderdale, FL.	12-011-0035	Near Road - Ft. Lauderdale	NEAR-ROAD	NO_2, NOx, CO, $PM_{2.5}$
Ft. Lauderdale, FL.	12-011-0034	Daniel Banu	non-near-road	CO, $PM_{2.5}$
Fort Lee, NJ.	34-003-0010	Fort Lee NR	NEAR-ROAD	NO_2, NOx, CO, $PM_{2.5}$
Fort Lee, NJ.	36-005-0110	IS 52	non-near-road	NO_2, NOx, $PM_{2.5}$
Fort Lee, NJ.	36-005-0133	Pfizer lab site*	non-near-road	NO_2, NOx, CO
Fort Lee, NJ.	34-039-0002*	Elizabeth Lab	non-near-road	CO
Fort Lee, NJ.	36-061-0135*	CCNY	non-near-road	CO
Fort Lee, NJ.	34-013-0003	Firehouse	non-near-road	CO
Fort Lee, NJ.	34-017-1002*	Jersey City	non-near-road	CO
Fort Lee, NJ.	36-081-0125	Queens College	NEAR-ROAD	NO_2, NOx, CO
Fort Worth, TX.	48-439-1053	Fort Worth California Parkway North	NEAR-ROAD	NO_2, NOx, CO
Fort Worth, TX.	48-113-0069	Hinton*	non-near-road	CO
Fort Worth, TX.	48-439-1002*	Fort Worth NW	non-near-road	NO_2, NOx
Fort Worth, TX.	48-439-3011	Arlington Municipal Airport	non-near-road	NO_2, NOx
Hartford, CT.	09-003-1003	McAuliffe Park	non-near-road	$PM_{2.5}$
Hartford, CT.	09-003-0025	Hartford - NEAR-ROAD	NEAR-ROAD	$PM_{2.5}$
Highland Heights, KY.	21-037-3002*	Northern Kentucky University	non-near-road	NO_2, NOx
Houston, TX.	48-201-0024	Houston Aldine	non-near-road	NO_2, NOx
Houston, TX.	48-201-0047	Lang	non-near-road	NO_2, NOx
Houston, TX.	48-201-1052	North Loop	NEAR-ROAD	NO_2, NOx, CO
Houston, TX.	48-201-1066	Houston Freeway	NEAR-ROAD	NO_2, NOx
Houston, TX.	48-201-0055	Houston Bayland Park	non-near-road	NO_2, NOx
Houston, TX.	48-201-0416*	Park Place	non-near-road	NO_2, NOx
Houston, TX.	48-201-1035	Clinton	non-near-road	NO_2, NOx, CO
Houston, TX.	48-201-1034*	Houston East	non-near-road	NO_2, NOx
Houston, TX.	48-201-1039	Houston Deer Park #2	non-near-road	NO_2, NOx, CO
Houston, TX.	48-201-0026	Channelview	non-near-road	NO_2, NOx

Houston, TX.	48-201-0029	Northwest Harris County	non-near-road	NO_2, NOx
Houston, TX.	48-039-1004*	Manvel Croix Park	non-near-road	NO_2, NOx
Houston, TX.	48-201-1050	Seabrook Friendship Park	non-near-road	NO_2, NOx
Indianapolis, IN.	18-097-0087	Indianapolis - I70	NEAR-ROAD	NO_2, NOx, CO, $PM_{2.5}$, BC
Indianapolis, IN.	18-097-0078	Washington Park	non-near-road	NO_2, NOx, CO, $PM_{2.5}$, BC
Indianapolis, IN.	18-097-0072	Illinois St.	non-near-road	CO
Indianapolis, IN.	18-097-0081	W. 18th St.	NEAR-ROAD	$PM_{2.5}$
Jacksonville, FL	12-031-0032	Kooker Park*	non-near-road	NO_2, NOx
Jacksonville, FL	12-031-0108	Pepsi Place	NEAR-ROAD	NO_2, NOx, CO
Jacksonville, FL	12-031-0084	Rosselle*	non-near-road	CO
Jacksonville, FL	12-031-0080	Playground*	non-near-road	CO
Jacksonville, FL.	12-086-0035	Perimeter Rd	NEAR-ROAD	NO_2, NOx
Jacksonville, FL.	12-086-4002	Lab Annex*	non-near-road	NO_2, NOx
Jacksonville, FL.	12-086-0027	Rosenstiel*	non-near-road	NO_2, NOx
Kansas City, MO.	29-095-0034	Troost, KC	non-near-road	NO_2, NOx, $PM_{2.5}$
Kansas City, MO.	29-095-0042	Blue Ridge, I-70	NEAR-ROAD	NO_2, NOx, CO, $PM_{2.5}$, BC
Kansas City, MO.	20-209-0021	JFK	non-near-road	NO_2, NOx, CO, $PM_{2.5}$
Kansas City, MO.	29-047-0005	Liberty	non-near-road	$PM_{2.5}$
Las Vegas, NV	32-003-1501	Near Road Rancho And Teddy	NEAR-ROAD	NO_2, CO, $PM_{2.5}$
Las Vegas, NV	32-003-1502	Near Road Casino Center	NEAR-ROAD	NO_2,
Las Vegas, NV	32-003-0561	Sunrise Acres*	non-near-road	*NO_2, *CO, $PM_{2.5}$
Las Vegas, NV	32-003-0075	Joe Neal	non-near-road	NO_2, $PM_{2.5}$
Las Vegas, NV	32-003-0540	Jerome Mack (Ncore)*	non-near-road	*NO_2, *CO, $PM_{2.5}$
Las Vegas, NV	32-003-0043	Paul Meyer	non-near-road	$PM_{2.5}$
Las Vegas, NV	32-003-0298	Green Valley	non-near-road	$PM_{2.5}$
Long Beach, CA.	06-037-4008	NR = Long Beach	NEAR-ROAD	NO_2, NOx
Long Beach, CA.	06-037-4006	Long Beach Hudson*	non-near-road	NO_2, NOx, CO
Long Beach, CA.	06-037-1302	Compton	non-near-road	NO_2, NOx
Louisville, KY.	21-111-0075	NR Durett Lane - Louisville	NEAR-ROAD	NO_2, NOx, CO
Louisville, KY.	21-111-0067	Cannons Lane*	non-near-road	NO_2, NOx, CO
Memphis, TN.	47-157-0075	Memphis – NCORE	non-near-road	CO
Memphis, TN.	47-157-0100	Near Road SW Tennessee	NEAR-ROAD	CO

		Community College		
Milwaukee, WI.	55-079-0056	College Ave	NEAR-ROAD	NO_2, NOx, $PM_{2.5}$
Milwaukee, WI.	55-079-0026	Milwaukee DNR	non-near-road	NO_2, NOx, $PM_{2.5}$
Milwaukee, WI.	55-133-0027	Waukehsa	non-near-road	$PM_{2.5}$
Milwaukee, WI.	55-079-0010	16th St. Health Center	non-near-road	$PM_{2.5}$
Minneapolis, MN.	27-053-0962	Near Road I-35/I-94	NEAR-ROAD	NO_2, NOx, CO, $PM_{2.5}$
Minneapolis, MN.	27-003-1002	Anoka County Airport	non-near-road	NO_2, NOx, CO, $PM_{2.5}$
Minneapolis, MN.	27-037-0480	Near Road I-35	NEAR-ROAD	NO_2, NOx
Minneapolis, MN.	27-037-0423	Flint Hills refinery	non-near-road	NO_2, NOx, CO
Minneapolis, MN.	27-123-0050	Lexington Ave.*	non-near-road	CO
Minneapolis, MN.	27-053-0954	Hennepin Center Arts*	non-near-road	CO
Minneapolis, MN.	27-037-0020	Flint Hills Refinery*	non-near-road	CO
Minneapolis, MN.	27-171-3201	St. Michael Elementary School	non-near-road	$PM_{2.5}$
Minneapolis, MN.	27-053-0963	Andersen School	non-near-road	$PM_{2.5}$
Minneapolis, MN.	27-123-0871	Harding High School	non-near-road	$PM_{2.5}$
Minneapolis, MN.	27-37-470	Apple Valley	non-near-road	$PM_{2.5}$
New Orleans, LA.	22-051-1001	Kenner	non-near-road	NO_2, NOx
New Orleans, LA.	22-071-0021	NR I-610	NEAR-ROAD	NO_2, NOx
Oakland, CA.	06-001-0012	Laney College	NEAR-ROAD	NO_2, NOx, CO, $PM_{2.5}$, BC
Oakland, CA.	06-001-0013	Berkeley Aquatic Park	NEAR-ROAD	NO_2, NOx, CO, $PM_{2.5}$, BC
Oakland, CA.	06-001-0011	Oakland West	non-near-road	NO_2, NOx, CO, $PM_{2.5}$
Oakland, CA.	06-001-0009	Oakland	non-near-road	NO_2, NOx, CO, $PM_{2.5}$
Oakland, CA.	06-013-1004	San Pablo	non-near-road	CO, $PM_{2.5}$
Oakland, CA.	06-041-0001	San Rafael	non-near-road	CO, $PM_{2.5}$
Oakland, CA.	06-075-0005	San Francisco *	non-near-road	CO, $PM_{2.5}$
Oklahoma City, OK.	40-109-0033	OKC Central	non-near-road	NO_2, NOx, $PM_{2.5}$
Oklahoma City, OK.	40-109-0097	NR – OKC	NEAR-ROAD	NO_2, NOx, CO, $PM_{2.5}$
Oklahoma City, OK.	40-109-1037	OKC North	non-near-road	CO, $PM_{2.5}$
Oklahoma City, OK.	40-027-0049	Moore Water Tower	non-near-road	$PM_{2.5}$

Ontario, CA.	06-071-0026	Ontario Near Road	NEAR-ROAD	NO_2, NOx, CO
Ontario, CA.	06-071-0027	Ontraio-Route60 NR	NEAR-ROAD	NO_2, NOx
Ontario, CA.	06-071-1004	Upland	non-near-road	NO_2, NOx, CO
Ontario, CA.	06-037-1701	Pomona	non-near-road	NO_2, NOx, CO
Ontario, CA.	06-071-2002	Fontana	non-near-road	NO_2, NOx, CO
Ontario, CA.	06-065-8005	Mira Loma	non-near-road	CO
Ontario, CA.	06-071-9004	San Bernardino	non-near-road	CO
Philadelphia, PA	34-007-0002	Camden Spruce St.	Non-near-road	CO
Philadelphia, PA	42-101-0048	North East Waste*	non-near-road	CO*, $PM_{2.5}$
Philadelphia, PA	42-101-0076	Car-Barn Mont	NEAR-ROAD	CO, $PM_{2.5}$
Philadelphia, PA	42-101-0075	Torresdale Station	NEAR-ROAD	CO
Philadelphia, PA	42-101-0055	Ritner*	non-near-road	$PM_{2.5}$
Philadelphia, PA	42-101-0057	Fire Admin Building*	non-near-road	$PM_{2.5}$
Philadelphia, PA	42-091-0013	Trailer	non-near-road	$PM_{2.5}$
Phoenix, AZ.	04-013-4019	Diablo	NEAR-ROAD	NO_2, CO, $PM_{2.5}$
Phoenix, AZ.	04-013-4003	S. Phoenix	non-near-road	CO, $PM_{2.5}$
Phoenix, AZ.	04-013-1003	Mesa	non-near-road	CO, $PM_{2.5}$
Phoenix, AZ.	04-013-4020	33rd	NEAR-ROAD	NO_2,
Phoenix, AZ.	04-013-0019	West Phoenix	non-near-road	NO_2, CO, $PM_{2.5}$
Phoenix, AZ.	04-013-9997	JLG Supersite*	non-near-road	NO_2, CO, $PM_{2.5}$
Phoenix, AZ.	04-013-3002	Central Phoenix	non-near-road	NO_2, CO
Phoenix, AZ.	04-013-4011	Buckeye	non-near-road	NO_2
Phoenix, AZ.	04-013-2001	Glendale	non-near-road	$PM_{2.5}$
Phoenix, AZ.	04-013-1004	N. Phoenix	non-near-road	$PM_{2.5}$
Phoenix, AZ.	04-013-9812	Durango Complex	non-near-road	$PM_{2.5}$
Phoenix, AZ.	04-013-4005	Tempe	non-near-road	$PM_{2.5}$
Pittsburgh, PA	42-003-0008	Lawrenceville	non-near-road	CO, $PM_{2.5}$
Pittsburgh, PA	42-003-1376	Pittsburgh – NEAR-ROAD	NEAR-ROAD	NO_2, CO, $PM_{2.5}$
Pittsburgh, PA	42-003-0031	Flag Plaza*	non-near-road	CO
Pittsburgh, PA	42-003-0002	Avalon	non-near-road	$PM_{2.5}$
Pittsburgh, PA	42-003-0064	Liberty	non-near-road	$PM_{2.5}$
Portland, OR.	41-051-0080	Portland - SE Lafayette	non-near-road	NO_2, NOx, CO
Portland, OR.	41-067-0005	Near Road Portland	NEAR-ROAD	NO_2, NOx, CO, BC
Providence, RI.	44-007-0030	Providence NEAR-ROAD	NEAR-ROAD	NO_2, NOx, BC, CO, $PM_{2.5}$
Providence, RI.	44-007-1010	Francis School	non-near-road	NO_2, NOx, BC, CO, $PM_{2.5}$

Providence, RI.	44-007-0022	Urban League Building Rooftop	non-near-road	BC, $PM_{2.5}$
Raleigh, NC.	37-183-0021	Triple Oak	NEAR-ROAD	NO_2, NOx, CO, $PM_{2.5}$
Raleigh, NC.	37-183-0014	Millbrook School	non-near-road	NO_2, NOx, CO, $PM_{2.5}$
Raleigh, NC	37-183-0015	Durham Armory	non-near-road	$PM_{2.5}$
Richmond, VA.	51-760-0025	Bryan Park	NEAR-ROAD	NO_2, CO
Richmond, VA.	51-087-0014	Math Science Innovation Center*	non-near-road	CO
Rochester, NY	36-055-1007	Rochester*	non-near-road	CO
Rochester, NY	36-055-0015	Rochester - NEAR-ROAD	NEAR-ROAD	NO_2, CO
Sacramento, CA.	06-067-0015	Bercut Drive	NEAR-ROAD	NO_2, NOx, CO, BC
Sacramento, CA.	06-067-0010	1309 T Street*	non-near-road	NO_2, NOx
Sacramento, CA.	06-067-0006	Del Paso Manor	non-near-road	NO_2, NOx, CO, BC
Sacramento, CA.	06-067-0002	North Highlands	non-near-road	CO
San Antonio, TX.	48-029-0032	San Antonio Northwest	non-near-road	NO_2, NOx
San Antonio, TX.	48-029-1069	SA I-35	NEAR-ROAD	NO_2, NOx
San Antonio, TX.	48-029-0059	Calaveras Lake	non-near-road	NO_2, NOx
San Diego, CA.	06-073-1022	El Cajon – Lexington Elementary	non-near-road	CO
San Diego, CA.	06-073-1017	San Diego - NEAR-ROAD	NEAR-ROAD	NO_2, CO
San Jose, CA.	06-085-0006	Knox Avenue	NEAR-ROAD	NO_2, NOx, CO, $PM_{2.5}$
San Jose, CA.	06-085-0005	Jackson	non-near-road	NO_2, NOx, CO, $PM_{2.5}$
Seattle, WA.	53-033-0080	Seattle-Beacon hill	non-near-road	NO_2, NOx, CO, $PM_{2.5}$
Seattle, WA.	53-033-0030	Near Road 10th & Weller	NEAR-ROAD	NO_2, NOx, CO, $PM_{2.5}$, BC
Seattle, WA.	53-033-0005	Lynnwood – 212th	non-near-road	$PM_{2.5}$
Seattle, WA.	53-033-0057	Duwamish	non-near-road	$PM_{2.5}$
St. Louis, MO.	17-163-0010	IEPA-RAPS Trailer, East St. Louis	non-near-road	NO_2, CO
St. Louis, MO.	29-510-0085	Blair Street	non-near-road	NO_2, CO, $PM_{2.5}$
St. Louis, MO.	29-510-0086	Margareta Cat B Core Slam	non-near-road	NO_2,
St. Louis, MO.	29-510-0094	Forest Park	NEAR-ROAD	NO_2, CO, $PM_{2.5}$
St. Louis, MO.	29-189-0016	Rider Trail I70	NEAR-ROAD	NO_2,
St. Louis, MO.	29-099-0019	Arnold West	non-near-road	$PM_{2.5}$
St. Louis, MO.	29-189-3001	Ladue*	non-near-road	$PM_{2.5}$

St. Louis, MO.	29-510-0093	Branch St.	non-near-road	$PM_{2.5}$
Tacoma, WA.	53-053-0029	Tacoma L Street	non-near-road	$PM_{2.5}$
Tacoma, WA.	53-053-0024	Tacoma NEAR-ROAD	NEAR-ROAD	$PM_{2.5}$
Tampa Bay, FL.	12-057-0113	Munro Street	NEAR-ROAD	NO_2, NOx, CO, $PM_{2.5}$, BC
Tampa Bay, FL.	12-103-0027	Sawgrass Lake Park	NEAR-ROAD	NO_2, CO
Tampa Bay, FL.	12-103-0018	Azalea Park	non-near-road	NO_2, NOx, $PM_{2.5}$
Tampa Bay, FL.	12-057-3002	Sydney	non-near-road	CO, $PM_{2.5}$
Tampa Bay, FL.	12-103-2008	Gateway	non-near-road	CO
Washington, DC.	51-013-0020	Aurora Hills Visitor Center*	non-near-road	NO_2, NOx, CO
Washington, DC.	11-001-0043	McMillan	non-near-road	NO_2, NOx, CO
Washington, DC.	11-001-0050	Takoma Rec Center	non-near-road	NO_2, NOx
Washington, DC.	51-059-0031	DC – Fairfqax Springfield	NEAR-ROAD	CO
Washington, DC.	11-001-0051	NR – DC	NEAR-ROAD	NO_2, NOx, CO

Table D-2: Summary statistics of the number of near-road sites and comparisons with non-near-road sites

	NO_2	$PM_{2.5}$	CO
Number of near-road sites that have a non-near-road monitor within city boundary/10 miles, but outside of the control zone	55	29	36
Number of comparisons made	91	72	70
AQS Rural Sites	8	4	2
AQS Suburban Sites	40	33	26
AQS Urban Sites	43	35	42

Table D-3: P-values from a one-tailed t-test (H_0: $\mu_{diff} = 0$; H_a: $\mu_{diff} > 0$ ($\mu_{non\text{-}near\text{-}road} > \mu_{NEAR\text{-}ROAD}$); $\alpha = 0.05$) comparing two-year average NO_2, $PM_{2.5}$, and CO concentrations at near-road sites and non-near-road sites. The non-urban comparison is the assessment of near-road monitors against suburban and rural sites combined.

	NO_2	$PM_{2.5}$	CO
All site comparison	1.9×10^{-22}	4.6×10^{-3}	6.6×10^{-7}
Urban comparison	2.6×10^{-8}	***0.051***	2.5×10^{-4}
Suburban comparison	1.6×10^{-15}	***0.032***	9.4×10^{-4}
Rural comparison	4.7×10^{-4}	***0.078***	0.089
non-urban comparison	3.2×10^{-19}	1.1×10^{-2}	2.0×10^{-5}

Table D-4: Locations where the near-road observation is exceeded by the non-near-road site concentration averaged over two years

	$PM_{2.5}$ (sites above 1.5 µg m^{-3}) *28 total site comparisons were higher		
	NEAR-ROAD Site (AQS Site ID No.)	Non-near-road Site (AQS Site ID No.)	Concentration (µg m^{-3})
1	Berkeley Aquatic Park (06-001-0013)	Oakland West (06-001-0011)	3.2
2	Pittsburgh NEAR-ROAD (42-003-1376)	Liberty (42-003-0064)	3.1
3	Denver I-25 (08-031-0027)	Tri County Health (08-001-0008)	2.1
4	Phoenix Diablo (04-013-4019)	Durango Complex (04-013-9812)	1.9
5	Kansas City I-70 (20-095-0042)	JFK (20-209-0021)	1.5

	NO_2		
	NEAR-ROAD Site (AQS Site ID No.)	Non-near-road Site (AQS Site ID No.)	Concentration (ppb)
1	NYC Queens College (36-81-0125)	IS 52 (36-005-0110)	2.0
2	Detroit Near Road – Livonia (26-163-0095)	Allen Park (26-163-1010)	1.7
3	St. Louis Rider Trail I-70 (29-189-0016)	Blair Street (29-510-0085)	1.2
4	Philadelphia Car-Barn Montgomery I - 76 (42-101-0076)	Camden Spruce Street (34-007-0002)	1.1
5	Fort Lee NR (34-003-0010)	IS 52 (36-005-0110)	0.26
6	Buffalo Near Road (36-029-0023)	Buffalo (36-029-0005)	0.16
7	St. Louis Forest Park (29-510-0094)	Blair Street (29-510-0085)	0.14

	CO (sites above 0.10 ppm) *15 total site comparisons were higher		
	NEAR-ROAD Site (AQS Site ID No.)	Non-near-road Site (AQS Site ID No.)	Concentration (ppm)
1	Indpls.-I70 (18-097-0087)	Indpls. - Illinois St. (18-097-0072)	0.40
2	Detroit Near Road – Livonia (26-163-0095)	Allen Park (26-163-1010)	0.19
3	Cleveland NR (39-035-0073)	Galleria (39-035-0051)	0.18
4	Columbus Smoky Row (39-049-0038)	Morse Rd. (39-049-0005)	0.11

Table D-5: Non-near-road sites that are identified in state Air Monitoring Network Plans that are source-oriented or identified as highest concentration. $PM_{2.5}$ two-year average concentration differences between near-road and non-near-road sites are also provided. A positive value indicates the near-road monitor has higher concentration than the non-near-road monitor.

Non-near-road site (AQS Site ID#)	Air Monitoring Network Plan Identification	$PM_{2.5}$ concentration difference (µg m^{-3})
Oakland West (06-001-0011)	Source-oriented (Port of Oakland)	-3.2; -0.70
Pittsburgh – Liberty (42-003-0064)	Highest Concentration; 3 km downwind of US Steel Clairton Coke Work	-3.1
Phoenix – Durango (04-013-9812)	Highest Concentration	-1.8
Las Vegas – Sunrise Acres (32-003-0561)	Highest Concentration	-0.36
St. Louis – Branch St. (29-510-0093)	Source-oriented	-0.32
Milwaukee – Waukesha (55-133-0027)	Source-oriented	-0.14
Milwaukee – 16th St. (55-079-0010)	Highest Concentration	0.32
LA-Van Buren (06-065-8005)	Highest Concentration	1.77
Providence – Urban League (44-007-0022)	Highest Concentration	1.88
Providence – East (44-007-1010)	Highest Concentration	1.90

Table D-6: Monthly differences of two-year average (95% Confidence Interval) NO_2, $PM_{2.5}$, and CO concentrations between the near-road sites and non-near-road sites. A positive value indicates the near-road sites have higher two-year average concentrations than the non-near-road sites.

	NO_2 (ppb)		$PM_{2.5}$ (µg m^{-3})		CO (ppm)	
	All sites	*Urban sites*	*All sites*	*Urban sites*	*All sites*	*Urban sites*
Jan.	5.7 (4.8-6.7)	4.4 (2.9-5.9)	0.24 (-0.32-0.80)	0.40 (-0.32-0.80)	0.07 (0.04- 0.10)	0.07 (0.03-0.11)
Feb.	5.8 (4.7-6.8)	4.8 (2.9-6.1)	0.32 (-0.05-0.69)	0.09 (-0.05-0.68)	0.09 (0.06 0.12)	0.08 (0.04-0.12)
March	6.5 (5.5-7.6)	5.0 (3.4 -6.6)	0.34 (-0.01-0.69)	0.24 (-0.01-0.68)	0.08 (0.05-0.11)	0.07 (0.04-0.11)
April	6.8 (5.8-7.7)	5.3 (3.8 -6.8)	0.46 (0.14-0.78)	0.39 (0.14-0.78)	0.09 (0.06-0.11)	0.07 (0.03-0.11)
May	6.9 (6.0-7.9)	5.8 (4.3 -7.4)	0.36 (0.03-0.70)	0.29 (-0.04-0.71)	0.09 (0.06-0.12)	0.08 (0.04-0.12)
June	6.3 (5.3-7.2)	5.5 (4.0-7.4)	0.36 (0.02-0.70)	0.19 (-0.02-0.69)	0.10 (0.07-0.14)	0.09 (0.05-0.14)
July	5.9 (5.0-6.8)	5.1 (3.5-7.1)	0.28 (-0.11-0.67)	0.05 (-0.11-0.67)	0.13 (0.10 -0.16)	0.12 (0.08-0.16)
Aug.	6.3 (5.3-7.4)	5.6 (3.9 -6.6)	0.26 (-0.16-0.67)	0.09 (-0.16-0.67)	0.12 (0.09-0.15)	0.10 (0.06-0.14)
Sept.	6.2 (5.3-7.2)	5.3 (3.6-7.3)	0.50 (0.05-0.95)	0.14 (-0.05-0.95)	0.11 (0.07-0.14)	0.09 (0.05-0.13)
Oct.	6.1 (5.0-7.1)	4.8 (3.3-6.9)	0.39 (-0.07-0.84)	0.22 (-0.07-0.84)	0.09 (0.05-0.12)	0.09 (0.05-0.13)
Nov.	5.5 (4.4-6.5)	4.1 (2.4 -6.4)	0.97 (0.47-1.5)	0.77 (0.47-1.5)	0.09 (0.06-0.13)	0.09 (0.05-0.14)
Dec.	5.6 (4.5-6.7)	4.2 (2.5-5.8)	1.01 (0.17-1.8)	1.0 (0.17-1.8)	0.06 (0.03-0.10)	0.07 (0.02-0.12)

Table D-7: $PM_{2.5}$ monitoring sites used in this study that exceed the US National Ambient Air Quality (NAAQS) primary annual average standard (12 μg m^{-3}) or 24 hour standard (35 μg m^{-3}). Here we use 2017 and 2018 year data and assess on a two-year rolling average not three as prescribed by the NAAQS. The asterisk (*) indicates sites that were sited as "source-oriented" or "highest exposures".

Site (AQS Site ID#)	NEAR-ROAD or non-near-road	$PM_{2.5}$ concentration (μg m^{-3})	NAAQS standard
CA. Laney College (06-001-0012)	Near-road	13.1	Annual average
CA. Oakland West (06-001-0011)*	Non-near-road	13.4	Annual average
PA. Pittsburgh Liberty (42-003-0064)*	Non-near-road	13.7	Annual average
CA. Long Beach South (06-037-4004)	Non-near-road	14.0	Annual average
CA. Long Beach (06-037-4008)	Near-road	14.8	Annual average
CA. Mira Loma Van Buren (06-065-8005)*	Non-near-road	15.7	Annual average
CA. Upland (06-071-1004)*	Non-near-road	16.4	Annual average
CA. Riverside – Ontario (06-071-0027)	Near-road	17.3	Annual average
WA. Seattle (53-053-0024)	Near-road	35.1	24-hour
WA. Tacoma (53-053-0024)	Non-near-road	35.9	24-hour
WA. Seattle (53-033-0030)	Non-near-road	37.4	24-hour
CA. Long Beach (06-037-4008)	Near-road	37.9	24-hour
CA. Riverside – Ontario (06-071-0027)	Near-road	40.1	24-hour
CA. Laney College (06-001-0012)	Non-near-road	46.1	24-hour
CA. Laney College (06-001-0012)	Near-road	46.2	24-hour
CA. San Jose (06-085-0006)	Non-near-road	47.0	24-hour
CA. San Jose (06-085-0006)	Near-road	47.4	24-hour
CA. Oakland West (06-001-0011)*	Non-near-road	49.4	24-hour
CA. San Rafael (06-041-0001)	Non-near-road	50.5	24-hour
CA. San Pablo (06-013-1004)	Non-near-road	51.0	24-hour
CA. Berkeley (06-001-0013)	Near-road	53.2	24-hour
CA. Oakland (06-001-0009)	Non-near-road	53.3	24-hour
CA. Upland (06-071-1004)*	Non-near-road	55.6	24-hour
CA. Riverside – Ontario (06-071-0027)	Near-road	78.4	24-hour
CA. Long Beach South (06-037-4004)	Non-near-road	80.3	24-hour
CA. Mira Loma Van Buren (06-065-8005)*	Non-near-road	89.2	24-hour
CA. Long Beach (06-037-4008)	Near-road	111.0	24-hour

Table D-8: Near-road sites where the low wind speed (WS < 1 m s^{-1}) and downwind condition does not result in the highest average concentration. Also indicated is whether there is a highway (that is not the target roadway of the near-road monitor) that is within the decay to background distance for each pollutant ($L_{PM2.5}$ = 350m and L_{NO2}= L_{CO} = 970m)

Site (AQS Site ID#)	Pollutant	Major highway that is not the target highway within decay to background distance
CA. Riverside (06-071-0027)	$PM_{2.5}$, NO_2	No
IN. Indianapolis (18-097-0087)	$PM_{2.5}$	No
NV. Las Vegas (32-003-1501)	$PM_{2.5}$, NO_2, CO	No
TX. San Antonio (48-029-1069)	$PM_{2.5}$, NO_2, CO	Yes for NO_2 & CO, no $PM_{2.5}$
CA. Anaheim (06-059-0008)	CO, NO_2	No
TX. Houston (48-201-1052)	CO, NO_2	Yes
MI. Detroit (26-163-0093)	CO, NO_2	Yes
CO. Denver (08-031-0027)	CO, NO_2	Yes
AZ. Phoenix (04-013-4019)	CO, NO_2	Yes
CA. Riverside (06-071-0026)	CO, NO_2	No
WA. Seattle (53-033-0030)	CO	No
WA. Seattle/Tacoma (53-053-0024)	NO_2	Yes
OK. Oklahoma City (40-109-0097)	CO, NO_2	Yes
TX. Dallas Fort Worth (48-113-1053)	CO, NO_2	Yes
AL. Birmingham (01-073-2059)	CO, NO_2	Yes
TX. Austin (48-453-1068)	CO, NO_2	Yes
OR. Portland (41-067-0005)	CO, NO_2	Yes
NC. Charlotte (37-119-0045)	CO	No
MN. Minneapolis (27-037-0480)	NO_2	No
MN. Minneapolis (27-053-0962)	CO, NO_2	Yes
MO. Kansas City (29-095-0042)	CO, NO_2	Yes
WI. Milwaukee (55-079-0026)	CO	Yes
OH. Cleveland (39-035-0073)	CO	Yes
AZ. Phoenix (04-013-4020)	NO_2	Yes
CA. Fresno (06-019-2016)	NO_2	No
TX. Houston (48-201-1066)	NO_2	No
TX. Dallas (48-113-1067)	NO_2	Yes

Table D-9: Mean Coefficients of Divergence (COD) between the near-road sites and non-near-road sites. If the non-near-road site had a higher two-year average concentration than the near-road site, we treated it as a negative COD. The non-urban comparison is the assessment of near-road monitors against suburban and rural sites combined.

	NO_2	$PM_{2.5}$	CO
All site comparison	0.38 (0.34-0.42)	0.06 (4.2×10^{-3}-0.13)	0.19 (0.11-0.24)
Urban comparison	0.26 (0.20-0.33)	0.03 (-0.02-0.10)	0.16 (0.07-0.24)
Suburban comparison	0.45 (0.42-0.47)	0.08 (-9.8×10^{-3}-0.19)	0.21 (0.11-0.32)
Rural comparison	0.56 (0.50-0.63)	0.13 (-0.02-0.05)	0.34 (0.32-0.37)
non-urban comparison	0.47 (0.44-0.49)	0.05 (3.8×10^{-3} -0.10)	0.23 (0.16-0.30)

Table D-10: $PM_{2.5}$ two-year average concentration difference ($\mu g\ m^{-3}$) between near-road and all non-near road sites (left) and near-road and non-near-road sites that are not "source-oriented" or "highest exposure" locations. The non-near-road sites that are "source-oriented" or "highest exposure" locations are provided in Table D-5.

	All Sites		**Without "source-oriented" or "highest exposure"**
	$PM_{2.5}$ concentration difference ($\mu g\ m^{-3}$)		$PM_{2.5}$ concentration difference ($\mu g\ m^{-3}$)
All Sites	0.50 (0.17-0.84)		0.64 (0.28– 1.01)
Urban non-near-road sites	0.42* (-0.08-0.90)		0.70 (0.02-1.38)
Suburban non-near-road sites	0.52 (-0.02-1.1)		0.55 (0.05-1.05)
Rural non-near-road sites	0.92* (-0.63-2.5)		0.85 (-1.2-2.9)

APPENDIX E. SUPPLEMENTAL MATERIAL FOR CHAPTER 6

E.1 Figure from the Supplementary Material

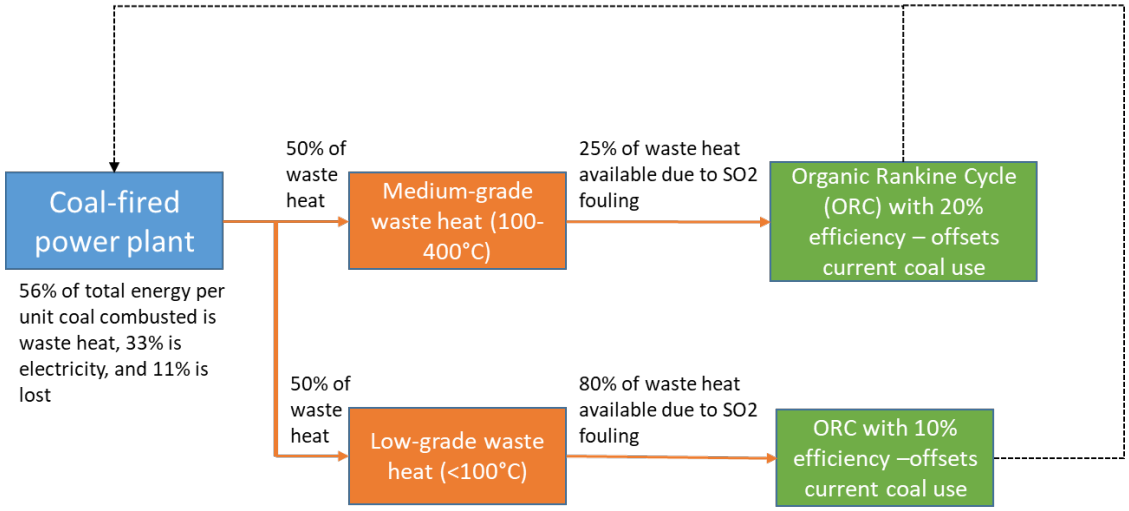

Figure E-1: Waste-heat pathway and efficiencies at coal-fired Thermal Power Stations (TPSs)

REFERENCES

1. Fu X*, et al.* (2013) Emission inventory of primary pollutants and chemical speciation in 2010 for the Yangtze River Delta region, China. *Atmospheric Environment* 70:39-50.

2. Nagpure AS, Ramaswami A, & Russell A (2015) Characterizing the Spatial and Temporal Patterns of Open Burning of Municipal Solid Waste (MSW) in Indian Cities. *Environmental Science & Technology* 49(21):12904-12912.

3. Kelly KE*, et al.* (2017) Ambient and laboratory evaluation of a low-cost particulate matter sensor. *Environmental Pollution* 221:491-500.

4. Zheng T, Bergin, M. H., Johnson, K. K., Tripathi, S. N., Shirodkar, S., Landis, M. S., Sutaria, R., and Carlson, D. E. (2018) Field evaluation of low-cost particulate matter sensors in high and low concentration environments. *Atmos. Meas. Tech. Discuss.*

5. Dockery DW*, et al.* (1993) An Association between Air Pollution and Mortality in Six U.S. Cities. *New England Journal of Medicine* 329(24):1753-1759.

6. Lim SS*, et al.* (2012) A comparative risk assessment of burden of disease and injury attributable to 67 risk factors and risk factor clusters in 21 regions, 1990–2010: a systematic analysis for the Global Burden of Disease Study 2010. *The Lancet* 380(9859):2224-2260.

7. Burnett R*, et al.* (2018) Global estimates of mortality associated with long-term exposure to outdoor fine particulate matter. *Proceedings of the National Academy of Sciences* 115(38):9592.

8. Apte JS, Brauer M, Cohen AJ, Ezzati M, & Pope CA (2018) Ambient PM2.5 Reduces Global and Regional Life Expectancy. *Environmental Science & Technology Letters* 5(9):546-551.

9. Lelieveld J, Evans JS, Fnais M, Giannadaki D, & Pozzer A (2015) The contribution of outdoor air pollution sources to premature mortality on a global scale. *Nature* 525(7569):367-371.

10. Seto K*, et al.* (2014) Human Settlements, Infrastructure and Spatial Planning. *Climate change 2014*, (Cambridge University Press, New York, NY), pp 923-1000.

11. Ramaswami A*, et al.* (2012) A Social-Ecological-Infrastructural Systems Framework for Interdisciplinary Study of Sustainable City Systems. *Journal of Industrial Ecology* 16(6):801-813.

12. Ramaswami A, Russell AG, Culligan PJ, Sharma KR, & Kumar E (2016) Meta-principles for developing smart, sustainable, and healthy cities. *Science* 352(6288):940.

13. Bergin MH*, et al.* (2015) The Discoloration of the Taj Mahal due to Particulate Carbon and Dust Deposition. *Environmental Science & Technology* 49(2):808-812.

14. Lal RM*, et al.* (2016) Municipal solid waste and dung cake burning: discoloring the Taj Mahal and human health impacts in Agra. *Environmental Research Letters* 11(10):104009.

15. Ramaswami A*, et al.* (2017) Urban cross-sector actions for carbon mitigation with local health co-benefits in China. *Nature Climate Change* 7:736.

16. Johnson KK, Bergin MH, Russell AG, & Hagler GSW (2018) Field Test of Several Low-Cost Particulate Matter Sensors in High and Low Concentration Urban Environments. *Aerosol and Air Quality Research* 18(3):565-578.

17. HEI (2010) Traffic-Related Air Pollution: A Critical Review of the Literature on Emissions, Exposure, and Health Effects. HEI Special Report 17. (HEI Boston, MA).

18. Anonymous (2015) Two Hundred Sixty Second Report on Effects of Pollution on Taj. (Parliament of India Rajya Sabha, New Delhi).

19. M.P.; GPS (1990) The long-term concentration of sulphur dioxide at Taj Mahal due to the Mathura Refinery. *Atmospheric Environment* 24B(3):407-411.

20. S. NRGPB (1983) A gaussian model for predicting SO2 concentration in the city of Agra. *Atmospheric Environment* 17:2199-2203.

21. Sharma PKG, H.O. (1993) Dust pollution at the Taj Mahal - A case study. *Proceedings of the International RILEM/UNESCO Congress*, ed Thiel MJ, pp 11-18.

22. Hicks BB & Manju K (1987) Marble discoloration at the Taj Mahal: A proposed explanation. *ICOMOS 8th General Assembly and International Symposium* pp 325-332.

23. IHME (2012) The Global Burden of Disease 2010: Generating Evidence and Guiding.

24. Gupta SM, K.; Prasad, R.; Gupta, S; Kansal A.; (1998) Solid waste management in India: options and opportunities. *Resource, Conservation and Recycling* 24:137-154.

25. Shamjad PM*, et al.* (2015) Contribution of Brown Carbon to Direct Radiative Forcing over the Indo-Gangetic Plain. *Environmental Science & Technology* 49(17):10474-10481.

26. Stockwell CE*, et al.* (2016) Nepal Ambient Monitoring and Source Testing Experiment (NAMaSTE): Emissions of trace gases and light-absorbing carbon from wood and dung cooking fires, garbage and crop residue burning, brick kilns, and other sources. *Atmos. Chem. Phys. Discuss.* 2016:1-57.

27. Vreeland H*, et al.* (2016) Chemical Characterization and toxicity of particulate matter from roadside trash combustino in urban India. *Environmental Science & Technology*.

28. CPCB (2010) *Air Quality Monitoring, Emission Inventory and Source Apportionment Study for Indian Cities* (New Delhi, India), Government of India (Board CPC).

29. Allsopp M, Costner P, & Johnston P (2001) Incineration and human health. *Environ Sci & Pollut Res* 8(2):141-145.

30. McKay G (2002) Dioxin characterisation, formationand minimisation during municipal solid waste (MSW) incineration: review. *Chemical Engineering Journal* 86:343-368.

31. Anonymous (2010) IARC monographs on the evaluation of carcinogenic risks to humans, household use of solid fuels and high-temperature frying. (World Health Organization. International Agency for Research on Caner, France).

32. Harsdorff M (2012) *The economics of biogas: Creating green jobs in the dairy industry in India*, International Labour Organization (Organization IL).

33. Anonymous (2012) *Energy Sources of Indian Households for Cooking and Lighting*, Government of India (Office NSS).

34. Sharholy M, Ahmad K, Mahmood G, & Trivedi RC (2008) Municipal solid waste management in Indian cities - A review. *Waste management* 28(2):459-467.

35. Guerrero LA, Maas G, & Hogland W (2013) Solid waste management challenges for cities in developing countries. *Waste management* 33(1):220-232.

36. Sujauddin M, Huda SM, & Hoque AT (2008) Household solid waste characteristics and management in Chittagong, Bangladesh. *Waste management* 28(9):1688-1695.

37. Ramaswami A, Baidwan NK, & Nagpure AS (2016) Exploring social and infrastructural factors affecting open burning of municipal solid waste (MSW) in Indian cities: A comparative case study of three neighborhoods of Delhi. *Waste management & research : the journal of the International Solid Wastes and Public Cleansing Association, ISWA*.

38. Hoornweg D & Bhada-Tata P (2012) What a waste: a global review of solid waste management. ed Bank W (Washington, DC.).

39. Ramanathan V & Carmichael G (2008) Global and regional climate changes due to black carbon. *Nature Geosci* 1(4):221-227.

40. Tripathi SN (2005) Aerosol black carbon radiative forcing at an industrial city in northern India. *Geophysical Research Letters* 32(8).

41. Hamilton RS & Mansfield TA (1991) Airborne particulate elemental carbon: its sources, transport and contribution to dark smoke and soiling. *Atmospheric Environment* 25A:715-723.

42. Burnett RT*, et al.* (2015) An integrated risk function for estimating the global burden of disease attributable to ambient fine particulate matter exposure. (University of British Columbia).

43. Murray CJ (1994) Quantifying the burden of disease: the technical basis for disability-adjusted life years. *Bulletin of the World Health Organization* 72(3):429-445.

44. EPA US (2004) AERMOD: Description of Model Formulation).

45. Christian TJ*, et al.* (2010) Trace gas and particle emissions from domestic and industrial biofuel use and garbage burning in central Mexico. *Atmos. Chem. Phys.* 10(2):565-584.

46. Saud T*, et al.* (2012) Emission estimates of organic and elemental carbon from household biomass fuel used over the Indo-Gangetic Plain (IGP), India. *Atmospheric environment* 61:212-220.

47. Jayarathne T*, et al.* (2016) Nepal Ambient Monitoring and Source Testing Experiment (NAMaSTE): Emissions of particulate matter from wood and dung cooking fires, brick kilns, generators, trash and crop residue burning. *Atmos. Chem. Phys.*

48. Pachauri T, Satsangi A, Singla V, Lakhani A, & Kumari KM (2013) Characteristics and sources of carbonaceous aerosols in PM2. 5 during wintertime in Agra, India. *Aerosol and Air Quality Research* 13(3):977-991.

49. Russell LM (2003) Aerosol Organic-Mass-to-Organic-Carbon Ratio Measurements. *Environmental Science & Technology* 37(13):2982-2987.

50. Seinfeld JH & Pandis SN (2006) *Atmospheric Chemistry and Physics* (John Wiley & Sons, New York).

51. Ramaswami A, Milford JB, & Small MJ (2005) *Integrated environmental modeling: pollutant transport, fate, and risk in the environment* (J. Wiley).

52. Bond TC*, et al.* (2013) Bounding the role of black carbon in the climate system: A scientific assessment. *Journal of Geophysical Research: Atmospheres* 118(11):5380-5552.

53. Turpin BJ & Lim H-J (2001) Species Contributions to PM2.5 Mass Concentrations: Revisiting Common Assumptions for Estimating Organic Mass. *Aerosol Science and Technology* 35(1):602-610.

54. Wiedinmyer C, Yokelson RJ, & Gullett BK (2014) Global emissions of trace gases, particulate matter, and hazardous air pollutants from open burning of domestic waste. *Environ Sci Technol* 48(16):9523-9530.

55. Annepu RK (2012) Sustainable solid waste management in India. *Columbia University, New York*.

56. Yedla S & Parikh J (2001) Economic evaluation of a landfill system with gas recovery for municipal solid waste management: a case study. *Int. J. Environment and Pollution* 15:433-447.

57. Anonymous (2010) Air Quality Assessment, Emissions Inventory and Source Apportionment Studies: Mumbai. (National Environmental Engineering Research Institute).

58. Villalobos AM*, et al.* (2015) Source apportionment of carbonaceous fine particulate matter (PM2.5) in two contrasting cities across the Indo-Gangetic Plain. *Atmospheric Pollution Research* 6(3).

59. Sehmel GA & Hodgson WH (1978) *Model for predicting dry deposition of particles and gases to environmental surfaces* p Medium: P; Size: Pages: 44.

60. Davidson CI, Lindberg SE, Schmidt JA, Cartwright LG, & Landis LR (1985) Dry deposition of sulfate onto surrogate surfaces. *Journal of Geophysical Research: Atmospheres* 90(D1):2123-2130.

61. Mitchell R, Maher BA, & Kinnersley R (2010) Rates of particulate pollution deposition onto leaf surfaces: Temporal and inter-species magnetic analyses. *Environmental Pollution* 158(5):1472-1478.

62. Zufall MJ, Davidson CI, Caffrey PF, & Ondov JM (1998) Airborne Concentrations and Dry Deposition Fluxes of Particulate Species to Surrogate Surfaces Deployed in Southern Lake Michigan. *Environmental Science & Technology* 32(11):1623-1628.

63. Thatcher TL & Layton DW (1995) Deposition, resuspension, and penetration of particles within a residence. *Atmospheric Environment* 29(13):1487-1497.

64. Kirchstetter TW (2004) Evidence that the spectral dependence of light absorption by aerosols is affected by organic carbon. *Journal of Geophysical Research* 109(D21).

65. Viswanathan B & Kavi Kumar KS (2005) Cooking fuel use patterns in India: 1983–2000. *Energy Policy* 33(8):1021-1036.

66. Goldemberg J, Johansson TB, Reddy AK, & Williams RH (2004) A global clean cooking fuel initiative. *Energy for Sustainable Development* 8(3):5-12.

67. Anonymous (2006) *Detailed project report for solid waste management in Agra, Uttar Pradesh* (Lucknow), Government of India (R.C.U.E.S).

68. Chavez A & Ramaswami A (2013) Articulating a trans-boundary infrastructure supply chain greenhouse gas emission footprint for cities: Mathematical relationships and policy relevance. *Energy Policy* 54:376-384.

69. Hillman T & Ramaswami A (2010) Greenhouse gas emission footprints and energy use benchmarks for eight US cities. (ACS Publications).

70. Kennedy C*, et al.* (2009) Greenhouse gas emissions from global cities. (ACS Publications).

71. Creutzig F*, et al.* (2016) Urban infrastructure choices structure climate solutions. *Nature Climate Change* 6(12):1054.

72. Kennedy C, Ibrahim N, & Hoornweg D (2014) Low-carbon infrastructure strategies for cities. *Nature Climate Change* 4(5):343.

73. Ramaswami A*, et al.* (2012) Quantifying carbon mitigation wedges in US cities: near-term strategy analysis and critical review. *Environmental science & technology* 46(7):3629-3642.

74. Lund H*, et al.* (2014) 4th Generation District Heating (4GDH): Integrating smart thermal grids into future sustainable energy systems. *Energy* 68:1-11.

75. Brückner S*, et al.* (2015) Industrial waste heat recovery technologies: an economic analysis of heat transformation technologies. *Applied Energy* 151:157-167.

76. Zhu J & Chertow MR (2016) Greening industrial production through waste recovery:"Comprehensive utilization of resources" in China. *Environmental science & technology* 50(5):2175-2182.

77. West JJ*, et al.* (2013) Co-benefits of mitigating global greenhouse gas emissions for future air quality and human health. *Nature climate change* 3(10):885.

78. Amann M*, et al.* (2011) Cost-effective control of air quality and greenhouse gases in Europe: Modeling and policy applications. *Environmental Modelling & Software* 26(12):1489-1501.

79. Anonymous (2004) *AERMOD: Descirption of Model Formulation*, (EPA US).

80. Burnett RT*, et al.* (2014) An integrated risk function for estimating the global burden of disease attributable to ambient fine particulate matter exposure. *Environmental health perspectives* 122(4):397-403.

81. Tong K*, et al.* (2018) The collective contribution of Chinese cities to territorial and electricity-related CO2 emissions. *Journal of Cleaner Production* 189:910-921.

82. Zhang Y & Cao F (2015) Fine particulate matter (PM2. 5) in China at a city level, Sci. Rep., 5, 14884.

83. Meerow S, Newell JP, & Stults M (2016) Defining urban resilience: A review. *Landscape and Urban Planning* 147:38-49.

84. Egger S (2006) Determining a sustainable city model. *Environmental Modelling & Software* 21(9):1235-1246.

85. Corbett J & Mellouli S (2017) Winning the SDG battle in cities: how an integrated information ecosystem can contribute to the achievement of the 2030 sustainable development goals. *Information Systems Journal* 27(4):427-461.

86. Choi J, Hwang M, Kim G, Seong J, & Ahn J (2016) Supporting the measurement of the United Nations' sustainable development goal 11 through the use of national urban information systems and open geospatial technologies: a case study of south Korea. *Open Geospatial Data, Software and Standards* 1(1):4.

87. Pope CA & Dockery DW (2006) Health Effects of Fine Particulate Air Pollution: Lines that Connect. *Journal of the Air & Waste Management Association* 56(6):709-742.

88. Cohen AJ*, et al.* (2005) The global burden of disease due to outdoor air pollution. *Journal of Toxicology and Environmental Health, Part A* 68(13-14):1301-1307.

89. Green GF, Peterson M, Rodriguez DA, & Gordon-Larsen P (2017) Neighborhood sociodemographics and change in built infrastructure AU - Hirsch, Jana A. *Journal of Urbanism: International Research on Placemaking and Urban Sustainability* 10(2):181-197.

90. Engel-Yan J, Kennedy C, Saiz S, & Pressnail K (2005) Toward sustainable neighbourhoods: the need to consider infrastructure interactions. *Canadian Journal of Civil Engineering* 32(1):45-57.

91. Pfeiffer D & Cloutier S (2016) Planning for Happy Neighborhoods. *Journal of the American Planning Association* 82(3):267-279.

92. Diener E (2009) Subjective Well-Being. *The Science of Well-Being: The Collected Works of Ed Diener*, ed Diener E (Springer Netherlands, Dordrecht), pp 11-58.

93. Larsen RJ, Diener E, & Emmons RA (1985) An evaluation of subjective well-being measures. *Social Indicators Research* 17(1):1-17.

94. Luhmann M, Hawkley LC, Eid M, & Cacioppo JT (2012) Time frames and the distinction between affective and cognitive well-being. *J Res Pers* 46(4):431-441.

95. Zhu J & Fan Y (2018) Daily travel behavior and emotional well-being: Effects of trip mode, duration, purpose, and companionship. *Transportation Research Part A: Policy and Practice* 118:360-373.

96. Stone AA & Mackie CE (2013) *Subjective well-being: Measuring happiness, suffering, and other dimensions of experience* (National Academies Press).

97. Diener E & Chan MY (2011) Happy People Live Longer: Subjective Well-Being Contributes to Health and Longevity. *Applied Psychology: Health and Well-Being* 3(1):1-43.

98. Dolan P, Peasgood T, & White M (2008) Do we really know what makes us happy? A review of the economic literature on the factors associated with subjective well-being. *Journal of Economic Psychology* 29(1):94-122.

99. Payne LL, Orsega-Smith E, Roy M, & Godbey GC (2005) Local Park Use and Personal Health Among Older Adults: An Exploratory Study. *Journal of Park & Recreation Administration* 23(2).

100. Ma L, Kent J, & Mulley C (2018) Transport disadvantage, social exclusion, and subjective well-being: The role of the neighborhood environment—evidence from Sydney, Australia. *Journal of transport and land use* 11(1).

101. Servadio JL*, et al.* (2019) Demographic Inequities in Health Outcomes and Air Pollution Exposure in the Atlanta Area and its Relationship to Urban Infrastructure. *Journal of Urban Health* 96(2):219-234.

102. Lucas K (2012) Transport and social exclusion: Where are we now? *Transport Policy* 20:105-113.

103. Ettema D, Gärling T, Olsson LE, & Friman M (2010) Out-of-home activities, daily travel, and subjective well-being. *Transportation Research Part A: Policy and Practice* 44(9):723-732.

104. Li Y, Guan D, Tao S, Wang X, & He K (2018) A review of air pollution impact on subjective well-being: Survey versus visual psychophysics. *Journal of Cleaner Production* 184:959-968.

105. Chow JC (1995) Measurement methods to determine compliance with ambient air quality standards for suspended particles. *Journal of the Air & Waste Management Association* 45(5):320-382.

106. Rai AC*, et al.* (2017) End-user perspective of low-cost sensors for outdoor air pollution monitoring. *Science of The Total Environment* 607-608:691-705.

107. Hagler GSW, Williams R, Papapostolou V, & Polidori A (2018) Air Quality Sensors and Data Adjustment Algorithms: When Is It No Longer a Measurement? *Environmental Science & Technology* 52(10):5530-5531.

108. Cross ES, Williams, L. R., Lewis, D. K., Magoon, G. R., Onasch, T. B., Kaminsky, M. L., Worsnop, D. R., and Jayne, J. T. (2017) Use of electrochemical sensors for measurement of air pollution: correcting interference response and validating measurements. *Atmos. Meas. Tech.* 10:3575-3588.

109. Castell N*, et al.* (2017) Can commercial low-cost sensor platforms contribute to air quality monitoring and exposure estimates? *Environment International* 99:293-302.

110. EPA US (2015) Air pollutant average annual emissions, criteria pollutants national Tier 1 for 1970-2016 emissions trends data. Policies and guidance. Air pollutant emissions trends data.

111. Larson R & Csikszentmihalyi M (2014) The experience sampling method. *Flow and the foundations of positive psychology*, (Springer), pp 21-34.

112. Shiffman S, Stone AA, & Hufford MR (2008) Ecological momentary assessment. *Annual review of clinical psychology* 4:1-32.

113. Kahneman D, Krueger AB, Schkade DA, Schwarz N, & Stone AA (2004) A Survey Method for Characterizing Daily Life Experience: The Day Reconstruction Method. *Science* 306(5702):1776.

114. Fan Y*, et al.* (2015) SmarTrAC: A smartphone solution for context-aware travel and activity capturing.

115. Fan Y, Brown R, Das K, & Wolfson J (Understanding Trip Happiness using Smartphone-Based Data: The Effects of Trip-and Person-Level Characteristics.

116. Wagner DP, Neumeister DM, & Murakami E (1996) Global positioning systems for personal travel surveys. *National Traffic Data Acquisition Conference (1996: Albuquerque NM) National Traffic Data Acquisition Conference (NATDAC'96): proceedings Vol. 1*.

117. Ermagun A, Fan Y, Wolfson J, Adomavicius G, & Das K (2017) Real-time trip purpose prediction using online location-based search and discovery services. *Transportation Research Part C: Emerging Technologies* 77:96-112.

118. Nitsche P, Widhalm P, Breuss S, Brändle N, & Maurer P (2014) Supporting large-scale travel surveys with smartphones–A practical approach. *Transportation Research Part C: Emerging Technologies* 43:212-221.

119. Gong L, Morikawa T, Yamamoto T, & Sato H (2014) Deriving personal trip data from GPS data: A literature review on the existing methodologies. *Procedia-Social and Behavioral Sciences* 138:557-565.

120. Martin DB, Addona V, Wolfson J, Adomavicius G, & Fan Y (2017) Methods for Real-Time Prediction of the Mode of Travel Using Smartphone-Based GPS and Accelerometer Data. *Sensors* 17(9).

121. Kheirbek I, Haney J, Douglas S, Ito K, & Matte T (2016) The contribution of motor vehicle emissions to ambient fine particulate matter public health impacts in New York City: a health burden assessment. *Environmental Health* 15(1):89.

122. Clark LP, Millet DB, & Marshall JD (2014) National Patterns in Environmental Injustice and Inequality: Outdoor NO2 Air Pollution in the United States. *PLOS ONE* 9(4):e94431.

123. Clark LP, Millet DB, & Marshall JD (2017) Changes in Transportation-Related Air Pollution Exposures by Race-Ethnicity and Socioeconomic Status: Outdoor Nitrogen Dioxide in the United States in 2000 and 2010. *Environmental health perspectives* 125(9):097012.

124. Tessum CW*, et al.* (2019) Inequity in consumption of goods and services adds to racial–ethnic disparities in air pollution exposure. *Proceedings of the National Academy of Sciences*:201818859.

125. Woolf SA, L.; Dubay, L.; Simon, S.; Zimmerman, E.; Luk, K. (2015) How are income and wealth linked to health and longevity?

126. Strak M*, et al.* (2017) Long-term exposure to particulate matter, NO2 and the oxidative potential of particulates and diabetes prevalence in a large national health survey. *Environment International* 108:228-236.

127. Anderson KG, Kellie; Rinker, Katie (2019) *2020 Air Monitoring Network Plan for Minnesota Appendix A: 2019 Air Monitoring Site Descriptions*, Minnesota Pollution Control Agency.

128. Vreeland H*, et al.* (2018).

129. Zhang J*, et al.* (2019) Effects of individual ozone exposure on lung function in the elderly: a cross-sectional study in China. *Environ Sci & Pollut Res* 26(12):11690-11695.

130. Barkjohn KK*, et al.* (Using Low-cost sensors to Quantify the Effects of Air Filtration on Indoor and Personal Exposure Relevant PM2.5 Concentrations in Beijing, China. *Aerosol and Air Quality Research*.

131. Schneider P*, et al.* (2019) Toward a Unified Terminology of Processing Levels for Low-Cost Air-Quality Sensors. *Environmental Science & Technology* 53(15):8485-8487.

132. Snyder MG*, et al.* (2013) RLINE: A line source dispersion model for near-surface releases. *Atmospheric Environment* 77:748-756.

133. Milando CW & Batterman SA (2018) Operational evaluation of the RLINE dispersion model for studies of traffic-related air pollutants. *Atmospheric Environment* 182:213-224.

134. Frey HC (2018) Trends in onroad transportation energy and emissions. *Journal of the Air & Waste Management Association* 68(6):514-563.

135. Venkatram A*, et al.* (2013) Re-formulation of plume spread for near-surface dispersion. *Atmospheric Environment* 77:846-855.

136. Kim C, Park Y-s, & Sang S (2008) *Spatial and Temporal Analysis of Urban Traffic Volume*.

137. Liu B & Frey HC (2015) Variability in Light-Duty Gasoline Vehicle Emission Factors from Trip-Based Real-World Measurements. *Environ Sci Technol* 49(20):12525-12534.

138. Fujita EM*, et al.* (2012) Comparison of the MOVES2010a, MOBILE6. 2, and EMFAC2007 mobile source emission models with on-road traffic tunnel and remote sensing measurements. *Journal of the Air & Waste Management Association* 62(10):1134-1149.

139. Zhai X*, et al.* (2016) Calibrating R-LINE model results with observational data to develop annual mobile source air pollutant fields at fine spatial resolution: Application in Atlanta. *Atmospheric Environment* 147:446-457.

140. Kahneman D & Krueger AB (2006) Developments in the measurement of subjective well-being. *Journal of Economic perspectives* 20(1):3-24.

141. Fan Y, Brown R, Das K, & Wolfson J (2019) Understanding Trip Happiness using Smartphone-Based Data: The Effects of Trip- and Person-Level Characteristics. *Transport Findings*.

142. Schwartz J (2000) The distributed lag between air pollution and daily deaths. *Epidemiology* 11(3):320-326.

143. Kuhl-Stennes M, Field, H.S, Jackson, A. (2019) *Residential Wood Combustion Survey Results*, (Agency MPC).

144. Anonymous (US Census Bureau: American Community Survey 5-year Estimates 2012-2016.

145. Kerr D (2018) Rail lines set records as Metro Transit ridership tops 81.9 million in 2017. ed MetroTransit.

146. Lin M*, et al.* (2012) Regression analyses between recent air quality and visibility changes in megacities at four haze regions in China. *Aerosol Air Qual. Res* 12:1049-1061.

147. Jiang Z*, et al.* (2018) Unexpected slowdown of US pollutant emission reduction in the past decade. *Proceedings of the National Academy of Sciences* 115(20):5099.

148. Gauderman WJ*, et al.* (2005) Childhood Asthma and Exposure to Traffic and Nitrogen Dioxide. *Epidemiology* 16(6):737-743.

149. Parvez F & Wagstrom K (2019) A hybrid modeling framework to estimate pollutant concentrations and exposures in near road environments. *Science of The Total Environment* 663:144-153.

150. Batterman S (2013) The Near-Road Ambient Monitoring Network and Exposure Estimates for Health Studies. *EM (Pittsburgh, Pa.)* 2013(7):24-30.

151. Tian N, Xue J, & Barzyk TM (2012) Evaluating socioeconomic and racial differences in traffic-related metrics in the United States using a GIS approach. *Journal Of Exposure Science And Environmental Epidemiology* 23:215.

152. Chen H*, et al.* (2017) Living near major roads and the incidence of dementia, Parkinson's disease, and multiple sclerosis: a population-based cohort study. *The Lancet* 389(10070):718-726.

153. Liang D*, et al.* (2018) Use of high-resolution metabolomics for the identification of metabolic signals associated with traffic-related air pollution. *Environment International* 120:145-154.

154. Alexeeff SE*, et al.* (2018) High-resolution mapping of traffic related air pollution with Google street view cars and incidence of cardiovascular events within neighborhoods in Oakland, CA. *Environmental Health* 17(1):38.

155. Alemany S*, et al.* (Traffic-Related Air Pollution, APOE ε4 Status, and Neurodevelopmental Outcomes among School Children Enrolled in the BREATHE Project (Catalonia, Spain). *Environmental health perspectives* 126(8):087001.

156. Apte JS*, et al.* (2017) High-Resolution Air Pollution Mapping with Google Street View Cars: Exploiting Big Data. *Environmental Science & Technology* 51(12):6999-7008.

157. Gu P*, et al.* (2018) Intracity Variability of Particulate Matter Exposure Is Driven by Carbonaceous Sources and Correlated with Land-Use Variables. *Environmental Science & Technology* 52(20):11545-11554.

158. Robinson ES*, et al.* (2019) Land-Use Regression Modeling of Source-Resolved Fine Particulate Matter Components from Mobile Sampling. *Environmental Science & Technology* 53(15):8925-8937.

159. Goodkind AL, Tessum CW, Coggins JS, Hill JD, & Marshall JD (2019) Fine-scale damage estimates of particulate matter air pollution reveal opportunities for location-specific mitigation of emissions. *Proceedings of the National Academy of Sciences* 116(18):8775.

160. Baldauf R*, et al.* (2009) Near-road air quality monitoring: Factors affecting network design and interpretation of data. *Air Quality, Atmosphere & Health* 2(1):1-9.

161. Watkins NaB, R. (2012) *Near-road NO2 Monitoring Technical Assistance Document*, United State Environmental Protection Agency.

162. Askariyeh MH, Zietsman J, & Autenrieth R (2019) Traffic contribution to PM2.5 increment in the near-road environment. *Atmospheric Environment*:117113.

163. Watkins N (2016) Near-Road Air Quality Monitoring Network: Status and Data. *National Ambient Air Monitoring Conference*.

164. DeWinter JL, Brown SG, Seagram AF, Landsberg K, & Eisinger DS (2018) A national-scale review of air pollutant concentrations measured in the U.S. near-road monitoring network during 2014 and 2015. *Atmospheric Environment* 183:94-105.

165. Seagram AF, Brown SG, Huang S, Landsberg K, & Eisinger DS (2019) National Assessment of Near-Road Air Quality in 2016: Multi-Year Pollutant Trends and Estimation of Near-Road PM2.5 Increment. *Transportation Research Record* 2673(2):161-171.

166. Hankey S & Marshall JD (2015) On-bicycle exposure to particulate air pollution: Particle number, black carbon, PM2.5, and particle size. *Atmospheric Environment* 122:65-73.

167. Liang D*, et al.* (2018) Errors associated with the use of roadside monitoring in the estimation of acute traffic pollutant-related health effects. *Environmental Research* 165:210-219.

168. Larsen M, Benders H, & Dann T (2014) Comparison of particulate monitoring methods at fort air partnership monitoring stations. *FAP Report Dec*.

169. Schwab JJ, Felton HD, Rattigan OV, & Demerjian KL (2006) New York State urban and rural measurements of continuous PM2.5 mass by FDMS, TEOM, and BAM. *Journal of the Air & Waste Management Association (1995)* 56(4):372-383.

170. Zhu K, Zhang J, & Lioy PJ (2007) Evaluation and Comparison of Continuous Fine Particulate Matter Monitors for Measurement of Ambient Aerosols. *Journal of the Air & Waste Management Association* 57(12):1499-1506.

171. Le T-C*, et al.* (2019) On the concentration differences between PM2.5 FEM monitors and FRM samplers. *Atmospheric Environment*:117138.

172. Anonymous (2016) "2016 U.S. Gazetteer Files". U.S. Gazetteer Files. United States Census Bureau. (United States Census Bureau).

173. Anonymous (US Environmental Protection Agency.Air Quality System Data Mart [internet database] available at http://www.epa.gov/ttn/airs/aqsdatamart. Accessed Dec. 1, 2018

174. Xie M*, et al.* (2012) Intra-urban spatial variability of PM(2.5)-bound carbonaceous components. *Atmospheric environment (Oxford, England : 1994)* 60:486-494.

175. Mavroidis I & Chaloulakou A (2011) Long-term trends of primary and secondary NO2 production in the Athens area. Variation of the NO2/NOx ratio. *Atmospheric Environment* 45(38):6872-6879.

176. Hilker N*, et al.* (2019) Traffic-related air pollution near roadways: discerning local impacts from background. *Atmos. Meas. Tech.* 12(10):5247-5261.

177. Brown SG, Penfold B, Mukherjee A, Landsberg K, & Eisinger DS (2019) Conditions Leading to Elevated PM2. 5 at Near-Road Monitoring Sites: Case Studies in Denver and Indianapolis. *International journal of environmental research and public health* 16(9):1634.

178. Qin M*, et al.* (2019) Improving ozone simulations in the Great Lakes Region: The role of emissions, chemistry, and dry deposition. *Atmospheric Environment* 202:167-179.

179. McDonald BC*, et al.* (2018) Modeling Ozone in the Eastern U.S. using a Fuel-Based Mobile Source Emissions Inventory. *Environmental Science & Technology* 52(13):7360-7370.

180. Knoderer C, Nguyen, D., Alrick, D. (2018) *2017 Air Monitoring Newtork Plan*, Bay Area Air Quality Management District (Measurement Ma).

181. Ruyter de Wildt M, Eskes H, & Boersma KF (2012) The global economic cycle and satellite-derived NO2 trends over shipping lanes. *Geophysical Research Letters* 39(1).

182. Eyring V*, et al.* (2010) Transport impacts on atmosphere and climate: Shipping. *Atmospheric Environment* 44(37):4735-4771.

183. Nam E*, et al.* (2010) Temperature Effects on Particulate Matter Emissions from Light-Duty, Gasoline-Powered Motor Vehicles. *Environmental Science & Technology* 44(12):4672-4677.

184. Donahue NM, Robinson AL, Trump ER, Riipinen I, & Kroll JH (2014) Volatility and Aging of Atmospheric Organic Aerosol. *Atmospheric and Aerosol Chemistry*, eds McNeill VF & Ariya PA (Springer Berlin Heidelberg, Berlin, Heidelberg), pp 97-143.

185. Offenberg JH*, et al.* (2017) Predicting Thermal Behavior of Secondary Organic Aerosols. *Environmental Science & Technology* 51(17):9911-9919.

186. Russell AR, Valin LC, Bucsela EJ, Wenig MO, & Cohen RC (2010) Space-based Constraints on Spatial and Temporal Patterns of NOx Emissions in California, 2005−2008. *Environmental Science & Technology* 44(9):3608-3615.

187. McClure CD & Jaffe DA (2018) US particulate matter air quality improves except in wildfire-prone areas. *Proceedings of the National Academy of Sciences*.

188. Platt SM*, et al.* (2017) Gasoline cars produce more carbonaceous particulate matter than modern filter-equipped diesel cars. *Scientific Reports* 7(1):4926.

189. May AA*, et al.* (2014) Gas- and particle-phase primary emissions from in-use, on-road gasoline and diesel vehicles. *Atmospheric Environment* 88:247-260.

190. Preble CV, Cados TE, Harley RA, & Kirchstetter TW (2018) In-Use Performance and Durability of Particle Filters on Heavy-Duty Diesel Trucks. *Environmental Science & Technology* 52(20):11913-11921.

191. Robert MA, Kleeman MJ, & Jakober CA (2007) Size and Composition Distributions of Particulate Matter Emissions: Part 2—Heavy-Duty Diesel Vehicles. *Journal of the Air & Waste Management Association* 57(12):1429-1438.

192. Robert MA, VanBergen S, Kleeman MJ, & Jakober CA (2007) Size and composition distributions of particulate matter emissions: Part 1—Light-duty gasoline vehicles. *Journal of the Air & Waste Management Association* 57(12):1414-1428.

193. Karjalainen P*, et al.* (2019) Strategies To Diminish the Emissions of Particles and Secondary Aerosol Formation from Diesel Engines. *Environmental Science & Technology* 53(17):10408-10416.

194. Pfister GG*, et al.* (2008) Contribution of isoprene to chemical budgets: A model tracer study with the NCAR CTM MOZART-4. *Journal of Geophysical Research: Atmospheres* 113(D5).

195. Miyoshi A, Hatakeyama S, & Washida N (1994) OH radical- initiated photooxidation of isoprene: An estimate of global CO production. *Journal of Geophysical Research: Atmospheres* 99(D9):18779-18787.

196. Chen L, Liang Z, Zhang X, & Shuai S (2017) Characterizing particulate matter emissions from GDI and PFI vehicles under transient and cold start conditions. *Fuel* 189:131-140.

197. Drozd GT*, et al.* (2016) Time Resolved Measurements of Speciated Tailpipe Emissions from Motor Vehicles: Trends with Emission Control Technology, Cold Start Effects, and Speciation. *Environmental Science & Technology* 50(24):13592-13599.

198. Lane TE, Donahue NM, & Pandis SN (2008) Effect of NOx on Secondary Organic Aerosol Concentrations. *Environmental Science & Technology* 42(16):6022-6027.

199. Kroll JH, Ng NL, Murphy SM, Flagan RC, & Seinfeld JH (2006) Secondary Organic Aerosol Formation from Isoprene Photooxidation. *Environmental Science & Technology* 40(6):1869-1877.

200. Song C, Na K, & Cocker DR (2005) Impact of the Hydrocarbon to NOx Ratio on Secondary Organic Aerosol Formation. *Environmental Science & Technology* 39(9):3143-3149.

201. Gordon TD*, et al.* (2014) Secondary organic aerosol formation exceeds primary particulate matter emissions for light-duty gasoline vehicles. *Atmos. Chem. Phys.* 14(9):4661-4678.

202. Zhao Y*, et al.* (2016) Intermediate Volatility Organic Compound Emissions from On-Road Gasoline Vehicles and Small Off-Road Gasoline Engines. *Environmental Science & Technology* 50(8):4554-4563.

203. Nordin E*, et al.* (2013) Secondary organic aerosol formation from idling gasoline passenger vehicle emissions investigated in a smog chamber. *Atmospheric Chemistry and Physics* 13(12):6101-6116.

204. Zhao Y*, et al.* (2017) Reducing secondary organic aerosol formation from gasoline vehicle exhaust. *Proceedings of the National Academy of Sciences* 114(27):6984.

205. Meng X, Hand JL, Schichtel BA, & Liu Y (2018) Space-time trends of PM2.5 constituents in the conterminous United States estimated by a machine learning approach, 2005–2015. *Environment International* 121:1137-1147.

206. Xu L, Suresh S, Guo H, Weber RJ, & Ng NL (2015) Aerosol characterization over the southeastern United States using high-resolution aerosol mass spectrometry: spatial and seasonal variation of aerosol composition and sources with a focus on organic nitrates. *Atmos. Chem. Phys.* 15(13):7307-7336.

207. McDonald BC, *et al.* (2018) Volatile chemical products emerging as largest petrochemical source of urban organic emissions. *Science* 359(6377):760.

208. Perez L, *et al.* (2013) Chronic burden of near-roadway traffic pollution in 10 European cities (APHEKOM network). *European Respiratory Journal* 42(3):594.

209. Jerrett M, *et al.* (2009) A Cohort Study of Traffic-Related Air Pollution and Mortality in Toronto, Ontario, Canada. *Environmental health perspectives* 117(5):772-777.

210. Hoffmann B, *et al.* (2006) Residence close to high traffic and prevalence of coronary heart disease. *European heart journal* 27(22):2696-2702.

211. Weichenthal S, *et al.* (2018) Spatial variations in the estimated production of reactive oxygen species in the epithelial lung lining fluid by iron and copper in fine particulate air pollution. *Environmental Epidemiology* 2(3):e020.

212. Bates JT, *et al.* (2015) Reactive Oxygen Species Generation Linked to Sources of Atmospheric Particulate Matter and Cardiorespiratory Effects. *Environmental Science & Technology* 49(22):13605-13612.

213. Kirkham PA & Barnes PJ (2013) Oxidative Stress in COPD. *Chest* 144(1):266-273.

214. Dhalla NS, Temsah RM, & Netticadan T (2000) Role of oxidative stress in cardiovascular diseases. *Journal of hypertension* 18(6):655-673.

215. Dellinger B, *et al.* (2001) Role of Free Radicals in the Toxicity of Airborne Fine Particulate Matter. *Chemical Research in Toxicology* 14(10):1371-1377.

216. Ayres JG, *et al.* (2008) Evaluating the Toxicity of Airborne Particulate Matter and Nanoparticles by Measuring Oxidative Stress Potential—A Workshop Report and Consensus Statement. *Inhalation Toxicology* 20(1):75-99.

217. Li N, *et al.* (2003) Ultrafine particulate pollutants induce oxidative stress and mitochondrial damage. *Environmental health perspectives* 111(4):455-460.

218. Sarnat JA, *et al.* (2018) Developing Multipollutant Exposure Indicators to Traffic Pollution: The Dorm Room Inhalation to Vehicle Emissions (DRIVE) study ed Institute HE.

219. Chowdhury S & Dey S (2016) Cause-specific premature death from ambient PM2.5 exposure in India: Estimate adjusted for baseline mortality. *Environment International* 91(Supplement C):283-290.

220. Jackson RB, *et al.* (2018) Global energy growth is outpacing decarbonization. *Environmental Research Letters* 13(12):120401.

221. Sharma D & Jain S (2019) Impact of intervention of biomass cookstove technologies and kitchen characteristics on indoor air quality and human exposure in rural settings of India. *Environment International* 123:240-255.

222. Pant P*, et al.* (2019) Monitoring particulate matter in India: recent trends and future outlook. *Air Quality, Atmosphere & Health* 12(1):45-58.

223. Venkataraman C*, et al.* (2017) Source influence on emission pathways and ambient PM2.5 pollution over India (2015-2050). *Atmos. Chem. Phys. Discuss.* 2017:1-38.

224. Botzen WJW, Gowdy JM, & Van Den Bergh JCJM (2008) Cumulative CO2 emissions: shifting international responsibilities for climate debt. *Climate Policy* 8(6):569-576.

225. Anonymous (*Census of India 2011: provisional population totals - India data sheet.* , (Office of the Registrar General Census Commissioner I).

226. Sadavarte P & Venkataraman C (2014) Trends in multi-pollutant emissions from a technology-linked inventory for India: I. Industry and transport sectors. *Atmospheric Environment* 99(Supplement C):353-364.

227. Guttikunda SK & Jawahar P (2014) Atmospheric emissions and pollution from the coal-fired thermal power plants in India. *Atmospheric Environment* 92(Supplement C):449-460.

228. CEA (2017) *Growth of Electricity Sector in India From 1947-2017* (New Delhi), Government of India (Power Mo).

229. Guttikunda SK & Jawahar P (2018) Evaluation of Particulate Pollution and Health Impacts from Planned Expansion of Coal-Fired Thermal Power Plants in India Using WRF-CAMx Modeling System. *Aerosol and Air Quality Research* 18(12):3187-3202.

230. Dharmadhikary S & Dixit S (2011) Thermal Power Plants on The Anvil: Implications and Need for Rationalisation. *Prayas Energy Group*.

231. Holloway S*, et al.* (2009) An assessment of the CO2 storage potential of the Indian subcontinent. *Energy Procedia* 1(1):2607-2613.

232. Chikkatur AP, Chaudhary A, & Sagar AD (2011) Coal Power Impacts, Technology, and Policy: Connecting the Dots. *Annual Review of Environment and Resources* 36(1):101-138.

233. Anonymous (2013) Black and Dirty - the Real Challenges Facing India's Coal Sector (Prayas Energy Group, Pune, India).

234. Anonymous (2012) Risks of Coal Based Electricity Generation in India. (World Institute of Sustainable Energy, Pune, India (2012)).

235. Anonymous (1992) *Report on Design and Operatin Parameters of Electrostatic Precipitators*, Central Pollution Control Board.

236. Zhang X (2016) Emission standards and control of PM2. 5 from coal-fired power plant. *IEA Clean Coal Centre: London, UK*.

237. Anonymous (2019) India's Energy Transition: The cost of meeting air pollution standards in the coal-fired electricity sector (International Institute for Sustainable Development; Global Subsidies Initatitive; Council on Energy, Environment and Water, International Institute for Sustainable Development).

238. Murata A*, et al.* (2016) Environmental co-benefits of the promotion of renewable power generation in China and India through clean development mechanisms. *Renewable Energy* 87(Part 1):120-129.

239. Tripathi L, Mishra AK, Dubey AK, Tripathi CB, & Baredar P (2016) Renewable energy: An overview on its contribution in current energy scenario of India. *Renewable and Sustainable Energy Reviews* 60:226-233.

240. Goel S*, et al.* (2014) Market potential study for organic Rankine cycle technology in India. *India: Indo-German Energy Forum*.

241. Sarkar R, Singh N, & Swapan Kumar D (2007) Effect of addition of pond ash and fly ash on properties of ash—clay burnt bricks. *Waste Management & Research* 25(6):566-571.

242. Verma RD, S; Arya, K.K.; Batra, P; Mhaske, P.S.; Siwal, P.D. (2017-18) *Central Electricity Authority: Annual Report*, Government of India (Power Mo).

243. Haleem A*, et al.* (2016) Critical factors for the successful usage of fly ash in roads & bridges and embankments: Analyzing indian perspective. *Resources Policy* 49:334-348.

244. Pandey A & Venkataraman C (2014) Estimating emissions from the Indian transport sector with on-road fleet composition and traffic volume. *Atmospheric Environment* 98:123-133.

245. Pandey A, Sadavarte P, Rao AB, & Venkataraman C (2014) Trends in multi-pollutant emissions from a technology-linked inventory for India: II. Residential, agricultural and informal industry sectors. *Atmospheric Environment* 99:341-352.

246. Madhawa Hettiarachchi HD, Golubovic M, Worek WM, & Ikegami Y (2007) Optimum design criteria for an Organic Rankine cycle using low-temperature geothermal heat sources. *Energy* 32(9):1698-1706.

247. CEA (2017-18) Load Generation Balance Reports. (Government of India, Ministry of Power, Central Electricity Authority).

248. Chacartegui R, Sánchez D, Muñoz JM, & Sánchez T (2009) Alternative ORC bottoming cycles FOR combined cycle power plants. *Applied Energy* 86(10):2162-2170.

249. Sarkar J & Bhattacharyya S (2015) Potential of organic Rankine cycle technology in India: Working fluid selection and feasibility study. *Energy* 90:1618-1625.

250. CII (2009) Manual on Waste Heat Recovery in Indian Cement Industry. (Confederation of Indian Industry and Asia-Pacific Partnership).

251. Khurana S, Banerjee R, & Gaitonde U (2002) Energy balance and cogeneration for a cement plant. *Applied Thermal Engineering* 22(5):485-494.

252. Cusworth DH*, et al.* (2018) Quantifying the influence of agricultural fires in northwest India on urban air pollution in Delhi, India. *Environmental Research Letters* 13(4):044018.

253. Hiloidhari M & Baruah DC (2011) Crop residue biomass for decentralized electrical power generation in rural areas (part 1): Investigation of spatial availability. *Renewable and Sustainable Energy Reviews* 15(4):1885-1892.

254. Bhuvaneshwari S, Hettiarachchi H, & Meegoda J (2019) Crop Residue Burning in India: Policy Challenges and Potential Solutions. *International Journal of Environmental Research and Public Health* 16:832.

255. Singh J, Panesar BS, & Sharma SK (2008) Energy potential through agricultural biomass using geographical information system—A case study of Punjab. *Biomass and Bioenergy* 32(4):301-307.

256. Morrow WR, Hasanbeigi A, Sathaye J, & Xu T (2014) Assessment of energy efficiency improvement and CO2 emission reduction potentials in India's cement and iron & steel industries. *Journal of Cleaner Production* 65:131-141.

257. STUDIES E (2003) Steel Statistical Yearbook. *World Steel Association, Brussels*.

258. Campana F*, et al.* (2013) ORC waste heat recovery in European energy intensive industries: Energy and GHG savings. *Energy Conversion and Management* 76:244-252.

259. Sharma V & Akhai S (2019) Trends in Utilization of Coal Fly Ash in India: A Review.

260. Haque EM (2013) Enablers and barriers for utilization of fly-ash in Indian cement industry. *International Journal of Advance Industrial Engineering* 1(1):31-35.

261. Harsha GS & Babu B (2016) Performance Evaluation of High Volume Fly Ash Concrete. *i-Manager's Journal on Structural Engineering* 5(2):39.

262. Rajarathnam U*, et al.* (2014) Assessment of air pollutant emissions from brick kilns. *Atmospheric Environment* 98:549-553.

263. Eliche-Quesada D, Sandalio-Pérez JA, Martínez Martínez S, Pérez-Villarejo L, & Sánchez-Soto P (2017) Investigation of use of coal fly ash in eco-friendly construction materials: Fired clay bricks and silica-calcareous non fired bricks. *Ceramics International* 44.

264. Bey I*, et al.* (2001) Global modeling of tropospheric chemistry with assimilated meteorology: Model description and evaluation. *Journal of Geophysical Research: Atmospheres* 106(D19):23073-23095.

265. Li M*, et al.* (2017) MIX: a mosaic Asian anthropogenic emission inventory under the international collaboration framework of the MICS-Asia and HTAP. *Atmos. Chem. Phys.* 17(2):935-963.

266. Chowdhury S*, et al.* (2019) Indian annual ambient air quality standard is achievable by completely mitigating emissions from household sources. *Proceedings of the National Academy of Sciences* 116(22):10711.

267. Apte JS & Pant P (2019) Toward cleaner air for a billion Indians. *Proceedings of the National Academy of Sciences* 116(22):10614.

268. Anonymous (2010) IARC monographs on the evaluation of carcinogenic risks to humans, household use of solid fuels and high-temperature frying. ed Cancer IAfRo (World Health Organization, France).

269. Woodbridge R, Sharma M, & Fuente D (2005) Atlas of Household Energy Consumption and Expenditure in India. *Chennai, India: Institute for Financial and Management Research*.

270. Anonymous (Census of India 2011: provisional population totals - India data sheet. (Office of the Registrar General Census Commisioner, India.).

271. Hinds WC (1982) Aerosol technology: properties, behavior, and measurement of airborne particles. *New York, Wiley-Interscience, 1982. 442 p.* 1.

272. Seinfeld JH & Pandis SN (2012) *Atmospheric chemistry and physics: from air pollution to climate change* (John Wiley & Sons).

273. Janhäll S, Andreae MO, & Pöschl U (2010) Biomass burning aerosol emissions from vegetation fires: particle number and mass emission factors and size distributions. *Atmos. Chem. Phys.* 10(3):1427-1439.

274. Barrie LA (1992) Scavenging ratios: black magic or a useful scientific tool. *Precipitation scavenging and atmosphere-surface exchange*), Vol 1.

275. Galloway JN, Savoie DL, Keene WC, & Prospero JM (1993) The temporal and spatial variability of scavenging ratios for NNS sulphate, nitrate, methonesulphonate and sodium in the atmosphere over the Northa Atlantic Ocean. *Atmos Environ* 27A:235-250.

276. Kane MM, Rendell AR, & Jickells D (1994) Atmospheric scavenging processes over the North Sea. *Atmos Environ* 28:2523-2530.

277. Wang ZW*, et al.* (2014) Elemental carbon in snow at Changbai Mountain, northeastern China: concentrations, scavenging ratios, and dry deposition velocities. *Atmos. Chem. Phys.* 14(2):629-640.

278. Cadle S & Dasch J (1988) Wintertime concentrations and sinks of atmospheric particulate carbon at a rural location in Northern Michigan. *Atmos Environ* 22:1373-1381.

279. Hegg DA, Clarke AD, Doherty SJ, & StrÖM J (2011) Measurements of black carbon aerosol washout ratio on Svalbard. *Tellus B* 63(5):891-900.

280. Guo L-C, Bao L-J, She J-W, & Zeng EY (2014) Significance of wet deposition to removal of atmospheric particulate matter and polycyclic aromatic hydrocarbons: A case study in Guangzhou, China. *Atmos Environ* 83:136-144.

281. Petzold A*, et al.* (2013) Recommendations for the interpretation of "black carbon" measurements. *Atmos. Chem. Phys. Discuss.* 13(4):9485-9517.

282. Favez O, Cachier H, Sciare J, Sarda-Estève R, & Martinon L (2009) Evidence for a significant contribution of wood burning aerosols to PM2.5 during the winter season in Paris, France. *Atmos Environ* 43(22–23):3640-3644.

283. Flagan RC & Seinfeld JH (2012) *Fundamentals of air pollution engineering* (Dover, Mineola, N.Y.) pp xiii, 562 p.

284. Slinn WGN (1983) Precipitation scavenging. *Atmospheric Sciences and Power Production - 1979*, (Division of Biomedical Environmental Research, U.S. Department of Energy, Washington, DC).

285. Ajayi GO (1984) Rain drop characteristics during a tropical thunderstorm and monsoon rainfall at Ile-If. *Antenna Telecommun* 39:515-522.

286. Parashar D, Gadi R, Mandal T, & Mitra A (2005) Carbonaceous aerosol emissions from India. *Atmos Environ* 39(40):7861-7871.

287. Krudysz MA, Froines JR, Fine PM, & Sioutas C (2008) Intra-community spatial variation of size-fractionated PM mass, OC, EC, and trace elements in the Long Beach, CA area. *Atmospheric Environment* 42(21):5374-5389.